The Development of Dualsteric Ligands for the Elucidation of Mode of Activation of Muscarinic Receptors and their Selective Signaling.

Dissertation zur Erlangung des
naturwissenschaftlichen Doktorgrades der Julius-
Maximilians-Universität Würzburg

vorgelegt von

Noura Riad

aus Kairo

Würzburg 2018

The present work was done during the period between September 2013 and September 2017 at the Institute of Pharmacy and Food Chemistry, Julius-Maximilians-University Würzburg, under the supervision of

Prof. Dr. Ulrike Holzgrabe

Head of the department of Pharmaceutical and Medicinal Chemistry.

Eingereicht bei der Fakultät für Chemie und Pharmazie am

Gutachter der schriftlichen Arbeit

1. Gutachter:

---

2. Gutachter:

Prüfer des öffentlichen Promotionskolloquiums

1. Prüfer:

---

2. Prüfer:

---

3. Prüfer:

Datum des öffentlichen Promotionskolloquiums

Doktorurkunde ausgehändigt am

Acknowledgement

List of publications and documentation of authorship

This section contains a list of individual contribution for each author to the publications reprinted in this thesis. The authors of the three published papers listed below thank Andreas Lorbach and Todd B. Marder (Institute of Inorganic Chermistry, Würzburg University) for the X-ray diffractometry data collection and structure solution.

Riad, **N. M.**; **Zlotos**, **D. P.**; **Holzgrabe**, **U.**, Crystal structure of 5, 11-dihydropyrido [2, 3-*b*][1, 4] benzodiazepin-6-one. *Acta Crystallographica Section E: Crystallographic Communications* **2015,** *71* (5), 304-305.

Author	1	2	3
Study design/concept development			x
Synthesis and crystallization	x		
Spectral data gathering	x		
Data analysis and interpretation	x	x	x
Manuscript planning	x	x	x
Manuscript writing	x	x	
Correction of manuscript	x	x	x
Supervision of Noura Riad			x

Riad, **N. M.**; **Zlotos, D.**; **Holzgrabe**, **U.**, 2-Amino-*N*-(2-chloropyridin-3yl) benzamide. *IUCrData* **2017,** *2* (10), x171536.

Author	1	2	3
Study design/concept development			x
Synthesis and crystallization	x		
Spectral data gathering	x		
Data analysis and interpretation	x	x	x
Manuscript planning	x	x	x
Manuscript writing	x	x	
Correction of manuscript	x	x	x
Supervision of Noura Riad			x

Riad, **N.**; **Zlotos**, **D.**; **Holzgrabe**, **U.**, 3-(2-Chloropyridin-3-yl) quinazoline-2, 4 (1*H*, 3*H*)-dione chloroform monosolvate. *IUCrData* **2017,** *2* (4), x170580.

Author	1	2	3
Study design/concept development			x
Synthesis and crystallization	x		
Spectral data gathering	x		
Data analysis and interpretation	x	x	x
Manuscript planning	x	x	x
Manuscript writing	x	x	
Correction of manuscript	x	x	x
Supervision of Noura Riad			x

Erklärung zu den Eigenanteilen des Doktoranden an Publikationen und Zweitpublikationsrechten bei einer kumulativen Dissertation.

Für alle in dieser kumulativen Dissertation verwendeten Manuskripte liegen die notwendigen Genehmigungen der Verlage („reprint permissions") für die Zweitpublikation vor.

Die Mitautorin der in dieser kumulativen Dissertation verwendeten Manuskripte ist sowohl über die Nutzung als auch über die oben angegebenen Eigenanteile informiert.

Die Beiträge der Mitautorin an den Publikationen sind in den vorausgehenden Tabellen aufgeführt.

Prof. Dr. Ulrike Holzgrabe   _____   _____

                                                          Ort, Datum   Unterschrift

Noura Riad   _____   _____

                                                          Ort, Datum   Unterschrift

Table of Contents

List of Figures

List of Tables

List of Abbreviations

Å	Angstrom
AC	Adenylyl Cyclase
ACh	Acetylcholine
AchE	Acetylcholinesterase
AchR	Acetycholine Receptor
ANS	Autonomic Nervous System
Asn	Asparagine
Asp	Aspartic acid
cAMP	Cyclic Adenosine Monophosphate
cGMP	Cyclic Guanosine Monophosphate
CH_2Cl_2	Dichloromethane
ChAT	Choline Acetyltransferase
$CHCl_3$	Chloroform
CHT	Choline High-affinity Transporter
CNS	Central Nervous System
COPD	Chronic Obstructive Pulmonary Disease
COSY	Correlation Spectroscopy
Cys	Cysteine
DAG	Diacylglycerol
DEPT	Distortionless Enhancement by Polarization Transfer
DMSO	Dimethyl Sulphoxide
EC	Extracellular Coil
Equiv.	Equivalent
ESI	Electrospray Ionization (ESI)
EtOAc	Ethyl Acetate
g	Gram
GABA	Gamma-Amino Butyric Acid
GDP	Guanosine Diphosphate
Glu	Glutamic acid
Gly	Glycine
Gly	Glycine
GPCRs	G-Protein coupled receptors
GTP	Guanosine Triphosphate
HMBC	Heteronuclear Multiple Bond Coherence

HMQC	Heteronuclear Multiple Quantum Coherence
Hz	Hertz
IC	Intracellular Coil
IP_3	Inositol-1,4,5-trisphosphate
KOtBu	Potassium tertiary butoxide
LC/MS	Liquid Chromatography/Mass Spectrometry
M	Molar
mAchR	Muscarinic Acetylcholine Receptor
MeOH	Methanol
Min	Minutes
Mol	Mole
Mp	Melting Point
MW	Molecular Weight
NA	Noradrenaline
nAchR	Nicotinic Acetylcholine Receptor
NAM	Negative Allosteric Modulator
NH_3	Ammonia
NMR	Nuclear Magnetic Resonance
NMS	N-Methyl Scopolamine
PAM	Positive Allosteric Modulator
PIP_2	Phosphatidyl-4,5-bisphosphates
PNS	Peripheral Nervous System
Ppm	Parts per million
PSNS	Parasympathetic Nervous System
QNB	Quinuclidinyl Benzilate
RP	Reverse Phase
SAM	Silent Allosteric Modulator
SiO_2	Silica gel
SNS	Sympathetic Nervous System
Thr	Threonine
TLC	Thin Layer Chromatography
TM	Transmembrane
Tyr	Tyrosine
UV	Ultraviolet
Vis	Visible
W	Watt

1. Introduction

1.1. The autonomic nervous system (ANS)

The nervous system communicates with the rest of the vertebrate body by sending electrical impulses from the central nervous system (CNS) through neurons to the peripheral nervous system (PNS), muscles and glands. Communication between neurons occurs via one of two key mechanisms; either the secretion of chemical messengers called neurotransmitters at chemical synapses, or the direct transmission of intercellular signals through gap junctions at electrical synapses.

The autonomic nervous system (ANS) is the branch of the PNS that controls the body's involuntary actions and visceral functions. Traditionally, the ANS is classified into the sympathetic nervous system (SNS) and the parasympathetic nervous system (PSNS). For both the SNS and PNS, signals through the inter-neuronal connections are communicated via the use of acetylcholine (ACh) as a neurotransmitter. Moreover, the postganglionic neurons in the PNS (as well as those of the SNS that innervate the sweat glands and the piloerector muscles) also transmit their signals to effector organs by the means of release of ACh, which binds to ACh receptors on these target organs. All other postganglionic neurons of the SNS, however, mediate their messages through the neurotransmitter noradrenaline (NA).[1-3]

1.2. The cholinergic transmission

ACh undergoes certain biosynthesis, storage and release processes in the cholinergic nervous system. The biosynthesis of ACh occurs in the terminal part of the cholinergic neuronal axon and is catalyzed by the enzyme choline acetyltransferase (ChAT), which links choline and acetyl coenzyme A. A prerequisite step for this synthesis is the uptake of choline from the synaptic cleft by a high affinity uptake system located on the synaptic terminals of these neurons. The synthesized ACh is stored inside vesicles in the presynaptic neuron.[4,5]

When a nerve impulse travels down the presynaptic neuron, voltage-dependent Ca^{2+} channels open. Elevation of intracellular Ca^{2+} levels inside the terminal bulb induces the release of ACh from its vesicles into the synaptic cleft. The binding of ACh to its complementary acetylcholine receptors (AChR) on the postsynaptic neuron or effector organ propagates further necessary cellular.[4, 5]

Finally, degradation of the ACh occurs, where ACh in cholinergic synapses is hydrolyzed by acetylcholinesterase (AChE) into choline and acetate. This is eventually followed by recycling of the choline precursor, where almost 50% of choline derived from the ACh hydrolysis is recovered by the choline high-affinity transporter (CHT).[5] The overall events occurring at the cholinergic synapse is illustrated in Figure 1.1.
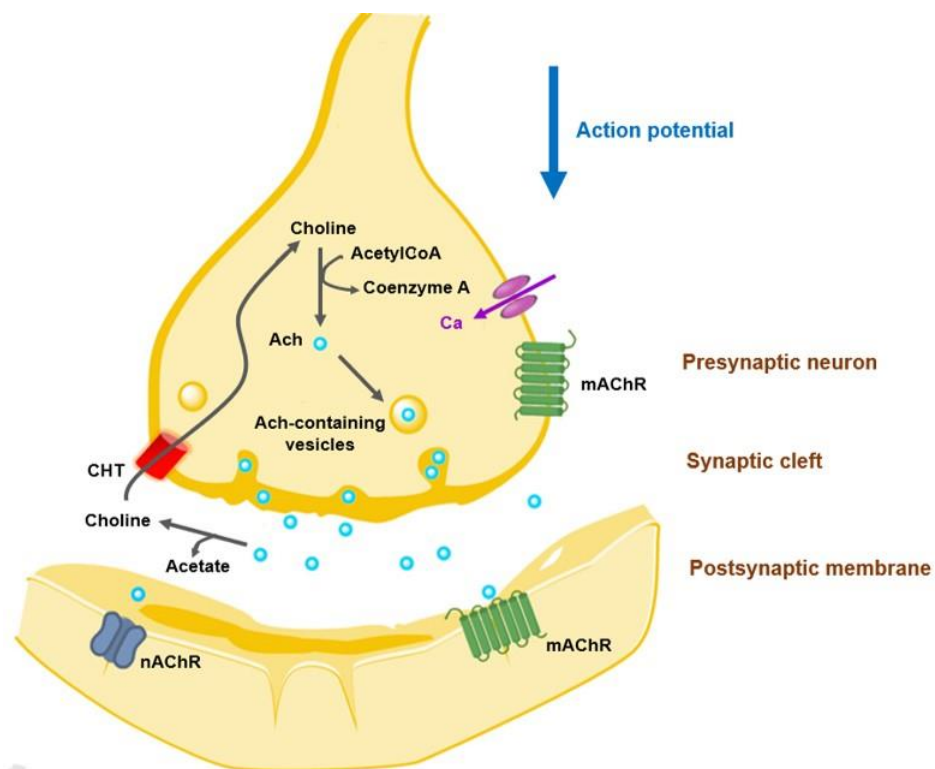
Figure 1.1: A schematic illustration of the cholinergic transmission.

The agonistic effect of ACh in the ANS are mediated through two types of receptors, the nicotinic acetylcholine receptors (nAChR) and the muscarinic acetylcholine receptors (mAChR), based on their abilities to be stimulated the natural alkaloidal agonists nicotine and muscarine, respectively.

mAChRs belong to the members of the superfamily of G protein-coupled receptors (GPCRs), which mediate slow metabolic responses through secondary messenger cascades. Meanwhile, nAChRs are considered ligand-gated ion channels, which mediate rapid signal transmission.[2, 6] The resultant neuromodulatory effect of ACh release in the ANS can be either excitatory or inhibitory based on the type of receptor stimulated on the postsynaptic cell.[7]

Drugs are able to modulate the cholinergic nervous system by directly binding to mAChRs or nAChRs, or indirectly by affecting the levels of ACh in the nervous system, for instance by inhibiting the AChE enzyme. Commonly, drugs affecting the parasympathetic system are found to bind to muscarinic receptors either as agonists (parasympathomimetics) or as antagonists (parasympatholytics).[8, 9]

1.3. G-protein coupled receptors (GPCRs)

G-protein coupled receptors (GPCRs) are the largest and most versatile group of membrane receptors in eukaryotes, where approximately 4% of the human exons encode for GPCRs. GPCR ligands constitute a diverse range of molecules such as biogenic amines, peptide and non-peptide neurotransmitters, hormones, growth factors, and lipids. Consequently, GPCRs are involved in wide spectrum of physiological functions such as vision, taste, olfaction, sympathetic and parasympathetic nervous functions, metabolism and immune regulation. Moreover, GPCRs are significant therapeutic targets in many pathological conditions including diabetes, neurodegeneration, cardiovascular disease, and psychiatric disorders. One-third to one-half of all marketed drugs function by the means of interaction with GPCRs.[1]

Despite the diversity of GPCR ligands, a common structural architecture is shared by all GPCRs and has been conserved over the years of evolution. Each GPCR consists of a core of seven transmembrane-spanning α-helical segments (TM1-TM7). These helices are linked by three intracellular coils (IC1-IC3) and three extracellular coils (EC1-EC3), with an intracellular C-terminal domain and an extracellular N-terminal domain. The extracellular coils form portions of the pockets onto which signaling molecules bind in order to interact

with the GPCR. Two cysteine residues are located in EC1 and EC2 (found in most GPCRs) and form disulfide bonds, a property which is crucial for the packing and stabilization of limited number conformations of the heptahelical structure.[1, 10, 11]

In spite of these similarities, individual GPCRs demonstrate unique combinations of signal transduction activities that involve several G-proteins. G-proteins, also known as guanine nucleotide-binding proteins, are distinctive proteins that act as molecular mediators in transmitting signals to the cell interior. The G-proteins that associate with GPCRs are heterotrimeric, having three distinct subunits; an alpha subunit (α), a beta subunit (β), and a gamma subunit (γ). Two of these subunits, the α- and β-subunits, are attached to the plasma membrane. The α-subunit binds either GTP or GDP depending on whether the G-protein is active or inactive, respectively. In the absence of a signal, GDP attaches to the α-subunit, and the entire G-protein-GDP complex binds to an adjacent GPCR. Upon ligand binding, a conformational change of the GPCR takes place. The activated GPCR in turn activates the G-protein by catalyzing the exchange of the bound GDP on the α-subunit for GTP. Consequently, the G-protein subunits dissociate into two parts; the GTP-bound α-subunit and a βγ dimer. These parts do not remain bound to the GPCR but rather they travel to interact with effector proteins such as enzymes and ion channels. The resultant effect involves changes in the concentration of intracellular signaling molecules such as cyclic adenosine monophosphate (cAMP), cyclic guanosine monophosphate (cGMP), inositol phosphates, diacylglycerol, arachidonic acid, and cytosolic ions, which in turn affects diverse cellular functions. Following ligand dissociation from the GPCR, and when the GTP is hydrolyzed back to GDP on the α-subunit using the GTPase activity of the G-protein, the three subunits re-assemble to form of an inactive heterotrimer, and the whole G-protein re-associates with the currently inactive GPCR, resulting in completion of the GPCR activation cycle, as shown in Figure 1.2.[1, 12, 13] The family of G-proteins includes the G_s, $G_{i/o}$, $G_{q/11}$, $G_{12/13}$.[14]
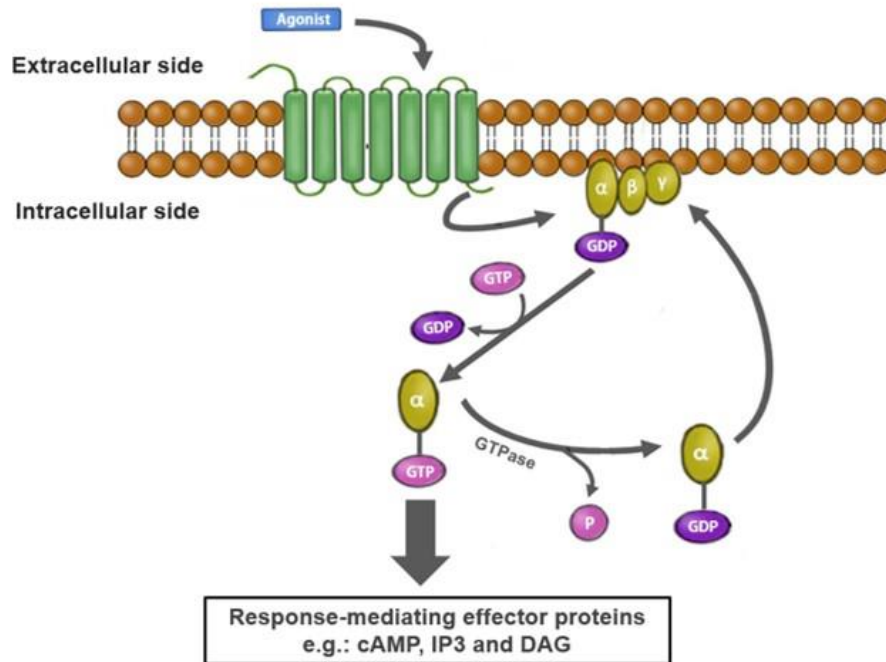
Figure 1.2 : A diagrammatic illustration of the GPCR activation cycle.

Based on sequence and structural similarities, GPCRs are classified into five main families; Rhodopsin (class A), Secretin (class B), Glutamate (class C), Adhesion and Frizzled/Taste, with each family demonstrating unique ligand binding properties. The largest class is class A, which accounts for approximately 85% of the GPCR genes. Muscarinic acetylcholine receptors belong to this class of GPCRs as well as the β-adrenergic receptors and the dopamine D_3 receptor.[1, 11, 15]

1.4. The muscarinic acetylcholine receptor (mAChR)

Based on the facts that the mAChR is a prototypical class A GPCR and that the cholinergic system has a high importance as previously discussed, the mAChR represents an important target for research.

1.4.1. Muscarinic acetylcholine receptors description, subtype classification, localization and involvement in physiological functions

mAChRs demonstrate a high level of sequence homology among their five subtypes at the so-called orthosteric binding site, while having a more variable domain at the extracellular region where it constitutes an allosteric binding site. Five metabotropic mAChRs subtypes are designated as M_1-M_5. The subtypes M_1, M_3 and M_5 exhibit coupling to $G_{q/11}$, whereas the subtypes M_2 and M_4 preferentially signal through the $G_{i/o}$-proteins.[6, 7, 16, 17]

The odd-numbered receptors (M_1, M_3, and M_5), coupling to $G_{q/11}$, activate phospholipase C (PLC) leading to the dissociation of phosphatidyl-4,5-bisphosphates (PIP_2) into two components; inositol-1,4,5-trisphosphate (IP_3) and diacylglycerol (DAG). IP_3 mediates Ca^{2+} release from the endoplasmic reticulum inside the cell, whereas DAG is responsible for activation of protein kinase C. The even-numbered receptors (M_2 and M_4), coupling to the $G_{i/o}$-proteins, inhibit adenylyl cyclase (AC) activity. These receptors also activate G-protein-gated potassium channels, which leads to hyperpolarization of the membrane in excitable cells. However, such categorization of final effect is not exclusive. For instance, M_1-type receptors can also cause adenylyl cyclase inhibition.[6, 18]

The mAChRs regulate heart rate, smooth muscle contraction, glandular secretion and various fundamental functions of the CNS. M_1, M_4 and M_5 receptors are mainly located in the CNS, being involved in complex responses such as memory, arousal and attention. M_1 receptors are also found on gastric parietal cells, exocrine glands and the autonomic ganglia. M_2 receptors are primarily localized in the heart, where their activation lowers the heart rate. M_3 receptors are found on smooth muscles in many areas in the body, where their activation produces responses on a variety of organs such as the bronchial tissue, the bladder and exocrine glands.[6, 16, 19]

Some mAChRs ligands designed through the field of research are selective for certain receptor subtypes and are often used as pharmacological tools for elucidating the function of the individual mAChRs. However, their specificity is not exclusive, for instance the M_2 receptor may be linked to $G_{i/o}$, $G_{q/11}$ or G_s.[6, 20]

1.4.2. Therapeutic targeting of muscarinic acetylcholine receptors in disease: potential alleviation of pathological conditions

The cholinergic manifestations of several diseases signify that mAChRs hold great potential as therapeutic targets. It has been reported that some M_1 receptor-selective agonists have the potential to remedy the symptoms of Alzheimer's disease and related cognitive disorders. Other findings suggest that ligands acting on M_1 and M_4 could exhibit antipsychotic activity. A correlation between mAChR and major depressive disorder was reported, where the use of muscarinic antagonists such as scopolamine decreased the levels of anxiety and alleviated depression. Muscarinic agonists may possibly be considered as therapeutic means to alleviate mania in cases with bipolar disorder. Moreover, the M_4 receptor, associated with the modulation of dopaminergic activity, could be targeted by selective antagonists to correct the imbalance in the level of dopamine in the brain that underlies the dyskinesia affiliated with Parkinson's disease. Studies propose that M_5 receptor antagonists could be useful for the treatment of drug abuse and substance dependence. It is also proposed that the stimulation of M_3 receptors could be useful for the treatment of type 2 diabetes. Furthermore, research proof suggests that mAChR-dependent signaling pathways and ligands can modulate cell proliferation and cancer progression, where mAChR antagonists could inhibit cell proliferation.[16, 17, 21, 22]

Among the clinically important ligands is pirenzepine, acting as an M_1-selective antagonist. Pirenzepine is known to inhibit gastric secretion, salivary and urinary function. The alkaloid atropine, a non-selective mAChR antagonist, is used in the treatment of myopia, but has undesired ocular and systemic side effects, therefore pirenzepine M_1-specific antagonist may alleviate side effects while remaining effective at decreasing the progression of myopia. Another alkaloid, scopolamine, is described to have antiemetic effect. Pirenzepine was also reported to counteract hypersalivation by its selective antagonistic activity on the M_4 receptor, which is stimulated by another known drug called clozapine. Clozapine is the only antipsychotic useful for treatment-resistant schizophrenia. Clozapine is a centrally-acting muscarinic antagonist at the M_1, M_2, M_3, and M_5 receptors, clozapine is a full agonist at the M_4 subtype. Peripherally-acting charged antagonists include tiotropium bromide, a drug which is used in COPD, as well as *N*-butyl scopolamine bromide which is used as an

antispasmodic drug. [16, 23, 24-32] Unfortunately, unavailability of subtype-selective ligands, lack of drugs deficient of side effects, as well as inconclusive physiological characterization of the role of each individual mAChR, are witnessed.[16]
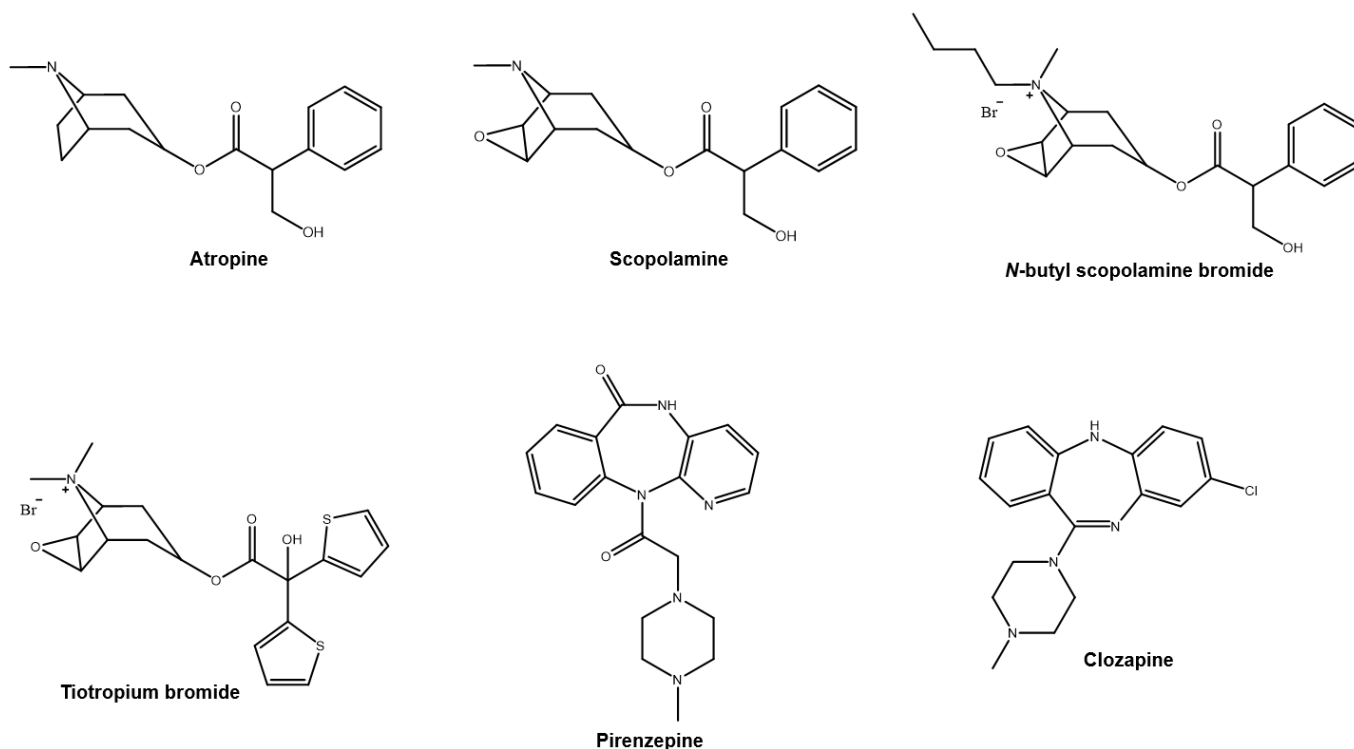
Figure 1.3: The structures of some muscarinic ligands in therapy.

1.4.3. Binding to the mAChR

Receptor ligands are classified based on the way they affect the receptor function or the location of their binding site, differentiating between orthosteric and allosteric ligands. More recent ligand design approaches describe a dualsteric means of binding, where one ligand has affinity to both the orthosteric and the allosteric site.[16, 33]

The published X-ray structures of class A GPCRs illustrate the topographically different locations of the orthosteric and allosteric binding sites.[34, 35]

Structural data have been reported for M_2 receptor in its active conformation, binding the agonist iperoxo, as well as in its inactive conformation, accomodating the antagonist

quinuclidinyl benzilate, QNB.[36] The M_3 receptor structure has also been reported in the inactive conformation, where the antagonist tiotropium bound.[37]

1.4.3.1. The orthosteric site

ACh binds to its orthosteric binding site of the mAChR as the endogenous agonist. Moreover, conventional agonists, antagonists and inverse agonists are typically able to occupy the same site as ACh based on structural similarities. The orthosteric binding site exhibits 20-50% sequence congruence within class A of GPCRs, with particularly high conservation among the individual subtypes of the mAChRs. Consequently, such property appears to be the underlying reason for the challenge to design selective orthosteric agonists and antagonists.[33]

ACh/agonist-binding mode on orthosteric site (orthosteric activation)

Crystal structure suggests that ACh binds to mAChRs in a narrow cleft enclosed by the ring-like arrangement of the seven transmembrane helices (the orthosteric binding site), about 10-15 Å away from the membrane surface.

Mutagenesis studies of the M_3 receptor suggest that the positively charged ammonium group of ACh forms an ionic bond with a highly conserved aspartate residue Asp147. Moreover, the efficient binding of ACh to the mAChR rely on the interactions between ACh and six other conserved amino acids; namely four tyrosine and two threonine residues. The asparagine residue Asn507 does not contribute to the binding of ACh to the orthosteric site, even though it is well-located for interaction with the bound ACh and proved to be conserved in all mAChR subtypes.[38] Figures 1.4 illustrates the detailed binding interactions between ACh and the M_3 receptor. Such interactions are expected between most orthosteric agonists and mAChRs.
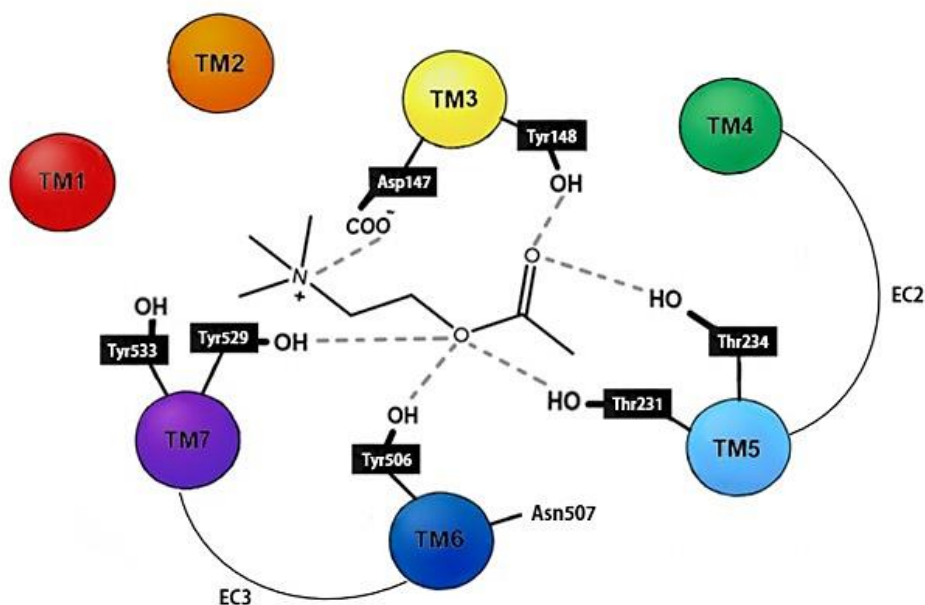
Figure 1.4 : The binding interaction of ACh and the residues in the orthosteric site of the M_3 receptor.

Studies done on the M_2 receptors suggested that the binding of ACh starts in its gauche form of the N-C1-C2-O dihedral angle. Subsequently, ACh goes through a conformational change from the gauche to the trans conformer when the ACh-bound M_2 receptor is activated and is bound to a G-protein, as shown in Figure 1.5.[39]
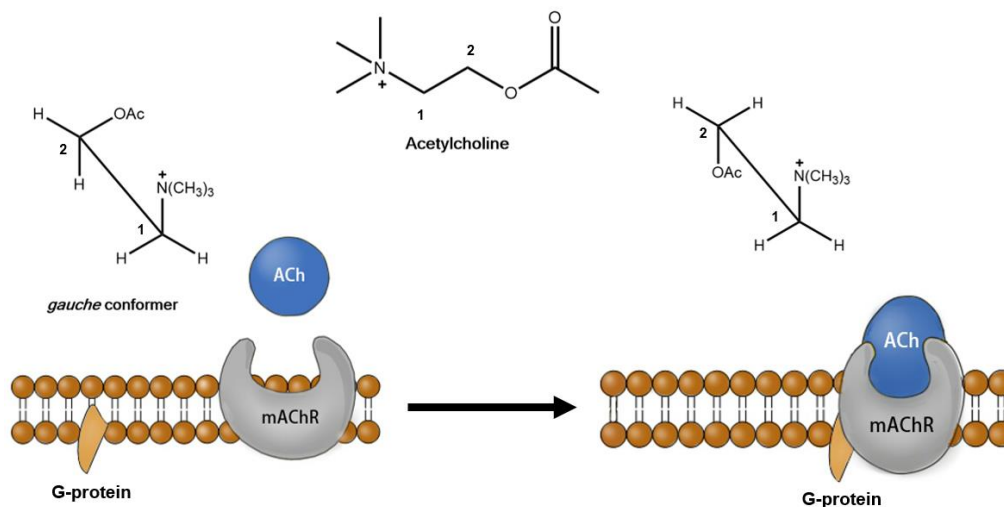
Figure 1.5: A diagrammatic illustration of the conformations of ACh involved in the mAChR activation.

On top of the list of agonists is iperoxo, which is a highly potent agonist for mAChRs. It is characterized by a Δ^2-isoxazoline ring system which highly enhances its binding affinity to the orthosteric site by a factor of 100 compared to ACh.[33, 40] The binding of iperoxo to the

orthosteric binding site is shown in Figure 1.6a, where the interactions with the receptor result in a closed shape of the orthosteric site (solvent-inaccessible).[16]

The three-dimensional conformational transition upon activation involves a cytoplasmic outwards movement of the transmembrane helical bundle and a corresponding inwards displacement of the extracellular domains, as illustrated in Figure 1.6b.[40] Moreover, it is also reported that the orthosteric site contracts to a smaller size to better fit the generally small agonist structure such as iperoxo and ACh, leading to better complementarity and justifying their agonistic action.[16]

In presence of an orthosteric agonist, the agonist-bound mAChR exists in a dymanic equilibrium (of different receptor conformations) between the active and the inactive conformations, suggesting that the receptor is "floppy" since the agonist can have multiple binding modes. A small alteration in the structure of the agonist can intensely affect the binding affinity for the active or the inactive receptor configuration.[41]
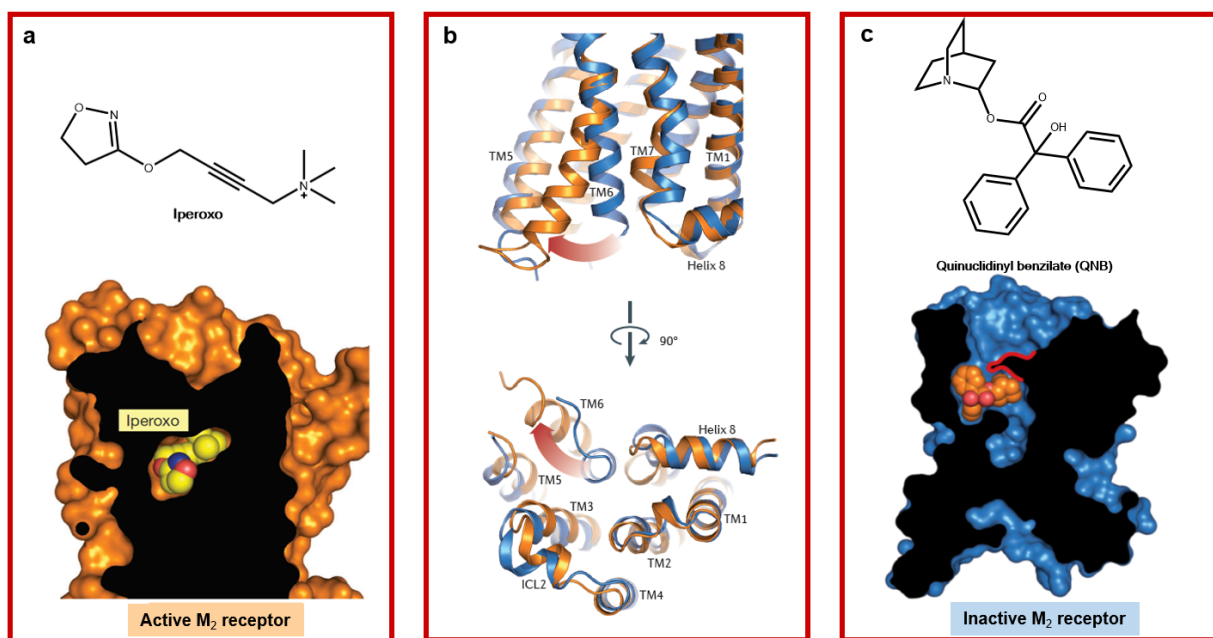
Figure 1.6: The M_2 receptor, **a**: The orthosteric binding site of the M_2 receptor showing the bound iperoxo, **b**: the conformation change of the transmembrane structure (particularly TM6) of the M_2 receptor upon transition from the inactive state (blue) to the active state (orange), **c**: the orthosteric binding site of the M_2 receptor showing the bound QNB. (modified from:[36]). Reprinted by permission of Macmillan Publishers Ltd.; Copyright © 2013.

Antagonist-binding mode on orthosteric site (orthosteric inhibition)

The asparagine residue Asn507 in TM6 participates in the improvement of the binding affinities of most antagonists (as proven by mutagenesis studies). The results demonstrated that the binding affinities of antagonists such as atropine-like agents (atropine, *N*-methyl atropine, scopolamine, and *N*-methyl scopolamine) and pirenzepine were diminished by factors ranging from 235 to 28,000 upon mutation, indicating that this conserved Asn residue provides a critical hydrogen bonding interaction in the binding mode of some mAChR antagonists.[38] Interaction through this Asn residue is considered a unique property of the mAChR family.[16]

As a first example to demonstrate the binding interactions of a competitive antagonist, *N*-methyl scopolamine (NMS), to the binding pocket of a M_3 receptor demonstrated ionic bonding between its quaternary nitrogen and Asp147 residue, similar to that reported for an agonist. Moreover, hydrogen bonding was found between Asn507 and NMS as is typical with most antagonists.[42] A second example of the antagonist quinuclidinyl benzilate (QNB), which was co-crystallized in the orthosteric binding site of M_2 receptor, is shown in Figure 1.6c.[36] Asn405 was shown to form hydrogen bonds with QNB, with limited interaction with Asn507, unlike most antagonists.[39]

Most of the well-known drugs of therapy (previously discussed) are considered orthosteric ligands (whether agonists or antagonists). Designing ligands that bind to the the orthosteric site provides high levels of binding affinity, however almost no subtype-selectivity. Interestingly, a tyrosine lid (made of the residues Tyr403, Tyr104 and Tyr426) was found to isolate the orthosteric site from the extracellular region. On the other side of that lid is the extracellular vestibule, which acts as the allosteric region and is formed of non-conserved amino acid residues. This opens a door to the utilization of this subtype-distinct allosteric region as means to design subtype-selective ligands.[16]

It is worthwhile to note that the orthosteric ligand has to pass the allosteric site on its journey to and from the orthosteric site. Consequently, it is proposed that orthosteric ligands may interact with residues of the allosteric site throughout their movement to and from the

orthosteric site, and hence they may regulate the topography of the orthosteric site by themselves.[43]

1.4.3.2. The allosteric site

Classical allosterism

Allosterism is typically described as the process by which the interaction of a chemical or protein at one location on a protein or macromolecular complex (the allosteric site) influences the binding or function of the same or another chemical or protein at a topographically distinct site.[44] The most commonly described allosterism is known as classical allostery, where the target of the allosteric modulation is a ligand concomitantly binding to an adjacent orthosteric site to the allosteric modulator.[35, 44]

Ligand-binding mode on the allosteric site

The non-conserved allosteric site is located between the extracellular coils EC2 and EC3. The loop EC2 of the M_2 receptor contains the crucial EDGE amino acid sequence (Glu172-Asp173-Gly174-Glu175) as well as Trp422 and Tyr177, whereas the essential residue Thr423 is on EC3.[16, 43]

Principles and pharmacological properties of allosteric modulators

Allosteric modulators induce conformational changes in the mAChR, consequently changes in the binding affinity of the orthosteric ligand may be observed as well as a possibility for the direct effect on the receptor signaling (intrinsic efficacy).[16, 44]

Cooperativity: allosteric-orthosteric interaction

The joint effect between concomitantly-bound allosteric and orthosteric ligands on a mAChR is bilateral and in the same direction; a phenomenon referred to as cooperativity.[33, 44]

Negative allosteric modulators (NAMs) are ligands that bind to the allosteric binding site and inhibit receptor function by decreasing the binding affinity of an orthosteric agonist

(negative binding cooperativity) and/or decreasing the efficacy of the agonist (negative activation cooperativity).[33]

Positive allosteric modulators (PAMs) are ligands that bind to the allosteric site and increase the overall binding of the concomitantly-bound orthosteric ligand. PAMs can only mediate their effect in the presence an orthosteric ligand and present an advantage of having no off-target effects. [33] An example of a PAM is the ligand LY2119620, which binds to the allosteric binding site of M_2 receptors in presence of an orthosteric agonist such as iperoxo. Upon binding, this PAM tends to stabilize the favourable configuration of the active receptor.[16] This is shown in the Figure 1.7 below.
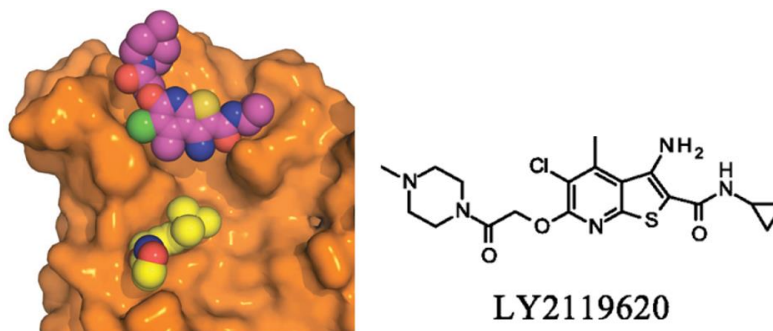
Figure 1.7: The structure of the M_2 receptor with the allosteric modulator LY2119620 (magenta) binding to its extracellular vestibule, and with a concomitantly bound iperoxo molecule (yellow) in the orthosteric binding site. (modified from:[36]). Reprinted by permission of Macmillan Publishers Ltd.; Copyright © 2013.

Silent or neutral allosteric modulators (SAMs) are ligands that bind to the allosteric site but have no effect on the affinity or efficacy of an orthosteric agonist (neutral cooperativity). They act as competitors at this binding site inducing a rightward shift of the dose-response curve of the concomitantly used allosteric modulators and can be regarded as antagonists of other allosteric modulators.[33]

Allosteric ligands which have the ability to activate the receptor in the absence of orthosteric agonists are referred to as allosteric agonists, ago-allosteric modulators or ago-potentiators. A number of PAMs were reported to be allosteric agonists as well, even though their agonistic activity is only seen at higher concentrations than those required for PAM activity.[33]

Characteristics of allosteric modulators providing the advantages of their use

➢ *Saturability.* This means that, above a certain concentration of the modulator, all the receptor allosteric sites are occupied and no further activity is witnessed for the allosteric ligand. This saturability phenomenon is governed by the cooperativity between orthosteric and allosteric sites.[16]

➢ *Partner dependency (probe dependence).* This means that the magnitude and direction of the allosteric effect changes according to the orthosteric ligand concomitantly-bound for a certain receptor and allosteric modulator.[16] This is because a receptor which is bound by either an allosteric or an orthosteric ligand can be considered as a new entity that has changed in structure from the original receptor form and, as a consequence, has a different signaling action.[33]

➢ *Signal bias (biased agonism).* This feature is also referred to as stimulus bias or functional selectivity.[33, 45] This property refers to the ability of allosteric ligands to stabilize certain receptor conformations so that only some signaling behaviour is mediated at the expense of others, as portrayed in Figure 1.8.[16] This is because the flexible allosteric vestibule controls the extent of receptor movement and thereby governs the G-protein recruitment within a certain receptor subtype. For instance, the vestibule of the M_2 receptor should adopt a more spacious conformation to achieve G_s coupling over $G_{i/o}$ coupling.[40] The therapeutic value of signal bias is the ability to design ligands that selectively promote signaling pathways involved in alleviation of physiological conditions, without promoting those that produce unwanted side effects.[45]

➢ *mAChR subtype selectivity.* This feature can be achieved either by targeting a less conserved allosteric site on the receptor or through selective cooperativity with the orthosteric ligand.[16]

The difference between the monovalent orthosteric and allosteric ligands binding is illustrated in Figure 1.9.
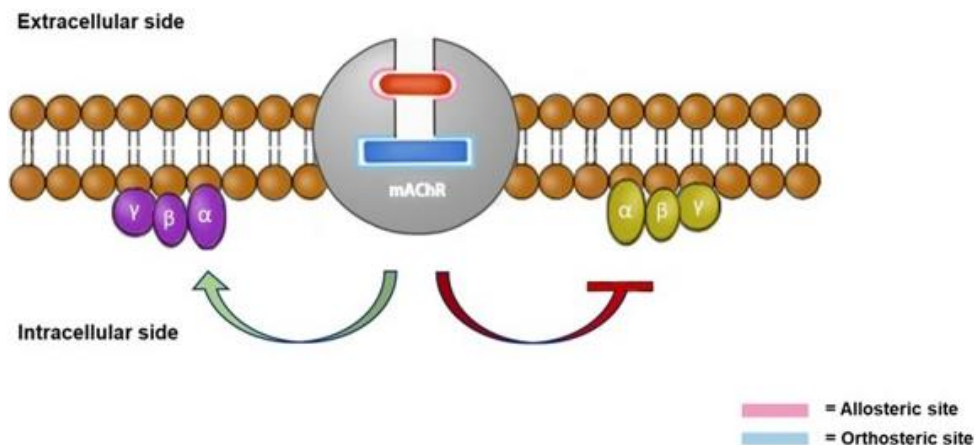
Figure 1.8: A schematic diagram of signal bias, as mediated by the presence of an allosteric ligand.
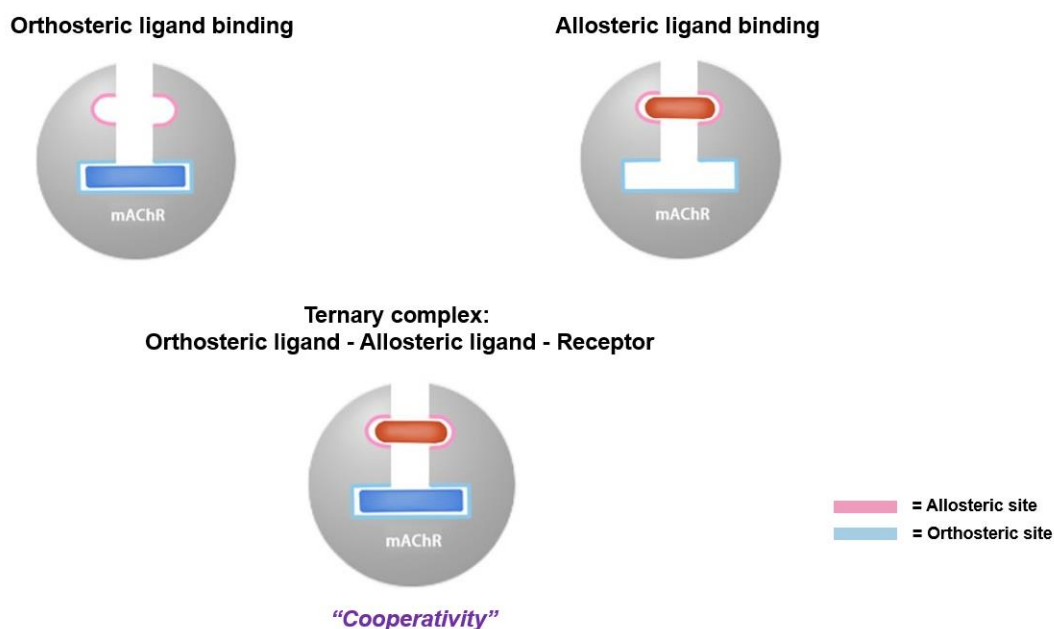
Figure 1.9: An illustration of the possible binding modes of monovalent ligands, which can bind orthosterically, allosterically, or concomitantly bind forming a ternary complex and exhibiting cooperativity.

Allosteric modulators in therapy

The first known allosteric modulators for therapeutic use were benzodiazepines, which have anxiolytic effect mediated by increasing the binding of the neurotransmitter γ-amino butyric acid (GABA).[33] Moreover other PAMs, such as those selective for M_1 and M_4 mAChR subtypes, have been reported for treatment of Alzheimer's disease and schizophrenia, respectively.[39] Cinacalcet (Mimpara®) is also a PAM towards Ca^{2+} at the

calcium-sensing receptor (CaSR) used to treat secondary hyperparathyroidism. Upon binding to the allosteric binding site, cinacalcet improves the receptor's sensitivity for extracellular Ca^{2+} and thus reduces the release of the parathyroid hormone (PTH) and bone resorption. In addition, a NAM called Maraviroc (Celsentry®) targets the human immunodeficiency virus (HIV), impairing its uptake into human host. This drug functions by allosterically binding to the CCR5 receptor (chemokine receptor 5) on the host cell, thus preventing this receptor from attaching to the envelope glycoprotein gp120 of the HIV. Furthermore, plerixafor (Mozobil®), acts as a SAM at the chemokine receptor CXCR4. This immunostimulatory ligand triggers the release stem cells into the blood for autogenic stem cell transplantation.[33] In conclusion, the clinical success of allosteric modulators suggest the research of such approach to attain improved therapeutic drugs.
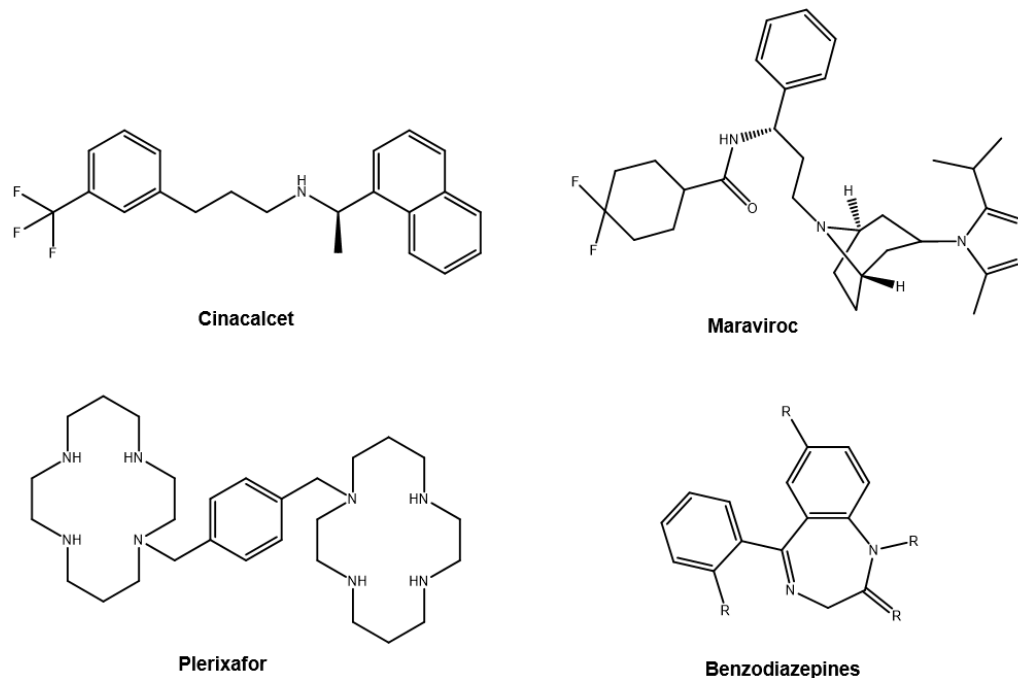
Figure 1.10: Structures of therapeutically useful allosteric modulators.

1.4.3.3. Dualsteric ligands

In a more advanced drug design approach, focus is on leading-edge dualsteric ligands targeting individual mAChR subtypes. Dualsteric ligands have two pharmacophoric

moieties, linked together as one molecular skeleton, to bind both the allosteric and orthosteric binding site on the same receptor, as shown in Figure 1.11.[16, 33, 34]

Figure 1.11: A schematic diagram of the dualsteric ligand approach, showing its 3 components: the orthosteric moiety, the allosteric moiety and the linker.

The dualsteric ligand approach was initially described as the "message-address" concept by R. Schwyzer.[46] Fundamentally, the "message" segment of the dualsteric ligand is responsible for receptor activation and hence binds with high affinity to the orthosteric binding site. The "address" segment of the dualsteric hybrid targets the uniquely non-conserved allosteric site of the receptor (subtype selectivity). The allosteric address portion of the dualsteric hybrid may further fine-tune the signaling behavior (signaling selectivity). An illustration of the "message-address" concept is shown in Figure 1.12. The linker segment in the middle of the dualsteric hybrid should have the appropriate length required for the successful binding of both the orthosteric and the allosteric moieties, without unnecessary length that may attribute to steric hindrance. The linker can be chemically made out of repeated segments of alkane groups, polyethyleneglycol or polyglycines, with the required flexibility/rigidity adjusted accordingly. The bridging functional groups may or may not be able to influence the receptor interactions and activation.[33, 47-50]

Since the dualsteric binding mode is mediated through one hybrid molecule, it is clearly differentiated from the standard ternary complex, which is formed using two distinct ligands binding to the allosteric and the orthosteric site concomitantly, as shown in Figure 1.13. In addition, the dualsteric binding mode is distinguishable from a multiple binding mode, where one small ligand oscillates between a purely allosteric and a purely orthosteric binding mode. Such flip-flop binding is restricted with dualsteric ligands because of their large size relatively high binding affinity.[43]
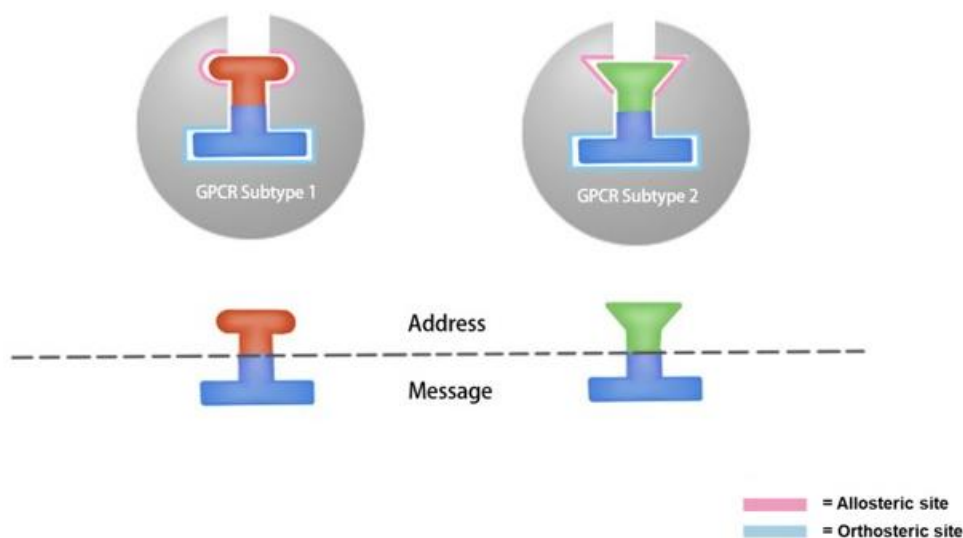
Figure 1.12: An illustration of the "message-address" concept.
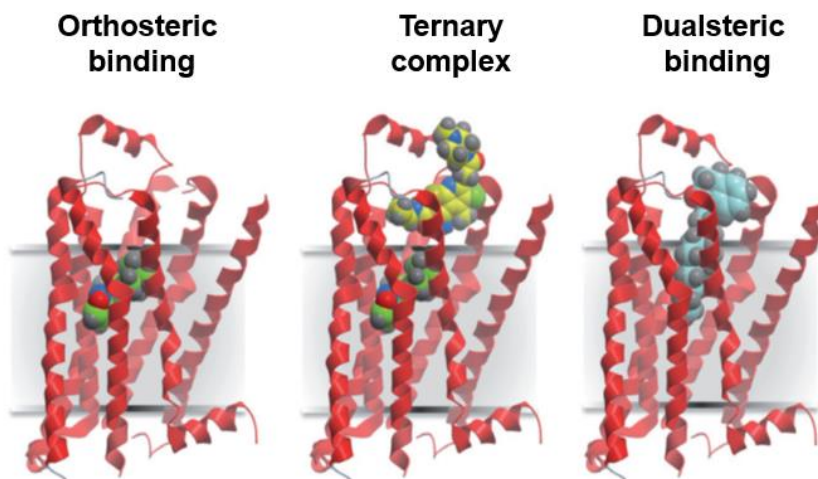
Figure 1.13: Three-dimensional models illustrating the difference in the binding mode between a monovalent orthosteric ligand, concomitantly-bound allosteric and orthosteric ligands (forming a ternary complex with the receptor), as well as dualsteric ligands. (modified from:[16]). Reprinted by permission of Macmillan Publishers Ltd.; Copyright © 2014.

Furthermore, dualsteric ligands exhibit dynamic ligand binding, meaning that the dualsteric hybrid can interchange between two binding modes; a pure dualsteric mode binding with both the orthosteric and allosteric binding sites and a purely allosteric binding mode occupying the allosteric binding site only, as shown in Figure 1.14. The shifting of this binding mode equilibrium towards one mode over the other occurs based on the ratio of

binding affinities of the orthosteric and allosteric moieties to their binding sites. The orthosteric segment of the dualsteric ligand should provide high binding affinity to embark a more favourable dualsteric binding mode.[48] Depending on the extent of dualsteric and allosteric binding, partial agonism can be designed.[34, 41, 50] Moreover, dynamic ligand binding was described to be the underlying reason for a phenomenon called protean agonism. Protean agonism refers to a feature of some dualsteric ligands which are able to act as agonists on receptors with low inherent activity, meanwhile acting as inverse agonists on inherently active receptor macromolecules.[51]
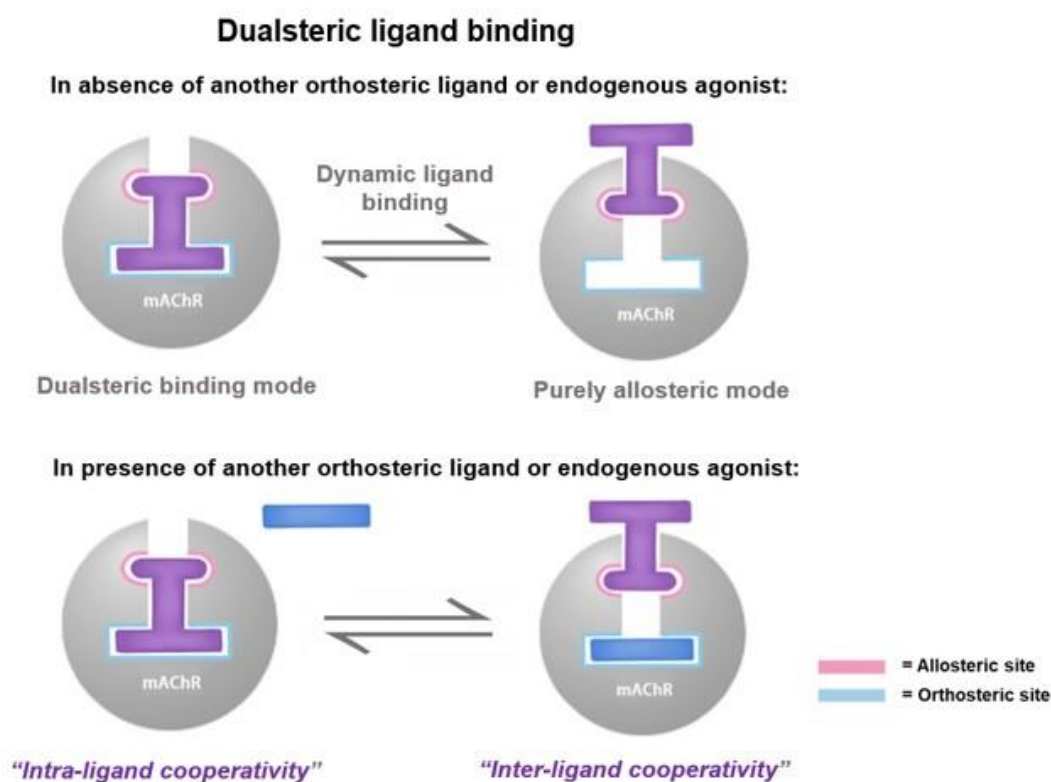
Figure 1.14: Dynamic ligand binding. A dualsteric ligand can demonstrate two binding modes: a dualsteric binding mode (cooperativity is observed) and a purely allosteric binding mode (cooperativity is observed in case of the presence of an orthosteric ligand).

The first dualsteric compounds

Successful examples of dualsteric hybrids consist of the superagonist iperoxo and the antagonistic allosteric phthalimido- or naphthalimidopropylamino molecules (derived from

the previously known W84 ligand) linked by a hexamethonium chain, as shown in Figure 1.15.[33, 34, 47] The hybrids provide both subtype selectivity (M_2-selectivity) as well as signal bias (functional selectivity), because these dualsteric hybrids prefer G_s recruitment over $G_{i/o}$ (as opposed to the functional preference of the orthosteric iperoxo alone).[33, 40, 52-54] Molecular switches have been reported for dualsteric ligands, where the M_2-selective dualsteric agonists were reported to convert to antagonistic activity merely by the introduction of a double bond into the Δ^2-isoxazoline ring of the iperoxo.[33, 41]
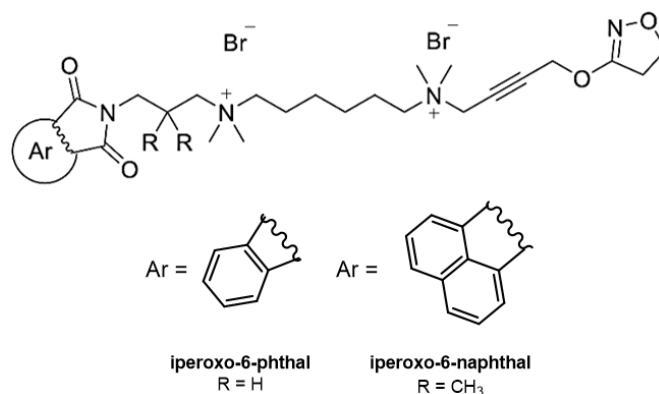
Figure 1.15: Structures of M_2-selective dualsteric ligands that are made up of iperoxo (orthosteric), phthalimido- or naphthalimidopropylamino (allosteric) and a six-carbon alkane linker.

Moreover, E. Heller et al. described the design of a M_2-selective dualsteric hybrid composed of AFDX-384 as an orthosteric moiety and phthalimidopropylamino as an allosteric moiety.[55] The rationale behind the use of AFDX-384 as an orthosteric antagonist was its feature of preferring the M_2 receptor subtype by being able to interact with some conserved residues present in the allosteric site,[43] while the phthalimidopropylamino part was used as a PAM.[54] In addition, M_1-selective dualsteric hybrids have been described. These ligands involved the use of the M_1 antagonist pirenzepine as the orthosteric moiety linked to one of several fluorescent allosteric moieties, as exemplified by the hybrid Bo(15)PZ, as shown in Figure 1.16.[56]

The expansion in the field of research of the dualsteric approach is highly demanded by the significant therapeutic potential of dualsteric hybrids selectively targeting mAChR subtypes, as well as the possibility for unraveling the molecular transduction pathways mediated by these receptors.
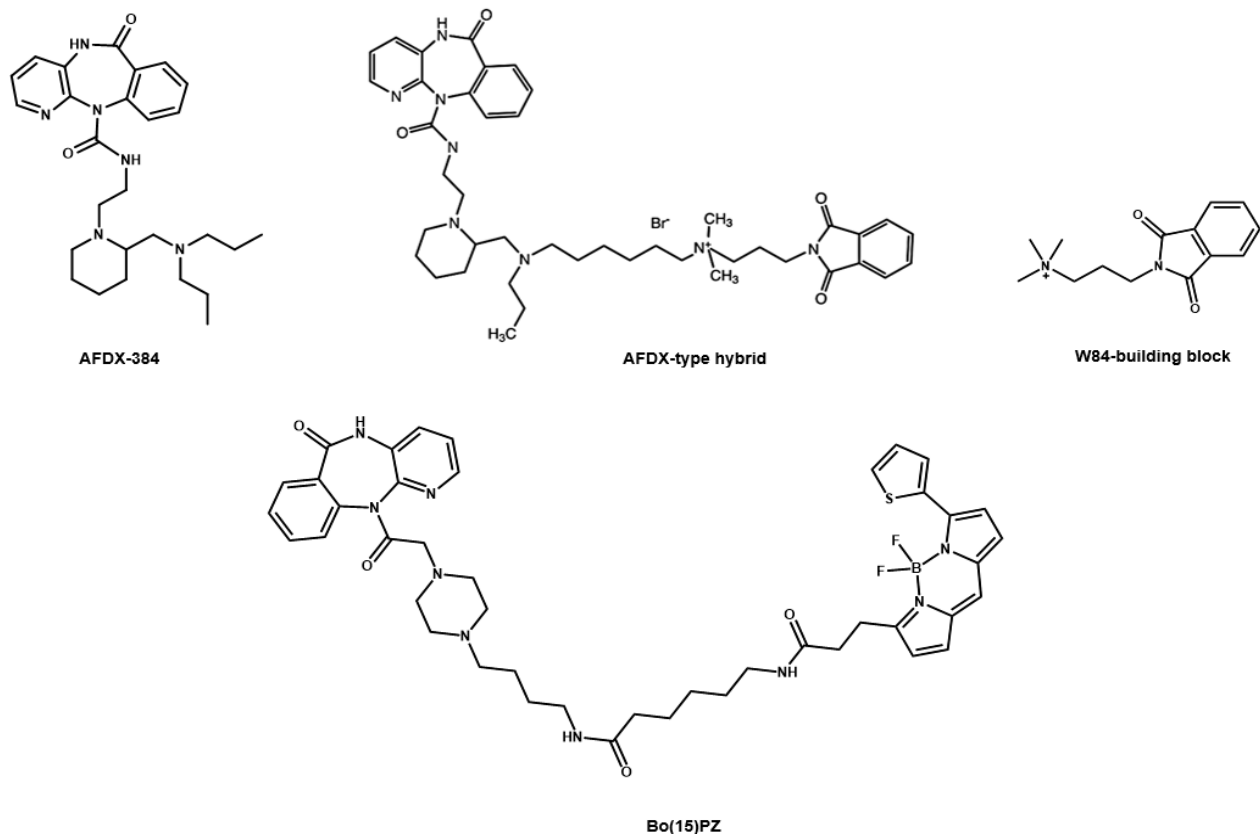
Figure 1.16: Structures of AFDX-384, the W84-building block, AFDX-type hybrid and Bo(15)PZ.

2. Aim of the work

GPCRs are significant therapeutic targets in many physiological conditions, where between one-third and one-half of all marketed drugs work by the means of acting on GPCRs. The cholinergic manifestations of several diseases signifies that muscarinic receptors (mAChRs) hold great potential as therapeutic targets, demanding treatment by the means of ligands of mAChR.

In the more advanced dualsteric drug design approach, allosteric and orthosteric moieties can be combined within one molecule to exploit the high affinity of ligand-binding to the orthosteric site and the structural diversity of the allosteric site to target an individual mAChR subtype, resulting in leading-edge dualsteric ligands. These mAChR subtype-selective dualsteric ligands provide the means to avoid the undesired side effects of non-selective orthosteric drugs, selectively promote signaling pathways involved in alleviation of pathological conditions, as well as aid in the elucidation of the physiological and pathological role of individual mAChR subtypes and highlight the molecular transduction mechanisms involved. These advantages essentially dictated the aim of this work to be the research and synthesis of dualsteric ligands targeting mAChR subtypes.

Firstly, a project attempting re-tracing the synthesis of the M_2-prefering AFDX-384 molecule was done (Figure 2.1), in an aim to open the gateway for future synthesis and inspection of AFDX-type dualsteric hybrids.
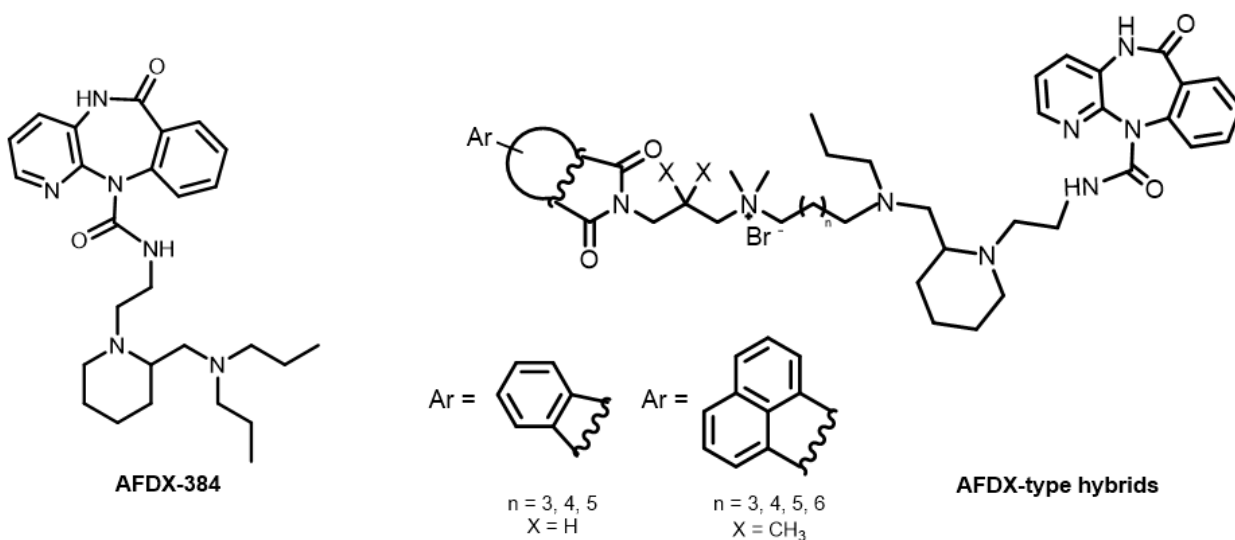
Figure 2.1: Structure of AFDX-384 and AFDX-type hybrids.

Secondly, dualsteric ligands involving variable orthosteric and allosteric moieties have been synthesized to constitute a second project, fruitfully resulting in the hybrid shown in Figure 2.2. Within each group of dualsteric hybrids, various linker lengths have been used in synthesis.

Phthalimide/1,8-naphthalimide-clozapine hybrids
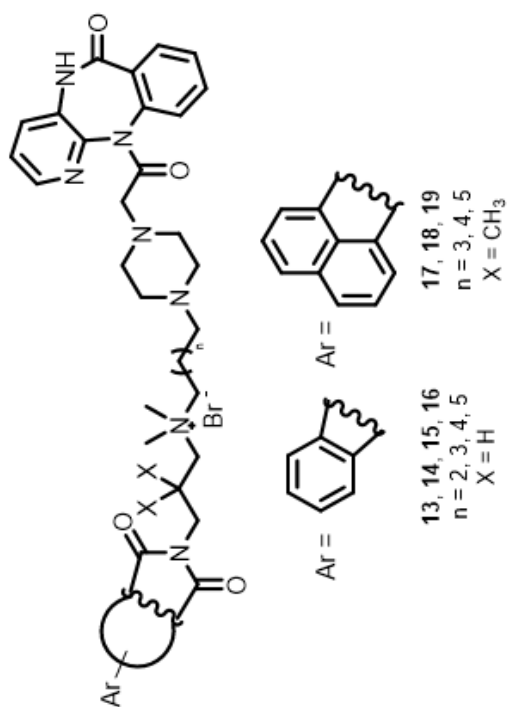
Ar =

21, 22
n = 4, 5
X = H

Ar =

23, 24, 25
n = 2, 4, 5
X = CH$_3$

Acetylcholine-clozapine hybrids

35, 36
n = 4, 6

Phthalimide/1,8-naphthalimide-pirenzepine hybrids

Ar =

13, 14, 15, 16
n = 2, 3, 4, 5
X = H

Ar =

17, 18, 19
n = 3, 4, 5
X = CH$_3$

Iperoxo-clozapine hybrids

30, 31, 32
n = 4, 6, 8
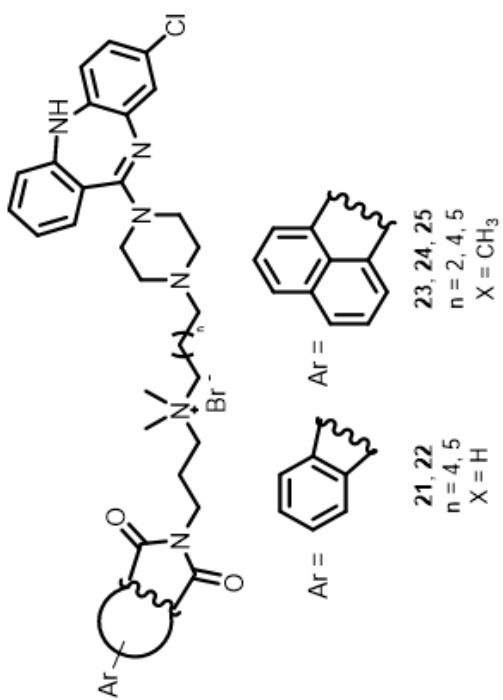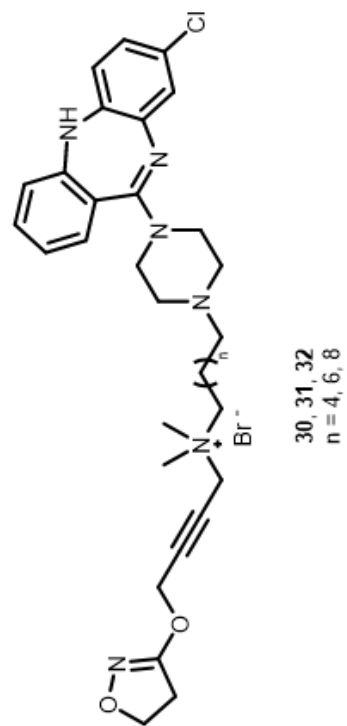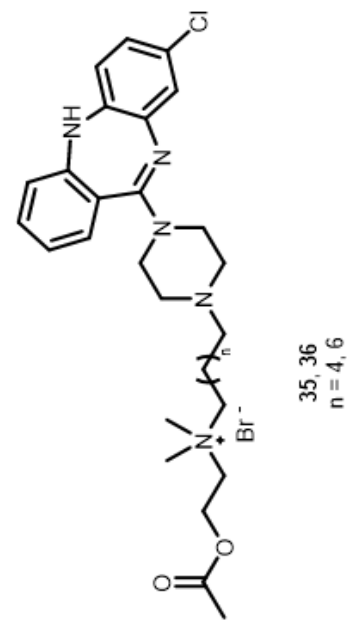
Figure 2.2: Structures of the dualsteric hybrids synthesized.

Pirenzepine-containing dualsteric hybrids were synthesized using the *N*-desmethyl pirenzepine as the orthosteric moiety and either a phthalimido- or 1,8-naphthalimidopropylamino moiety to bind the allosteric site, each hybrid with a different alkane chain length as the middle linker. Individually, pirenzepine is known as an orthosteric M_1-selective antagonist, while the phthalimide or naphthalimide "W84-derived" part is known to allosterically bind the M_2 receptor subtype as NAMs (producing antagonist/inverse agonist action).[25, 33]

Moreover, several clozapine-containing dualsteric hybrids were synthesized. Generally, clozapine is known to act as an orthosteric antagonist at the M_1, M_2, M_3 and M_5 receptors, and as an agonist at the M_4 subtype.[23] *N*-Desmethyl clozapine was reported to possess M_1-selectivity as allosteric agonist.[57] *N*-Desmethyl clozapine was involved as part of some of the synthesized dualsteric hybrids linked to either a phthalimido- or 1,8-naphthalimidopropylamino moiety with variable linker lengths. Furthermore, other dualsteric ligands were synthesized by adjoining *N*-desmethyl clozapine through different chain lengths to the non-selective super-agonistic iperoxo, to produce potentially M_1-selective hybrids. Similarly, additional dualsteric hybrids were synthesized involving *N*-desmethyl clozapine and the endogenous agonist acetylcholine.

The synthesized dualsteric ligands would eventually be pharmacologically tested using the appropriate FRET assays.

3. Results and discussion

3.1. Chapter 1: Synthesis of AFDX-384

The synthesis of the compound AFDX-384 was pursued in order to make it available as a reference compound for the biological testing and for the possible derivatization of dualsteric hybrids that are similar to it. AFDX-384 (5,11-dihydro-11-[[[2-[2-[(dipropylamino)methyl]-1-piperidinyl]ethyl]amino]carbonyl]-6*H*-pyrido[2,3-b][1,4] benzodiazepine-6-one) can be synthesized by combining its precursor units **IV**, 2-[2-[(dipropylamino)methyl]-1-piperidinyl]ethanamine, and **VIII**, the chloro acyl derivative of benzopyridodiazepine, as shown in Scheme 3.1. This final synthetic step was reported for a similar AFDX-type compound by E. Heller et al.[55] The synthesis of each of those intermediates is discussed below in brief.
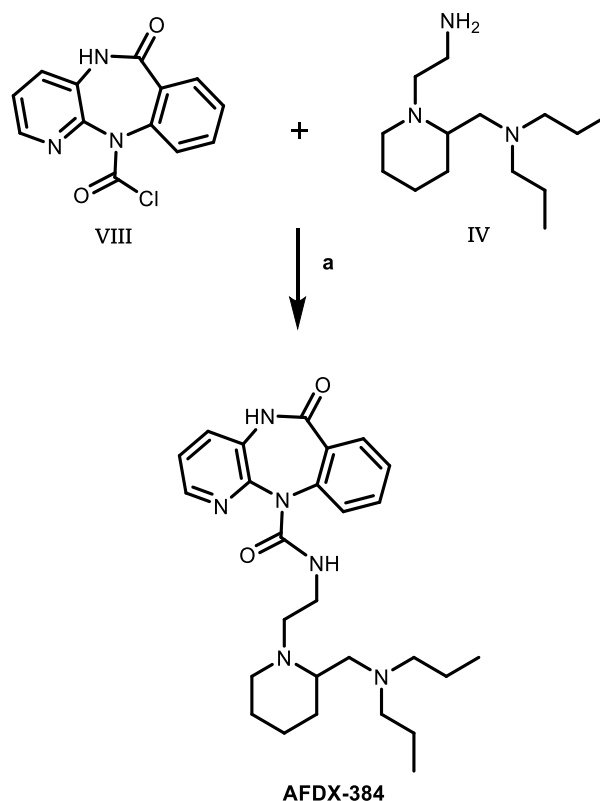
Scheme 3.1: The final synthesis step of AFDX-384 from its precusor molecules **IV** and **VIII**; **a**: Hünig's base, THF, microwave.[55]

Firstly, the synthesis of the initial molecule **IV** was achieved over several steps, as illustrated in Scheme 3.2. E. Heller reported the synthesis of a similar piperidinyl compound.[55] In short, 2-piperidine methanol was used as starting material, where it underwent a chlorination reaction using thionyl chloride. The resultant chlorinated intermediate, **I**, was subjected to a nucleophilic substitution reaction using dipropylamine to obtain the subsequent intermediate **II**. Bromo acetonitrile was used in the following step to produce the nitrile molecule **III** by means of the microwave. In the end, the nitrile **III** was reduced by means of $LiAlH_4$ and $AlCl_3$ to attain the desired piperidine derivative **IV**.[55]
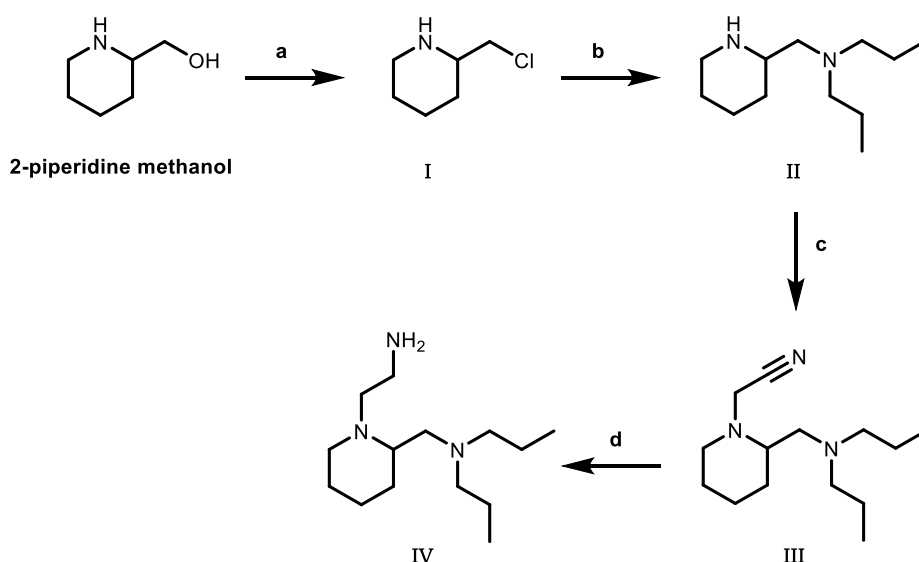
Scheme 3.2: The synthetic scheme for the intermediate piperidine derivative **IV**; [55] **a**: $SOCl_2$, $CHCl_3$, reflux for 1.5 hrs, **b**: dipropylamine, CH_2Cl_2, reflux for 3.5 hrs, **c**: K_2CO_3, EtOH, bromoacetonitrile, microwave (gradient of heating: 2 mins. to 78 °C, holding time: 2 hrs at 78 °C), **d**: $LiAlH_4$, $AlCl_3$, THF, reflux for 5 hrs.

Secondly, the synthesis of benzopyridodiazepine carbonyl chloride **VIII** was planned in 2 sequential steps: starting with the synthesis of the tricyclic benzopyridodiazepine ring system **VII**, followed by chloro acylation of the diazepine nitrogen.[55]

The conversion of 3-amino-2-chloropyridine and ethyl 2-aminobenzoate using KOtBu in the microwave resulted in a product whose ^{1}H NMR spectrum in $CDCl_3$ showed signals that were slightly different from those of the reported tricyclic compound **VII**.[55] Upon measurement of NMR in DMSO, an NH_2 signal was seen at $\delta_H = 6.47$ ppm with an

integration corresponding to 2 protons. This indicated that, instead of formation of the tricyclic ring, the ester of ethyl 2-aminobenzoate seem to have reacted with the amino group of 3-amino-2-chloropyridine resulting in the amide **V**, as shown in Scheme 3.3. The NMR spectra of both **V** and **VII** are shown in Figure 3.1 and 3.2, respectively (the atoms of the compounds are enumerated according to the same numbering pattern for the sake of comparisons of structures and the corresponding NMR signals).
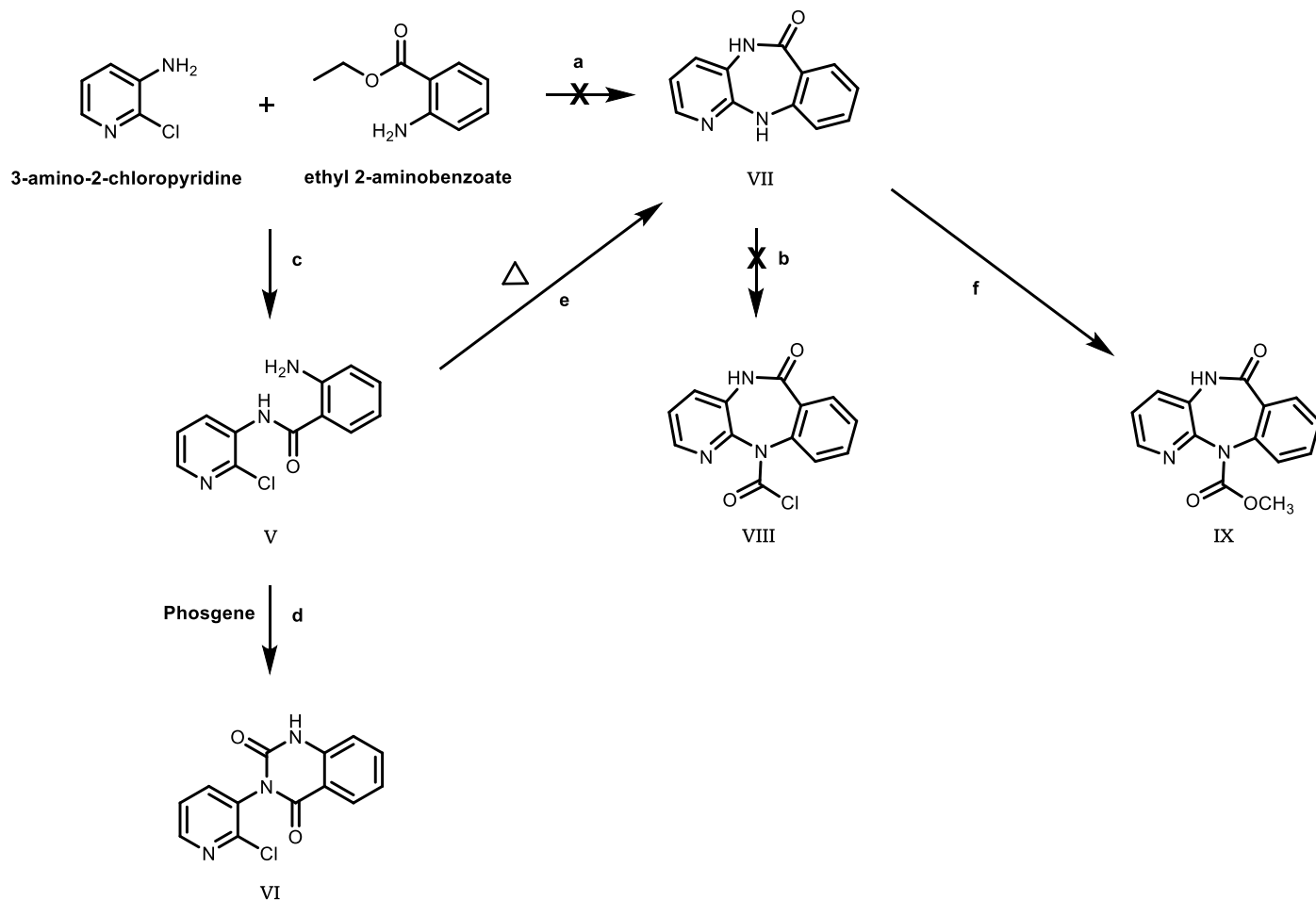
Scheme 3.3: The synthesis of compounds **V**, **VI**, **VII** and **IX**; **a** and **c**: KOtBu, dioxane, microwave, **b** and **d**: Hünig's base, dioxane, 20% phosgene in toluene, microwave, **e**: ethylene glycol, reflux for overnight, **f**: dioxane, 20% phosgene in toluene, reflux overnight.
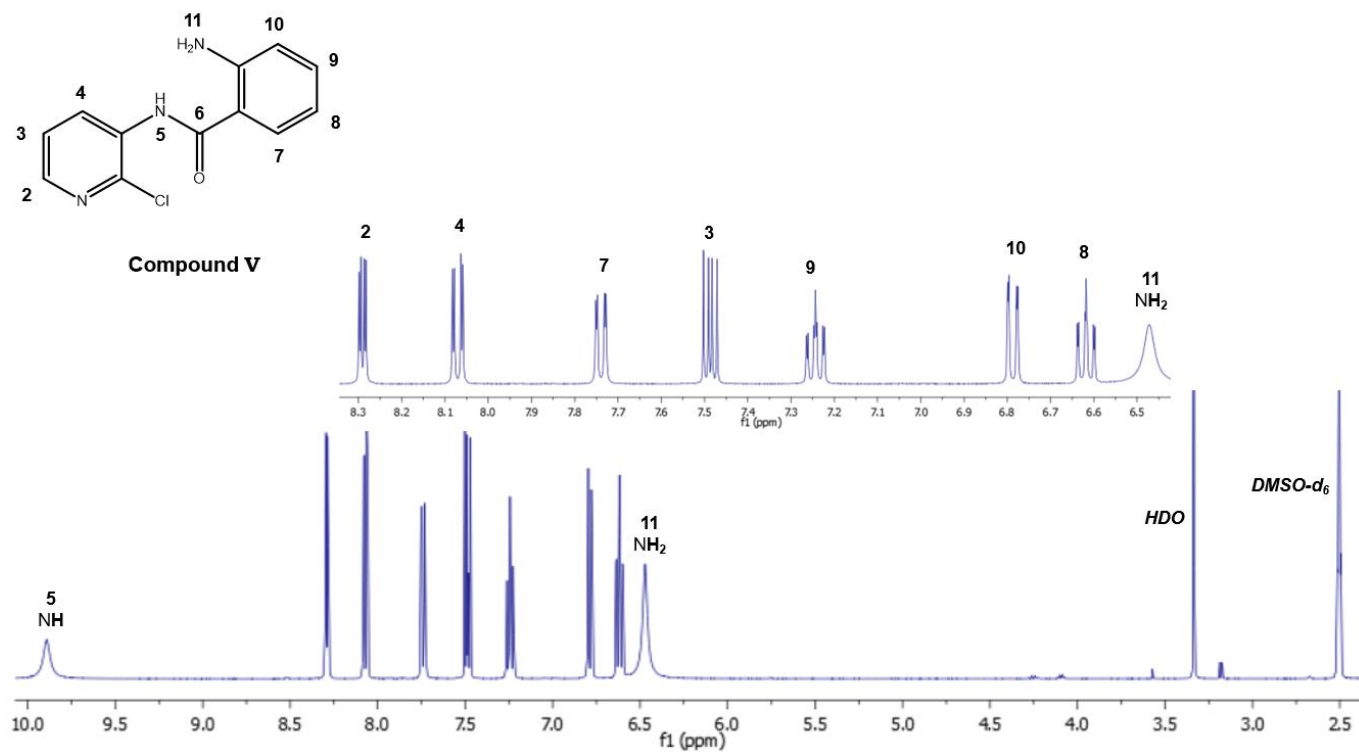
Figure 3.1: ^{1}H NMR (400 MHz) spectrum for compound **V** in DMSO-d[6].
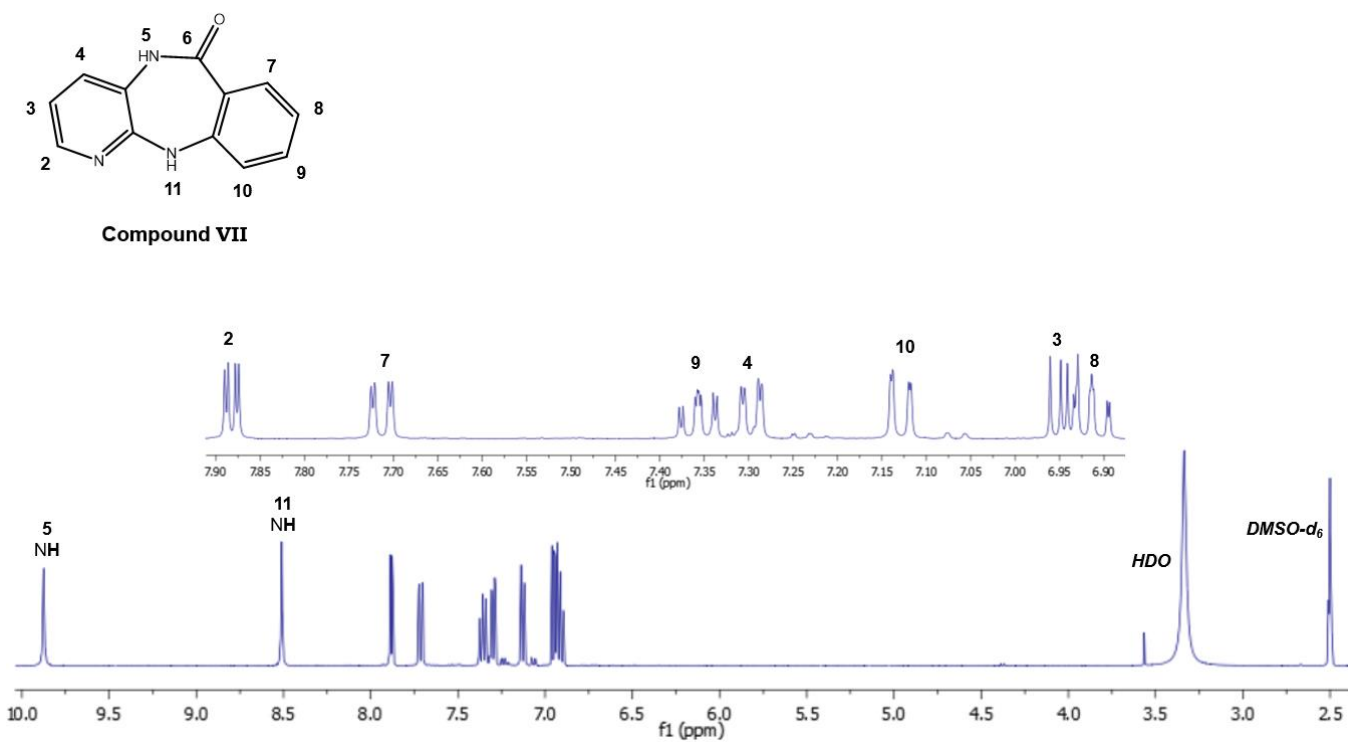
Figure 3.2: ^{1}H NMR (400 MHz) spectrum for compound **VII** in DMSO-d[6].[55]

The conversion with phosgene, which was performed in the assumption that the tricyclic system was formed and which had to be converted to **VIII**, gave a quinazolidine-2,4-dione **VI**, as shown in Scheme 3.3. The formation of compound **VI** was verified by NMR (Figure 3.3), where the introduced **C**=O appears at $\delta_C = 151.0$ ppm, however all signals appear at different chemical shifts to those of compound **VIII** as reported by E. Heller et al.[55] A comparative analysis of the ^{1}H and ^{13}C NMR data of the described **V**, **VI**, **VII** and **VIII** is shown in Table 3.1.
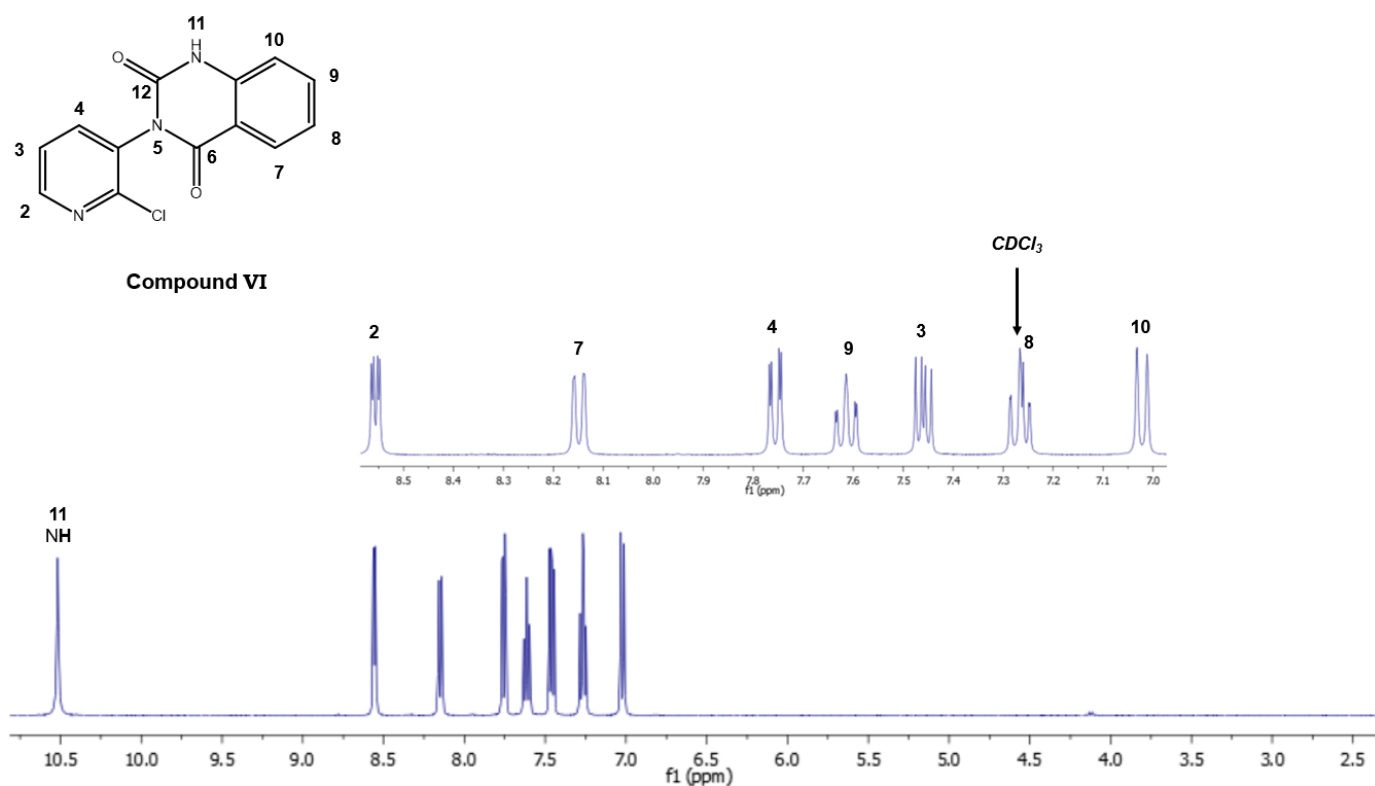
Figure 3.3: ^{1}H NMR (400 MHz) spectrum for compound **VIII** in CDCl₃.

	Compound V DMSO		Compound VI CDCl₃		Compound VII DMSO		Compound VIII DMSO		Compound IX DMSO	
	¹H (ppm)	¹³C (ppm)	¹H (ppm)	¹³C (ppm)	¹H (ppm)	¹³C (ppm)	¹H (ppm)	¹³C (ppm)	¹H (ppm)	¹³C (ppm)
2	8.29 dd	146.7	8.56 dd	149.9	7.88 dd	142.6	8.51 br	145.5	8.27 dd	144.8
3	7.49 dd	123.9	7.46 dd	123.4	6.95 dd	118.6	7.53-7.77* m	134.1	7.41 dd	124.4
4	8.07 dd	137.0	7.76 dd	139.6	7.30 dd	128.6	7.53-7.77* m	131.7	7.63-7.71* m	131.21
4a	-	132.8	-	129.9	-	124.2	-	135.10	-	131.1
5 NH	9.89 br	-	10.52 br	-	9.88 br	-	11.02 br	-	10.85 br	-
6 C=O	-	168.3	-	161.6	-	167.3	-	165.7	-	166.2
6a	-	113.9	-	114.3	-	147.3	-	125.10	-	129.7
7	7.74 dd	129.3	8.15 dd	128.7	7.71 dd	132.1	7.86 d	127.2	7.77 dd	130.7
8	6.62 ddd	115.4	7.27 ddd	124.0	6.92 ddd	121.0	7.53-7.77* m	126.2	7.44-7.50 m	128.3
9	7.24 ddd	133.2	7.61 ddd	135.9	7.36 ddd	133.5	7.53-7.77* m	126.1	7.63-7.71* m	133.2
10	6.79 dd	117.2	7.02 d	115.7	7.13 dd	119.6	7.53-7.77* m	118.9	7.52 dd	128.42
10a	-	150.7	-	138.9	-	121.8	-	139.50	-	140.4
11 NH	6.47 br	-	-	-	8.51 br	-	-	-	-	-
11a	-	146.7	-	150.4	-	151.1	-	144.20	-	145.1
12 C=O	-	-	-	151.0	-	-	-	147.4	-	153.4
13 OCH₃	-	-	-	-	-	-	-	-	3.65 s	53.3
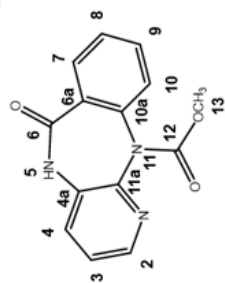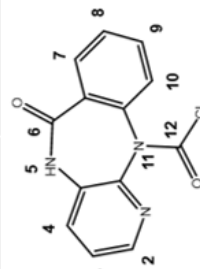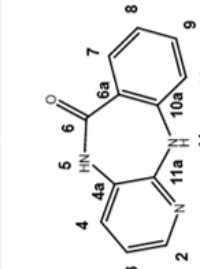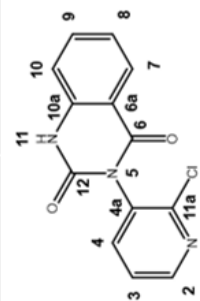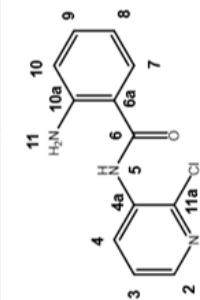
Table 3.1: A comparative analysis of the ¹H NMR (400 MHz) and ¹³C NMR (100 MHz) data of compounds **V**, **VI**, **VII**, **VIII** and **IX** in their corresponding deuterated solvents. It is to be noted that NMR measurements for all the compounds have been recorded in this study except for the values of compound **VII** and **VIII** which are reported by E. Heller et al.[55]

32

In order to confirm the structure **V** and **VI**, X-ray crystallography analysis was performed. The compound **V** was crystallized using methanol and toluene in a mixed solvent recrystallization technique, while the compound **VI** was crystallized from chloroform. Crystallography results indicative for the corresponding structures are shown below (for the experimental details, see Supplementary information):

➤ Compound **V**: the central amide group adopts an almost planar orientation (O=C—N—H torsion angle = 174°). The C12— C7—C6=O1 torsion angle is 145.9 (2)° and an intramolecular N—H⋯O hydrogen bond closes an *S*(6) ring. The aromatic rings are essentially coplanar [dihedral angle = 2.28 (9)°] (molecular structure shown in Figure 3.4a). In the crystal, molecules are linked by N—H⋯O and N—H⋯N hydrogen bonds to generate 100 sheets (Figure 3.4b and Table 3.2).[58]
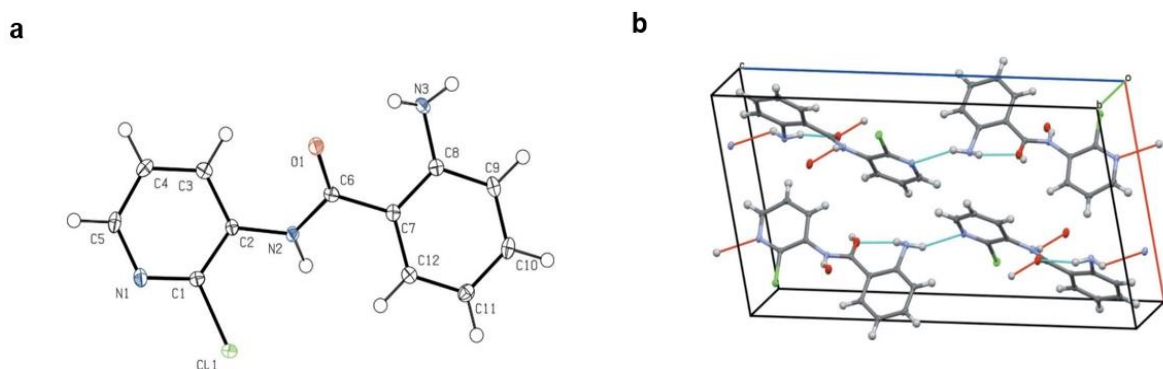
Figure 3.4: X-ray crystallography results for compound **V**, **a**: the molecular structure of **V**, with displacement ellipsoids drawn at the 50% probability level, **b**: a view along the c axis of the packing of **V**. Hydrogen bonds are shown as dashed lines.[58]

D—H⋯*A*	*D*—H	H⋯*A*	*D*⋯*A*	*D*—H⋯*A*
N3—H3*A*⋯O1	0.86	2.10	2.7734 (19)	135
N2—H2⋯O1[i]	0.88	2.07	2.882 (2)	152
N3—H3*B*⋯N1[ii]	0.86	2.42	3.087 (2)	134

Table 3.2: Hydrogen bond geometry for compound **V** (Å, º). Symmetry codes: (i) *x*, *y*−1, *z*; (ii) *x*, −*y*+3/2, *z*−1/2.[58]

➢ Compound **VI**: the compound was crystallized as a chloroform monosolvate. The pyridine ring (N1/C1–C5) is nearly perpendicular to the planar quinazoline ring (N2/N3/C6–C13; r.m.s.d. (root mean square deviation) = 0.04 Å), making a dihedral angle of 84.28 (9)° (molecular structure shown in Figure 3.5a). In the crystal, molecules are linked by pairs of N—H⋯O hydrogen bonds forming inversion dimers, with an R_2^2 (8) ring motif. The chloroform solvate molecules are linked to the organic molecule by C— H⋯N hydrogen bonds, and the dimers are linked by C—H⋯O hydrogen bonds, forming ribbons propagating along the a-axis direction (Figure 3.5b and Table 3.3).[59]
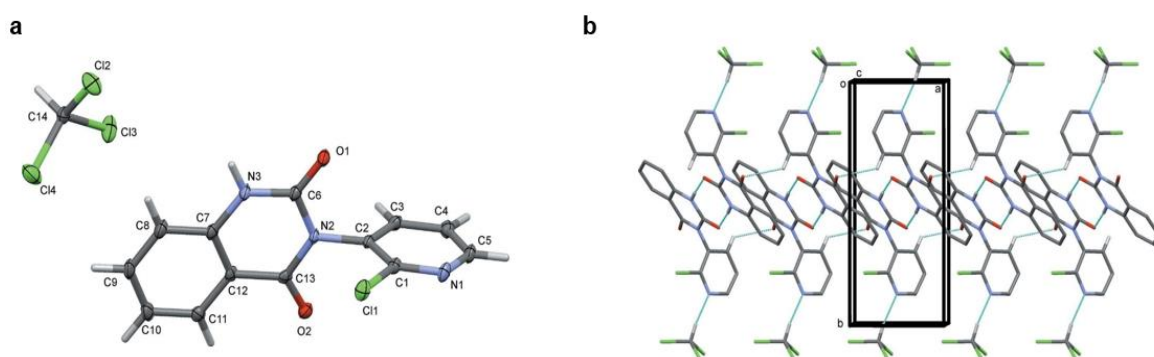
Figure 3.5: X-ray crystallography results for compound **VI** (crystallized as chloroform monosolvate), **a**: the molecular structure of the solvated compound **VI** CHCl$_3$, with the atom labelling and displacement ellipsoids drawn at the 50% probability level, **b**: A view along the c axis of the crystal packing of the solvated compound **VI** CHCl$_3$. The hydrogen bonds are shown as dashed lines.[59]

D—H⋯A	D—H	H⋯A	D⋯A	D—H⋯A
N3—H3⋯O1^i	0.88	1.91	2.791 (3)	175
C14—H14⋯N1^{ii}	1.00	2.39	3.200 (3)	137
C3—H3A⋯O2^{iii}	0.95	2.48	3.123 (3)	125

Table 3.3: Hydrogen bond geometry for the solvated compound **VI** CHCl$_3$ (Å, °). Symmetry codes: (i) −x+1, −y+1, −z+1; (ii) x, y−1, z; (iii) x+1, y, z.[59]

Ring closure of the amide **V** was attempted using KOtBu and dioxane by the means of microwave-assistance at 100 °C. Upon TLC reaction monitoring using EtOAc as eluent, no conversion was observed. In order to facilitate ring closure, the temperature was raised by using ethylene glycol according to literature.[60] After the workup and crystallization of the

product from methanol and toluene, the NMR spectra were in accordance with compound **VII**. The compound was obtained, however, in a low yield of 20%. X-ray crystallography analysis was performed for compound **VII** and the results are shown below (for the experimental details, see Supplementary information):

➢ Compound **VII**: the seven-membered ring adopts a boat conformation and the dihedral angle between the planes of the aromatic rings is 41.51(9)° (molecular structure shown in Figure 3.6a). In the crystal, molecules are linked into chains of alternating inversion dimers formed by pairs of N—H···O hydrogen bonds and pairs of N—H··· N hydrogen bonds. In both cases, R_2^2 (8) loops are generated (Figure 3.6b and Table 3.4).[61]
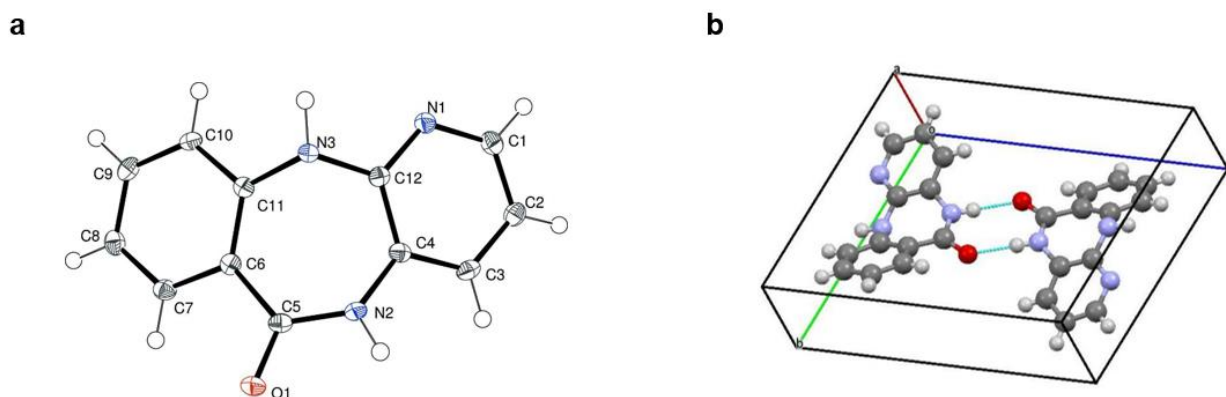
Figure 3.6: X-ray crystallography results for compound **VII**, **a**: the molecular structure of **VII**, with the atom labelling and displacement ellipsoids drawn at the 50% probability level, **b**: Unit-cell packing of **VII** showing two inverted molecules linked by hydrogen bonds indicated as dotted lines.[61]

D—H···A	D—H	H···A	D···A	D—H···A
N2—H2···O1^{i}	0.87 (2)	1.98 (2)	2.840 (2)	175 (2)
N3—H3···N1^{ii}	0.93 (2)	2.28 (2)	3.200 (2)	168.7 (19)

Table 3.4: Hydrogen bond geometry for compound **VII** (Å, °). Symmetry codes: (i) −x+1, −y+1, −z+1; (ii) x, y−1, z; (iii) x+1, y, z.[61]

The compound **VII** was subjected to the phosgene reaction for 2 hrs in the microwave, where no product was formed. The prolongation of time with the replacement of the use of

microwave with reflux overnight resulted in a small spot closely below the spot of **VII** upon TLC monitoring of the reaction (using a mixture of EtOAc/CH$_2$Cl$_2$ 2:1 as eluent). This product **IX** was purified by silica gel column chromatography using a solvent system consisting of EtOAc/CH$_2$Cl$_2$/MeOH 20:10:0.5 since the introduction of the more polar methanol into the mobile phase was necessary. Upon inspection of the NMR spectra of **IX**, the introduction of the extra **C**=O from phosgene could be confirmed, appearing at δ_C = 153.9 ppm. However, the product seems to have converted to the carbamate analogue rather than remaining as an acyl chloride, where the methyl group appears at δ_H = 3.65 ppm and δ_C = 53.1 ppm in the ^{1}H and ^{13}C NMR spectra, respectively (Figure 3.7) The NMR data is also displayed in the comparative analysis in Table 3.1. This is attributed to the use of methanol in the purification, which should be refrained in future trials.
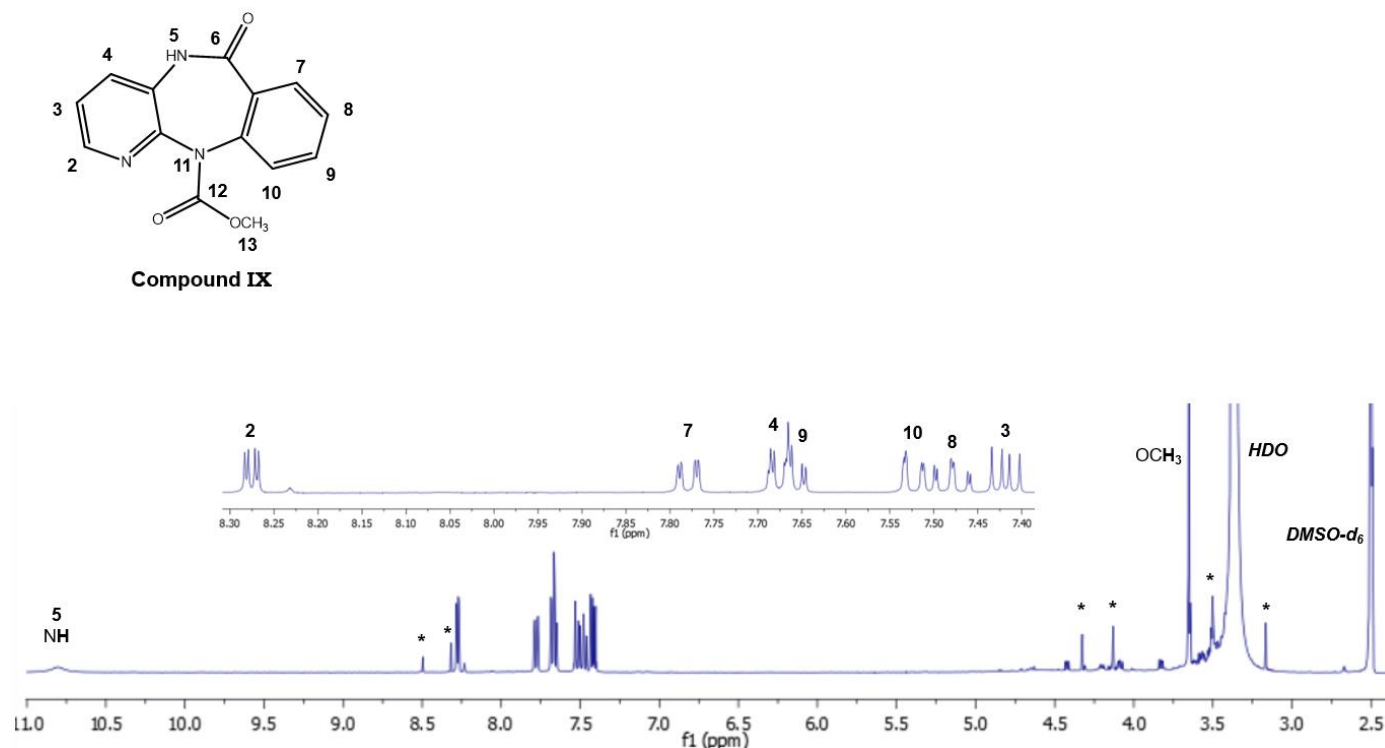
Compound IX

Figure 3.7: ^{1}H NMR (400 MHz) spectrum for compound **IX** in DMSO-d$_6$. *: Minor impurities as indicated and confirmed by two-dimensional NMR spectroscopy.

Another paper by H. Zare et al. reports the use of triphosgene (bis(trichloromethyl)carbonate) as a faster and simpler method to produce chloro acylated products in good yields with easy purification and an overall safer handling of the

procedure.[62] The technique described involves grinding compound **VII** with triphosgene and NaOH as a base for 5 min. This alternative reaction was tried out with very small amounts and hence initial yields were low, but it is considered a prospect for future optimization, possibly with use of its alternative solvent method,[63] to attain the target chloro acyl compound **VIII** and hence complete the AFDX-384 synthesis scheme.

3.2. Chapter 2: Synthesis of dualsteric hybrids

3.2.1. Chemistry

3.2.1.1. Synthesis of phthalimide/1,8-naphthalimide-pirenzepine hybrids 13-19

The hybrid compounds **13**-**19** were synthesized by linking the corresponding phthalimide or 1,8-naphthalimide intermediate (**2-5** or **8-10**, respectively) to *N*-desmethyl pirenzepine **12**. Each of these two entities were synthesized by means of several steps, as shown in Scheme 3.4. Three different reaction conditions were carried out and evaluated during the optimization process of the final step of the synthesis of these final compounds.

Phthalic anhydride   **1,8-Naphthalic anhydride**

Benzopyridodiazepine
VII

1
X = H

6
X = CH$_3$

11

2, 3, 4, 5
n = 2, 3, 4, 5
X = H

8, 9, 10
n = 3, 4, 5
X = CH$_3$

+

12

13, 14, 15, 16
n = 2, 3, 4, 5
X = H

17, 18, 19
n = 3, 4, 5
X = CH$_3$
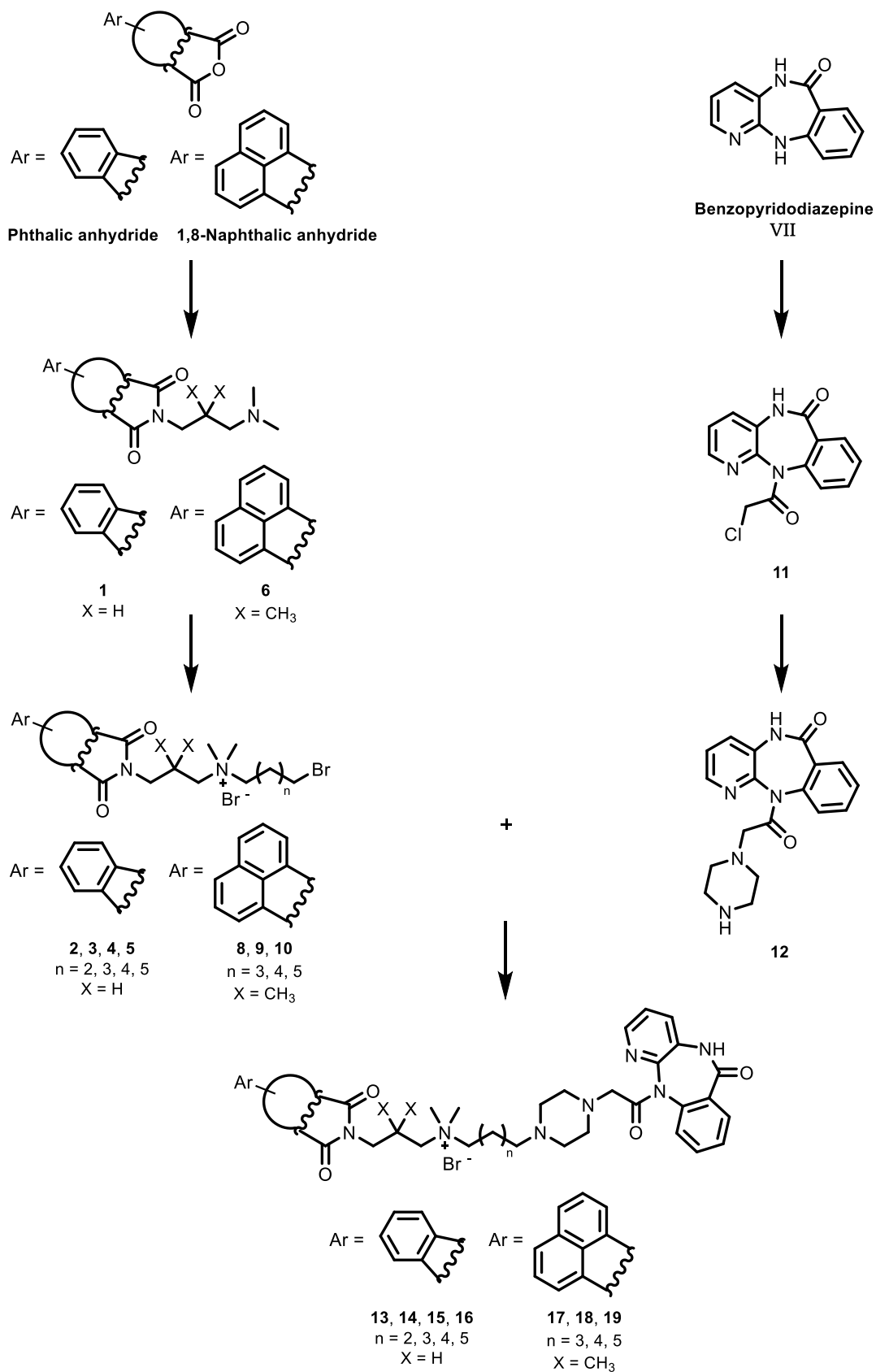
Scheme 3.4: Overall synthesis of phthalimide/1,8-naphthalimide-pirenzepine hybrids.

3.2.1.1.A. Synthesis of phthalimido/1,8-naphthalimido monoquaternary bromides 2-5 and 7-10

The synthesis of the phthalimido/1,8-naphthalimido bromide intermediates is essential for the consequent synthesis of the desired dualsteric hybrids. The phthalimide or naphthalimide "W84-derived" part is known to allosterically bind the M_2 receptor subtype as NAMs (producing antagonist/inverse agonist action).[33] The synthesis of these intermediates involves 2 steps, starting with the synthesis of the required initial imides followed by attaching bromide linkers with the appropriate length to these imides, creating quaternary amine compounds according to literature.[64]

Schmitz et al. reported the synthesis of the two imides, namely phthalimidopropylamine **1** and 1,8-naphthalimido-2,2-dimethylpropylamine **6**, which were used to synthesize the corresponding monoquaternary bromide intermediates.[64] As shown in Scheme 3.5, an equimolar mixture of the appropriate anhydride (either phthalic anhydride or 1,8-naphthalic anhydride) and the corresponding diamine derivative (N^1,N^1-dimethylpropane-1,3-diamine or N^1,N^1,2,2-tetramethylpropane-1,3-diamine) as well as a catalytic amount p-toluenesulfonic acid and weflon-tablets (PTFE with 10% graphite) in absolute toluene were heated in the microwave at 115 °C by using a Dean-Stark water separator (ramp: 30 °C/min, 800W). Upon completion of the reaction (approximately requires less than 1 hr; silica gel TLC monitoring was done using a mixture of EtOAc/petroleum ether 1:1 as eluent), the solvent was evaporated under reduced pressure followed by washing of the product with petroleum ether and crystallization from methanol. The imides **1** and **6** were obtained in approximately 90% yield as pale white and light brown crystals, respectively.
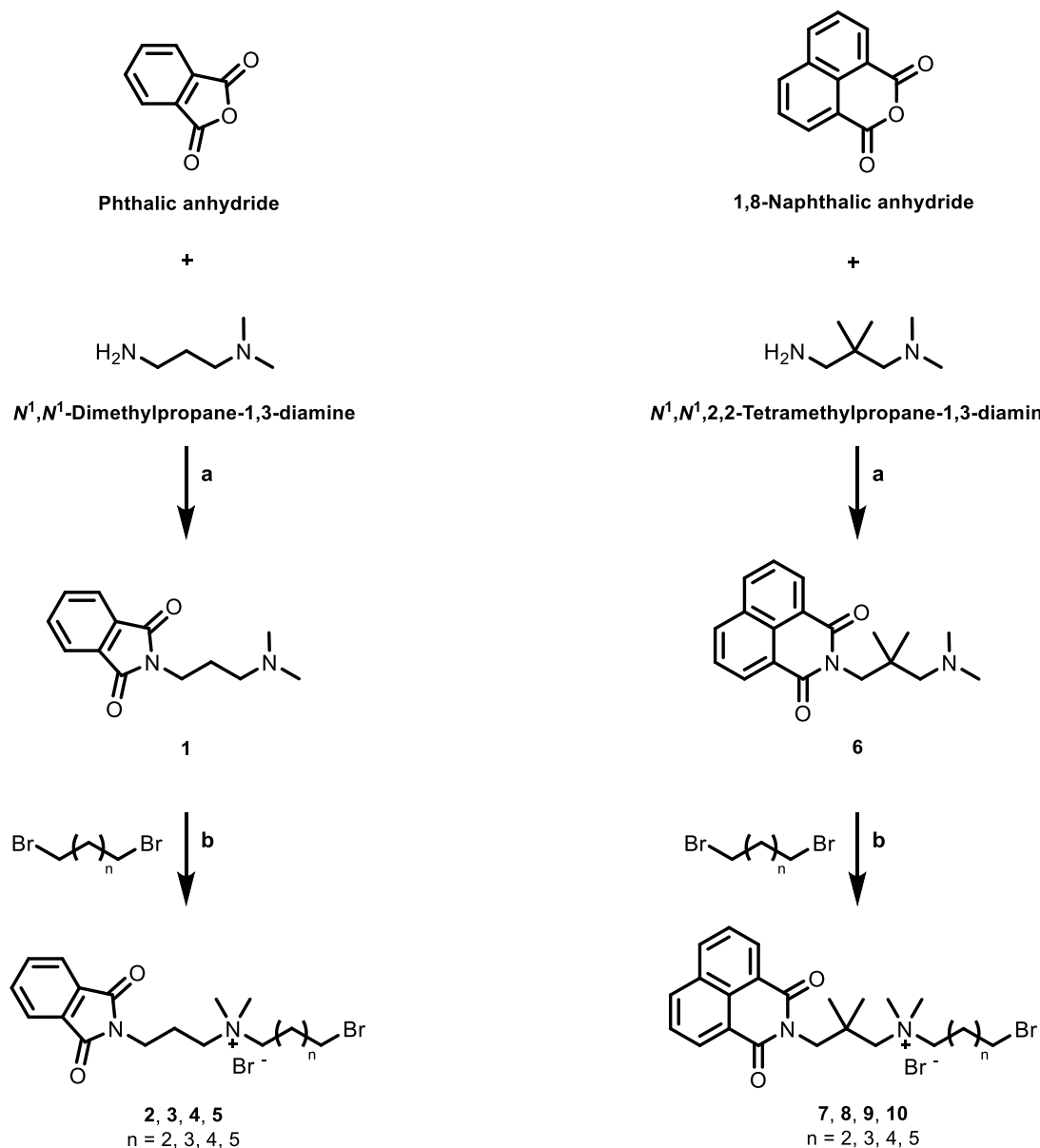
Scheme 3.5: Synthesis of phthalimido/1,8-naphthalimido monoquaternary bromide intermediates; **a**: *p*-toluenesulfonic acid, abs. toluene, Dean-Stark water separator, microwaves at 115 °C for 1 hr, **b**: microwaves at 80 °C for 3 hrs.

Subsequently, the desired phthalimido/1,8-naphthalimido monoquaternary bromides **2- 5** and **7-10** were synthesized from the imides **1** and **6**, as shown in Scheme 3.5 as well.[64] In brief, the corresponding imide was dissolved in a fifteen-fold excess of the suitable alkyl dibromide and heated in the microwave at 80 °C (ramp: 20 °C/min, 800W) for 3 hrs. The

products precipitated after cooling were washed with hot diethyl ether several times and obtained pure in 68% to 94% yields, respectively.

It is to be noted that the intermediates **2**, **3** and **8** were used only for the synthesis of pirenzepine-containing hybrids, while the intermediate **7** was only for the synthesis of clozapine-containing hybrids (later described in section 3.2.1.2.). The other bromide intermediates (**4**, **5**, **9** and **10**) were used to synthesize final compounds of both pirenzepine-containing and clozapine-containing dualsteric hybrids.

3.2.1.1.B. Synthesis of *N*-desmethyl pirenzepine 12

The essential tricyclic ring system to achieve the synthesis of the desired dualsteric ligands, which is to be coupled to the aforementioned phthalimido/1,8-naphthalimido bromide intermediates, is the well-known *N*-desmethyl pirenzepine **12**. This key entity is derived from the high affinity M_1-selective orthosteric antagonist pirenzepine. Such heterogeneity in binding to mAChRs is the reason behind the incorporation of *N*-desmethyl pirenzepine **12** in dualsteric subtype-targeting hybrids.[43, 56] This molecule is synthesized via 2 consecutive steps, the first of which is the synthesis of the chloroacetyl benzopyridodiazepine **11** according to literature,[56] followed by *N*-alkylation using piperazine to attain **12** according to a modification of a procedure for similar compounds in literature.[56]

In a concise description, the chloroacetyl intermediate **11** was obtained by the means of refluxing chloroacetyl chloride as a reagent with the benzopyridodiazepine **VII** (see Chapter 1) as starting material in presence of a base, as shown in Scheme 3.6.[56]
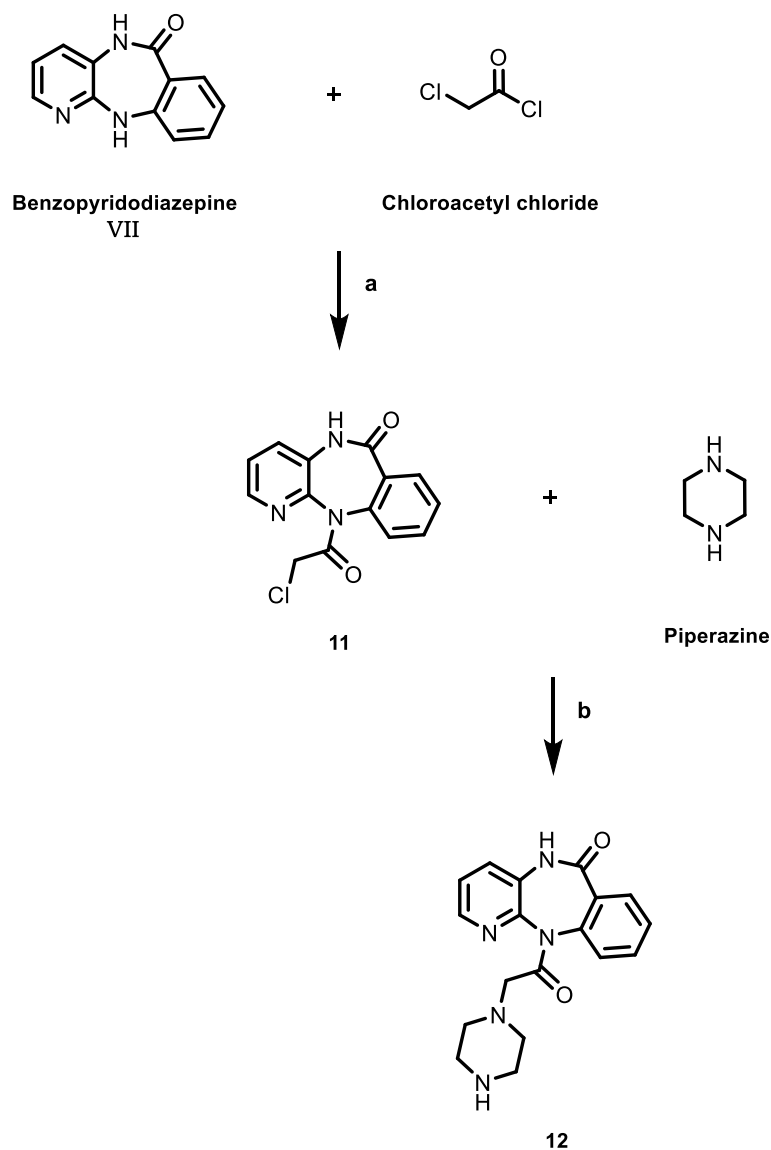
Scheme 3.6: Synthesis of *N*-desmethyl pirenzepine **12**; **a**: dioxane, Et₃N, reflux for 8 hrs, **b**: acetonitrile, KI/K₂CO₃, microwaves at 80 °C for 2 hrs.

The target *N*-desmethyl pirenzepine **12** was synthesized by using a large excess of piperazine (ratio of 1:20) to ensure *N*-alkylation of the chloroacetyl intermediate **11** and hence avoiding dimeric side products. Catalytic amount of KI was used as well as K_2CO_3 as base in the reaction, and the mixture in acetonitrile was heated under microwaves at 80 °C (ramp: 20 °C/min, 800W). The obtained product was extracted and further purified by silica gel chromatography (CHCl₃/MeOH/NH₃ 100:10:1) to give the desired compound **12** in 72% yield.[56]

3.2.1.1.C. Synthesis of phthalimide/1,8-naphthalimide-pirenzepine hybrids 13-19

The final step of the hybrids' synthesis is the connection of one of the phthalimido/1,8-naphthalimido bromide intermediates **2-5** or **8-10** (with the variable alkyl chain length) with *N*-desmethyl pirenzepine **12** (Scheme 3.7). The syntheses of the dualsteric hybrids was attempted using 3 different reaction conditions. Despite the success of synthesis with the initial trial, different methods and conditions were applied to optimize yields, reduce side products and hence easier purification of the products. The 3 reaction methods **I**, **II** and **III** were examined.
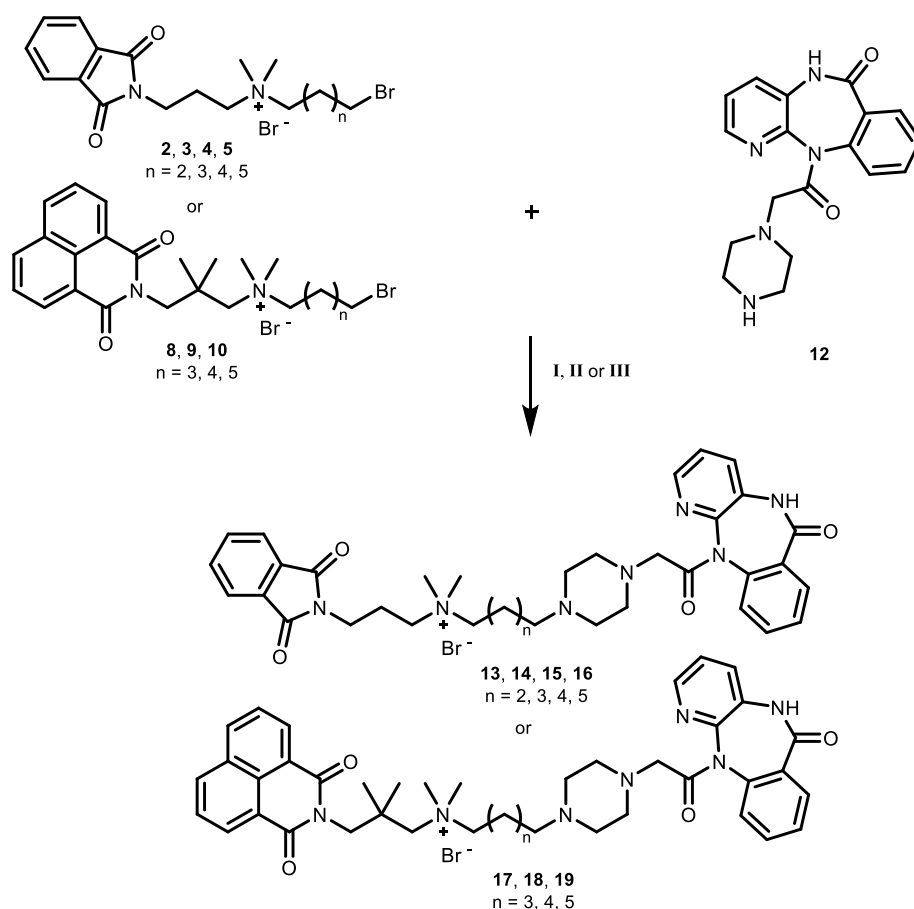
Scheme 3.7: Final step of the synthesis of phthalimide/1,8-naphthalimide-pirenzepine hybrids using 3 different reaction conditions; **I**: K$_2$CO$_3$/KI, acetonitrile, microwaves at 80 °C for 7 hrs, **II**: acetonitrile (without base or catalytst), microwaves at 80 °C for 7 hrs, **III**: acetonitrile (without base or catalytst), stirring at 35 °C for 7 days.

All 3 reaction methods involve the use of 1 equivalent of the corresponding intermediate **2-5** or **8-10** and 1.1 equivalent of *N*-desmethyl pirenzepine **12**, along with the use of dry acetonitrile as a solvent. This slight excess of **12** ensure the complete consumption of the bromo quaternary ammonium intermediate and hence facilitate purification of the final hybrid as the sole quaternary charged compound in the medium. Silica gel TLC monitoring was done using 0.2 M aqueous KNO_3/MeOH 2:3 as eluent for determine reaction completion. The 3 methods were applied to all combinations of starting products, as shown in Table 3.5.

Reaction **I** was characterized by the use of base (K_2CO_3) and catalyst (KI), and was facilitated by the means of microwaves at 80 °C for 7 hrs (ramp: 20 °C/min, 800W). However, the yield of the reaction was poor. The second synthesis trial (reaction method **II**) constitutes removal of the base and catalyst while maintaining the microwave heating condition. This resulted in improvement of yield. The highest yield for the final hybrid synthesis was achieved using reaction method **III**, where, besides the absence of the base and catalyst, only stirring under low temperature (35 °C). TLC monitoring showed that this method required a longer period (7 days) for reaction completion, but resulted in less side products.

Yield analysis of the 3 reaction conditions is summarized in Table 3.5. Final compounds **13**, **14** and **15** are the only hybrids ultimately synthesized using reaction method **II** in this work, while all the rest of the dualsteric ligands in this project were synthesized using the optimal method **III**, having variations only in the reaction durations.

RXN	CPD NO.	BASE	CATALYST	TEMP.	DURATION	MICROWAVE	YIELD
I	**13,14,15** (n=2,3,4)	K_2CO_3	KI	80 °C	7 hrs	YES (800 W)	10-12%
II	**13,14,15** (n=2,3,4)	-	-	80 °C	7 hrs	YES (800 W)	30-35%
III	**16** (n=5)	-	-	35 °C	7 days	-	45%

Table 3.5: Comparison between the 3 examined reaction conditions **I**, **II** and **III** for the final step of the synthesis of selected phthalimide/1,8-naphthalimide-pirenzepine hybrids and their corresponding yields. CPD NO.: compound number. TEMP.: temperature.

Several purification techniques were carried out in the process of attaining the highest purity of the synthesized hybrids, as shown in Table 3.6. Each purification trial was monitored by HLPC (a gradient method using a solvent system of 0.1% formic acid in water and 0.1% formic acid in methanol).

Initially, the phthalimide–pirenzepine hybrids **13**, **14** and **15** were subjected to purification using basic ALOX column chromatography (using a mixture of $CHCl_3$/MeOH/NH_3 100:10:1 as eluent system), and resulted in minor purity levels only (in the range of 60%). Due to the small remaining amount of compound **13**, only compound **14** and **15** were subjected to the second purification step using C18 reverse phase silica gel flash chromatography. The purification run was done using a linear gradient of water: solvent A and methanol: solvent B (B% from 0% to 100% in 60 min) followed by a plateau phase (100% methanol for 30 min), yielding pure product as the last fraction. Drastic improvement of purity was revealed by the subsequent HPLC chromatography of **14** and **15**, indicating that the ideal method of purification for these dualsteric hybrids was found, as shown in Table 3.6.

Consequently, purification of other dualsteric ligands, such as compound **17**, **18** and **19**, was achieved successfully by subjecting them to flash chromatography runs using C18 reverse phase silica gel columns. The substantial degree of purity of **17**, **18** and **19** was comparable to the respectable percentage of purity of the crystallized compound **16** from the same series. Therefore, crystallization from the reaction medium (acetonitrile) or, whenever crystallization was not attainable or hindered, C18 reverse phase silica gel flash chromatography (using H_2O/MeOH solvent system) were the 2 purification methods of choice for purification of all dualsteric hybrids.

PURIFICATION METHOD	CPD NO.	PURITY
BASIC ALOX CHROM.	**13** (n=2)	64%
BASIC ALOX + RP SiO$_2$ FLASH CHROM.	**14**,**15** (n=3,4)	98-99%
RP SiO$_2$ FLASH CHROM.	**17**,**18**,**19** (n=3,4,5)	93-96%
CRYSTALLIZATION	**16** (n=5)	94%

Table 3.6: Comparison between the different purification techniques used for phthalimide/1,8-naphthalimide-pirenzepine hybrids and their resultant percentages of purity as revealed by HPLC analysis. Basic ALOX column chromatography used a mixture of CHCl$_3$/MeOH/NH$_3$ 100:10:1 as eluent system, reverse phase silica gel flash chromatography used H$_2$O/MeOH as eluent system, and crystallization was achieved from the acetonitrile reaction mixture. CPD NO.: compound number. RP: reverse phase. SiO$_2$: silica gel. CHROM.: chromatography.

The compounds **13**, **14** and **15,** which were subjected to basic ALOX chromatography, were exposed to the ammonia in the mobile phase used. This ammonia appeared during the LC-MS runs for these compounds, where base peaks corresponding to m/z = [M-Br+NH$_4$] $^{2+}$ were seen in their mass spectra (ESI), as shown in Table 3.7. Meanwhile, the other hybrids, purified without ammonia, showed the expected base peaks corresponding to m/z = [M-Br+H] $^{2+}$ in their mass spectra (ESI).

CPD NO.	AMMONIA USED	M.	M/Z BASE PEAK	CORRESPONDS TO
13 (n=2)	✓	704.67	321.60	$[M-Br+NH_4]^{2+}$
14 (n=3)	✓	718.70	328.70	$[M-Br+NH_4]^{2+}$
15 (n=4)	✓	732.71	335.65	$[M-Br+NH_4]^{2+}$
16 (n=5)	✗	746.75	333.75	$[M-Br+H]^{2+}$
17 (n=3)	✗	796.81	358.70	$[M-Br+H]^{2+}$
18 (n=4)	✗	810.84	365.75	$[M-Br+H]^{2+}$
19 (n=5)	✗	824.87	372.75	$[M-Br+H]^{2+}$

Table 3.7: Comparison between m/z base peaks in the ESI mass spectra of phthalimide/1,8-naphthalimide-pirenzepine hybrids and their correlation to the use of ammonia during purification. CPD NO.: compound number. M.: molecular weight. RP: reverse phase. SiO_2: silica gel. CHROM.: chromatography.

The NMR spectrum of compound **15**, the phthalimide–pirenzepine analogue with a 6-carbon spacer length, is the representative example discussed (Figure 3.8). The indicator for the successful linkage of the 2 precursor entities, **4** and **12**, is the disappearance of the resonance signal corresponding to CH_2-Br (terminal methylene in the intermediate **4** at $δ_H$ = 3.41 – 3.32 ppm) and the presence of the more upfield **i**-methylene group in compound **15** ($δ_H$ = 2.18 ppm). The presence of the pirenzepine part of the molecule is manifested in the spectra of the hybrid 15 through the presence of the piperazine methylene groups appearing at $δ_H$ = 2.55 – 2.26 ppm and $δ_C$ = 53.6, 54.1 ppm. In addition, the resonance signal for CH_2-C=O methylene group (between piperazine and the benzopyridodiazepine ring) appears at $δ_H$ = 3.36 – 3.27 ppm. It is of interest to note that this methylene signal appears overlapping with the CD_3OD solvent signal and has been confirmed by two-dimensional NMR spectroscopy through HMQC and HMBC measurements (see Appendix). Three distinct carbonyl signals are exhibited in the ^{13}C NMR spectrum, accounting for CH_2-C=O, the NH-C=O of the benzopyridodiazepine ring and the 2 carbonyl groups of the phthalimide ring. The double methyl groups on the quaternary ammonium nitrogen resonate as a pronounced singlet at at $δ_H$ = 3.10 ppm and $δ_C$ = 51.1 ppm. All the other signals in both the ^1H and ^{13}C NMR spectra are in agreement with the elucidated characteristics of compound **15**.
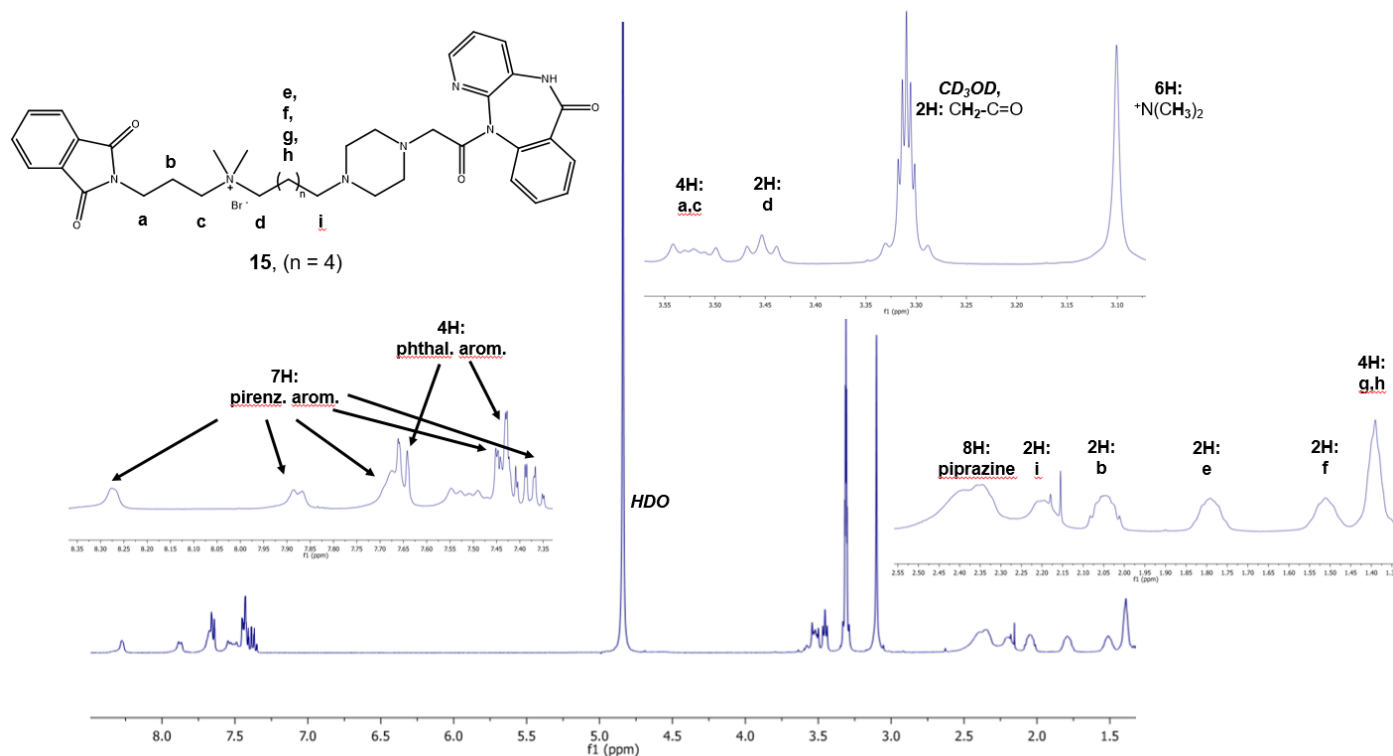
Figure 3.8: ^{1}H NMR spectrum for compound **15** (400 MHz, CD$_3$OD).

3.2.1.2. Synthesis of phthalimide/1,8-naphthalimide-clozapine hybrids 21-25

The hybrid compounds **21-25** were synthesized by linking the corresponding formerly described intermediates (**4, 5**, **7**, **9** or **10,** respectively) to *N*-desmethyl clozapine **20**. Before linkage can be made, the synthesis of the entity *N*-desmethyl clozapine **20** was achieved using clozapine as starting material, as shown in Scheme 3.8. The general procedure of synthesis and purification methods for these clozapine-containing hybrids were based on the optimally found methods discussed in the synthesis of the aforementioned pirenzepine-containing hybrids. The same default strategy was adopted for all other dualsteric hybrids as well.

Clozapine

20

Ar = **4, 5**
n = 4, 5
X = H

Ar = **7, 9, 10**
n = 2, 4, 5
X = CH$_3$

+

Ar = **21, 22**
n = 4, 5
X = H

Ar = **23, 24, 25**
n = 2, 4, 5
X = CH$_3$
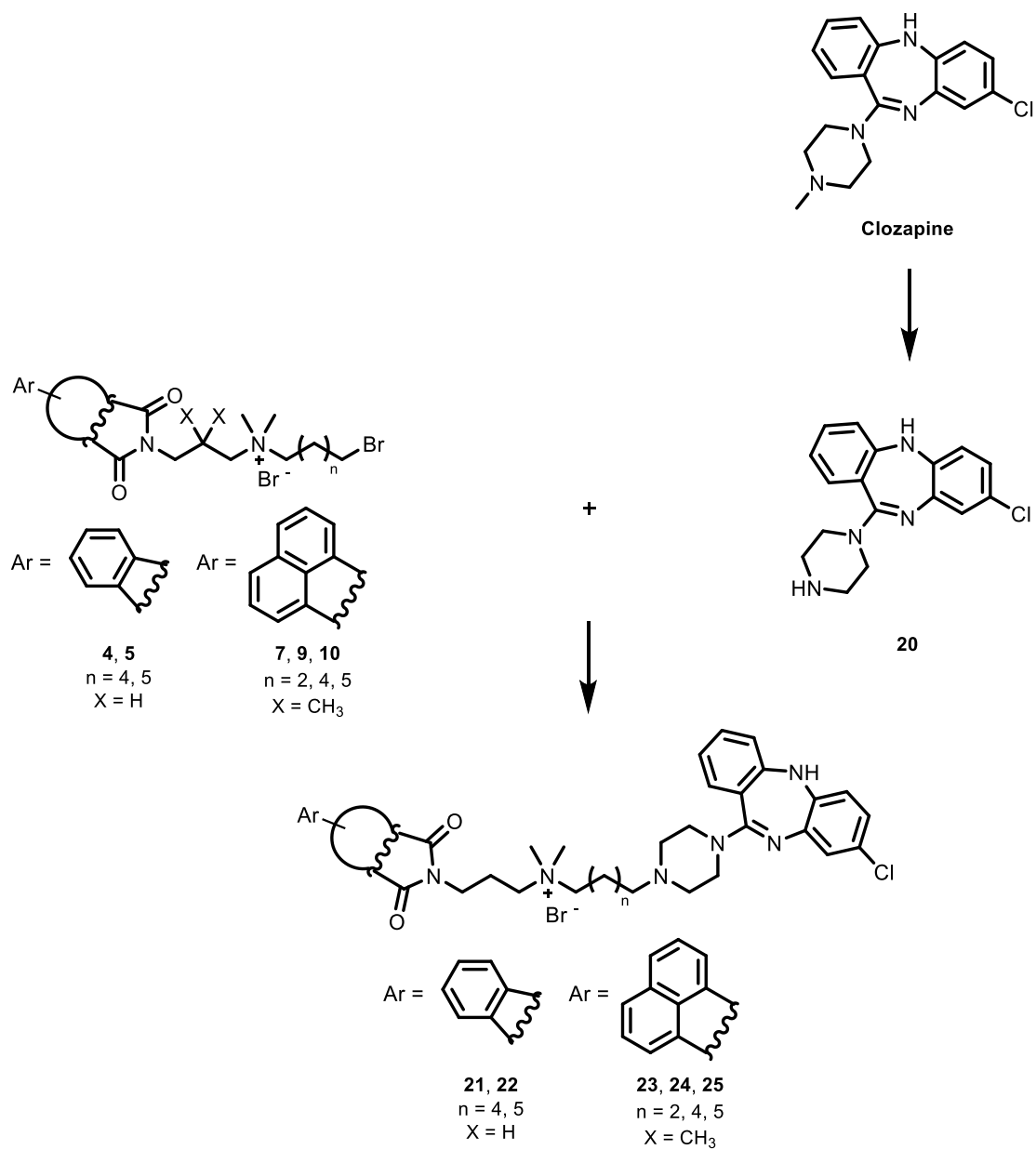
Scheme 3.8: Overall synthesis of phthalimide/1,8-naphthalimide-clozapine hybrids.

3.2.1.2.A. Synthesis of *N*-desmethyl clozapine 20

N-Desmethyl clozapine **20** was synthesized from clozapine as its precursor molecule. Clozapine is known to act as an orthosteric antagonist at the M_1, M_2, M_3 and M_5 receptors, and as an agonist at the M_4 subtype.[23] *N*-Desmethyl clozapine was reported to possess M_1-selectivity as allosteric agonist.[57] The starting material clozapine was extracted from purchased Clozapex® tablets (100 mg clozapine per tablet).

The compound **20** was a result of a one-step synthesis by the means of *N*-demethylation of the piperazine of clozapine (Scheme 3.9). In brief, an ice-cold solution of clozapine in 1,2-dichloroethane was subjected to the dropwise addition of an excess of *α*-chloroethyl chloroformate. Upon addition of this reagent, the solution turns from bright yellow to fluorescent red. Following the subsequent reflux overnight and solvent evaporation under reduced pressure, the resultant carbamate intermediate is hydrolyzed heating under reflux in methanol overnight to attain the secondary amine molecule **20** in 60% yield.[65]
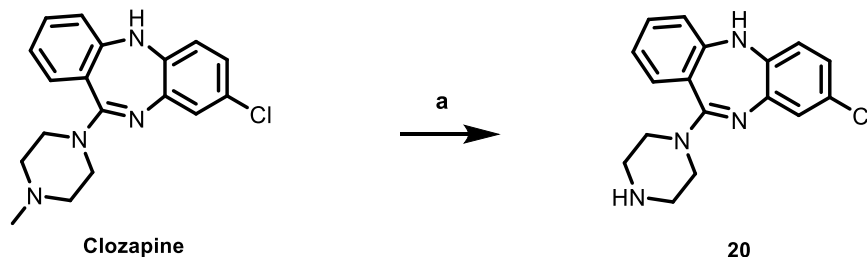
Scheme 3.9: Synthesis of *N*-desmethyl clozapine **20**; **a**: 1,2-dichloroethane, *α*-chloroethyl chloroformate, reflux overnight, followed by addition of methanol, reflux overnight.

3.2.1.2.B. Synthesis of phthalimide/1,8-naphthalimide-clozapine hybrids 21-25

The last step of the synthesis of these final compounds is the linking of the previously synthesized phthalimido/1,8-naphthalimido bromide intermediates **4**, **5**, **7**, **9** and **10**, respectively, to *N*-desmethyl clozapine **20** using the aforementioned reaction method **III**, as shown in Scheme 3.10. The synthesis required 5 days for completion (silica gel TLC

monitoring was done using 0.2 M aqueous KNO_3/MeOH 2:3 as eluent). These final hybrids were purified either by crystallization from the reaction mixture or by RP silica gel flash chromatography (using the same gradient run method affirmed for the aforemention pirenzepine-containing hybrids by means of H_2O/MeOH solvent system).
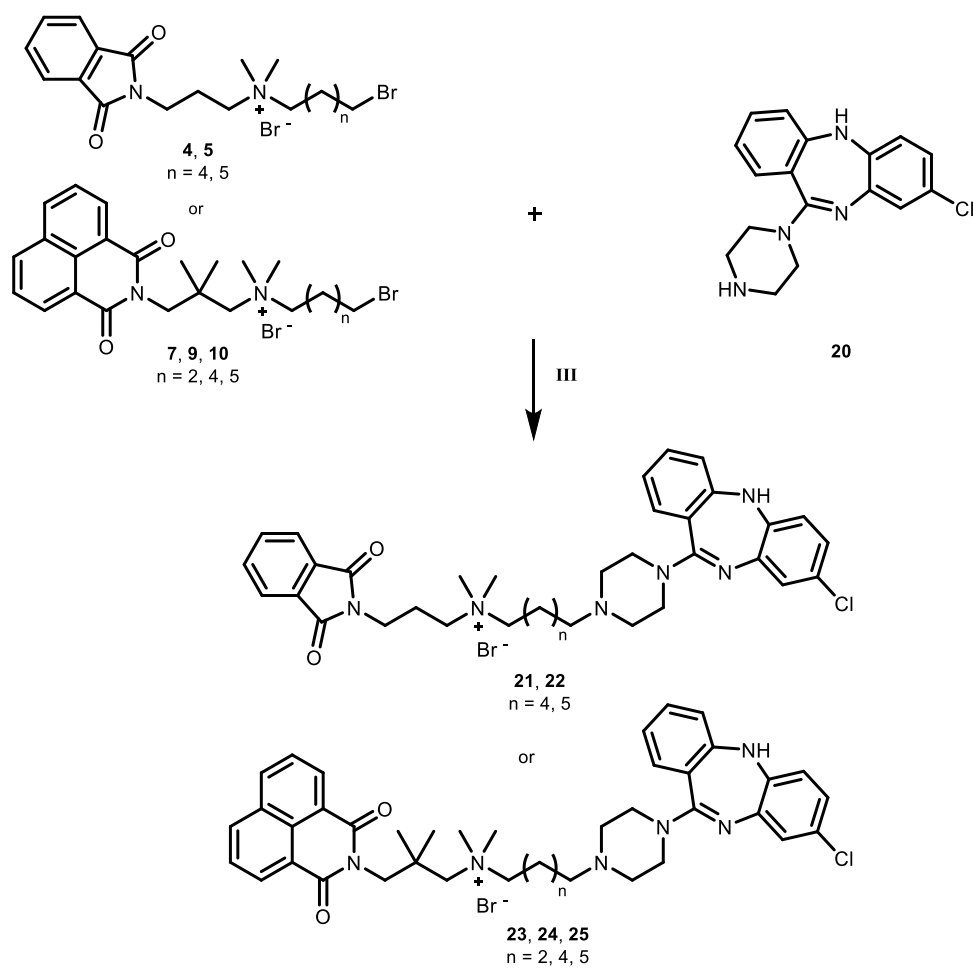
Scheme 3.10: Final step of the synthesis of phthalimide/1,8-naphthalimide-clozapine hybrids; **III**: acetonitrile, stirring at 35 °C for 5 days.

The ^{1}H NMR spectrum of compound **24** (Figure 3.9) exhibits the absence of the resonance signal corresponding to CH_2-Br (terminal methylene in the intermediate **9** at $\delta_H = 3.51 - 3.41$ ppm in CD_3OD) and the presence of the more upfield **i**-methylene group (CH_2-N) in compound **24** ($\delta_H = 3.45 - 3.23$ ppm in DMSO-d$_6$). Some of the characteristic features of the clozapine part in the ^{13}C NMR spectrum are the C=N signal ($\delta_C = 162.2$ ppm), the C-

C=N signal (δ_C = 154.3 ppm) and the C-Cl signal (δ_C = 142.4 ppm). The assignment of the signals in the ^{13}C NMR spectrum of **24** is confirmed by two-dimensional NMR spectroscopy through HMBC measurement (see Appendix). In addition, the resonance signals that distinguish the naphthalimide part, such as the methyl $C(CH_3)_2$ signal (δ_H = 1.25 ppm, δ_C = 25.5 ppm), appear in both ^1H and ^{13}C NMR spectra.
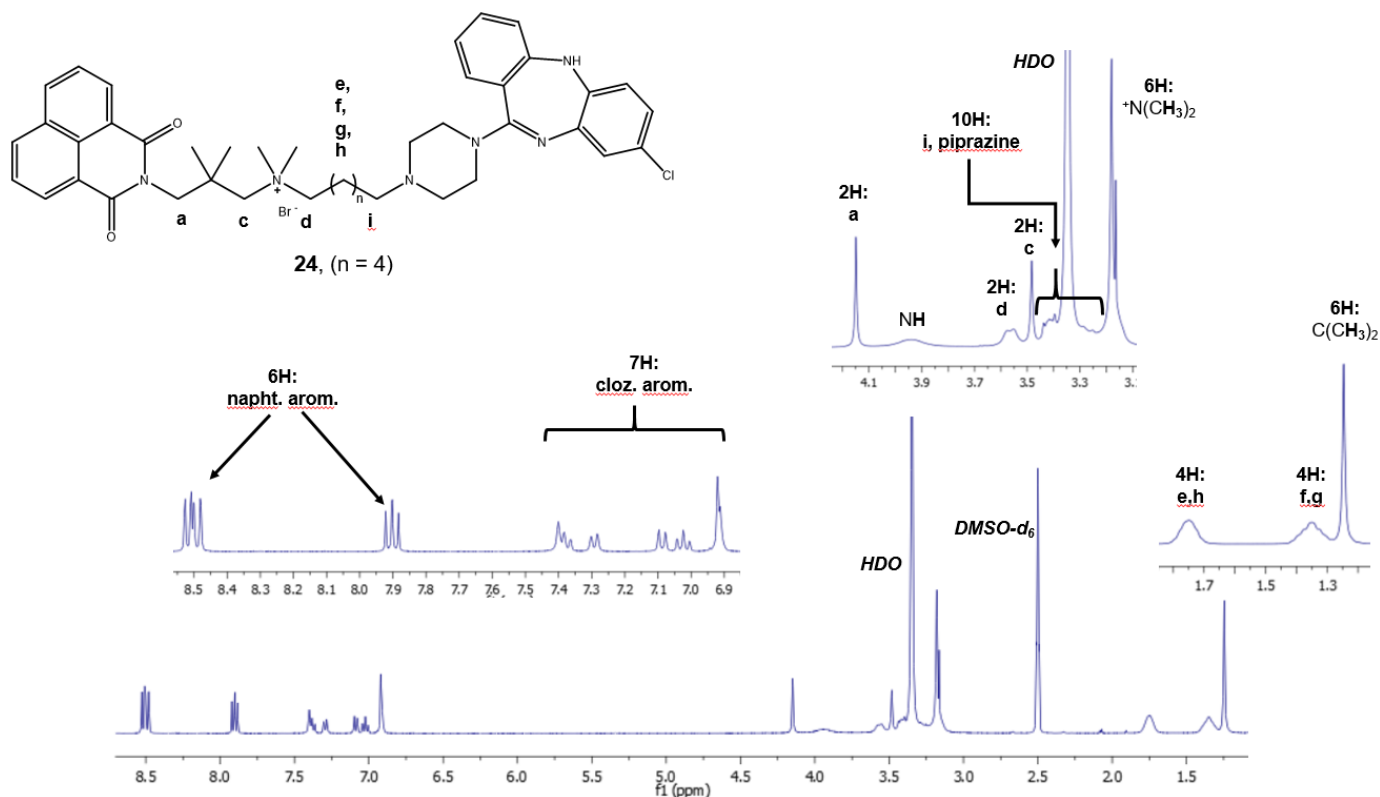
Figure 3.9: ^1H NMR spectrum for compound **24** (400 MHz, DMSO-d_6).

3.2.1.3. Synthesis of iperoxo-clozapine hybrids 30-32

The third group of final compounds constitutes the hybrids **30-32** which are composed of the iperoxo monoquaternary bromides **27-29** respectively, and *N*-desmethyl clozapine **20**. Iperoxo is a non-selective super-agonist of mAchRs, whose high binding affinity makes it a good candidate for incorporation in dualsteric hybrids.[33] Beside the previously described synthesis of **20**, the iperoxo bromide intermediates were also synthesized over several steps according to literature,[66-68] as shown in Scheme 3.11.
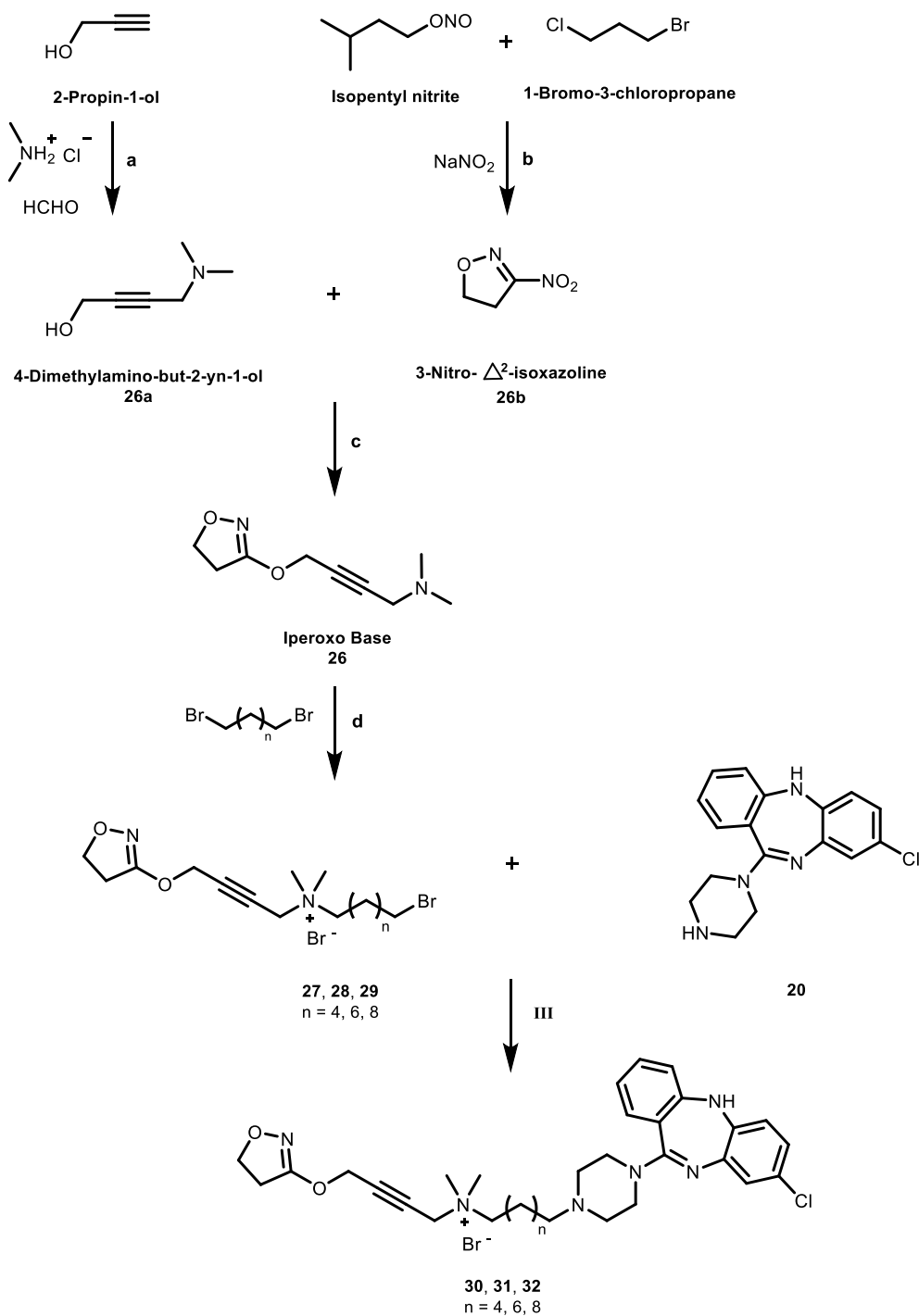
Scheme 3.11: Overall synthesis of iperoxo-clozapine hybrids; **a**: dimethylammonium hydrochloride, aqueous formaldehyde solution, copper sulfate pentahydrate as catalyst, 80 °C for 4 hrs, **b**: isopentyl nitrite, 1-bromo-3-chloropropane, sodium nitrite, DMSO, stirring at room temperature for 3 hrs, **c**: sodium hydride, THF, reflux for 8 hrs, **d**: acetonitrile, KI/K$_2$CO$_3$, microwaves at 80 °C for 5 hrs, **III**: acetonitrile, stirring at 35 °C for 4 days.

3.2.1.3.A. Synthesis of iperoxo monoquaternary bromides 27-29

The synthesis of the key iperoxo intermediates **27**-**29**, with the different carbon chain lengths, involves 2 important steps: Initially, the synthesis of the crucial iperoxo base, followed by the attachment of the appropriate linker chain.

Kloeckner et al. described the 2-step synthesis of the iperoxo base **26** (*N*-desmethyl iperoxo) through the synthesis of its 2 precursor molecules namely 4-dimethylamino-but-2-yn-1-ol **26a** and 3-nitro-Δ^2-*isoxazoline* **26b**.[66] Firstly, **26a** was synthesized via a Mannich reaction using a basic aqueous solution of dimethylammonium hydrochloride (pH=9), 40% formaldehyde aqueous solution, 2-propin-1-ol and an aqueous solution of copper sulfate pentahydrate as a catalyst. The pH of the solution was then adjusted to 8 using 2 M sodium hydroxide solution, heated at 80 °C for 4 hrs and treated with 25% aqueous ammonia solution. After work-up, **26a** was obtained as a yellow oil in 65% yield. Secondly, **26b** was synthesized by conversion of 1-bromo-3-chloropropane with sodium nitrite and isopentyl nitrite in DMSO. The mixture was then stirred at room temperature for 24 hrs and extracted with dichloromethane to obtain **26b** as yellow oil in 45% yield. The iperoxo base **26** was formed using the precursors **26a** and **26b** by means of sodium hydride and was obtained as orange oil in 62% yield.

Finally, the needed iperoxo monoquaternary bromides **27**- **29** were synthesized from the iperoxo base **26** (Scheme 3.11), based on slight modification of the reported literature.[67, 68] In short, an acetonitrile mixture containing **26**, 15 equivalents of the appropriate alkyl dibromide and a catalytic amount of 1:1 mixture of KI/K_2CO_3 were heated in the microwave 80 °C (ramp: 20 °C/min, 800W) for about 5 hrs. Following cooling of the mixture, filtration was done and the attained filtrate was evaporated under reduced pressure to obtain an oily residue, from which the target product was precipitated using diethyl ether and acquired by vacuum filtration. The pure iperoxo spacer compounds **27**, **28** and **29** were successfully synthesized in yields ranging from 57% to 79%.

3.2.1.3.B. Synthesis of iperoxo-clozapine hybrids 30-32

The synthesis of the iperoxo-clozapine dualsteric hybrids **30-32** was concluded by the coupling of the iperoxo bromide intermediates **27**- **29**, respectively, to *N*-desmethyl clozapine **20** by the same strategy approved in this project using reaction method **III** (as shown in Scheme 3.11) and a small variation of the reaction time (4 days, based on TLC monitoring). These final compounds were purified either by crystallization from the reaction mixture or by RP silica gel flash chromatography (by means of H_2O/MeOH solvent system).

The NMR data of compound **30** is the representative example of iperoxo-clozapine hybrids discussed (Figure 3.10). The iperoxo entity exhibits the clear resonance signals for the 2-butynyl carbon fragment, with 2 methylene groups $C{\equiv}C\text{-}CH_2\text{-}N^+$ and $O\text{-}CH_2\text{-}C{\equiv}C$ at $\delta_H =$ 4.91 ppm and $\delta_H = 4.44 - 4.35$ ppm, respectively, in the ^1H NMR spectrum. The ethyne carbons appear as 2 quaternary carbon signals at $\delta_C = 76.6$ ppm and 87.7 ppm in the ^{13}C NMR spectrum. Moreover, the 2 methylene groups of the Δ^2-isoxazoline ring appear in both spectra and have been confirmed via two-dimensional NMR spectroscopy (see Appendix).
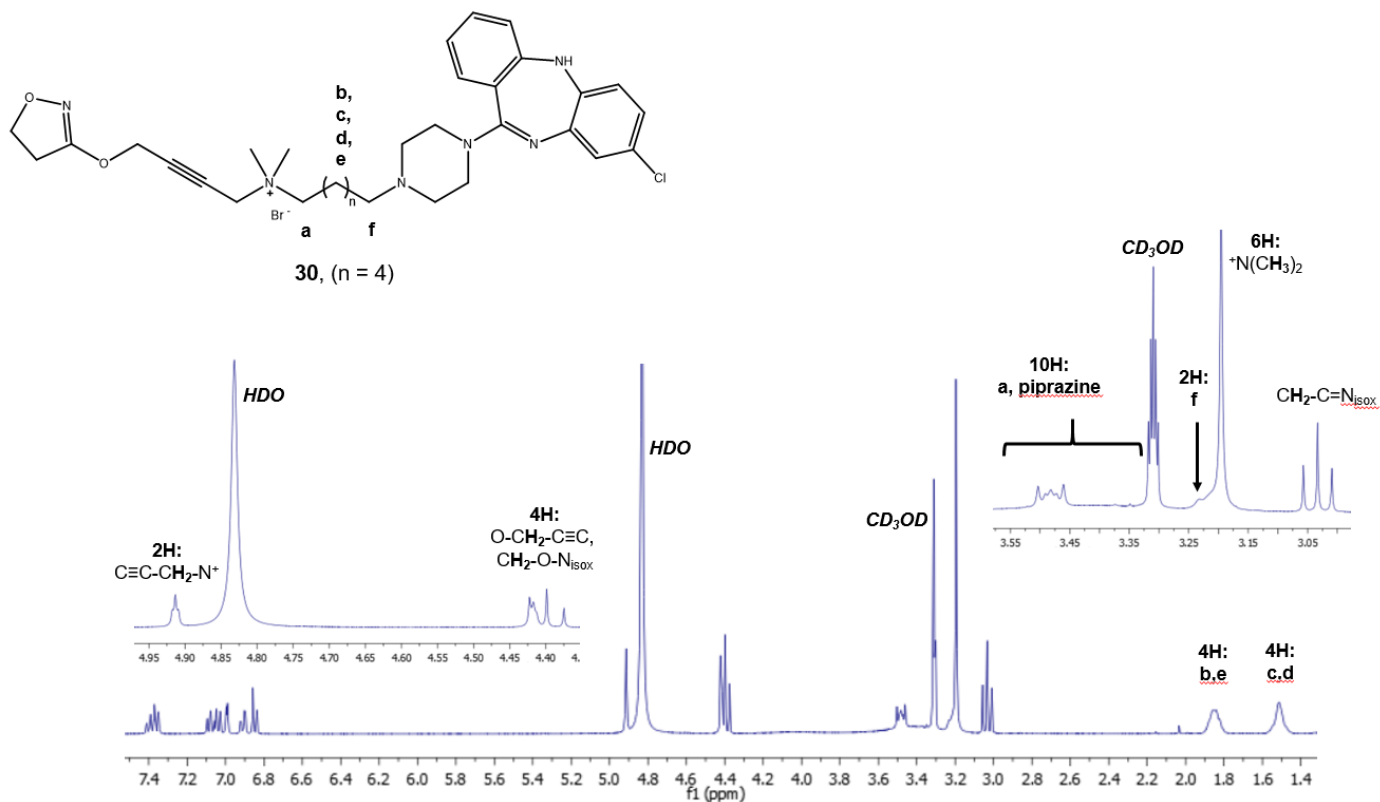
Figure 3.10: ^{1}H NMR spectrum for compound **30** (400 MHz, CD$_3$OD).

3.2.1.4. Synthesis of acetylcholine-clozapine hybrids 35 and 36

The acetylcholine-clozapine hybrids **35** and **36** are dualsteric compounds made up of the acetylcholine monoquaternary bromides **33** and **34**, respectively, linked to *N*-desmethyl clozapine **20**. Acetylcholine, being an endogenous orthosteric agonist, has high binding affinity to mAchRs.[69] This makes it of great use in dualsteric muscarinic hybrids. The synthesis of the 2 acetylcholine bromide intermediates was the initial step for the synthesis of the hybrids according to literature,[70] as shown in Scheme 3.12.
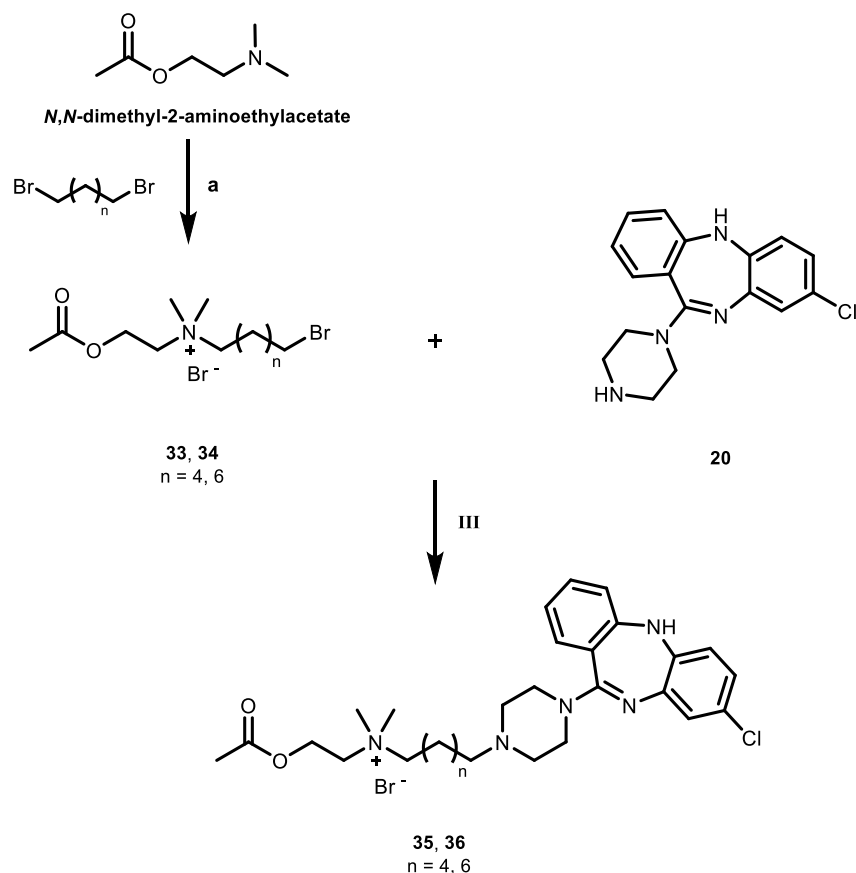
Scheme 3.12: Overall synthesis of acetylcholine-clozapine hybrids; **a**: acetonitrile, reflux for 3 hrs, **III**: acetonitrile, stirring at 35 °C for 3 days.

3.2.1.4.A. Synthesis of acetylcholine monoquaternary bromides 33 and 34

Uppal et al. detailed the synthesis of acetylcholine intermediates.[70] Concisely, the synthesis entailed the use of *N,N*-dimethyl-2-aminoethylacetate and a fifteen-fold excess of the required alkyl dibromide (either 1,6-dibromohexane or 1,8-dibromoctane) in acetonitrile as solvent whilst heating under reflux for 3 hrs (Scheme 3.12). Following cooling, the pure product was precipitated using diethyl ether and obtained by vacuum filtration as a white solid. The monoquaternary compounds **33** and **34** were attained in 70% and 81% yields, respectively.

3.2.1.4.B. Synthesis of acetylcholine-clozapine hybrids 35 and 36

Using reaction method **III**, the synthesis of acetylcholine-clozapine hybrids required the shortest reaction time among all synthesized hybrid groups (0.2 M aqueous KNO_3/MeOH 2:3 as eluent for silica gel TLC monitoring), needing 3 days only (Scheme 3.12). Hybrid **35** was purified by RP silica gel flash chromatography (by means of H_2O/MeOH solvent system), while hybrid **36** was crystallization from the reaction mixture.

Out of the 2 acetylcholine-clozapine hybrids, compound **35** is the elective 6-carbon analogue used to exemplify the NMR evidence of the correct synthesis (Figure 3.11). The acetylcholine segment is depicted in the spectra of **35** by the appearance of the methyl singlet of CH_3-C=O at δ_H = 2.11 ppm and δ_C = 20.7 ppm, with its carbonyl signal at δ_C = 171.61 ppm in the ^{13}C NMR spectrum. Both methylene groups of the same segment are accounted for, where O-**CH₂**-CH_2-N^+ appears at δ_H = 4.53 ppm, δ_C = 58.7 ppm, and O-CH_2-**CH₂**-N^+ appears at δ_H = 3.76 − 3.68 ppm, δ_C = 63.7 ppm, and are confirmed by two-dimensional NMR measurements (see Appendix).
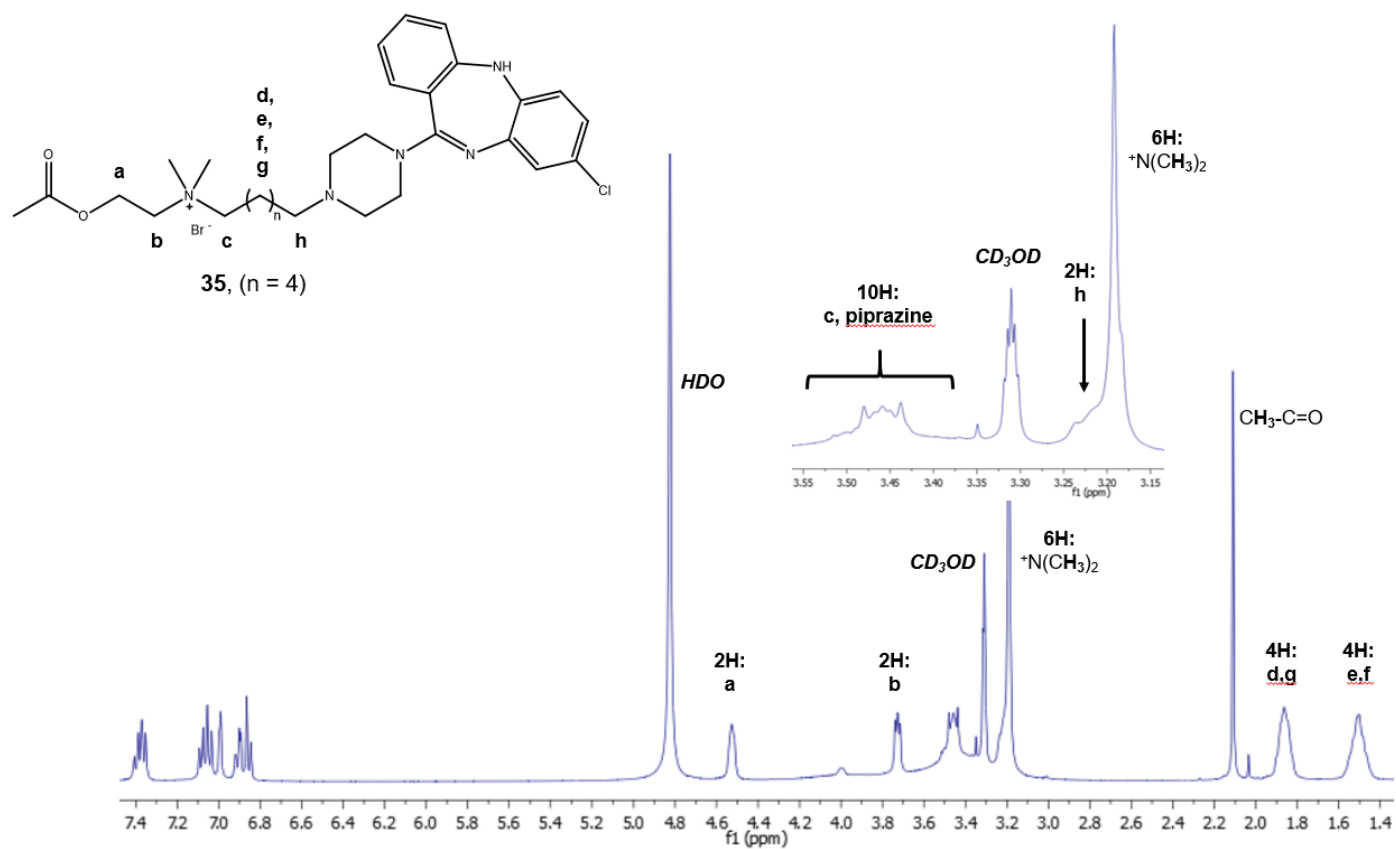
Figure 3.11: ^{1}H NMR spectrum for compound **35** (400 MHz, CD$_3$OD).

3.2.2. Pharmacology

Due to the vast availability of drugs and molecules acting on GPCRs, tools and pharmacological methods to test these resultant interactions have been widely developed. Fluorescence resonance energy transfer (FRET), also called Förster resonance energy transfer, is an imaging technique that allows visualization of ligand – receptor interaction since this type of microscopy depends on the ability to detect fluorescent signals from the interactions of labeled molecules in cells. FRET is a distance-dependent process by which energy is transferred from an excited molecular fluorophore (the donor) to another fluorophore (the acceptor) by means of intermolecular long-range interaction. FRET assays can be considered a reliable measurement of the vicinity of labelled proteins at distances between 10-100 Å, being particularly most accurate when the donor and acceptor are positioned within the Förster radius (the distance at which half the excitation energy of the donor is transferred to the acceptor, typically 3-6 nm).[71] FRET assays utilize these genetically-encoded proteins being attached on the target GPCR. One or both of these proteins is required to be fluorescent. Upon ligand binding, the receptor undergoes conformational change and hence resulting in a change the measured fluorescence. The results are recorded as the appearance of the fluorescence of the acceptor or the quenching of the fluorescence of the donor.[71, 72] FRET is well suited to report both protein-protein interactions (intermolecular FRET) and conformational changes (intramolecular FRET).[73, 74]

The commonly used biosensors are cyan fluorescent protein (CFP) on the C-terminus, and either yellow fluorescent protein (YFP) or a six-amino acid short sequence (CCPGCC) involving tetracysteine that is able to bind a fluorophore called fluoresceine arsenical hairpin binder (FlAsH) on the third loop of the GPCR.[74-76] The latterly mentioned biosensor has the advantage of having a small size and hence less disruption of the protein mobility during the assay.[76]

Dualsteric or bitopic ligands are compounds that have affinity to more than one binding site on GPCRs, such as the orthosteric and allosteric regions, and provide a very strong foundation for the design of new drugs.[75] The synthesized dualsteric hybrids of this project

are being tested using FRET assays as means to the inspection of the optimal linker length of the molecule, which allows the ideal conformational change of the GPCR, as well as the nature of the orthosteric and allosteric moieties. In addition to the elucidation of the conformational changes upon binding of the dualsteric hybrids, it has to be confirmed that these hybrids are able to bind in dualsteric and purely allosteric manners by means of FRET experiments. The GPCRs involved in these studies, which are in progress, are M_1 or M_2 muscarinic receptors accordingly.

4. A. Summary

GPCRs, particularly muscarinic receptors (mAChRs), are significant therapeutic targets in many physiological conditions. The significance of dualsteric hybrids selectively targeting mAChR subtypes is their great advantage in avoiding undesired side effects. This is attained by exploitation of the high affinity of ligand-binding to the orthosteric site and the structural diversity of the allosteric site to target an individual mAChR subtype, as well as offering signal bias to avoiding undesired transduction pathways. Furthermore, dualsteric targeting of mAChR subtypes helps in the elucidation of the physiological role of each individual mAChR subtype.

The first project was the attempt of synthesis of the M_2-preferring ligand AFDX-384. AFDX-384 is known to preferentially bind to the M_2 receptor subtype as an orthosteric antagonist, with partial interaction with residues in the allosteric site. This project aimed to re-trace the synthesis route of AFDX-384, to open the door to its upscaling and the future synthesis of AFDX-type dualsteric ligands. The multi-step synthesis of AFDX-384 is achieved through the synthesis of its 2 precursors, the chloro acyl derivative **VIII** and the piperidinyl derivative **IV**, as shown in Figure 4.1.
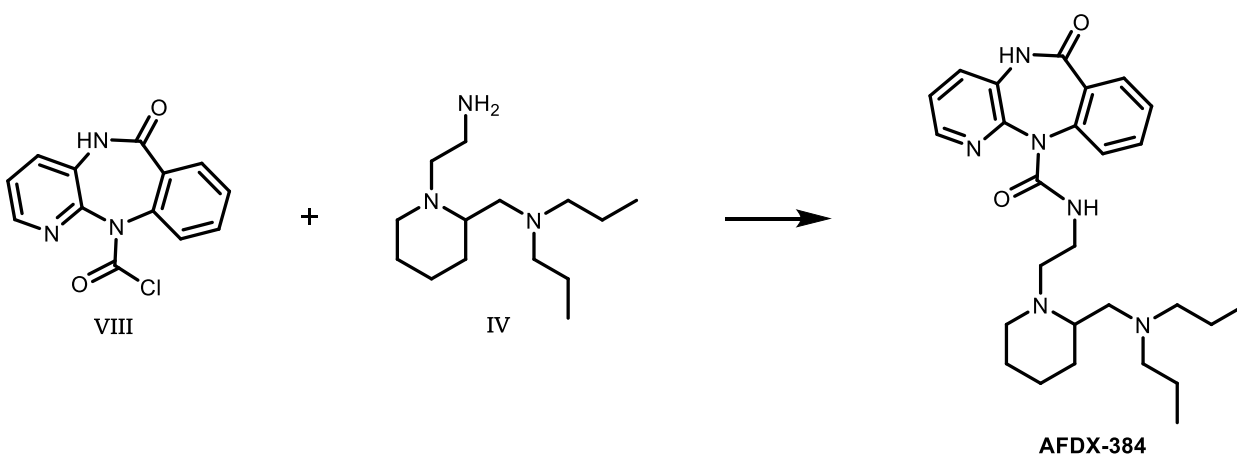
Figure 4.1: The synthesis of AFDX-384 from its precursor molecules **IV** and **VIII**.

Upscaled synthesis of the piperidinyl derivative **IV** was attained. Synthesis of the chloro acyl compound **VIII** was attempted. Several trials to synthesize the benzopyridodiazepine nucleus as well as its chloro-acylation resulted in the production of the novel crystal structures **V** and **VI** (Figure 4.2). X-ray crystallography was also done for crystallized molecules of the closed-ring benzopyridodiazepine **VII** that was previously synthesized. Chloro-acylation reactions of compound **VII** using phosgene seem to be attainable when done using reflux overnight. However, the use of methanol to aid in elution during silica gel column chromatography converted the expected product to the carbamate analogue **IX**. Hence, further attempts in purification should refrain from the use of methanol. The use of triphosgene instead of phosgene demonstrates a cleaner route for further upscaled synthesis.
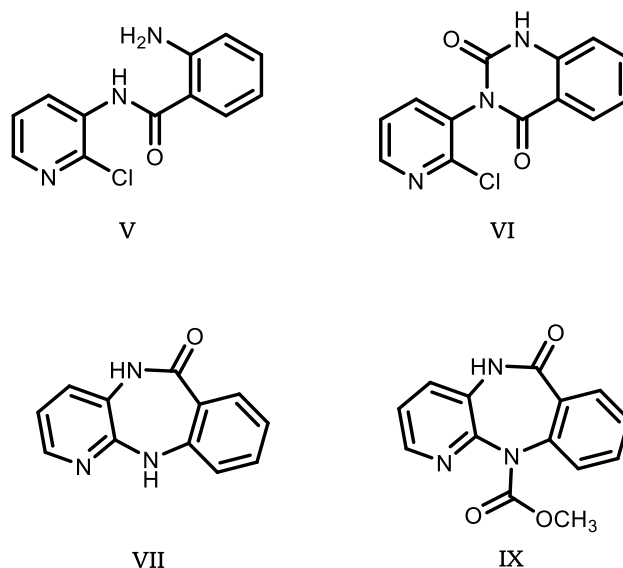
Figure 4.2: The structures of compounds **V**, **VI** and **VII** (for which X-ray crystallography has been made), as well as the carbamate product **IX**.

The second project was the synthesis of dualsteric ligands involving variable orthosteric and allosteric moieties. Four different types of hybrids have been created over multiple steps. Dualsteric ligands have been synthesized using either a phthalimido- or 1,8-naphthalimidopropylamino moiety as the allosteric-binding group, coupled to either *N*-desmethyl pirenzepine or *N*-desmethyl clozapine using variable chain lengths. Furthermore, the synthesis of the dualsteric ligands involving *N*-desmethyl clozapine linked

to either the super-agonist iperoxo or acetylcholine, and being connected using variable alkane chain lengths (Figure 4.3).

Several reaction conditions have been investigated throughout the analysis of the optimal condition to conduct the critical final step of synthesis of these dualsteric hybrids, which involves the linking of the two segments of the hybrid together. The optimal method, which produced the least side products and highest yield, was to connect the two intermediates of the compound in absence of base, catalyst or microwaves while stirring at 35 °C for several days using acetonitrile as solvent (silica gel TLC monitoring, 0.2 M aqueous KNO_3/MeOH 2:3). The ideal purification methods for the final compounds were found to be either crystallization from the reaction medium or using C18 reverse phase silica gel flash chromatography (using H_2O/MeOH solvent system). All the hybrids will be subjected to pharmacological testing using the appropriate FRET assays.

Phthalimide/1,8-naphthalimide-clozapine hybrids
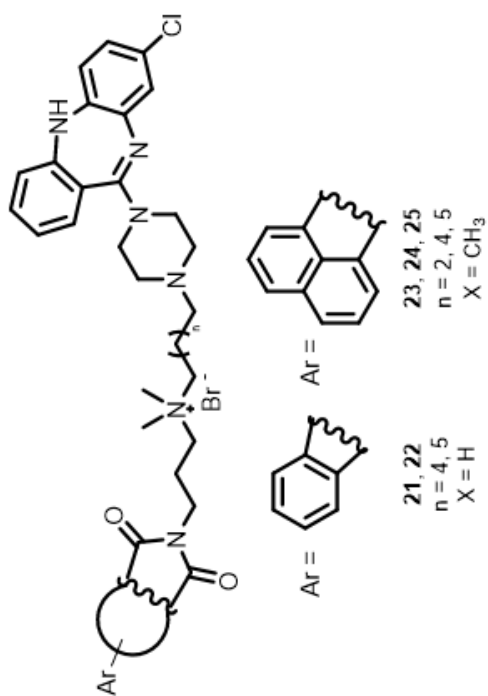
Ar =

21, 22
n = 4, 5
X = H

Ar =

23, 24, 25
n = 2, 4, 5
X = CH₃

Phthalimide/1,8-naphthalimide-pirenzepine hybrids

Ar =

13, 14, 15, 16
n = 2, 3, 4, 5
X = H

Ar =

17, 18, 19
n = 3, 4, 5
X = CH₃

Acetylcholine-clozapine hybrids

35, 36
n = 4, 6

Iperoxo-clozapine hybrids

30, 31, 32
n = 4, 6, 8
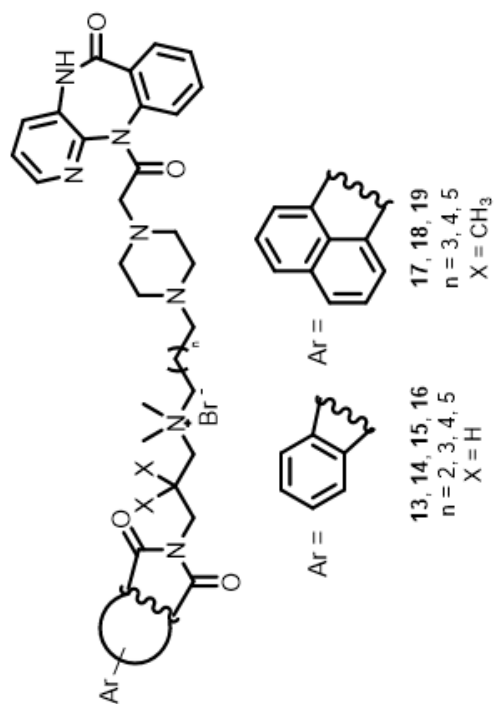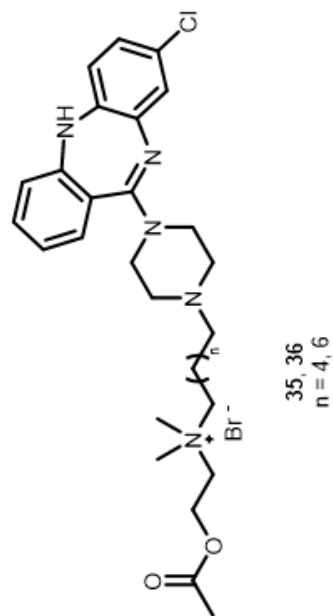
Figure 4.3: Dualsteric ligands.

4. B. Zusammenfassung

G-Protein-gekoppelte Rezeptoren (GPCRs), besonders die Familie der muscarinischen Rezeptoren, stellen wichtige therapeutische Zielstrukturen für die Behandlung einer Vielzahl an Erkrankungen dar. Die Besonderheit dualsterischer Hybridliganden, die selektiv an den muskarinischen Acetylcholinrezeptor (mAChR) binden liegt darin begründet, dass so ungewünschte Nebenwirkungen vermieden werden können. Dies wird durch die Ausnutzung der hohen Bindungsaffinität an die orthostere Stelle sowie die strukturelle Vielfältigkeit der allosteren Bindestelle erreicht, wodurch bestimmte mAChR-Subtypen adressiert und eine funktionelle Selektivität erreicht werden kann, die unerwünschte Signaltransduktionswege umgeht. Desweiteren kann die dualstere Adressierung der mAChR-Subtypen dazu beitragen, die physiologische Funktion eines jeden Rezeptors zu bestimmen und aufzuklären.

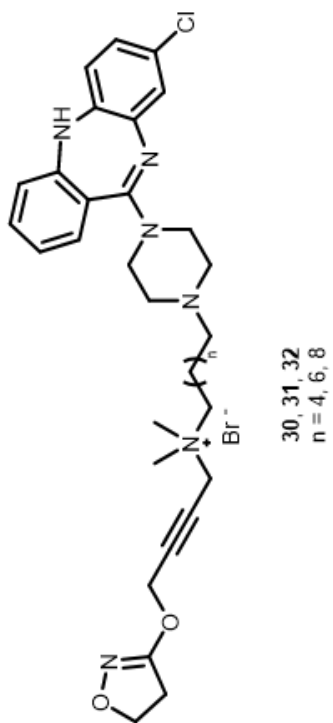Das Ziel des ersten Teilprojektes war die Synthese des bevorzugt an M_2 bindenden Liganden AFDX-384. Von diesem ist bekannt, als orthosterer Agonist bevorzugt an den M_2-Rezeptorsubtyp zu binden und zum Teil Interaktionen in der allosteren Bindestelle einzugehen. Hierbei sollte die Darstellungsroute von AFDX-384 nachvollzogen werden, um eine Synthese in größerem Maßstab zu entwickeln und die Herstellung weiterer dualsterer Liganden vom AFDX-Typ zu ermöglichen. Die mehrstufige Synthese von AFDX-384 geht von zwei Vorstufen aus, dem Chloracyl **VIII** sowie dem Piperidinylderivat **IV** (Abbildung 4.4).
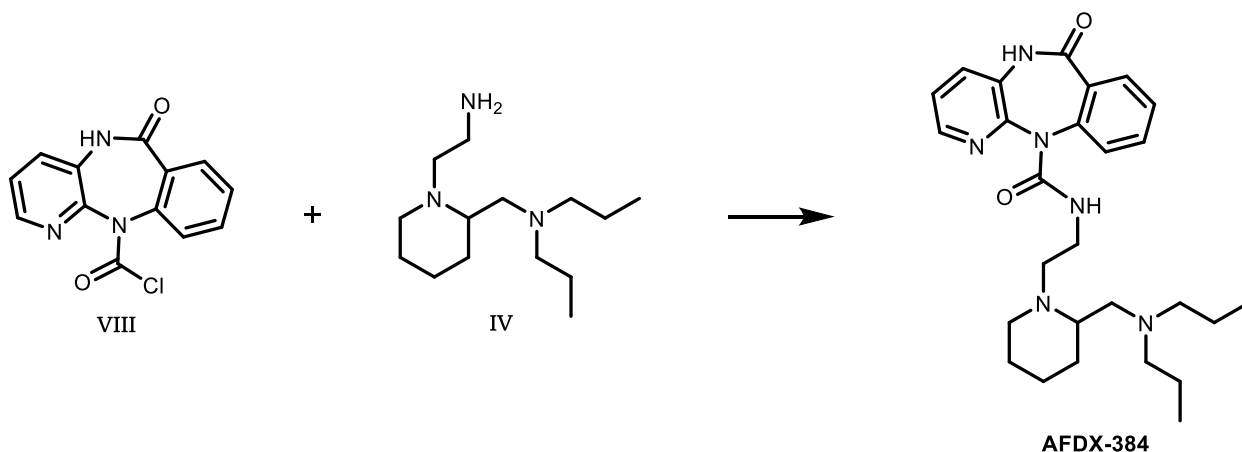
Abbildung 4.4: Synthese von AFDX-384 ausgehend von den Vorstufen **IV** und **VIII**.

Zunächst wurde das *Upscaling* der Synthese von **IV** erreicht und die Darstellung von **VIII** versucht. Mehrere Versuche, den Benzopyridodiazepin-Kern sowie das entsprechende chloracetylierte Derivat zu erhalten, führten zur Bildung der neuen Strukturen **V** und **VI** (Abbildung 4.5). Das zuvor synthetisierte, ringgeschlossene Benzopyridodiazepin **VII** wurde mittels Röntgenkristallstrukturanalyse charakterisiert. Die Chloracylierung von **VII** schien mittels Phosgens und unter Rückfluss über Nacht möglich zu sein. Allerdings wurde das Reaktionsprodukt durch den Einfluss von Methanol, das während der chromatographischen Reinigung als Fließmittel verwendet wurde, in das Carbamat-Analogon **IX** überführt. Daher sollten künftige Reinigungsschritte ohne die Zuhilfenahme von Methanol erfolgen. Durch den Einsatz von Triphosgen anstelle von Phosgen wird eine eindeutigere, direktere Syntheseroute zum weiteren *Upscaling* erreicht.
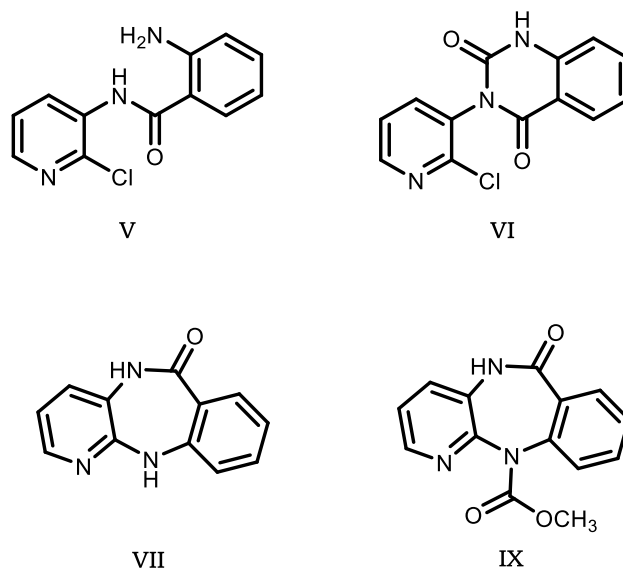
Abbildung 4.5: Strukturen der Verbindungen **V**, **VI** und **VII** (für diese wurden Röntgen-Kristallstruzkturanalysen durchgeführt) sowie des Carbamates **IX**.

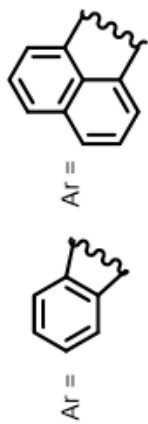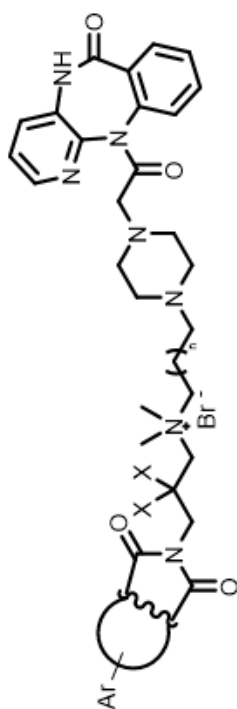Im Rahmen des zweiten Teilprojektes wurden dualstere Liganden hergestellt, die variable orthostere und allostere Molekülteile besitzen. Durch mehrstufige Syntheseverfahren konnten vier verschiedene Typen von Hybriden hergestellt werden. Dualstere Liganden wurden dadurch erhalten, dass entweder Phthalimido- oder 1,8-Naphthalimidopropylamino-Gruppen als allostere Bindegruppe durch einen flexiblen und

verschieden langen *Linker* mit *N*-Demethylpirenzepin oder *N*-Demethylclozapin verknüpft wurden. Außerdem wurden dualstere Liganden hergestellt, in denen *N*-Demethylclozapin durch einen variablen *Linker* entweder an den Superagonisten Iperoxo oder an Acetylcholin geknüpft ist (Abbildung 4.6).

Der kritischste Schritt der Synthese ist die Verknüpfung der beiden Linkersegmente am Ende des Herstellungsweges. Hierfür wurden mehrere Reaktionsbedingungen untersucht, um die Kopplung optimal zu ermöglichen. Die beste Methode, bei der die wenigsten Nebenprodukte und die größten Ausbeuten erzielt wurden besteht darin, die beiden letzten Zwischenstufen in Abwesenheit einer Base, Katalysatoren oder Mikrowellenstrahlung in Acetonitril zu lösen und bei 35 °C mehrere Tage zu rühren (Reaktionskontrolle: Dünnschichtchromatographie an Kieselgel, Fließmittel: 0,2 M wässrige KNO_3/MeOH 2:3). Als bestes Reinigungsverfahren stellten sich entweder die Kristallisation aus dem Reaktionsmedium oder die Verwendung einer Flash-Chromatographie-Apparatur an C18-Kieselgel dar (Eluent: H_2O/MeOH). Alle synthetisierten Hybridmoleküle werden noch einer pharmakologischen Charakterisierung unter Anwendung geeigneter FRET-Testsysteme unterzogen.

Phthalimide/1,8-Naphthalimide-Clozapin Liganden

23, 24, 25
n = 2, 4, 5
X = CH₃

21, 22
n = 4, 5
X = H

Ar =

Ar =

Phthalimide/1,8-Naphthalimide-Pirenzepin Liganden

17, 18, 19
n = 3, 4, 5
X = CH₃

13, 14, 15, 16
n = 2, 3, 4, 5
X = H

Ar =

Ar =
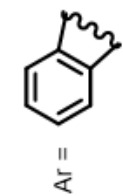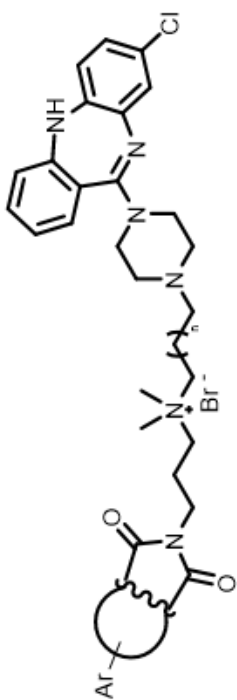
Acetylcholin-Clozapin Liganden

35, 36
n = 4, 6

Iperoxo-Clozapin Liganden

30, 31, 32
n = 4, 6, 8
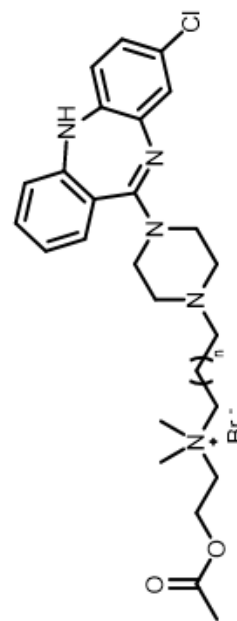
Figure 4.6: Dualsteriche Hybridliganden.

5. Experimental

A. General specifications

A.1. Instruments

NMR Spectroscopy

The ^{1}H (400.13 MHz) and ^{13}C (100.61 MHz) NMR spectra were recorded on a Bruker Avance 400 Ultra Shield^{TM} spectrometer (Bruker Biospin, Ettlingen, Germany) instrument using tetramethylsilan as internal standard δ = 0 ppm. Residual undeuterated solvent signals were used as reference (^{1}H, ^{13}C): DMSO-d_6 at 2.50 ppm, 39.5 ppm; CD_3OD = 3.31 ppm, 49.0 ppm; $CDCl_3$ = 7.26 ppm, 77.2 ppm. Coupling constants (_J_-values) are given in Hertz. All the signals of the final compounds were confirmed using two-dimensional NMR experiments (COSY, HMQC and HMBC). The multiplicities of the resonance signal are represented with the following symbols: s = singlet, br = broad, d = doublet, dd = doublet of doublet, ddd = doublet of doublet of doublet, t = triplet, m = multiplet.

Infrared Spectroscopy

All infrared measurements for the final compounds were conducted on Jasco FT-IR-6100 Spectrometer of Jasco Laborund Datentechnik GmbH (Groß-Umstadt, Deutschland) at room temperature, and underwent ATR correction.

Mass Spectroscopy

The molecular weights of all final compounds were acquired on a Shimadzu LC/MS-2020 instrument (Hilden, Germany) using Electrospray ionization (ESI), DGU-20A3R degassing unit, a LC20AB liquid chromatograph and a SPDA-20A UV-VIS detector.

Purity

The peak purity of the final compounds were confirmed on an analytical Shimadzu HPLC instrument (Hilden, Germany) equipped with a DGU-20A3R degassing unit, a LC20AB liquid chromatograph, and a SPD20A UV/Vis detector. The stationary phase was a Synergi fusion-RP (150 x 4.6 mm, 4 µm) column (Phenomenex, Aschaffenburg, Germany). The

following gradient elution was conducted: solvent A: water with 0.1% formic acid, solvent B: MeOH with 0.1% formic acid. Solvent A from 0% to 100% in 13 mins., then 100% A maintained for 5 mins., followed by a decrease of A from 100% to 5% in 1 mins., and finally maintaining 5% of A for 4 mins. The flow rate was adjusted to 1.0 mL/min. UV detection was performed at 254 nm.

Melting point

All melting points of the final compounds were measured using Coesfield MPM-H2-melting point instrument (Dortmund, Deutschland).

Microwave

All microwave reactions were done a MLS-Ethos-CFR-Microwave (Leutkirch, Germany). Each microwave reaction condition is mentioned with each appropriate condition.

A.2. Chromatography methods

Column chromatography

For silica gel column chromatography, silica gel 60 (SiO_2, 0.063-0.2 mm) was purchased from Merck (Darmstadt, Deutschland). For basic ALOX column chromatography, CHROMABOND® Alox B was purchased from Machery-Nagel (Düren, Deutschland) (high purity basic aluminium oxide, pore volume: 0.90 mL/g, particle size: 60 - 150 µm, pH: 9.5 ± 0.5).

Flash chromatography

Flash column chromatography was performed on an Interchim Puri-Flash 430 instrument using a PuriFlash column C18/HP (reverse phase silica gel) and connected to an Interchim Flash ELSD as well as UV detector (Montluçon, France).

Thin layer chromatography

Thin layer chromatography (TLC) for conducted for reaction monitoring silica gel 60 F_{254} (Merck, Darmstadt, Germany) or basic ALOX UV_{254} (Machery-Nagel, Düren, Deutschland). Non UV-active compounds were viewed in an I_2 chamber.

A.3. Chemicals

All starting materials, reagents and solvents (technical and HPLC grade) were purchased from Sigma Aldrich, Schnelldorf, Germany. Dry solvents used in synthesis were distilled over molecular sieve with 4 Å pore size. Only distilled water was used during synthesis or work-up. Millipore water was used for HPLC and LC/MS runs.

B. Chapter 1: Synthesis of the intermediates of AFDX-384

The intermediate compounds **I-IV** synthesized during the course of the attempt of synthesis of AFDX-384 were based on previously reported procedures.[55]

Synthesis and spectral data of 2-amino-*N*-(2-chloropyridin-3yl)benzamide **V**, 3-(2-chloropyridin-3-yl)quinazoline-2,4(1*H*,3*H*)-dione **VI** and 5,11-dihydropyrido-[2,3-b][1,4]benzodiazepin-6-one **VII** are discussed below.[58, 59, 61]

5.1. 2-Amino-*N*-(2-chloropyridin-3-yl)benzamide V
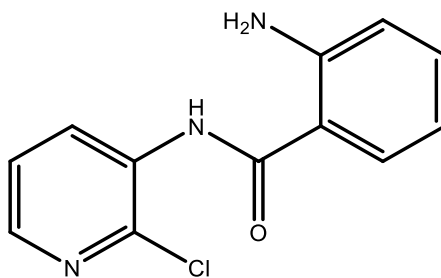
V

($C_{12}H_{10}ClN_3O$, MW: 247.68 g/mol)

3-Amino-2-chloropyridine (2.57 g, 20.0 mmol), ethyl 2-aminobenzoate (3.39 g, 20.5 mmol) and KOtBu (7.29 g, 65.0 mmol) were suspended in dry 1,4-dioxane (100 mL) under argon. The mixture was heated by microwaves (gradient of heating: 2 min to 60 °C; holding time: 10 min at 60 °C; gradient of heating: 3 min from 60-100 °C; holding time: 2.5 h at 100 °C). After cooling to 25 °C, the solution was treated with an aqueous solution of 1 M NaH_2PO_4 (60 mL) and stirred for 30 min. After phase separation, the organic phase was dried using anhydrous Na_2SO_4. The dioxane was evaporated under reduced pressure and the residue was treated with 50 mL water. The solid obtained was filtered, dried and purified by silica chromatography (ethyl acetate/petroleum ether 1:1) to obtain **V** (1.16 g, 23% yield).[58]

Compound **V**: pale-yellow solid; mp = 204 °C; R_f = 0.78 (silica gel, ethyl acetate/petroleum ether 1:1).[58]

IR (ATR), ṽ [cm^{-1}]: 3433 (NH), 3330, 3286 (NH_2), 3073 (CH), 1644 (C=O amide), 1616, 1578, 1569, 1503, 1486, 1391, 802, 743, 735.[58]

^{1}H NMR (400 MHz, DMSO-d$_6$, δ [ppm]): 9.89 (br, 1H, N**H**), 8.29 (dd*, J* = 4.7, 1.8 Hz, 1H, **H**-6$_{pyrid.}$), 8.07 (dd, *J* = 7.9, 1.8 Hz, 1H, **H**-4$_{pyrid.}$), 7.74 (dd, *J* = 8.1,1.5 Hz, 1H, **H**-6$_{benz.}$), 7.49 (dd, *J* = 7.9, 4.7 Hz, 1H, **H**-5$_{pyrid.}$), 7.24 (ddd, *J* = 8.4,7.1, 1.5 Hz, 1H, **H**-4$_{benz.}$), 6.79 (dd, *J* = 8.4, 1.2 Hz, 1H, **H**-3$_{benz.}$), 6.62 (ddd, *J* = 8.1, 7.1, 1.2 Hz, 1H, **H**-5$_{benz.}$), 6.47 (br, 2H, **NH$_2$**).[58]

^{13}C NMR (100 MHz, DMSO-d$_6$, δ [ppm]): 168.3 (**C**=O), 150.7 (**C**-2), 146.7 (**C**-Cl), 146.7 (**C**-6$_{pyrid.}$), 137.0 (**C**-4$_{pyrid.}$), 133.2 (**C**-4), 132.8 (**C**-3$_{pyrid.}$), 129.3 (**C**-6), 123.9 (**C**-5$_{pyrid.}$), 117.2 (**C**-3), 115.4 (**C**-5), 113.9 (**C**-1).[58]

MS (ESI), m/z: 248.20 [M+H]$^+$.[58]

5.2. 3-(2-Chloropyridin-3-yl)quinazoline-2,4(1*H*,3*H*)-dione VI
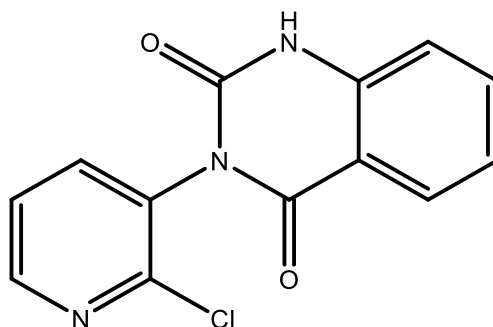
VI

(C$_{13}$H$_{18}$ClN$_3$O$_2$, MW: 273.68 g/mol)

Compound **V** (4.22 g, 20.0 mmol) and Hünig's base (7.0 mL, 40.0 mmol) were dissolved in dry 1,4-dioxane (150 mL) under argon. A solution of 20% phosgene in toluene (18.5 mL, 35.0 mmol) was added dropwise over 30 min. The solution was heated using microwaves (gradient of heating: 3 min to 85 °C; holding time: 2 hrs at to 85 °C). After cooling to 85 °C, the mixture was quenched with 1 M NaH$_2$PO$_4$ (100 mL) and stirred for 1 hr at room temperature. After phase separation, the organic phase was dried using anhydrous Na$_2$SO$_4$. The dioxane was evaporated and the solid obtained was filtered by suction and dried over P$_4$O$_{10}$, giving a white solid. The product **VI** was crystallized from chloroform (4.68 g, 86% yield).[59]

Compound **VI**: colourless block-like crystals; mp = 237 °C.[59]

IR (ATR), ṽ [cm^{-1}]: 3348 (NH), 3072 (CH), 1680 (C=O), 1730 (C=O), 1580, 734.[59]

^{1}H NMR (400 MHz, CDCl$_3$, δ [ppm]): 10.52 (br,1H, N**H**), 8.56 (dd, J = 4.8, 1.8 Hz, 1H, **H**-6$_{pyrid.}$), 8.15 (dd, J = 7.9, 1.1 Hz, 1H, **H**-5$_{quinaz.}$), 7.76 (dd, J = 7.8, 1.8 Hz, 1H, **H**-4$_{pyrid.}$), 7.61 (ddd, J = 8.1, 7.0, 1.1 Hz, 1H, **H**-7$_{quinaz.}$), 7.46 (dd, J = 7.8, 4.8 Hz, 1H, **H**-5$_{pyrid.}$), 7.27 (ddd, J = 7.9, 7.0, 1.0 Hz, 1H, **H**-6$_{quinaz.}$), 7.02 (dd, J = 8.1, 1.0 Hz, 1H, **H**-8$_{quinaz.}$).[59]

^{13}C NMR (100 MHz, CDCl$_3$, δ [ppm]): 161.6 (4-**C**=O), 151.0 (2-**C**=O), 150.4 (**C**-Cl), 149.9 (**C**-6$_{pyrid.}$), 139.6 (**C**-4$_{pyrid.}$), 138.9 (**C**-8a$_{quinaz.}$), 135.9 (**C**-7$_{quinaz.}$), 129.9 (**C**-3$_{pyrid.}$), 128.7 (**C**-5$_{quinaz.}$), 124.0 (**C**-6$_{quinaz.}$), 123.4 (**C**-5$_{pyrid.}$), 115.7 (**C**-8$_{quinaz.}$), 114.3 (**C**-4a$_{quinaz.}$).[59]

MS (ESI), m/z: 274.60 [M+H]$^+$.[59]

5.3. Synthesis of 5,11-dihydro-6*H*-pyrido [2,3-*b*][1,4] benzodiazepine-6-one VII
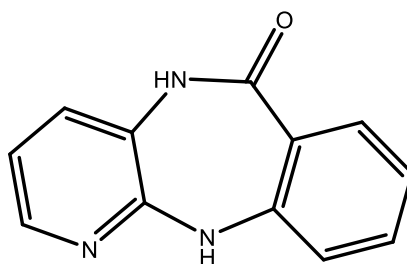
VII

**(C$_{12}$H$_9$N$_3$O, MW: 211.22 g/mol)**

Compound **V** (100 mg, 0.40 mmol) was dissolved in 100 mL of ethylene glycol and heated under reflux overnight. During the workup of the reaction, the product was extracted in toluene, followed by evaporation of the solvent under reduced pressure and finally crystallization of the product from methanol and toluene to obtain **VII** (17 mg, 20% yield).[60]

Compound **VII**: colourless crystals; R$_f$ = 0.54 (silica gel, EtOAc).

The spectroscopic data for this compound are in accordance with the literature.[55]

5.4. Methyl-6-oxo-5,6-dihydro-11*H*-benzo[e]pyrido[3,2-*b*][1,4]diazepine-11-carboxylate **IX**
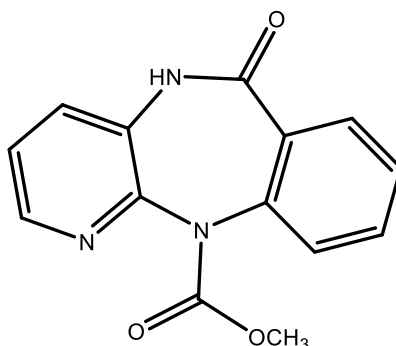
IX

(C14H11N3O3, MW: 269.26 g/mol)

Compound **V** (50 mg, 0.20 mmol) and Hünig's base (0.1 mL, 0.40 mmol) were dissolved in dry 1,4-dioxane (150 mL) under argon. A solution of 20% phosgene in toluene (0.2 mL, 0.35 mmol) was added dropwise over a period of 30 min. The solution was heated under reflux overnight. After cooling to room temperature, the mixture was quenched with 1 M NaH2PO4 (100 mL) and stirred for 1 hr. After phase separation, the organic phase was dried using anhydrous Na2SO4. The solvent was then evaporated under reduced pressure and the residue was purified by silica gel chromatography (EtOAc/CH2Cl2/MeOH 20:10:0.5) to give **IX** (15 mg, 28% yield). (Modified from literature:[55]).

Compound **IX**: pale white powder; R_f = 0.31 (silica gel, EtOAc/CH2Cl2/MeOH 20:10:0.5).

^{1}H NMR (400 MHz, DMSO-d_6, δ [ppm]): 10.85 (s, 1H, N**H**), 8.27 (dd, *J* = 4.6, 1.7 Hz, 1H, **H**-2), 7.77 (dd, *J* = 7.8, 1.3 Hz, 1H, **H**-7), 7.71 − 7.63 (m, 2H, **H**-4, **H**-9), 7.52 (dd, *J* = 8.1, 0.8 Hz, 1H, **H**-10), 7.50 − 7.44 (m, 1H, **H**-8), 7.41 (dd, *J* = 8.0, 4.6 Hz, 1H, **H**-3), 3.65 (s, 3H, OC**H3**).

^{13}C NMR (100 MHz, DMSO-d_6, δ [ppm]): 166.2 (6-**C**=O), 153.4 (12-**C**=O), 145.1 (**C**-11a), 144.8 (**C**-2), 140.4 (**C**-10a), 133.2 (**C**-9), 131.1 (**C**-4a), 130.8 (**C**-4), 130.7 (**C**-7), 129.7 (**C**-6a), 128.3 (**C**-8), 128.0 (**C**-10), 124.4 (**C**-3), 53.3 (OC**H3**).

C. Chapter 2: Synthesis of dualsteric hybrids

The procedures reported in literature were used for the synthesis of phthalimidopropylamine **1**,[64] 1,8-naphthalimidopropylamine **6**,[64] and the iperoxo base **26**.[66]

5.5. Synthesis of phthalimide/1,8-naphthalimide-pirenzepine hybrids 13-19

5.5.1. General procedure A for the synthesis of phthalimido/1,8-napthalimido monoquaternary bromides 2-5 and 7-10

The corresponding imide (1 equiv.), either phthalimidopropylamine **1** or 1,8-naphthalimidopropylamine **6**, was dissolved in an excess of the corresponding alkyl dibromide (15 equiv.) and stirred in the microwave at 80 °C (ramp: 20 °C/min, 800W). The reaction was generally found to be completed after approximately 3 hrs (silica gel TLC monitoring, $CHCl_3$/MeOH/NH_3 100:10:1). After cooling to room temperature, the obtained precipitate was filtered off and washed with hot diethyl ether.[64]

5.5.1.1. 4-Bromo-*N*-(3-(1,3-dioxoisoindolin-2-yl)propyl)-*N*,*N*-dimethylbutan-1-aminium bromide 2
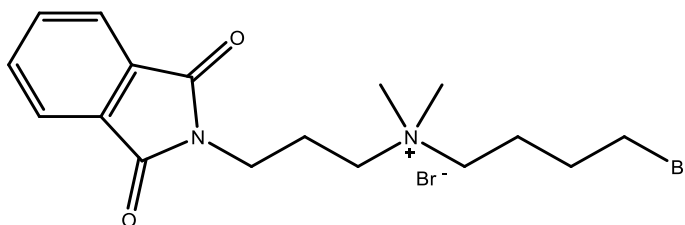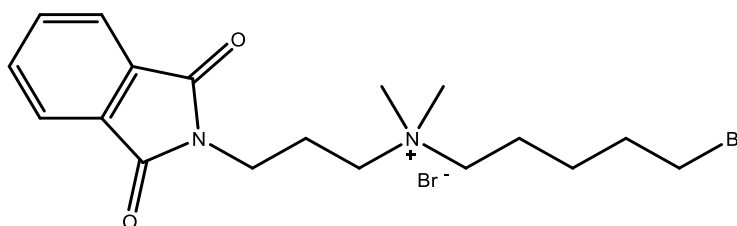

2

($C_{17}H_{24}Br_2N_2O_2$, MW: 448.19 g/mol)

Phthalimidopropylamine **1** (1.00 g, 4.31 mmol) and 1,4-dibromobutane (7.7 mL, 64.65 mmol) were used as reactants to give **2** (1.64 g, 85% yield).

Compound **2**: white solid; R_f = 0.26 (silica gel, CHCl$_3$/MeOH/NH$_3$ 100:10:1).

The spectroscopic data for this compound are in accordance with the literature.[77]

5.5.1.2. 5-Bromo-*N*-(3-(1,3-dioxoisoindolin-2-yl)propyl)-*N*,*N*-dimethylpentan-1-aminium bromide 3

3

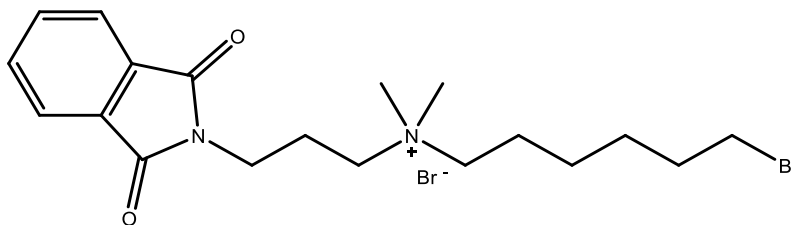**(C$_{18}$H$_{26}$Br$_2$N$_2$O$_2$, MW: 462.23 g/mol)**

Phthalimidopropylamine **1** (1.00 g, 4.31 mmol) and 1,5-dibromopentane (8.8 mL, 64.65 mmol) were used as reactants to give **3** (1.43 g, 72% yield).

Compound **3**: white solid; R_f = 0.30 (silica gel, CHCl$_3$/MeOH/NH$_3$ 100:10:1).

^{1}H NMR (400 MHz, CD$_3$OD, δ [ppm]): 7.89 – 7.84 (m, 2H, arom.), 7.84 – 7.79 (m, 2H, arom.), 3.81 (t, *J* = 6.5 Hz, 2H, N$_{phth}$-**CH$_2$**), 3.52 – 3.43 (m, 4H, **CH$_2$**-N$^+$, $^+$N-**CH$_2$**), 3.41 – 3.33 (m, 2H, **CH$_2$**-Br), 3.12 (s, 6H, $^+$N(**CH$_3$**)$_2$), 2.26 – 2.14 (m, 2H, N$_{phth}$-CH$_2$-**CH$_2$**), 1.98 – 1.87 (m, 2H, $^+$N-CH$_2$-**CH$_2$**), 1.85 – 1.74 (m, 2H, $^+$N-CH$_2$-(CH$_2$)$_2$-**CH$_2$**), 1.58 – 1.46 (m, 2H, $^+$N-CH$_2$-CH$_2$-**CH$_2$**).

^{13}C NMR (100 MHz, CD$_3$OD, δ [ppm]): 169.8 (2C, **C**=O), 135.5 (2C, **CH**$_{arom.}$), 133.3 (2C, **C**$_{arom.}$), 124.2 (2C, **CH**$_{arom.}$), 65.3 (**CH$_2$**-Br), 63.0 (**CH$_2$**-N$^+$), 51.4 (2C, $^+$N(**CH$_3$**)$_2$), 35.8 (N$_{phth}$-**CH$_2$**), 33.9 ($^+$N-**CH$_2$**), 33.2 ($^+$N-CH$_2$-**CH$_2$**), 25.9 ($^+$N-CH$_2$-CH$_2$-**CH$_2$**), 23.3 (N$_{phth}$-CH$_2$-**CH$_2$**), 22.8 ($^+$N-CH$_2$-(CH$_2$)$_2$-**CH$_2$**).

5.5.1.3. 6-Bromo-*N*-(3-(1,3-dioxoisoindolin-2-yl)propyl)-*N*,*N*-dimethylhexan-1-aminium bromide 4

4

(C$_{19}$H$_{28}$Br$_2$N$_2$O$_2$, MW: 474.05 g/mol)
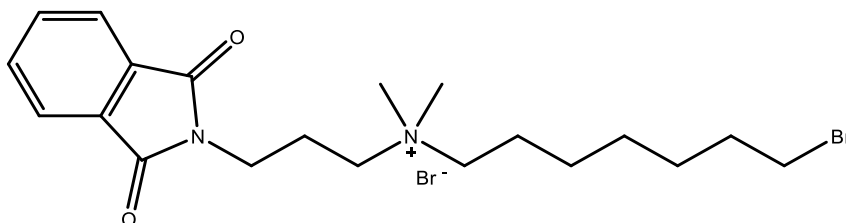
Phthalimidopropylamine **1** (1.00 g, 4.31 mmol) and 1,6-dibromohexane (9.9 mL, 64.65 mmol) were used as reactants to give **4** (1.39 g, 68% yield).

Compound **4**: white solid; R$_f$ = 0.29 (silica gel, CHCl$_3$/MeOH/NH$_3$ 100:10:1).

The spectroscopic data for this compound are in accordance with the literature.[78, 79]

5.5.1.4. 7-Bromo-*N*-(3-(1,3-dioxoisoindolin-2-yl)propyl)-*N*,*N*-dimethylheptan-1-aminium bromide 5


5

(C$_{20}$H$_{30}$Br$_2$N$_2$O$_2$, MW: 490.28 g/mol)

Phthalimidopropylamine **1** (1.00 g, 4.31 mmol) and 1,7-dibromoheptane (11.0 mL, 64.65 mmol) were used as reactants to give **5** (1.92 g, 91% yield).

Compound **5**: white solid; R_f = 0.32 (silica gel, CHCl$_3$/MeOH/NH$_3$ 100:10:1).

The spectroscopic data for this compound are in accordance with the literature.[80]

5.5.1.5. 4-Bromo-*N*-(3-(1,3-dioxo-1*H*-benzo[*de*]isoquinolin-2(3*H*)-yl)-2,2-dimethylpropyl)-*N,N*-dimethylbutan-1-aminium bromide 7
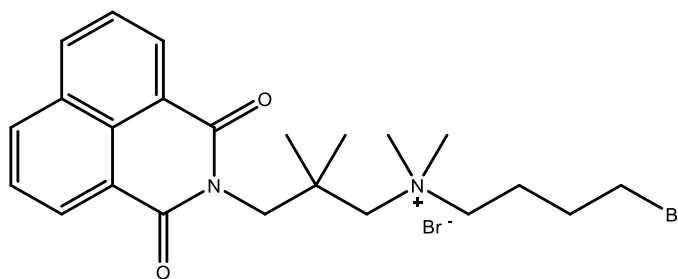
7

(C$_{23}$H$_{30}$Br$_2$N$_2$O$_2$, MW: 526.31 g/mol)

1,8-Naphthalimidopropylamine **6** (1.00 g, 3.23 mmol) and 1,4-dibromobutane (5.8 mL, 48.45 mmol) were used as reactants to give **7** (1.24 g, 73% yield).

Compound **7**: beige solid; R_f = 0.24 (silica gel, CHCl$_3$/MeOH/NH$_3$ 100:10:1).

The spectroscopic data for this compound are in accordance with the literature.[79]

5.5.1.6. 5-Bromo-*N*-(3-(1,3-dioxo-1*H*-benzo[*de*]isoquinolin-2(3*H*)-yl)-2,2-dimethylpropyl)-*N*,*N*-dimethylpentan-1-aminium bromide 8
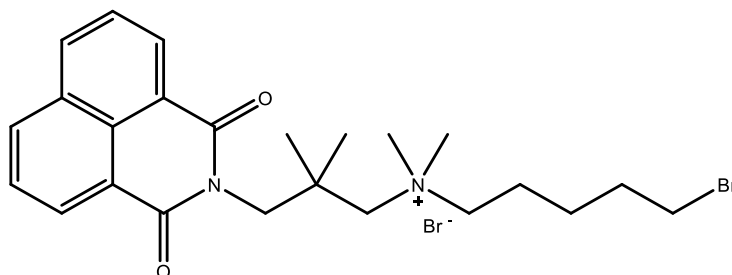

8

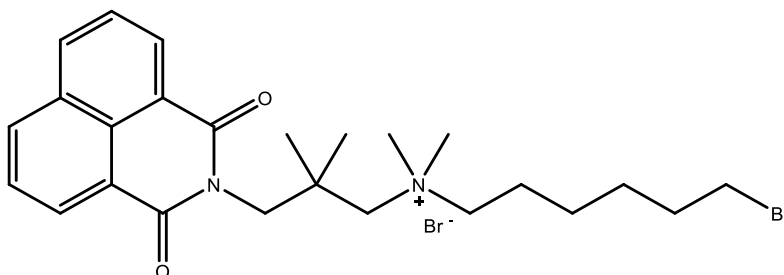**(C$_{24}$H$_{32}$Br$_2$N$_2$O$_2$, MW: 540.34 g/mol)**

1,8-Naphthalimidopropylamine **6** (1.00 g, 3.23 mmol) and 1,5-dibromopentane (6.6 mL, 48.45 mmol) were used as reactants to give **8** (1.41 g, 81% yield).

Compound **8**: beige solid; R$_f$ = 0.26 (silica gel, CHCl$_3$/MeOH/NH$_3$ 100:10:1).

^{1}H NMR (400 MHz, CD$_3$OD, δ [ppm]): 8.60 (dd, *J* = 7.3, 1.0 Hz, 2H, arom.), 8.40 (dd, *J* = 8.4, 1.0 Hz, 2H, arom.), 7.89 – 7.81 (m, 2H, arom.), 4.32 (s, 2H, N$_{naphth}$-**CH$_2$**), 3.54 (s, 2H, **CH$_2$**-N$^+$), 3.52 – 3.44 (m, 4H, $^+$N-**CH$_2$**, **CH$_2$**-Br), 3.29 (s, 6H, $^+$N(**CH$_3$**)$_2$), 2.00 – 1.88 (m, 4H, $^+$N-CH$_2$-**CH$_2$**, $^+$N-CH$_2$-(CH$_2$)$_2$-**CH$_2$**), 1.57 – 1.49 (m, 2H, $^+$N-CH$_2$-CH$_2$-**CH$_2$**), 1.35 (s, 6H, C(**CH$_3$**)$_2$).

^{13}C NMR (100 MHz, CD$_3$OD, δ [ppm]): 166.8 (2C, **C**=O), 135.8 (2C, **C**H$_{arom.}$), 133.2 (**C**$_{arom.}$), 132.6 (2C, **C**H$_{arom.}$), 129.4 (**C**$_{arom.}$), 128.3 (2C, **C**H$_{arom.}$), 123.6 (2C, **C**$_{arom.}$), 69.8, 66.9, 53.2 (2C, $^+$N(**C**H$_3$)$_2$), 50.1, 40.5 (**C**(CH$_3$)$_2$), 34.0, 33.1, 27.8, 26.5 (2C, C(**C**H$_3$)$_2$), 23.1.

5.5.1.7. 6-Bromo-*N*-(3-(1,3-dioxo-1*H*-benzo[*de*]isoquinolin-2(3*H*)-yl)-2,2-dimethylpropyl)-*N*,*N*-dimethylhexan-1-aminium bromide 9
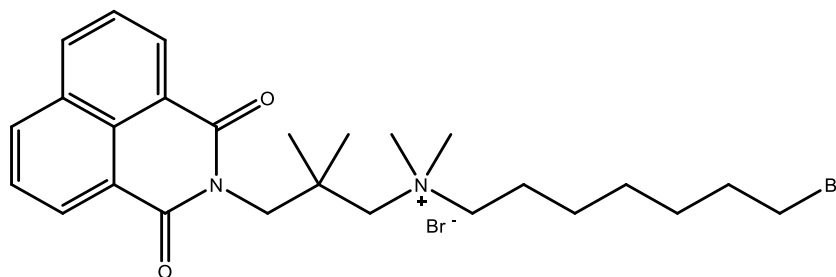

9

(C25H34Br2N2O2, MW: 554.37 g/mol)

1,8-Naphthalimidopropylamine **6** (1.00 g, 3.23 mmol) and 1,6-dibromohexane (7.5 mL, 48.45 mmol) were used as reactants to give **9** (1.68 g, 94% yield).

Compound **9**: beige solid; R_f = 0.28 (silica gel, CHCl₃/MeOH/NH₃ 100:10:1).

The spectroscopic data for this compound are in accordance with the literature.[53]

5.5.1.8. 7-Bromo-*N*-(3-(1,3-dioxo-1*H*-benzo[*de*]isoquinolin-2(3*H*)-yl)-2,2-dimethylpropyl)-*N*,*N*-dimethylheptan-1-aminium bromide 10


10

(C26H36Br2N2O2, MW: 568.39 g/mol)

1,8-Naphthalimidopropylamine **6** (1.00 g, 3.23 mmol) and 1,7-dibromoheptane (8.3 mL, 48.45 mmol) were used as reactants to give **10** (1.40 g, 76% yield).

Compound **10**: beige solid; R_f = 0.25 (silica gel, $CHCl_3$/MeOH/NH_3 100:10:1).

The spectroscopic data for this compound are in accordance with the literature.[80]

### 5.5.2. 11-(2-Chloroacetyl)-5,11-dihydro-6H-benzo[e]pyrido[3,2-b][1,4]diazepin-6-one 11
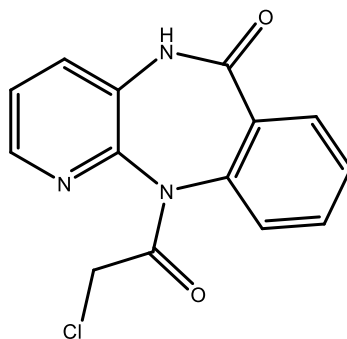
11

($C_{14}H_{10}ClN_3O_2$, MW: 287.70 g/mol)

A suspension of the benzopyridodiazepine **VII** (see Chapter 1) (2.56 g, 12.13 mmol) in dioxane (50 mL) was refluxed for 15 min and then allowed to cool to room temperature before adding Et_3N (2.1 mL, 14.62 mmol). Chloroacetyl chloride (1.2 mL, 14.62 mmol) was added dropwise, under stirring, to this solution during a period of 30 min. The mixture was then refluxed for 8 hrs. After the mixture was cooled, the precipitate was removed by filtration on a celite pad and washed with dioxane. The crude filtrate was evaporated and purified by silica gel column chromatography (EtOAc/hexane 3:7 to 7:3) to give **11** (2.25 g, 64.5% yield).[56]

Compound **11**: pale white solid; R_f = 0.37 (silica gel, EtOAc/hexane 7:3).

The spectroscopic data for this compound are in accordance with the literature.[56]

5.5.3. 11-(2-(Piperazin-1-yl)acetyl)-5,11-dihydro-6H-benzo[e]pyrido[3,2-b][1,4]diazepin-6-one 12
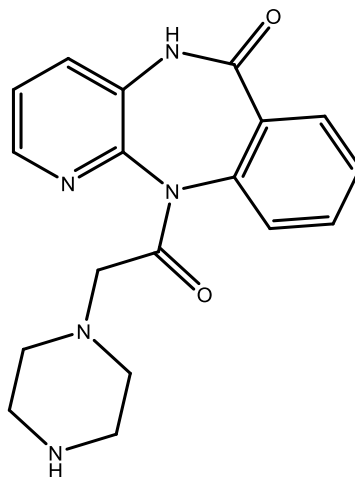
12

($C_{18}H_{19}N_5O_2$, MW: 337.38 g/mol)

To a solution of the chloroacetyl intermediate **11** (0.76 g, 2.64 mmol) in acetonitrile (100 mL), 20-fold excess amount of piperazine (4.55 g, 52.83 mmol) was added. To this solution, catalytic amount of a 1:1 mixture of KI/K_2CO_3 was added. The mixture was then stirred in the microwave for 2 hrs at 80 °C (ramp: 20 °C/min, 800W). The solvent was evaporated under reduced pressure, after which the residue was allowed to attain room temperature. To this residue, distilled water (50 mL) and $CHCl_3$ (50 mL) were added. The mixture was shaken and the phases were separated in a separating funnel. The aqueous phase was then washed with $CHCl_3$ (3 X 50 mL), combining all the organic phases which were then washed with distilled water, dried over Na_2SO_4 and evaporated under reduced pressure. The residue was purified by silica gel chromatography after dissolution in minimum amount of the mobile phase ($CHCl_3$/MeOH/NH_3 100:10:1) to give *N*-desmethyl pirenzepine **12** (0.64 g, 72% yield). This molecule is synthesized according to a modification of a procedure for similar compounds in literature.[56]

Compound **12**: pale white solid; R_f = 0.21 (silica gel, $CHCl_3$/MeOH/NH_3 100:10:1).

The spectroscopic data for this compound are in accordance with the literature.[67]

5.5.4. General procedure B for the synthesis of phthalimide-pirenzepine hybrids 13-15

To a stirred acetonitrile solution of the corresponding intermediate **2**, **3** or **4** (1 equiv.), *N*-desmethyl pirenzepine **12** (1.1 equiv.) was added and dissolved. The reaction was stirred in the microwave for 7 hrs at 80 °C (ramp: 20 °C/min, 800W), after which the solvent was evaporated under reduced pressure (silica gel TLC monitoring, 0.2 M aqueous KNO_3/MeOH 2:3). The residue was purified using basic ALOX column chromatography, with or without further purification using C18 reverse phase silica gel flash chromatography using a linear gradient of water: solvent A and methanol: solvent B (B% from 0% to 100% in 60 min) followed by a plateau phase (100% methanol for 30 min) yielding the pure product **13**, **14** or **15**, respectively, as the last fraction using UV detection.

5.5.4.1. *N*-(3-(1,3-Dioxoisoindolin-2-yl)propyl)-*N,N*-dimethyl-4-(4-(2-oxo-2-(6-oxo-5,6-dihydro-11*H*-benzo[*e*]pyrido[3,2-*b*][1,4]diazepin-11-yl)ethyl)piperazin-1-yl)butan-1-aminium bromide 13
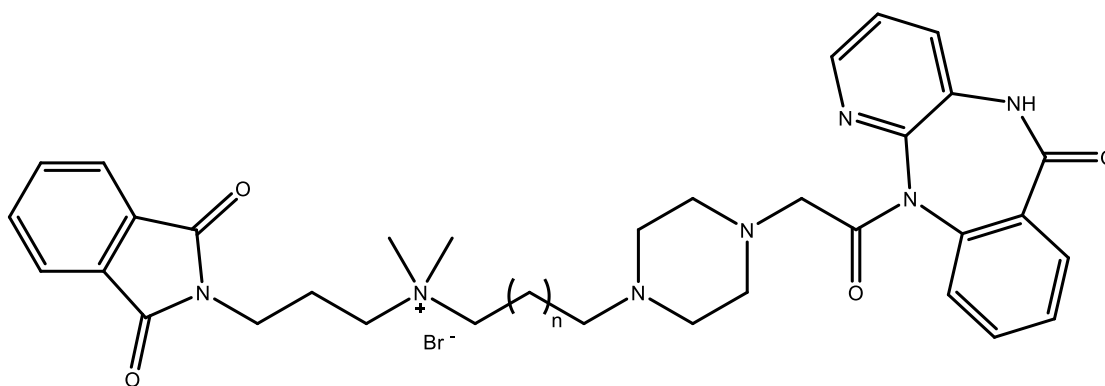
13, (n = 2)

(C_{35}H_{42}BrN_7O_4, MW: 704.66 g/mol)

The intermediate **2** (142 mg, 0.27 mmol) and *N*-desmethyl pirenzepine **12** (100 mg, 0.30 mmol) were used as reactants, and the product was purified using only basic ALOX column chromatography (CHCl$_3$/MeOH/NH$_3$ 100:10:1) to give **13** (66 mg, 35% yield).

Compound **13**: pale white solid; R_f = 0.40 (silica gel, 0.2 M aqueous KNO$_3$/MeOH 2:3).

IR (ATR), ṽ [cm^{-1}]: 3368, 3033, 2959, 2839, 1770, 1647, 1597, 1458, 1402, 1359, 1262.

^{1}H NMR (400 MHz, CD$_3$OD, δ [ppm]): 8.31 (s, 1H, **H**-2$_{pirenz-arom.}$), 7.97 – 7.79 (m, 3H, **H**-10$_{pirenz-arom.}$ (1H), phth. (2H)), 7.71 – 7.64 (m, 1H, **H**-8$_{pirenz-arom.}$), 7.61 – 7.43 (m, 6H, , **H**-3$_{pirenz-arom.}$ (1H), **H**-4$_{pirenz-arom.}$ (1H), **H**-7$_{pirenz-arom.}$ (1H), **H**-9$_{pirenz-arom.}$ (1H), phth. (2H)), 3.66 (d, *J* = 14.4 Hz, 1H, C**H$_2$**-C=O), 3.59 – 3.39 (m, 6H, N$_{phth}$-C**H$_2$**, C**H$_2$**-N$^+$, $^+$N-C**H$_2$**), 3.30 – 3.05 (m, 9H, C**H$_2$**-C=O (1H), N(C**H$_2$CH$_2$**)$_2$N (8H)), 3.16 (s, 6H, $^+$N(C**H$_3$**)$_2$), 2.52 (br, 2H, $^+$N-CH$_2$-(CH$_2$)$_2$-C**H$_2$**), 2.11 (br, 2H, N$_{phth}$-CH$_2$-C**H$_2$**), 1.93 (br, 2H, $^+$N-CH$_2$-C**H$_2$**), 1.83 (br, 2H, $^+$N-CH$_2$-CH$_2$-C**H$_2$**).

^{13}C NMR (100 MHz, CD$_3$OD, δ [ppm]): 170.7 (2C, N$_{phth}$-**C**=O), 169.8 (NH-**C**=O), 168.9 (CH$_2$-**C**=O), 146.1, 141.6, 135.5, 134.3, 133.4, 133.0 (2C, **C**$_{phth.}$), 132.6, 132.2, 132.0, 130.8, 129.7 (2C, **C**H$_{phth.}$), 128.8, 126.0 (2C, **C**H$_{phth.}$), 124.3, 64.8, 63.3, 60.8 (**C**H$_2$-C=O), 57.0 (2C, N(CH$_2$**C**H$_2$)$_2$N-CH$_2$-C=O), 52.9 (2C, N(**C**H$_2$CH$_2$)$_2$N-CH$_2$-C=O), 51.7 (2C, $^+$N(**C**H$_3$)$_2$), 50.5, 37.4, 24.2, 22.0, 21.1.

MS (ESI), m/z: 321.60 [M-Br+NH$_4$]$^{2+}$

HPLC purity: 64%

5.5.4.2. *N*-(3-(1,3-Dioxoisoindolin-2-yl)propyl)-*N,N*-dimethyl-5-(4-(2-oxo-2-(6-oxo-5,6-dihydro-11*H*-benzo[*e*]pyrido[3,2-*b*][1,4]diazepin-11-yl)ethyl)piperazin-1-yl)pentan-1-aminium bromide 14
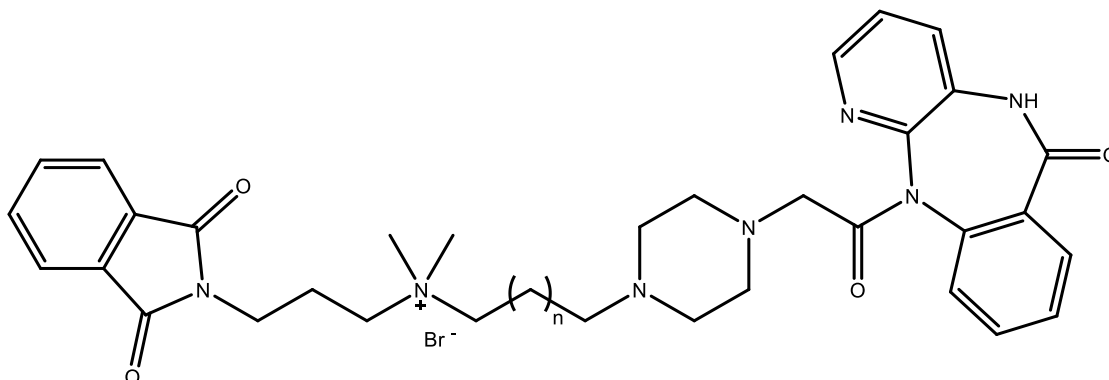
14, (n = 3)

($C_{36}H_{44}BrN_7O_4$, MW: 718.68 g/mol)

The intermediate **3** (145 mg, 0.27 mmol) and *N*-desmethyl pirenzepine **12** (100 mg, 0.30 mmol) were used as reactants and, and the product was purified using basic ALOX column chromatography (CHCl$_3$/MeOH/NH$_3$ 100:10:1), with further purification using C18 reverse phase silica gel flash chromatography (H$_2$O/MeOH solvent system) to give **14** (62 mg, 32% yield).

Compound **14**: pale white solid; R_f = 0.42 (silica gel, 0.2 M aqueous KNO$_3$/MeOH 2:3).

IR (ATR), ṽ [cm^{-1}]: 3362, 2945, 2821, 1734, 1648, 1558, 1457, 1362, 1267.

^{1}H NMR (400 MHz, CD$_3$OD, δ [ppm]): 8.27 (s, 1H, **H-2**$_{pirenz-arom.}$), 7.88 (d, *J* = 5.6 Hz, 1H, **H-10**$_{pirenz-arom.}$), 7.72 – 7.61 (m, 3H, **H-4**$_{pirenz-arom.}$ (1H), phth. (2H)), 7.58 – 7.47 (m, 2H, **H-8**$_{pirenz-arom.}$, **H-9**$_{pirenz-arom.}$), 7.47 – 7.41 (m, 3H, **H-7**$_{pirenz-arom.}$ (1H), phth. (2H)), 7.40 – 7.34 (m, 1H, **H-3**$_{pirenz-arom.}$), 3.64 – 3.40 (m, 6H, N$_{phth}$-**CH$_2$**, **CH$_2$**-N$^+$, $^+$N-**CH$_2$**), 3.37 – 3.26 (m, 2H, **CH$_2$**-C=O), 3.10 (s, 6H, $^+$N(**CH$_3$**)$_2$), 2.34 (br, 8H, N(**CH$_2$CH$_2$**)$_2$N), 2.17 (br, 2H, $^+$N-CH$_2$-(CH$_2$)$_3$-**CH$_2$**), 2.05 (br, 2H, N$_{phth}$-CH$_2$-**CH$_2$**), 1.80 (br, 2H, $^+$N-CH$_2$-**CH$_2$**), 1.60 – 1.49 (m, 2H, $^+$N-CH$_2$-(CH$_2$)$_2$-**CH$_2$**), 1.41 – 1.31 (m, 2H, $^+$N-CH$_2$-CH$_2$-**CH$_2$**).

^{13}C NMR (100 MHz, CD$_3$OD, δ [ppm]): 176.1 (2C, N$_{phth}$-**C**=O), 173.4 (NH-**C**=O), 171.5 (CH$_2$-**C**=O), 145.7, 140.8, 136.1, 134.0, 132.7 (2C, **C**$_{phth.}$), 131.8, 131.6, 130.8, 130.4, 129.7 (2C, **CH**$_{phth.}$), 129.4, 128.5 (2C, **CH**$_{phth.}$), 125.7, 125.7, 65.4 (**CH**$_2$-C=O), 63.6, 58.9 (2C, N(CH$_2$**CH**$_2$)$_2$N-CH$_2$-C=O), 53.6 (2C, N(**CH**$_2$CH$_2$)$_2$N-CH$_2$-C=O), 53.3, 51.0 (2C, $^+$N(**CH**$_3$)$_2$), 37.2 (2C), 26.7, 25.2, 24.0, 23.2.

MS (ESI), m/z: 328.70 [M-Br+NH$_4$] $^{2+}$

HPLC purity: 98%

5.5.4.3. *N*-(3-(1,3-Dioxoisoindolin-2-yl)propyl)-*N,N*-dimethyl-6-(4-(2-oxo-2-(6-oxo-5,6-dihydro-11*H*-benzo[e]pyrido[3,2-*b*][1,4]diazepin-11-yl)ethyl)piperazin-1-yl)hexan-1-aminium bromide 15
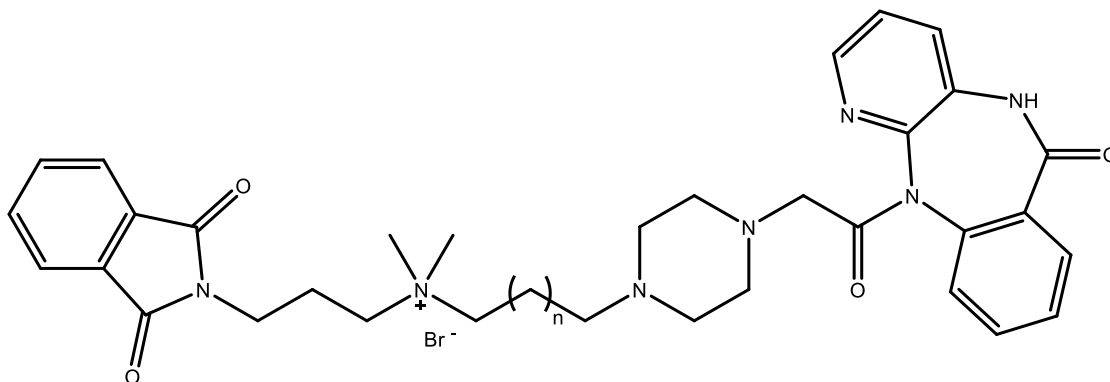
15, (n = 4)

(C$_{37}$H$_{46}$BrN$_7$O$_4$, MW: 732.71 g/mol)

The intermediate **4** (107 mg, 0.27 mmol) and *N*-desmethyl pirenzepine **12** (100 mg, 0.30 mmol) were used as reactants, and the product was purified using basic ALOX column chromatography (CHCl$_3$/MeOH/NH$_3$ 100:10:1), with further purification using C18 reverse phase silica gel flash chromatography (H$_2$O/MeOH solvent system) to give **15** (58 mg, 30% yield).

Compound **15**: pale white solid; R_f = 0.44 (silica gel, 0.2 M aqueous KNO_3/MeOH 2:3).

IR (ATR), $\tilde{\nu}$ [cm^{-1}]: 3402, 2935, 2823, 1656, 1561, 1459, 1367, 1263.

^{1}H NMR (400 MHz, CD$_3$OD, δ [ppm]): 8.28 (s, 1H, **H**-2$_{pirenz-arom.}$), 7.88 (d, J = 7.1 Hz, 1H, **H**-10$_{pirenz-arom.}$), 7.73 – 7.62 (m, 3H, **H**-4$_{pirenz-arom.}$ (1H), phth. (2H)), 7.57 – 7.47 (m, 2H, **H**-8$_{pirenz-arom.}$, **H**-9$_{pirenz-arom.}$), 7.46 – 7.41 (m, 3H, **H**-7$_{pirenz-arom.}$ (1H), phth. (2H)), 7.41 – 7.34 (m, 1H, **H**-3$_{pirenz-arom.}$), 3.60 – 3.48 (m, 4H, N$_{phth}$-**CH$_2$**, **CH$_2$**-N$^+$), 3.45 (t, J = 5.9 Hz, 2H, $^+$N-**CH$_2$**), 3.36 – 3.27 (m, 2H, C**H$_2$**-C=O), 3.10 (s, 6H, $^+$N(C**H$_3$**)$_2$), 2.35 (br, 8H, N(C**H$_2$CH$_2$**)$_2$N), 2.18 (br, 2H, $^+$N-CH$_2$-(CH$_2$)$_4$-C**H$_2$**), 2.05 (br, 2H, N$_{phth}$-CH$_2$-C**H$_2$**), 1.79 (br, 2H, $^+$N-CH$_2$-C**H$_2$**), 1.51 (br, 2H, $^+$N-CH$_2$-CH$_2$-C**H$_2$**), 1.39 (br, 4H, $^+$N-CH$_2$-(CH$_2$)$_2$-C**H$_2$**, $^+$N-CH$_2$-(CH$_2$)$_3$-C**H$_2$**).

^{13}C NMR (100 MHz, CD$_3$OD, δ [ppm]): 176.0 (2C, N$_{phth}$-**C**=O), 173.4 (NH-**C**=O), 171.4 (CH$_2$-**C**=O), 148.2, 145.8, 141.7, 140.7, 136.2 (2C, **C**$_{phth.}$), 134.3, 132.7, 132.0, 131.7, 130.8 (2C, **C**H$_{phth.}$), 129.5, 129.3 (2C, **C**H$_{phth.}$), 128.5, 125.8, 65.7 (**C**H$_2$-C=O), 63.6, 61.9, 59.1 (2C, N(CH$_2$**C**H$_2$)$_2$N-CH$_2$-C=O), 53.6 (2C, N(**C**H$_2$CH$_2$)$_2$N-CH$_2$-C=O), 53.2, 51.1 (2C, $^+$N(**C**H$_3$)$_2$), 37.4 (2C), 27.9, 27.1, 24.1, 23.4.

MS (ESI), m/z: 335.65 [M-Br+NH$_4$]$^{2+}$

HPLC purity: 99%

5.5.5. General procedure C for the synthesis of phthalimide/1,8-naphthalimide-pirenzepine hybrids 16-19

To a stirred acetonitrile solution of the corresponding intermediate **5**, **8**, **9** or **10** (1 equiv.), *N*-desmethyl pirenzepine **12** (1.1 equiv.) was added and dissolved. The reaction was stirred at 35 °C under inert conditions for 7 days (silica gel TLC monitoring, 0.2 M aqueous KNO₃/MeOH 2:3). The product either directly crystallized from the reaction mixture during the reaction time and was hence obtained by vacuum filtration followed by washing with cold acetonitrile, or, in case of no crystallization, the product was obtained by evaporation of the solvent under reduced pressure followed by purification using C18 reverse phase silica gel flash chromatography using a linear gradient of water: solvent A and methanol: solvent B (B% from 0% to 100% in 60 min) followed by a plateau phase (100% methanol for 30 min) yielding the pure product **16**, **17**, **18** or **19**, respectively, as the last fraction using UV detection.

5.5.5.1. *N*-(3-(1,3-Dioxoisoindolin-2-yl)propyl)-*N,N*-dimethyl-7-(4-(2-oxo-2-(6-oxo-5,6-dihydro-11*H*-benzo[e]pyrido[3,2-b][1,4]diazepin-11-yl)ethyl)piperazin-1-yl)heptan-1-aminium bromide 16
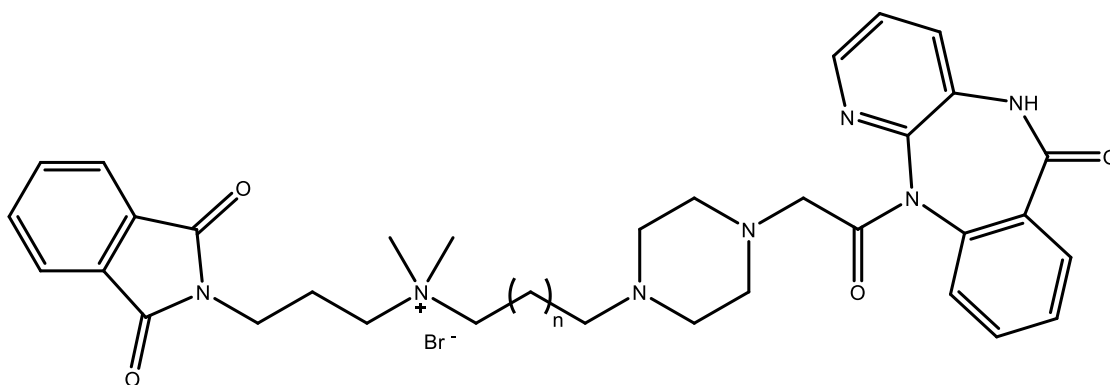
16, (n = 5)

(C₃₈H₄₈BrN₇O₄, MW: 746.75 g/mol)

The intermediate **5** (114 mg, 0.28 mmol) and *N*-desmethyl pirenzepine **12** (103 mg, 0.31 mmol) were used as reactants, and the crystallized product was filtered under vacuum and washed with cold acetonitrile to give **16** (93 mg, 45% yield).

Compound **16**: pale white solid; mp = 123 °C; R_f = 0.46 (silica gel, 0.2 M aqueous KNO_3/MeOH 2:3).

IR (ATR), $\tilde{v}$ [cm^{-1}]: 3421, 2980, 2681, 2606, 1769, 1707, 1651, 1456, 1394, 1350, 1264.

^{1}H NMR (400 MHz, CDCl$_3$, δ [ppm]): 8.17 (d, J = 5.9 Hz, 2H, **H**-2$_{pirenz-arom.}$, **H**-4$_{pirenz-arom.}$), 7.82 – 7.62 (m, 5H, **H**-10$_{pirenz-arom.}$ (1H), phth. (4H)), 7.60 – 7.50 (m, 2H, **H**-7$_{pirenz-arom.}$, **H**-8$_{pirenz-arom.}$), 7.40 – 7.32 (m, 1H, **H**-9$_{pirenz-arom.}$), 7.29 – 7.23 (m, 1H, **H**-3$_{pirenz-arom.}$), 3.92 (d, J = 13.7 Hz, 1H, C**H$_2$**-C=O), 3.82 (br, 2H, N$_{phth}$-C**H$_2$**), 3.58 (br, 4H, C**H$_2$**-N$^+$, $^+$N-C**H$_2$**), 3.49 (br, 4H, N(CH$_2$C**H$_2$**)$_2$N-CH$_2$-C=O), 3.30 (s, 6H, $^+$N(C**H$_3$**)$_2$), 3.27 – 3.03 (m, 5H, N(C**H$_2$**CH$_2$)$_2$N-CH$_2$-C=O (4H), C**H$_2$**-C=O (1H)), 2.96 – 2.56 (m, 4H, $^+$N-CH$_2$-C**H$_2$**, $^+$N-CH$_2$-(CH$_2$)$_5$-C**H$_2$**), 2.26 (br, 2H, N$_{phth}$-CH$_2$-C**H$_2$**), 2.09 – 1.72 (s, 4H, $^+$N-CH$_2$-(CH$_2$)$_3$-C**H$_2$**, $^+$N-CH$_2$-(CH$_2$)$_4$-C**H$_2$**), 1.39 (br, 4H, $^+$N-CH$_2$-CH$_2$-C**H$_2$**, $^+$N-CH$_2$-(CH$_2$)$_2$-C**H$_2$**).

^{13}C NMR (100 MHz, CDCl$_3$, δ [ppm]): 168.4 (2C, N$_{phth}$-**C**=O), 166.9 (CH$_2$-**C**=O), 161.0 (NH-**C**=O), 147.8, 144.1, 140.3, 134.5 (2C, **C**H$_{phth.}$), 132.9, 131.9 (2C, **C**$_{phth.}$), 131.5, 131.4, 131.1, 129.6, 128.4, 128.3, 123.9, 123.6 (2C, **C**H$_{phth.}$), 64.8, 62.2, 60.6 (**C**H$_2$-C=O), 56.5 (2C, N(CH$_2$**C**H$_2$)$_2$N-CH$_2$-C=O), 51.5 (2C, $^+$N(**C**H$_3$)$_2$), 50.8 (2C, N(**C**H$_2$CH$_2$)$_2$N-CH$_2$-C=O), 49.8, 49.0, 35.1, 27.2, 25.2, 22.8, 22.7, 22.2.

MS (ESI), m/z: 333.75 [M-Br+H]$^{2+}$

HPLC purity: 94%

5.5.5.2. *N*-(3-(1,3-Dioxo-1*H*-benzo[*de*]isoquinolin-2(3*H*)-yl)-2,2-dimethylpropyl)-*N,N*-dimethyl-5-(4-(2-oxo-2-(6-oxo-5,6-dihydro-11*H*-benzo[*e*]pyrido[3,2-*b*][1,4]diazepin-11-yl)ethyl)piperazin-1-yl)pentan-1-aminium bromide 17
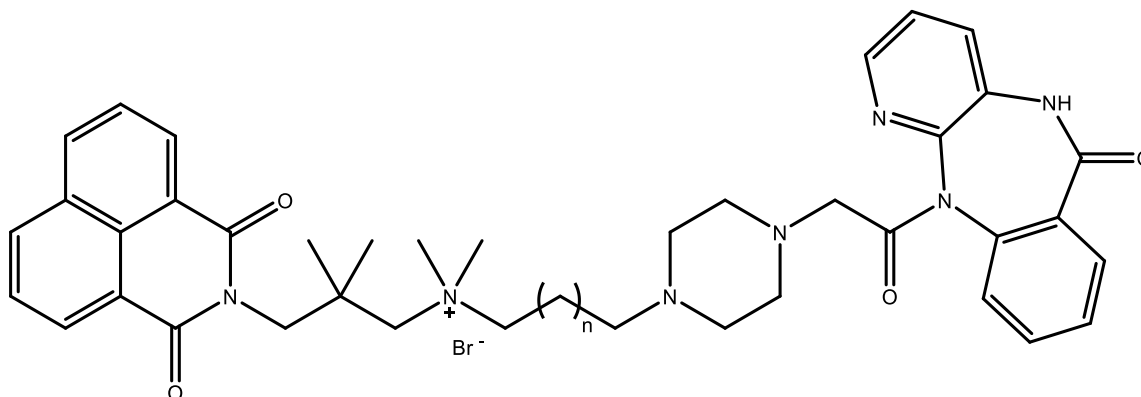
17, (n = 3)

(C$_{42}$H$_{50}$BrN$_7$O$_4$, MW: 796.81 g/mol)

The intermediate **8** (145 mg, 0.27 mmol) and *N*-desmethyl pirenzepine **12** (100 mg, 0.30 mmol) were used as reactants, and the product was purified using C18 reverse phase silica gel flash chromatography (H$_2$O/MeOH solvent system) to give **17** (66 mg, 31% yield).

Compound **17**: beige solid; R$_f$ = 0.39 (silica gel, 0.2 M aqueous KNO$_3$/MeOH 2:3).

IR (ATR), ṽ [cm^{-1}]: 3363, 2980, 1737, 1653, 1587, 1507, 1457, 1374, 1338, 1233.

^{1}H NMR (400 MHz, CDCl$_3$, δ [ppm]): 8.58 – 8.47 (m, 2H, naphth.), 8.28 – 8.16 (m, 2H, naphth.), 8.12 (d, *J* = 4.8 Hz, 1H, **H-2**$_{pirenz-arom.}$), 8.02 (d, *J* = 7.9 Hz, 1H, **H-4**$_{pirenz-arom.}$), 7.83 (d, *J* = 7.7 Hz, 1H, **H-10**$_{pirenz-arom.}$), 7.79 – 7.66 (m, 2H, naphth.), 7.59 – 7.47 (m, 2H, **H-7**$_{pirenz-arom.}$, **H-8**$_{pirenz-arom.}$), 7.35 – 7.28 (m, 1H, **H-9**$_{pirenz-arom.}$), 7.22 (dd, *J* = 7.9, 4.8 Hz, 1H, **H-3**$_{pirenz-arom.}$), 4.32 (s, 2H, N$_{naphth}$-**CH$_2$**), 3.73 (d, *J* = 15.1 Hz, 1H, CH$_2$-C=O), 3.67 – 3.60 (m, 2H, $^+$N-**CH$_2$**), 3.57 (s, 2H, **CH$_2$**-N$^+$), 3.51 (s, 6H, $^+$N(**CH$_3$**)$_2$), 2.96 (d, *J* = 15.1 Hz, 1H, CH$_2$-C=O), 2.50 – 2.19 (m, 6H, N(CH$_2$**CH$_2$**)$_2$N-CH$_2$-C=O (4H), $^+$N-CH$_2$-(CH$_2$)$_3$-**CH$_2$** (2H)), 2.19 – 1.96 (m, 4H, N(**CH$_2$**CH$_2$)$_2$N-CH$_2$-C=O), 1.90 (br, 2H, $^+$N-CH$_2$-**CH$_2$**), 1.49 (br, 2H, $^+$N-CH$_2$-(CH$_2$)$_2$-**CH$_2$**), 1.39 – 1.31 (m, 2H, $^+$N-CH$_2$-CH$_2$-**CH$_2$**), 1.31 (s, 6H, C(**CH$_3$**)$_2$).

^{13}C NMR (100 MHz, CDCl$_3$, δ [ppm]): 170.3 (CH$_2$-**C**=O), 168.3 (NH-**C**=O), 165.3 (2C, N$_{naphth}$-**C**=O), 143.9, 140.5, 134.7 (2C, **CH**$_{naphth.}$), 132.5, 132.0 (2C, **CH**$_{naphth.}$), 131.7 (2C, **CH**$_{pirenz-arom.}$), 131.1, 129.8, 128.2 (2C, **CH**$_{pirenz-arom.}$), 127.3 (2C, **CH**$_{naphth.}$), 124.7, 122.2 (2C, **C**$_{naphth.}$), 72.4, 68.5, 61.8 (**CH**$_2$-C=O), 60.0, 57.6 (2C, N(CH$_2$**CH**$_2$)$_2$N-CH$_2$-C=O), 53.0 (2C, $^+$N(**CH**$_3$)$_2$), 52.7 (2C, N(**CH**$_2$CH$_2$)$_2$N-CH$_2$-C=O), 48.4, 39.3 (**C**(CH$_3$)$_2$), 26.6 (2C, C(**CH**$_3$)$_2$), 25.1, 24.4, 22.6.

MS (ESI), m/z: 358.70 [M-Br+H]$^{2+}$

HPLC purity: 93%

5.5.5.3. *N*-(3-(1,3-Dioxo-1*H*-benzo[*de*]isoquinolin-2(3*H*)-yl)-2,2-dimethylpropyl)-*N*,*N*-dimethyl-6-(4-(2-oxo-2-(6-oxo-5,6-dihydro-11*H*-benzo[e]pyrido[3,2-*b*][1,4]diazepin-11-yl)ethyl)piperazin-1-yl)hexan-1-aminium bromide 18
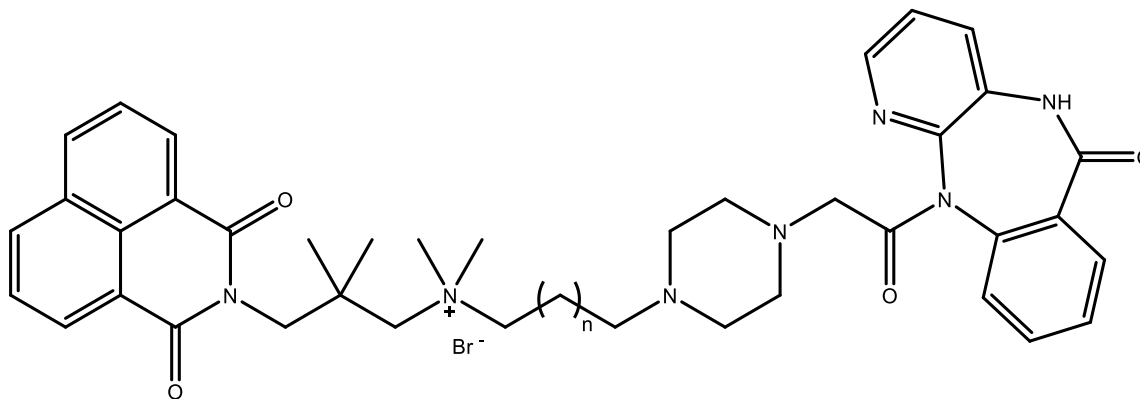
18, (n = 4)

(C$_{43}$H$_{52}$BrN$_7$O$_4$, MW: 810.84 g/mol)

The intermediate **9** (149 mg, 0.27 mmol) and *N*-desmethyl pirenzepine **12** (100 mg, 0.30 mmol) were used as reactants, and the product was purified using C18 reverse phase silica gel flash chromatography (H$_2$O/MeOH solvent system) to give **18** (69 mg, 31% yield).

Compound **18**: beige solid; R$_f$ = 0.43 (silica gel, 0.2 M aqueous KNO$_3$/MeOH 2:3).

IR (ATR), ṽ [cm^{-1}]: 3362, 2926, 2853, 1737, 1654, 1587, 1457, 1375, 1338, 1234.

^{1}H NMR (400 MHz, CDCl$_3$, δ [ppm]): 8.62 – 8.50 (m, 2H, naphth.), 8.30 – 8.18 (m, 2H, naphth.), 8.12 (d, J = 4.7 Hz, 1H, **H**-2$_{pirenz-arom.}$), 8.02 (d, J = 7.9 Hz, 1H, **H**-4$_{pirenz-arom.}$), 7.82 (d, J = 7.6 Hz, 1H, **H**-10$_{pirenz-arom.}$), 7.80 – 7.68 (m, 2H, naphth.), 7.59 – 7.43 (m, 2H, **H**-7$_{pirenz-arom.}$, **H**-8$_{pirenz-arom.}$), 7.36 – 7.29 (m, J = 6.9 Hz, 1H, **H**-9$_{pirenz-arom.}$), 7.21 (dd, J = 7.9, 4.7 Hz, 1H, **H**-3$_{pirenz-arom.}$), 4.33 (s, 2H, N$_{naphth}$-C**H$_2$**), 3.72 (d, J = 14.1 Hz, 1H, C**H$_2$**-C=O), 3.68 – 3.62 (m, 2H, $^+$N-C**H$_2$**), 3.60 (s, 2H, C**H$_2$**-N$^+$), 3.53 (s, 6H, $^+$N(C**H$_3$**)$_2$), 3.00 (d, J = 14.1 Hz, 1H, C**H$_2$**-C=O), 2.54 – 2.22 (m, 6H, N(CH$_2$C**H$_2$**)$_2$N-CH$_2$-C=O (4H), $^+$N-CH$_2$-(CH$_2$)$_4$-C**H$_2$** (2H)), 2.21 – 1.94 (m, 4H, N(C**H$_2$**CH$_2$)$_2$N-CH$_2$-C=O), 1.78 (br, 2H, $^+$N-CH$_2$-C**H$_2$**), 1.50 – 1.20 (m, 6H, $^+$N-CH$_2$-CH$_2$-C**H$_2$**, $^+$N-CH$_2$-(CH$_2$)$_2$-C**H$_2$**, $^+$N-CH$_2$-(CH$_2$)$_3$-C**H$_2$**), 1.33 (s, 6H, C(C**H$_3$**)$_2$).

^{13}C NMR (100 MHz, CDCl$_3$, δ [ppm]): 170.3 (CH$_2$-**C**=O), 167.8 (NH-**C**=O), 165.4 (2C, N$_{naphth}$-**C**=O), 143.6, 140.7, 134.7 (2C, **C**H$_{naphth.}$), 132.6, 132.0 (2C, **C**H$_{naphth.}$), 131.7 (2C, **C**H$_{pirenz-arom.}$), 131.0, 130.0, 128.2 (2C, **C**H$_{pirenz-arom.}$), 127.3 (2C, **C**H$_{naphth.}$), 123.8, 122.2 (2C, **C**$_{naphth.}$), 72.3, 68.7, 61.4 (**C**H$_2$-C=O), 59.1, 57.8 (2C, N(CH$_2$**C**H$_2$)$_2$N-CH$_2$-C=O), 53.2 (2C, $^+$N(**C**H$_3$)$_2$), 52.7 (2C, N(**C**H$_2$CH$_2$)$_2$N-CH$_2$-C=O), 48.6, 39.4 (**C**(CH$_3$)$_2$), 29.8, 26.6 (2C, C(**C**H$_3$)$_2$), 25.2, 22.3.

MS (ESI), m/z: 365.75 [M-Br+H]$^{2+}$

HPLC purity: 95%

5.5.5.4. *N*-(3-(1,3-Dioxo-1*H*-benzo[de]isoquinolin-2(3*H*)-yl)-2,2-dimethylpropyl)-*N,N*-dimethyl-7-(4-(2-oxo-2-(6-oxo-5,6-dihydro-11*H*-benzo[e]pyrido[3,2-b][1,4]diazepin-11-yl)ethyl)piperazin-1-yl)heptan-1-aminium bromide 19
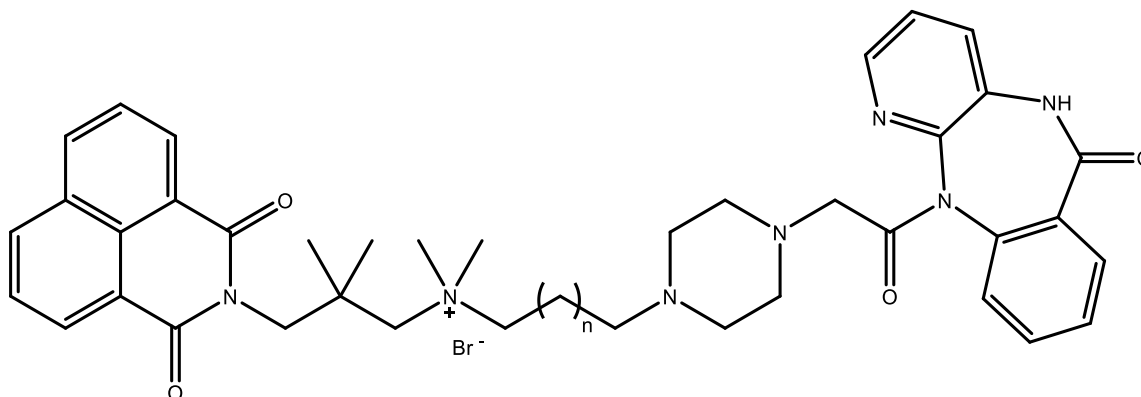
19, (n = 5)

($C_{44}H_{54}BrN_7O_4$, MW: 824.87 g/mol)

The intermediate **10** (130 mg, 0.23 mmol) and *N*-desmethyl pirenzepine **12** (85 mg, 0.25 mmol) were used as reactants, and the product was purified using C18 reverse phase silica gel flash chromatography (H_2O/MeOH solvent system) to give **19** (65 mg, 34% yield).

Compound **19**: beige solid; R_f = 0.45 (silica gel, 0.2 M aqueous KNO_3/MeOH 2:3).

IR (ATR), ṽ [cm^{-1}]: 3362, 2922, 2851, 1735, 1655, 1587, 1507, 1458, 1377, 1338, 1235.

^{1}H NMR (400 MHz, $CDCl_3$, δ [ppm]): 8.58 – 8.50 (m, 2H, naphth.), 8.28 – 8.18 (m, 2H, naphth.), 8.10 (d, *J* = 4.7 Hz, 1H, **H-2**$_{pirenz-arom.}$), 7.97 (d, *J* = 7.9 Hz, 1H, **H-4**$_{pirenz-arom.}$), 7.82 (d, *J* = 7.6 Hz, 1H, **H-10**$_{pirenz-arom.}$), 7.79 – 7.71 (m, 2H, naphth.), 7.57 – 7.42 (m, 2H, **H-7**$_{pirenz-arom.}$, **H-8**$_{pirenz-arom.}$), 7.34 – 7.27 (m, 1H, **H-9**$_{pirenz-arom.}$), 7.19 (dd, *J* = 7.9, 4.7 Hz, 1H, **H-3**$_{pirenz-arom.}$), 4.31 (s, 2H, N$_{naphth}$-**CH₂**), 3.78 – 3.69 (m, 2H, $^+$N-**CH₂**), 3.66 – 3.59 (m, 1H, **CH₂**-C=O), 3.54 (s, 2H, **CH₂**-N$^+$), 3.49 (s, 6H, $^+$N(**CH₃**)₂), 3.08 (d, *J* = 14.3 Hz, 1H, **CH₂**-C=O), 2.47 – 2.18 (m, 6H, N(CH₂**CH₂**)₂N-CH₂-C=O (4H), $^+$N-CH₂-(CH₂)₅-**CH₂** (2H)), 2.11 (br, 4H, N(**CH₂**CH₂)₂N-CH₂-C=O), 1.80 (br, 2H, $^+$N-CH₂-**CH₂**), 1.34 (br, 8H, $^+$N-CH₂-CH₂-**CH₂**, $^+$N-CH₂-(CH₂)₂-**CH₂**, $^+$N-CH₂-(CH₂)₃-**CH₂**, $^+$N-CH₂-(CH₂)₄-**CH₂**), 1.31 (s, 6H, C(**CH₃**)₂).

^{13}C NMR (100 MHz, CDCl$_3$, δ [ppm]): 170.2 (CH$_2$-**C**=O), 168.5 (NH-**C**=O), 165.3 (2C, N$_{naphth}$-**C**=O), 143.8, 140.8, 134.7 (2C, **C**H$_{naphth.}$), 132.4, 132.0 (2C, **C**H$_{naphth.}$), 131.7 (2C, **C**H$_{pirenz-arom.}$), 130.9, 129.1, 128.2 (2C, **C**H$_{pirenz-arom.}$), 127.3 (2C, **C**H$_{naphth.}$), 124.0, 122.2 (2C, **C**$_{naphth.}$), 72.2, 68.5, 61.2 (**C**H$_2$-C=O), 59.7, 58.1 (2C, N(CH$_2$**C**H$_2$)$_2$N-CH$_2$-C=O), 53.0 (2C, $^+$N(**C**H$_3$)$_2$), 52.9 (2C, N(**C**H$_2$CH$_2$)$_2$N-CH$_2$-C=O), 48.5, 39.3 (**C**(CH$_3$)$_2$), 31.0, 26.9, 26.59 (2C, C(**C**H$_3$)$_2$), 25.9, 22.9.

MS (ESI), m/z: 372.75 [M-Br+H] $^{2+}$

HPLC purity: 96%

5.6. Synthesis of phthalimide/1,8-naphthalimide-clozapine hybrids 21-25

5.6.1. 8-Chloro-11-(piperazin-1-yl)-5H-dibenzo[b,e][1,4]diazepine 20
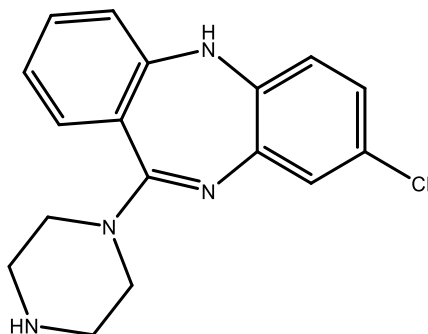
20

(C$_{17}$H$_{17}$ClN$_4$, MW: 312.80 g/mol)

Prior to the synthesis of *N*-desmethyl clozapine **20**, the starting material clozapine was extracted from purchased Clozapex® tablets (100 mg clozapine per tablet). The extraction technique involved crushing of 20 of the pale yellow uncoated tablets and adding the ground powder to a mixture of equal volumes (100 mL) of dichloromethane and distilled water. After shaking and phase separation, the dichloromethane phase was collected and the aqueous phase was washed with dichloromethane (3 x 100 mL). The combined organic solutions were washed with distilled water, dried with Na$_2$SO$_4$ and evaporated to obtain pure clozapine. The structure and purity of clozapine was confirmed using NMR spectroscopy, HPLC and LC-MS.

To a solution of clozapine (1.78 g, 5.45 mmol) in 1,2-dichloroethane (100 mL), 3-fold excess of *α*-chloroethyl chloroformate (1.8 mL, 16.34 mmol) was added dropwise (over 15 min) at 0 °C. The solution was then refluxed overnight. The solvent was evaporated under reduced pressure, after 100 mL of methanol was added to residue and refluxed at 50 °C overnight. The solvent was re-evaporated under reduced pressure and the residue was purified by silica gel chromatography (CHCl$_3$/MeOH/NH$_3$ 100:10:1) to give the *N*-desmethyl clozapine **20** (1.02 g, 60% yield).[65]

Compound **20**: bright yellow solid; R_f = 0.41 (silica gel, CHCl$_3$/MeOH/NH$_3$ 100:10:1).

^{1}H NMR (400 MHz, CDCl$_3$, δ [ppm]): 7.32 – 7.20 (m, 2H, **H**-3$_{arom.}$, **H**-1$_{arom.}$), 7.05 (d, J = 1.7 Hz, 1H, **H**-9$_{arom.}$), 7.03 – 6.96 (m, 1H, **H**-2$_{arom.}$), 6.85 – 6.73 (m, 2H, **H**-7$_{arom.}$, **H**-4$_{arom.}$), 6.59 (d, J = 8.3 Hz, 1H, **H**-6$_{arom.}$), 5.00 (s, 1H, N**H**-5), 3.40 (s, 4H, NH(CH$_2$C**H$_2$**)$_2$N), 2.89 (s, 4H, NH(C**H$_2$**CH$_2$)$_2$N), 2.15 (s, 1H, N**H**(CH$_2$CH$_2$)$_2$N).

^{13}C NMR (100 MHz, CDCl$_3$, δ [ppm]): 163.2 (**C**=N), 152.8 (**C**-11a$_{arom.}$ (**C**-C=N)), 141.9 (**C**-8$_{arom.}$ (**C**-Cl)), 140.6 (**C**-5a$_{arom.}$), 132.0 (**C**-3$_{arom.}$), 130.3 (**C**-1$_{arom.}$), 129.0 (**C**-9a$_{arom.}$), 126.8 (**C**-9$_{arom.}$), 123.5 (**C**-4a$_{arom.}$), 123.1 (**C**-2$_{arom.}$, **C**-7$_{arom.}$), 120.1 (**C**-4$_{arom.}$, **C**-6$_{arom.}$), 48.7 (2C, NH(CH$_2$**C**H$_2$)$_2$N), 46.0 (2C, NH(**C**H$_2$CH$_2$)$_2$N).

5.6.2. General procedure D for the synthesis of phthalimide/1,8-naphthalimide-clozapine hybrids 21-25

To a stirred acetonitrile solution of the corresponding intermediate **4**, **5**, **7**, **9** or **10** (1 equiv.), *N*-desmethyl clozapine **20** (1.1 equiv.) was added and dissolved. The reaction was stirred at 35 °C under inert conditions for 5 days (silica gel TLC monitoring, 0.2 M aqueous KNO$_3$/MeOH 2:3). The product either directly crystallized from the reaction mixture during the reaction time and was hence obtained by vacuum filtration followed by washing with cold acetonitrile, or, in case of no crystallization, the product was obtained by evaporation of the solvent under reduced pressure followed by purification using C18 reverse phase silica gel flash chromatography using a linear gradient of water: solvent A and methanol: solvent B (B% from 0% to 100% in 60 min) followed by a plateau phase (100% methanol for 30 min) yielding the pure product **21**, **22**, **23**, **24** or **25**, respectively, as the last fraction using UV detection.

5.6.2.1. 6-(4-(8-Chloro-5*H*-dibenzo[*b,e*][1,4]diazepin-11-yl)piperazin-1-yl)-*N*-(3-(1,3-dioxoisoindolin-2-yl)propyl)-*N,N*-dimethylhexan-1-aminium bromide 21
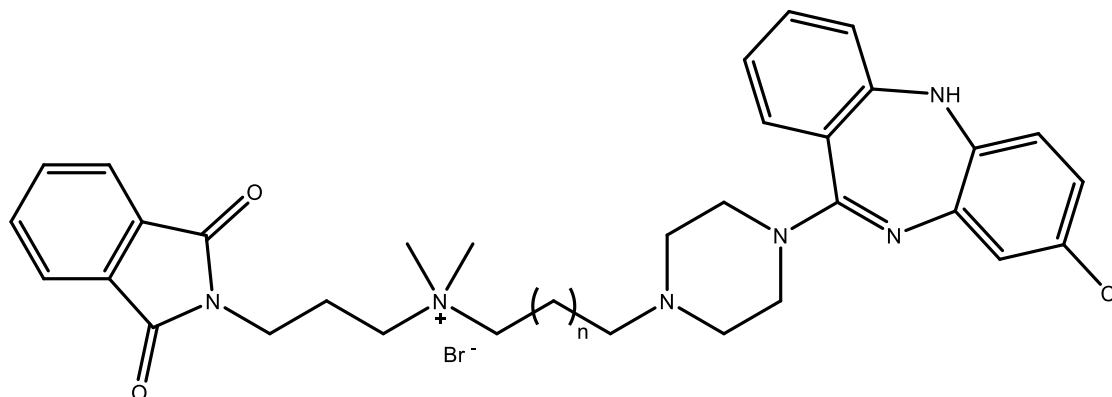
21, (n = 4)

($C_{36}H_{44}BrClN_6O_2$, MW: 708.14 g/mol)

The intermediate **4** (202 mg, 0.51 mmol) and *N*-desmethyl clozapine **20** (175 mg, 0.56 mmol) were used as reactants, and the crystallized product was filtered under vacuum and washed with cold acetonitrile to give **21** (228 mg, 63% yield).

Compound **21**: dull yellow solid; mp = 185 °C; R_f = 0.38 (silica gel, 0.2 M aqueous KNO_3/MeOH 2:3).

IR (ATR), ṽ [cm^{-1}]: 3265, 2971, 1771, 1716, 1615, 1558, 1457, 1396, 1362.

^{1}H NMR (400 MHz, DMSO-d_6, δ [ppm]): 7.92 – 7.82 (m, 4H, phth.), 7.37 (t, *J* = 7.7 Hz, 1H, **H**-3$_{cloz-arom.}$), 7.30 (d, *J* = 7.5 Hz, 1H, **H**-7$_{cloz-arom.}$), 7.12 (d, *J* = 7.9 Hz, 1H, **H**-6$_{cloz-arom.}$), 7.02 (t, *J* = 7.5 Hz, 1H, **H**-2$_{cloz-arom.}$), 6.98 – 6.88 (m, 3H, **H**-1$_{cloz-arom.}$, **H**-4$_{cloz-arom.}$, **H**-9$_{cloz-arom.}$), 3.92 (br, 1H, N**H**), 3.66 (t, *J* = 6.2 Hz, 2H, N$_{phth}$-C**H₂**), 3.55 (br, 2H, C**H₂**-N⁺), 3.41 – 3.20 (m, 8H, N(C**H₂**C**H₂**)₂N), 3.27 (br, 2H, ⁺N-C**H₂**), 3.15 (br, 2H, ⁺N-CH₂-(CH₂)₄-C**H₂**), 3.01 (s, 6H, ⁺N(C**H₃**)₂), 2.06 (br, 2H, N$_{phth}$-CH₂-C**H₂**), 1.73 (br, 2H, ⁺N-CH₂-(CH₂)₃-C**H₂**), 1.65 (br, 2H, ⁺N-CH₂-C**H₂**), 1.32 (br, 4H, ⁺N-CH₂-CH₂-C**H₂**, ⁺N-CH₂-(CH₂)₂-C**H₂**).

^{13}C NMR (100 MHz, DMSO-d_6, δ [ppm]): 168.0 (2C, **C**=O), 162.3 (**C**=N), 154.3 (**C**-C=N), 142.4 (**C**-Cl), 141.1, 134.5 (2C, **C**H$_{phth.}$), 132.6 (2C, **C**$_{phth.}$), 131.7, 129.9, 126.7, 125.8,

123.4, 123.1 (2C, **CH**phth.), 122.6, 122.1, 120.9, 120.5, 63.0, 60.8, 55.4, 50.5 (4C, N(**CH**$_2$**CH**$_2$)$_2$N), 50.0 (2C, $^+$N(**CH**$_3$)$_2$), 34.7, 25.4, 25.1, 22.8, 21.6, 21.4.

MS (ESI), m/z: 314.40 [M-Br+H] $^{2+}$

HPLC purity: 92%

5.6.2.2. 7-(4-(8-Chloro-5*H*-dibenzo[*b,e*][1,4]diazepin-11-yl)piperazin-1-yl)-*N*-(3-(1,3-dioxoisoindolin-2-yl)propyl)-*N*,*N*-dimethylheptan-1-aminium bromide 22
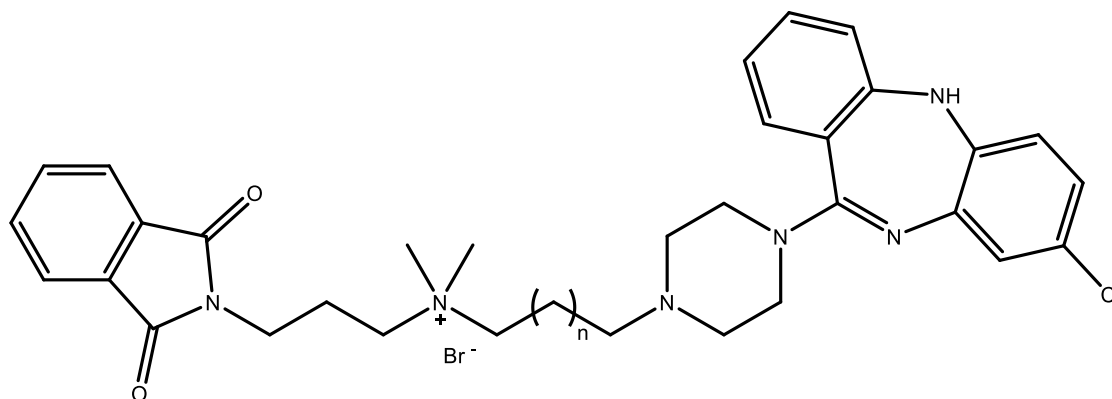
22, (n = 5)

(C$_{37}$H$_{46}$BrClN$_6$O$_2$, MW: 722.17 g/mol)

The intermediate **5** (222 mg, 0.54 mmol) and *N*-desmethyl clozapine **20** (186 mg, 0.60 mmol) were used as reactants, and the product was purified using C18 reverse phase silica gel flash chromatography (H$_2$O/MeOH solvent system) to give **22** (216 mg, 55% yield).

Compound **22**: dull yellow solid; R$_f$ = 0.42 (silica gel, 0.2 M aqueous KNO$_3$/MeOH 2:3).

IR (ATR), ṽ [cm^{-1}]: 3398, 2927, 2670, 1770, 1704, 1604, 1559, 1458, 1396, 1372.

^{1}H NMR (400 MHz, DMSO-d$_6$, δ [ppm]): 7.93 – 7.84 (m, 4H, phth.), 7.38 (t, *J* = 7.9 Hz, 1H, **H**-3cloz-arom.), 7.29 (d, *J* = 7.3 Hz, 1H, **H**-7cloz-arom.), 7.09 (d, *J* = 8.0 Hz, 1H, **H**-6cloz-arom.), 7.02

(t, J = 7.4 Hz, 1H, **H**-3cloz-arom.), 6.95 − 6.89 (m, 3H, **H**-1cloz-arom., **H**-4cloz-arom., **H**-9cloz-arom.), 3.93 (br, 1H, N**H**), 3.66 (t, J = 6.3 Hz, 2H, Nphth-C**H₂**), 3.58 − 3.49 (m, 2H, C**H₂**-N⁺), 3.49 − 3.20 (m, 8H, N(C**H₂**C**H₂**)₂N), 3.25 (br, 2H, ⁺N-C**H₂**), 3.15 (br, 2H, ⁺N-CH₂-(CH₂)₅-C**H₂**), 2.99 (s, 6H, ⁺N(C**H₃**)₂), 2.05 (br, 2H, Nphth-CH₂-C**H₂**), 1.76 − 1.56 (m, 4H, ⁺N-CH₂-C**H₂**, ⁺N-CH₂-(CH₂)₄-C**H₂**), 1.38 − 1.20 (m, 6H, ⁺N-CH₂-CH₂-C**H₂**, ⁺N-CH₂-(CH₂)₂-C**H₂**, ⁺N-CH₂-(CH₂)₃-C**H₂**).

¹³C NMR (100 MHz, DMSO-d₆, δ [ppm]): 168.0 (2C, **C**=O), 162.2 (**C**=N), 154.3 (**C**-C=N), 142.4 (**C**-Cl), 134.5 (2C, **C**Hphth.), 132.6 (2C, **C**phth.), 131.7, 129.8, 126.74, 125.7, 123.5, 123.1 (2C, **C**Hphth.), 122.5, 122.1, 120.9, 120.5, 118.1, 63.1, 60.7, 55.5, 50.5 (4C, N(**C**H₂**C**H₂)₂N), 50.0 (2C, ⁺N(**C**H₃)₂), 43.9, 34.6, 27.9, 25.8, 25.5, 22.9, 21.6.

MS (ESI), m/z: 321.35 [M-Br+H] ²⁺

HPLC purity: 88%

5.6.2.3. 4-(4-(8-Chloro-5*H*-dibenzo[*b,e*][1,4]diazepin-11-yl)piperazin-1-yl)-*N*-(3-(1,3-dioxo-1*H*-benzo[*de*]isoquinolin-2(3*H*)-yl)-2,2-dimethylpropyl)-*N,N*-dimethylbutan-1-aminium bromide 23
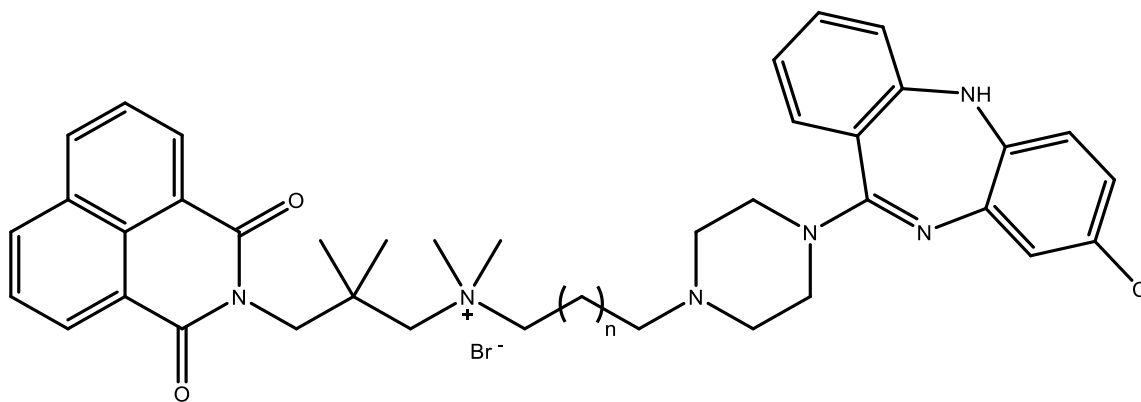
23, (n = 2)

(C₄₀H₄₆BrClN₆O₂, MW: 758.20 g/mol)

The intermediate **7** (181 mg, 0.34 mmol) and *N*-desmethyl clozapine **20** (118 mg, 0.38 mmol) were used as reactants, and the crystallized product was filtered under vacuum and washed with cold acetonitrile to give **23** (134 mg, 51% yield).

Compound **23**: dull yellow solid; mp = 155 °C; R_f = 0.44 (silica gel, 0.2 M aqueous KNO_3/MeOH 2:3).

IR (ATR), ṽ [cm^{-1}]: 3421, 3235, 2958, 1748, 1704, 1655, 1608, 1458, 1377, 1340, 1234.

^{1}H NMR (400 MHz, DMSO-d_6, δ [ppm]): 8.54 – 8.43 (m, 4H, naphth.), 7.88 (t, *J* = 7.8 Hz, 2H, naphth.), 7.38 – 7.32 (m, 1H, **H**-3$_{cloz-arom.}$), 7.22 (d, *J* = 7.3 Hz, 1H, **H**-7$_{cloz-arom.}$), 7.09 (d, *J* = 7.8 Hz, 1H, **H**-6$_{cloz-arom.}$), 7.01 (t, *J* = 7.5 Hz, 1H, **H**-2$_{cloz-arom.}$), 6.95 – 6.90 (m, 1H, **H**-9$_{cloz-arom.}$), 6.89 – 6.84 (m, 2H, **H**-1$_{cloz-arom.}$, **H**-4$_{cloz-arom.}$), 4.13 (s, 2H, N$_{napht}$-**CH$_2$**), 3.65 (br, 1H, N**H**), 3.59 (br, 2H, C**H$_2$**-N$^+$), 3.48 (br, 2H, $^+$N-C**H$_2$**), 3.47 – 3.23 (m, 8H, N(C**H$_2$**C**H$_2$**)$_2$N), 3.43 (br, 2H, $^+$N-CH$_2$-(CH$_2$)$_2$-C**H$_2$**), 3.18 (s, 6H, $^+$N(C**H$_3$**)$_2$), 1.79 (br, 2H, $^+$N-CH$_2$-C**H$_2$**), 1.57 (br, 2H, $^+$N-CH$_2$-CH$_2$-C**H$_2$**), 1.25 (s, 6H, C(C**H$_3$**)$_2$).

^{13}C NMR (100 MHz, DMSO-d_6, δ [ppm]): 164.7 (2C, **C**=O), 162.6 (**C**=N), 154.2 (**C**-C=N), 142.3 (**C**-Cl), 134.4 (2C, **C**H$_{naphth.}$), 132.2, 131.3, 131.1, 131.0 (2C, **C**H$_{naphth.}$), 129.8, 127.5, 127.4, 127.3 (2C, **C**H$_{naphth.}$), 126.7, 125.8, 125.6, 122.4, 122.3 (2C, **C**$_{naphth.}$), 120.8, 120.4, 71.6, 66.7, 61.6, 52.1 (2C, $^+$N(**C**H$_3$)$_2$), 50.3 (4C, N(**C**H$_2$**C**H$_2$)$_2$N), 48.9, 39.2 (**C**(CH$_3$)$_2$), 25.5 (2C, C(**C**H$_3$)$_2$), 20.0 (2C).

MS (ESI), m/z: 339.35 [M-Br+H] $^{2+}$

HPLC purity: 96%

5.6.2.4. 6-(4-(8-Chloro-5*H*-dibenzo[*b,e*][1,4]diazepin-11-yl)piperazin-1-yl)-*N*-(3-(1,3-dioxo-1*H*-benzo[*de*]isoquinolin-2(3*H*)-yl)-2,2-dimethylpropyl)-*N,N*-dimethylhexan-1-aminium bromide 24
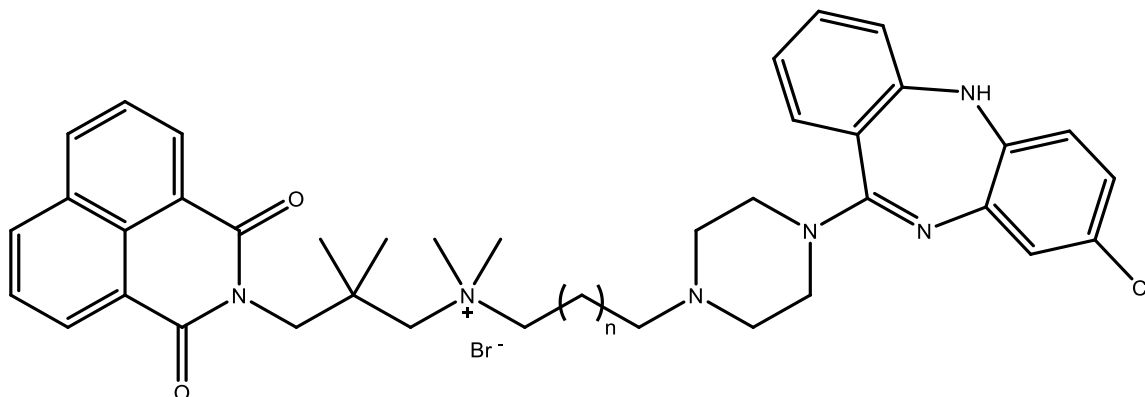
24, (n = 4)

(C₄₂H₅₀BrClN₆O₂, MW: 786.26 g/mol)

The intermediate **9** (200 mg, 0.36 mmol) and *N*-desmethyl clozapine **20** (124 mg, 0.40 mmol) were used as reactants, and the crystallized product was filtered under vacuum and washed with cold acetonitrile to give **24** (181 mg, 64% yield).

Compound **24**: dull yellow solid; mp = 231 °C; R_f = 0.39 (silica gel, 0.2 M aqueous KNO₃/MeOH 2:3).

IR (ATR), ṽ [cm⁻¹]: 3421, 3285, 2937, 1703, 1656, 1618, 1459, 1376, 1339, 1234.

¹H NMR (400 MHz, DMSO-d₆, δ [ppm]): 8.56 – 8.45 (m, 4H, naphth.), 7.90 (t, *J* = 7.9 Hz, 2H, naphth.), 7.43 – 7.34 (m, 1H, **H**-3ₑₗₒz-arom.), 7.29 (d, *J* = 7.7 Hz, 1H, **H**-7cloz-arom.), 7.09 (d, *J* = 7.7 Hz, 1H, **H**-6cloz-arom.), 7.02 (t, *J* = 7.9 Hz, 1H, **H**-2cloz-arom.), 6.94 – 6.87 (m, 3H, **H**-1cloz-arom., **H**-4cloz-arom., **H**-9cloz-arom.), 4.15 (s, 2H, Nnaphth-**CH₂**), 3.94 (br, 1H, **NH**), 3.56 (br, 2H, ⁺N-**CH₂**), 3.48 (s, 2H, **CH₂**-N⁺), 3.41 (br, 2H, ⁺N-CH₂-(CH₂)₄-**CH₂**), 3-39 – 3.26 (m, 8H, N(**CH₂CH₂**)₂N), 3.18 (s, 6H, ⁺N(**CH₃**)₂), 1.75 (br, 4H, ⁺N-CH₂-**CH₂**, ⁺N-CH₂-(CH₂)₃-**CH₂**), 1.35 (br, 4H, ⁺N-CH₂-CH₂-**CH₂**, ⁺N-CH₂-(CH₂)₂-**CH₂**), 1.25 (s, 6H, C(**CH₃**)₂).

¹³C NMR (100 MHz, DMSO-d₆, δ [ppm]): 164.7 (2C, **C**=O), 162.2 (**C**=N), 154.3 (**C**-C=N), 142.4 (**C**-Cl), 141.1, 134.4 (2C, **CH**naphth.), 132.6, 131.3, 130.9 (2C, **CH**naphth.), 129.8, 127.5,

127.3 (2C, $CH_{naphth.}$), 126.8, 125.8, 123.5, 122.5, 122.3 (2C, $C_{naphth.}$), 122.1, 120.9, 120.5, 71.7, 67.1, 55.4, 52.0 (2C, $^+N(CH_3)_2$), 50.5 (4C, $N(CH_2CH_2)_2N$), 48.9, 39.2 ($C(CH_3)_2$), 25.5 (2C, $C(CH_3)_2$), 25.2 (2C), 22.9, 21.9.

MS (ESI), m/z: 353.40 [M-Br+H]$^{2+}$

HPLC purity: 97%

5.6.2.5. 7-(4-(8-Chloro-5*H*-dibenzo[*b,e*][1,4]diazepin-11-yl)piperazin-1-yl)-*N*-(3-(1,3-dioxo-1*H*-benzo[*de*]isoquinolin-2(3*H*)-yl)-2,2-dimethylpropyl)-*N,N*-dimethylheptan-1-aminium bromide 25
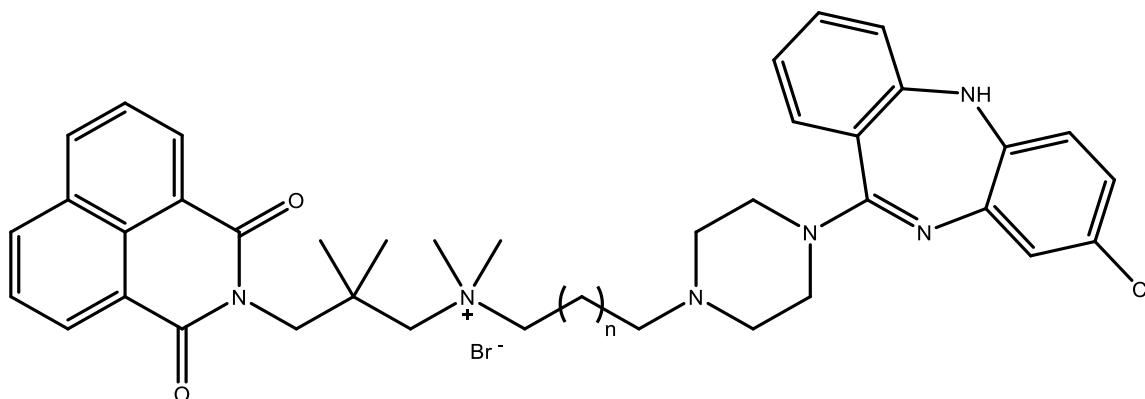
25, (n = 5)

($C_{43}H_{52}BrClN_6O_2$, MW: 800.28 g/mol)

The intermediate **10** (92 mg, 0.16 mmol) and *N*-desmethyl clozapine **20** (56 mg, 0.18 mmol) were used as reactants, and the product was purified using C18 reverse phase silica gel flash chromatography (H_2O/MeOH solvent system) to give **25** (74 mg, 57% yield).

Compound **25**: dull yellow solid; R_f = 0.42 (silica gel, 0.2 M aqueous KNO_3/MeOH 2:3).

IR (ATR), $\tilde{v}$ [cm^{-1}]: 3245, 2927, 2854, 1701, 1655, 1603, 1559, 1458, 1376, 1338, 1235.

^{1}H NMR (400 MHz, CDCl$_3$, δ [ppm]): 8.59 (dd, J = 7.3, 0.9 Hz, 2H, naphth.), 8.26 (dd, J = 8.3, 0.8 Hz, 2H, naphth.), 7.79 (t, J = 7.6 Hz, 2H, naphth.), 7.30 – 7.19 (m, 2H, **H**-1$_{\text{cloz-arom.}}$, **H**-3$_{\text{cloz-arom.}}$), 7.03 (d, J = 2.4 Hz, 1H, **H**-9$_{\text{cloz-arom.}}$), 7.01 – 6.94 (m, 1H, **H**-2$_{\text{cloz-arom.}}$), 6.87 (d, J = 7.9 Hz, 1H, **H**-4$_{\text{cloz-arom.}}$), 6.79 (dd, J = 8.3, 2.4 Hz, 1H, **H**-7$_{\text{cloz-arom.}}$), 6.66 (d, J = 8.3 Hz, 1H, **H**-6$_{\text{cloz-arom.}}$), 4.30 (s, 2H, N$_{\text{naphth}}$-**CH$_2$**), 3.71 (br, 2H, $^+$N-**CH$_2$**), 3.57 – 3.49 (m, 8H, N(**CH$_2$CH$_2$**)$_2$N), 3.52 (s, 2H, **CH$_2$**-N$^+$), 3.45 (s, 6H, $^+$N(**CH$_3$**)$_2$), 2.50 (br, 2H, $^+$N-CH$_2$-(CH$_2$)$_5$-**CH$_2$**), 2.39 – 2.30 (m, 2H, $^+$N-CH$_2$-(CH$_2$)$_4$-**CH$_2$**), 1.77 (br, 2H, $^+$N-CH$_2$-**CH$_2$**), 1.54 – 1.44 (m, 2H, $^+$N-CH$_2$-(CH$_2$)$_3$-**CH$_2$**), 1.34 (br, 4H, $^+$N-CH$_2$-CH$_2$-**CH$_2$**, $^+$N-CH$_2$-(CH$_2$)$_2$-**CH$_2$**), 1.30 (s, 6H, C(**CH$_3$**)$_2$).

^{13}C NMR (100 MHz, CDCl$_3$, δ [ppm]): 165.4 (2C, **C**=O), 163.0 (**C**=N), 153.0 (**C**-C=N), 142.0 (**C**-Cl), 140.7, 134.8 (2C, **C**H$_{\text{naphth.}}$), 132.1 (2C, **C**H$_{\text{naphth.}}$), 132.0, 131.8, 130.4, 129.0, 128.2, 127.3, 126.8 (2C, **C**H$_{\text{naphth.}}$), 123.5, 123.2, 123.1, 122.2 (2C, **C**$_{\text{naphth.}}$), 120.3, 120.2, 72.2, 68.3, 58.7, 53.3 (2C, N(CH$_2$**CH$_2$**)$_2$N-C=N), 53.1 (2C, $^+$N(**CH$_3$**)$_2$), 50.7, 48.5, 46.6 (2C, N(**CH$_2$**CH$_2$)$_2$N-C=N), 39.3 (**C**(CH$_3$)$_2$), 29.3, 27.4, 26.7, 26.6 (2C, C(**CH$_3$**)$_2$), 23.3.

MS (ESI), m/z: 360.50 [M-Br+H] $^{2+}$

HPLC purity: 99%

5.7. Synthesis of iperoxo-clozapine hybrids 30-32

5.7.1. General procedure E for the synthesis of iperoxo monoquaternary bromides 27-29

The iperoxo base **26** (1 equiv.) and an excess amount of the corresponding alkyl dibromide (15 equiv.) were dissolved in acetonitrile (10 mL). To this solution, catalytic amount of a 1:1 mixture of KI/K_2CO_3 was added. The mixture was then stirred in the microwave at 80 °C (ramp: 20 °C/min, 800W). The reaction was generally found to be completed after approximately 5 hrs (silica gel TLC monitoring, $CHCl_3/MeOH/NH_3$ 100:10:1, I_2 detection). After cooling to room temperature, the mixture was filtered and the filtrate was evaporated under reduced pressure to obtain a brown oil. The oil was dissolved in acetonitrile and the product was precipitated using diethyl ether to obtain **27**, **28** or **29** as pure product. The procedure is modified from reported literature of similar compounds.[67, 81]

5.7.1.1. 6-Bromo-*N*-(4-((4,5-dihydroisoxazol-3-yl)oxy)but-2-yn-1-yl)-*N,N*-dimethylhexan-1-aminium bromide 27
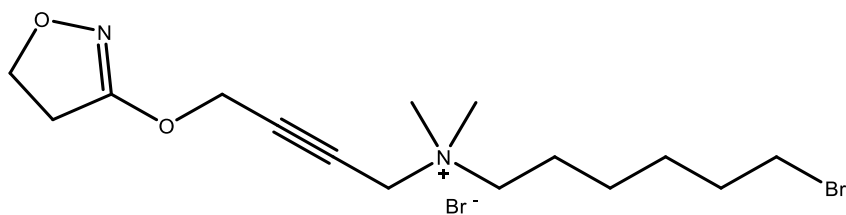

27

($C_{15}H_{26}Br_2N_2O_2$, MW: 426.19 g/mol)

The iperoxo base **26** (180 mg, 1.00 mmol) and 1,6-dibromohexane (2.3 mL, 15.00 mmol) were used as reactants to give **27** (339 mg, 79% yield).

Compound **27**: pale yellow solid; R_f = 0.55 (silica gel, $CHCl_3/MeOH/NH_3$ 100:10:1).

The spectroscopic data for this compound are in accordance with the literature.[67]

5.7.1.2. 8-Bromo-*N*-(4-((4,5-dihydroisoxazol-3-yl)oxy)but-2-yn-1-yl)-*N,N*-dimethyloctan-1-aminium bromide 28
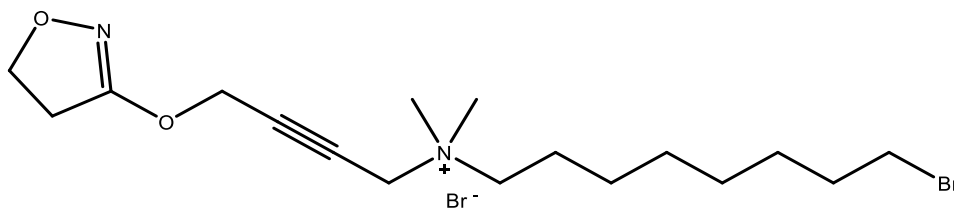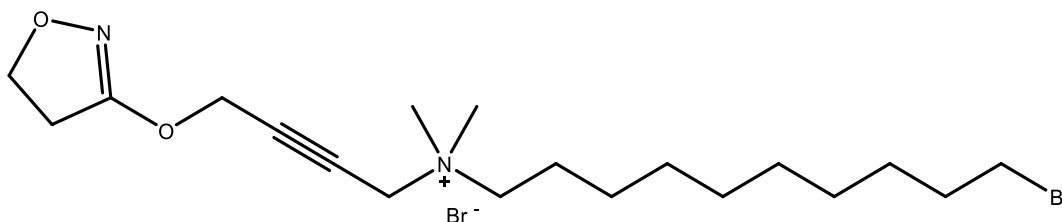

28

(C$_{17}$H$_{30}$Br$_2$N$_2$O$_2$, MW: 454.25 g/mol)

The iperoxo base **26** (0.50 g, 2.70 mmol) and 1,8-dibromooctane (7.6 mL, 41.20 mmol) were used as reactants to give **28** (0.7 g, 57% yield).

Compound **28**: yellowish-orange solid; R$_f$ = 0.46 (silica gel, CHCl$_3$/MeOH/NH$_3$ 100:10:1).

The spectroscopic data for this compound are in accordance with the literature.[67]

5.7.1.3. 10-Bromo-*N*-(4-((4,5-dihydroisoxazol-3-yl)oxy)but-2-yn-1-yl)-*N,N*-dimethyldecan-1-aminium bromide 29

29

(C$_{19}$H$_{34}$Br$_2$N$_2$O$_2$, MW: 482.30 g/mol)

The iperoxo base **26** (0.50 g, 2.70 mmol) and 1,10-dibromodecane (12.36 g, 41.20 mmol) were used as reactants to give **29** (0.79 g, 61% yield).

Compound **29**: yellowish-orange solid; R_f = 0.43 (silica gel, CHCl$_3$/MeOH/NH$_3$ 100:10:1).

^{1}H NMR (400 MHz, CDCl$_3$, δ [ppm]): 4.92 (s, 2H, C≡C-**CH$_2$**-N$^+$), 4.80 (s, 2H, O-**CH$_2$**-C≡C), 4.40 (t, J = 9.6 Hz, 2H, **CH$_2$**-O-N$_{isox}$), 3.65 – 3.55 (m, 2H, **CH$_2$**-Br), 3.43 (s, 6H, $^+$N(**CH$_3$**)$_2$), 3.38 (t, J = 6.8 Hz, 2H, $^+$N-**CH$_2$**), 2.99 (t, J = 9.6 Hz, 2H, **CH$_2$**-C=N$_{isox}$), 1.87 – 1.65 (m, 4H, $^+$N-CH$_2$-**CH$_2$**, $^+$N-CH$_2$-(CH$_2$)$_7$-**CH$_2$**), 1.45 – 1.28 (m, 12H, $^+$N-CH$_2$-CH$_2$-**CH$_2$**, $^+$N-CH$_2$-(CH$_2$)$_2$-**CH$_2$**, $^+$N-CH$_2$-(CH$_2$)$_3$-**CH$_2$**, $^+$N-CH$_2$-(CH$_2$)$_4$-**CH$_2$**, $^+$N-CH$_2$-(CH$_2$)$_5$-**CH$_2$**, $^+$N-CH$_2$-(CH$_2$)$_6$-**CH$_2$**).

^{13}C NMR (100 MHz, CDCl$_3$, δ [ppm]): 166.8 (**C**=N$_{isox}$), 86.5 (O-CH$_2$-**C**≡C), 76.1 (O-CH$_2$-C≡**C**), 70.1 (**C**H$_2$-O-N$_{isox}$), 64.2, 57.4 (O-**C**H$_2$-C≡C), 54.9 (C≡C-**C**H$_2$-N$^+$), 50.6 (2C, $^+$N(**C**H$_3$)$_2$), 34.2, 33.0 (**C**H$_2$-C=N$_{isox}$), 32.8, 29.3, 29.3, 29.2, 28.7, 28.1, 26.2, 23.0.

5.7.2. General procedure F for the synthesis of iperoxo-clozapine hybrids 30-32

To a stirred acetonitrile solution of the corresponding intermediate **27**, **28** or **29** (1 equiv.), *N*-desmethyl clozapine **20** (1.1 equiv.) was added and dissolved. The reaction was stirred at 35 °C under inert conditions for 4 days (silica gel TLC monitoring, 0.2 M aqueous KNO₃/MeOH 2:3). The product either directly crystallized from the reaction mixture during the reaction time and was hence obtained by vacuum filtration followed by washing with cold acetonitrile, or, in case of no crystallization, the product was obtained by evaporation of the solvent under reduced pressure followed by purification using C18 reverse phase silica gel flash chromatography using a linear gradient of water: solvent A and methanol: solvent B (B% from 0% to 100% in 60 min) followed by a plateau phase (100% methanol for 30 min) yielding the pure product **30**, **31** or **32**, respectively, as the last fraction using UV detection.

5.7.2.1. 6-(4-(8-Chloro-5*H*-dibenzo[*b,e*][1,4]diazepin-11-yl)piperazin-1-yl)-*N*-(4-((4,5-dihydroisoxazol-3-yl)oxy)but-2-yn-1-yl)-*N,N*-dimethylhexan-1-aminium bromide 30
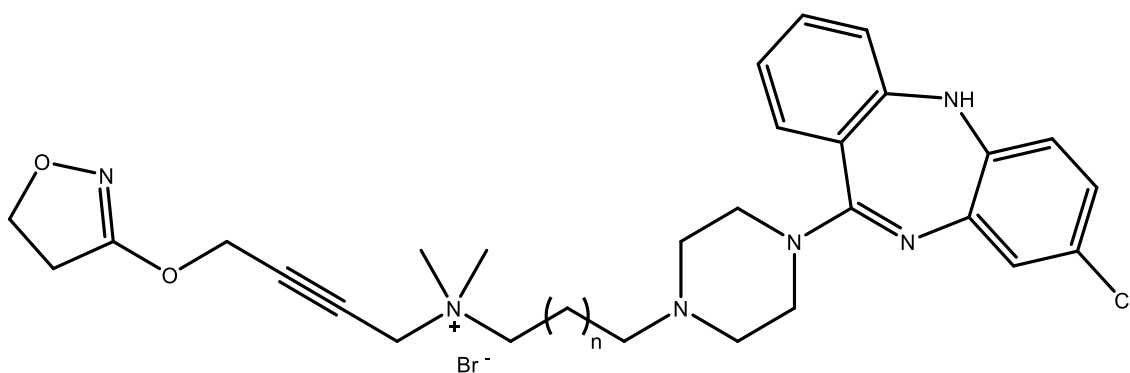
30, (n = 4)

(C₃₂H₄₂BrClN₆O₂, MW: 658.08 g/mol)

The intermediate **27** (200 mg, 0.47 mmol) and *N*-desmethyl clozapine **20** (161 mg, 0.52 mmol) were used as reactants, and the crystallized product was filtered under vacuum and washed with cold acetonitrile to give **30** (195 mg, 48% yield).

Compound **30**: yellowish-brown solid; mp = 180 °C; R_f = 0.44 (silica gel, 0.2 M aqueous KNO_3/MeOH 2:3).

IR (ATR), ṽ [cm^{-1}]: 3274, 2948, 1734, 1608, 1568, 1461, 1433, 1378, 1337, 1227.

^{1}H NMR (400 MHz, MeOD, δ [ppm]): 7.42 – 7.33 (m, 2H, **H**-1$_{cloz-arom.}$, **H**-3$_{cloz-arom.}$), 7.08 (td, *J* = 7.7, 1.1 Hz, 1H, **H**-2$_{cloz-arom.}$), 7.04 (d, *J* = 8.0 Hz, 1H, **H**-4$_{cloz-arom.}$), 6.99 (d, *J* = 2.3 Hz, 1H, **H**-9$_{cloz-arom.}$), 6.94 – 6.82 (m, 2H, **H**-6$_{cloz-arom.}$, **H**-7$_{cloz-arom.}$), 4.91 (s, 2H, C≡C-**CH$_2$**-N$^+$), 4.44 – 4.35 (m, 4H, O-C**H$_2$**-C≡C, C**H$_2$**-O-N$_{isox}$), 3.64 – 3.31 (m, 8H, N(C**H$_2$CH$_2$**)$_2$N), 3.51 – 3.44 (m, 2H, $^+$N-C**H$_2$**), 3.27 – 3.20 (m, 2H, $^+$N-CH$_2$-(CH$_2$)$_4$-C**H$_2$**), 3.20 (s, 6H, $^+$N(C**H$_3$**)$_2$), 3.03 (t, *J* = 9.6 Hz, 2H, C**H$_2$**-C=N$_{isox}$), 1.84 (br, 4H, $^+$N-CH$_2$-C**H$_2$**, $^+$N-CH$_2$-(CH$_2$)$_3$-C**H$_2$**), 1.52 (br, 4H, $^+$N-CH$_2$-CH$_2$-C**H$_2$**, $^+$N-CH$_2$-(CH$_2$)$_2$-C**H$_2$**).

^{13}C NMR (100 MHz, MeOD, δ [ppm]): 168.7 (**C**=N$_{isox}$), 164.2 (**C**=N$_{cloz}$), 155.6 (**C**-C=N$_{cloz}$), 142.5 (**C**-Cl), 141.9, 134.1, 131.2, 129.7, 127.4, 125.4, 124.3, 123.9, 121.7, 121.5, 87.7 (O-CH$_2$-**C**≡C), 76.6 (O-CH$_2$-C≡**C**), 71.2 (**C**H$_2$-O-N$_{isox}$), 65.2, 58.3 (O-**C**H$_2$-C≡C), 58.0 (C≡C-**C**H$_2$-N$^+$), 55.3, 52.6 (2C, N(**C**H$_2$CH$_2$)$_2$N-C=N$_{cloz}$), 51.3 (2C, $^+$N(**C**H$_3$)$_2$), 46.1 (2C, N(CH$_2$**C**H$_2$)$_2$N-C=N$_{cloz}$), 33.7 (**C**H$_2$-C=N$_{isox}$), 26.9, 26.5, 24.7, 23.4.

MS (ESI), m/z: 289.35 [M-Br+H]$^{2+}$

HPLC purity: 99%

5.7.2.2. 8-(4-(8-Chloro-5*H*-dibenzo[*b,e*][1,4]diazepin-11-yl)piperazin-1-yl)-*N*-(4-((4,5-dihydroisoxazol-3-yl)oxy)but-2-yn-1-yl)-*N,N*-dimethyloctan-1-aminium bromide 31
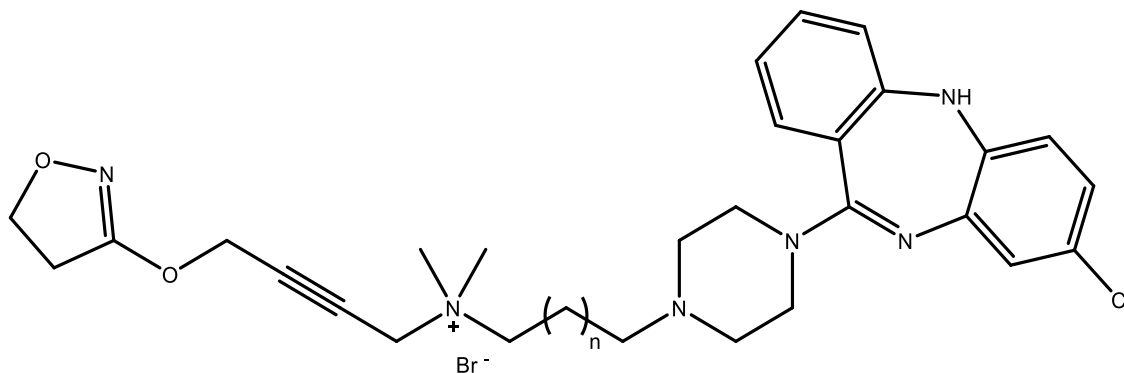
31, (n = 6)

(C$_{34}$H$_{46}$BrClN$_6$O$_2$, MW: 686.14 g/mol)

The intermediate **28** (204 mg, 0.45 mmol) and *N*-desmethyl clozapine **20** (154 mg, 0.49 mmol) were used as reactants, and the product was purified using C18 reverse phase silica gel flash chromatography (H$_2$O/MeOH solvent system) to give **31** (130 mg, 42% yield).

Compound **31**: yellowish-brown solid; R$_f$ = 0.38 (silica gel, 0.2 M aqueous KNO$_3$/MeOH 2:3).

IR (ATR), ṽ [cm^{-1}]: 3421, 3242, 2928, 2855, 1604, 1560, 1458, 1430, 1374, 1339, 1235.

^{1}H NMR (400 MHz, MeOD, δ [ppm]): 7.42 – 7.32 (m, 2H, **H**-1$_{cloz-arom.}$, **H**-3$_{cloz-arom.}$), 7.10 – 7.02 (m, 2H, **H**-2$_{cloz-arom.}$, **H**-4$_{cloz-arom.}$), 6.98 (d, *J* = 2.3 Hz, 1H, **H**-9$_{cloz-arom.}$), 6.92 – 6.83 (m, 2H, **H**-6$_{cloz-arom.}$, **H**-7$_{cloz-arom.}$), 4.91 (s, 2H, C≡C-**CH₂**-N$^+$), 4.43 – 4.36 (m, 4H, O-**CH₂**-C≡C, **CH₂**-O-N$_{isox}$), 3.79 – 3.59 (m, 4H, N(**CH₂**CH₂)₂N-C=N$_{cloz}$), 3.51 – 3.43 (m, 2H, $^+$N-**CH₂**), 3.38 – 3.32 (m, 4H, N(CH₂**CH₂**)₂N-C=N$_{cloz}$), 3.19 (s, 6H, $^+$N(**CH₃**)₂), 3.15 – 3.08 (m, 2H, $^+$N-CH₂-(CH₂)₆-**CH₂**), 3.03 (t, *J* = 9.6 Hz, 2H, **CH₂**-C=N$_{isox}$), 1.80 (br, 4H, $^+$N-CH₂-**CH₂**, $^+$N-CH₂-(CH₂)₅-**CH₂**), 1.45 (br, 8H, $^+$N-CH₂-CH₂-**CH₂**, $^+$N-CH₂-(CH₂)₂-**CH₂**, $^+$N-CH₂-(CH₂)₃-**CH₂**, $^+$N-CH₂-(CH₂)₄-**CH₂**).

^{13}C NMR (100 MHz, MeOD, δ [ppm]): 168.7 (**C**=N$_{isox}$), 164.3 (**C**=N$_{cloz}$), 155.6 (**C**-C=N$_{cloz}$), 143.3 (**C**-Cl), 142.4, 134.0, 131.2, 129.6, 127.4, 125.2, 124.3, 123.6, 121.7, 121.5, 87.7 (O-CH$_2$-**C**≡C), 76.6 (O-CH$_2$-C≡**C**), 71.2 (**C**H$_2$-O-N$_{isox}$), 65.5, 58.4 (O-**C**H$_2$-C≡C), 58.3 (C≡C-**C**H$_2$-N$^+$), 55.2, 52.7 (2C, N(**C**H$_2$CH$_2$)$_2$N-C=N$_{cloz}$), 51.2 (2C, $^+$N(**C**H$_3$)$_2$), 46.0 (2C, N(CH$_2$**C**H$_2$)$_2$N-C=N$_{cloz}$), 33.7 (**C**H$_2$-C=N$_{isox}$), 29.8, 29.7, 27.5, 27.1, 25.2, 23.6.

MS (ESI), m/z: 303.35 [M-Br+H]$^{2+}$

HPLC purity: 87%

5.7.2.3. 10-(4-(8-Chloro-5*H*-dibenzo[*b,e*][1,4]diazepin-11-yl)piperazin-1-yl)-*N*-(4-((4,5-dihydroisoxazol-3-yl)oxy)but-2-yn-1-yl)-*N,N*-dimethyldecan-1-aminium bromide 32
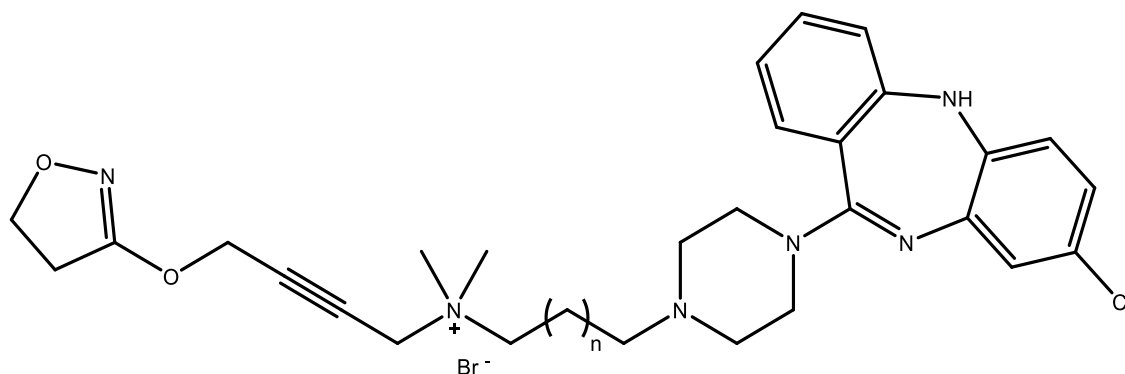
32, (n = 8)

(C$_{36}$H$_{50}$BrClN$_6$O$_2$, MW: 714.09 g/mol)

The intermediate **29** (229 mg, 0.48 mmol) and *N*-desmethyl clozapine **20** (163 mg, 0.52 mmol) were used as reactants, and the product was purified using C18 reverse phase silica gel flash chromatography (H$_2$O/MeOH solvent system) to give **32** (102 mg, 30% yield).

Compound **32**: yellowish-brown solid; R$_f$ = 0.41 (silica gel, 0.2 M aqueous KNO$_3$/MeOH 2:3).

IR (ATR), ṽ [cm^{-1}]: 3280, 2926, 2852, 1603, 1561, 1460, 1375, 1296, 1237.

^{1}H NMR (400 MHz, MeOD, δ [ppm]): 7.36 – 7.30 (m, 1H, **H**-3$_{cloz-arom.}$), 7.28 – 7.24 (m, 1H, **H**-1$_{cloz-arom.}$), 7.05 – 6.96 (m, 2H, **H**-2$_{cloz-arom.}$, **H**-4$_{cloz-arom.}$), 6.94 (d, J = 2.2 Hz, 1H, **H**-9$_{cloz-arom.}$), 6.87 – 6.76 (m, 2H, **H**-6$_{cloz-arom.}$, **H**-7$_{cloz-arom.}$), 4.35 (s, 2H, C≡C-**CH$_2$**-N$^+$), 4.24 (s, 2H, O-**CH$_2$**-C≡C), 4.16 (t, J = 8.8 Hz, 2H, **CH$_2$**-O-N$_{isox}$), 3.41 (br, 4H, N(**CH$_2$**CH$_2$)$_2$N-C=N$_{cloz}$), 2.66 (t, J = 8.8 Hz, 2H, **CH$_2$**-C=N$_{isox}$), 2.54 (br, 4H, N(**CH$_2$**CH$_2$)$_2$N-C=N$_{cloz}$), 2.42 – 2.33 (m, 2H, $^+$N-C**H$_2$**), 2.32 – 2.24 (m, 2H, $^+$N-CH$_2$-(CH$_2$)$_8$-**CH$_2$**), 2.21 (s, 6H, $^+$N(**CH$_3$**)$_2$), 1.49 (br, 4H, $^+$N-CH$_2$-C**H$_2$**, $^+$N-CH$_2$-(CH$_2$)$_7$-**CH$_2$**), 1.42 – 1.29 (m, 12H, $^+$N-CH$_2$-CH$_2$-**CH$_2$**, $^+$N-CH$_2$-(CH$_2$)$_2$-**CH$_2$**, $^+$N-CH$_2$-(CH$_2$)$_3$-**CH$_2$**, $^+$N-CH$_2$-(CH$_2$)$_4$-**CH$_2$**, $^+$N-CH$_2$-(CH$_2$)$_5$-**CH$_2$**, $^+$N-CH$_2$-(CH$_2$)$_6$-**CH$_2$**).

^{13}C NMR (100 MHz, MeOD, δ [ppm]): 169.9 (**C**=N$_{isox}$), 165.3 (**C**=N$_{cloz}$), 155.5 (**C**-C=N$_{cloz}$), 143.6 (**C**-Cl), 143.1, 133.4, 131.3, 129.3, 127.2, 124.4, 124.4, 123.8, 121.5, 121.3, 88.1 (O-CH$_2$-**C**≡C), 77.3 (O-CH$_2$-C≡**C**), 69.7 (**CH$_2$**-O-N$_{isox}$), 60.8, 59.8 (O-**C**H$_2$-C≡C), 59.8 (C≡C-**C**H$_2$-N$^+$), 55.1, 54.1 (2C, N(**CH$_2$**CH$_2$)$_2$N-C=N$_{cloz}$), 48.2 (2C, N(CH$_2$**CH$_2$**)$_2$N-C=N$_{cloz}$), 48.1 (**C**H$_2$-C=N$_{isox}$), 45.4 (2C, $^+$N(**CH$_3$**)$_2$), 30.6 (2C), 30.5, 28.7, 28.6, 28.6, 28.3, 27.5.

MS (ESI), m/z: 317.40 [M-Br+H]$^{2+}$

HPLC purity: 99%

5.8. Synthesis of acetylcholine-clozapine hybrids 35 and 36

5.8.1. General procedure G for the synthesis of acetylcholine monoquaternary bromides 33 and 34

To a solution of *N,N*-dimethyl-2-aminoethylacetate (1 equiv.) and an excess of the corresponding alkyl dibromide (15 equiv.) were dissolved in acetonitrile (30 mL) under inert atmosphere. The reaction mixture was refluxed for 3 hrs, followed by cooling to room temperature and evaporation of solvent to dryness under reduced pressure. The residue was then dissolved in acetonitrile and the product was precipitated using diethyl ether. The precipitate of pure **33** or **34** was collected.[70]

5.8.1.1. *N*-(2-Acetoxyethyl)-6-bromo-*N,N*-dimethylhexan-1-aminium bromide 33
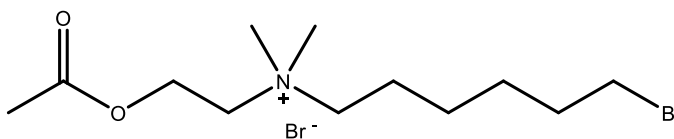
33

(C$_{12}$H$_{25}$Br$_2$NO$_2$, MW: 375.15 g/mol)

N,N-Dimethyl-2-aminoethylacetate (400 mg, 3.05 mmol) and 1,6-dibromohexane (7.0 mL, 45.74 mmol) were used as reactants to give **33** (0.80 g, 70% yield).

Compound **33**: white solid.

^{1}H NMR (400 MHz, CDCl$_3$, δ [ppm]): 4.56 (br, 2H, O-C**H$_2$**-CH$_2$-N$^+$), 4.06 (br, 2H, O-CH$_2$-C**H$_2$**-N$^+$), 3.69 – 3.61 (m, 2H, C**H$_2$**-Br), 3.45 (s, 6H, $^+$N(C**H$_3$**)$_2$), 3.40 (t, *J* = 6.6 Hz, 2H, $^+$N-C**H$_2$**), 2.10 (s, 3H, C**H$_3$**-C=O), 1.91 – 1.75 (m, 4H, $^+$N-CH$_2$-C**H$_2$**, $^+$N-CH$_2$-(CH$_2$)$_3$-C**H$_2$**), 1.58 – 1.47 (m, 2H, $^+$N-CH$_2$-CH$_2$-C**H$_2$**), 1.47 – 1.37 (m, 2H, $^+$N-CH$_2$-(CH$_2$)$_2$-C**H$_2$**).

^{13}C NMR (100 MHz, CDCl$_3$, δ [ppm]): 170.0 (CH$_3$-**C**=O), 65.4, 62.5 (O-CH$_2$-**CH$_2$**-N$^+$), 57.9 (O-**C**H$_2$-CH$_2$-N$^+$), 52.0 (2C, $^+$N(**CH$_3$**)$_2$), 33.7, 32.3, 27.7, 25.5, 22.8, 21.1 (**C**H$_3$-C=O).

5.8.1.2. *N*-(2-Acetoxyethyl)-8-bromo-*N,N*-dimethyloctan-1-aminium bromide 34

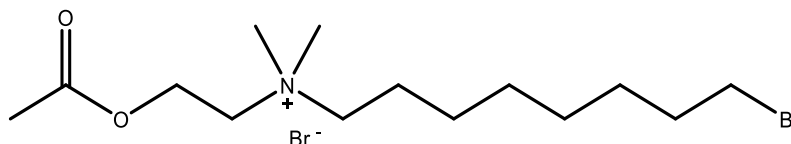**34**

(C$_{14}$H$_{29}$Br$_2$NO$_2$, MW: 403.20 g/mol)

N,N-Dimethyl-2-aminoethylacetate (400 mg, 3.05 mmol) and 1,8-dibromoctane (8.4 mL, 45.74 mmol) were used as reactants to give **34** (1.00 g, 81% yield).

Compound **34**: white solid.

^{1}H NMR (400 MHz, CDCl$_3$, δ [ppm]): 4.55 – 4.53 (m, 2H, O-C**H$_2$**-CH$_2$-N$^+$), 4.08 – 4.06 (m, 2H, O-CH$_2$-C**H$_2$**-N$^+$), 3.63 – 3.59 (m, 2H, C**H$_2$**-Br), 3.46 (s, 6H, $^+$N(C**H$_3$**)$_2$), 3.37 (t, *J* = 6.8 Hz, 2H, $^+$N-C**H$_2$**), 2.08 (s, 3H, C**H$_3$**-C=O), 1.83 – 1.75 (m, 4H, $^+$N-CH$_2$-C**H$_2$**, $^+$N-CH$_2$-(CH$_2$)$_5$-C**H$_2$**), 1.42 – 1.30 (m, 8H, $^+$N-CH$_2$-CH$_2$-C**H$_2$**, $^+$N-CH$_2$-(CH$_2$)$_2$-C**H$_2$**, $^+$N-CH$_2$-(CH$_2$)$_3$-C**H$_2$**, $^+$N-CH$_2$-(CH$_2$)$_4$-C**H$_2$**).

^{13}C NMR (100 MHz, CDCl$_3$, δ [ppm]): 170.1 (CH$_3$-**C**=O), 65.6, 62.5 (O-CH$_2$-**CH$_2$**-N$^+$), 57.9 (O-**C**H$_2$-CH$_2$-N$^+$), 52.0 (2C, $^+$N(**CH$_3$**)$_2$), 34.2, 32.7, 29.2, 28.6, 28.1, 26.3, 23.0, 21.1 (**C**H$_3$-C=O).

5.8.2. General procedure H for the synthesis of acetylcholine-clozapine hybrids 35 and 36

To a stirred acetonitrile solution of the corresponding intermediate **33** or **34** (1.5 equiv.), *N*-desmethyl clozapine **20** (1 equiv.) was added and dissolved. The reaction was stirred at 35 °C under inert conditions for 3 days (silica gel TLC monitoring, 0.2 M aqueous KNO_3/MeOH 2:3). The product either directly crystallized from the reaction mixture during the reaction time and was hence obtained by vacuum filtration followed by washing with cold acetonitrile, or, in case of no crystallization, the product was obtained by evaporation of the solvent under reduced pressure followed by purification using C18 reverse phase silica gel flash chromatography using a linear gradient of water: solvent A and methanol: solvent B (B% from 0% to 100% in 60 min) followed by a plateau phase (100% methanol for 30 min) yielding the pure product **35** or **36**, respectively, as the last fraction using UV detection.

5.8.2.1. *N*-(2-Acetoxyethyl)-6-(4-(8-chloro-5*H*-dibenzo[*b,e*][1,4]diazepin-11-yl)piperazin-1-yl)-*N,N*-dimethylhexan-1-aminium bromide 35
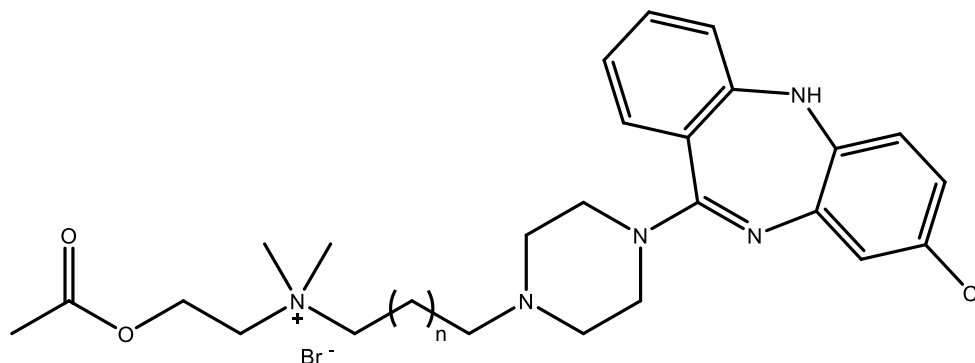
35, (n = 4)

(C$_{29}$H$_{41}$BrClN$_5$O$_2$, MW: 607.03 g/mol)

The intermediate **33** (207 mg, 0.55 mmol) and *N*-desmethyl clozapine **20** (115 mg, 0.37 mmol) were used as reactants, and the product was purified using C18 reverse phase silica gel flash chromatography (H$_2$O/MeOH solvent system) to give **35** (115 mg, 51% yield).

Compound **35**: straw yellow solid; R$_f$ = 0.49 (silica gel, 0.2 M aqueous KNO$_3$/MeOH 2:3).

IR (ATR), ṽ [cm^{-1}]: 2970, 1734, 1716, 1541, 1507, 1457, 1375, 1219.

^{1}H NMR (400 MHz, MeOD, δ [ppm]): 7.43 – 7.33 (m, 2H, **H**-1$_{cloz\text{-}arom.}$, **H**-3$_{cloz\text{-}arom.}$), 7.11 – 7.02 (m, 2H, **H**-2$_{cloz\text{-}arom.}$, **H**-4$_{cloz\text{-}arom.}$), 6.99 (d, *J* = 2.2 Hz, 1H, **H**-9$_{cloz\text{-}arom.}$), 6.94 – 6.83 (m, 2H, **H**-6$_{cloz\text{-}arom.}$, **H**-7$_{cloz\text{-}arom.}$), 4.53 (br, 2H, O-C**H₂**-CH₂-N$^+$), 3.76 – 3.68 (m, 2H, O-CH₂-C**H₂**-N$^+$), 3.64 – 3.33 (m, 8H, N(C**H₂CH₂**)$_2$N), 3.48 – 3.42 (m, 2H, $^+$N-C**H₂**), 3.28 – 3.20 (m, 2H, $^+$N-CH₂-(CH₂)$_4$-C**H₂**), 3.19 (s, 6H, $^+$N(C**H₃**)$_2$), 2.11 (s, 3H, C**H₃**-C=O), 1.86 (br, 4H, $^+$N-CH₂-C**H₂**, $^+$N-CH₂-(CH₂)$_3$-C**H₂**), 1.51 (br, 4H, $^+$N-CH₂-CH₂-C**H₂**, $^+$N-CH₂-(CH₂)$_2$-C**H₂**).

^{13}C NMR (100 MHz, MeOD, δ [ppm]): 171.6 (CH₃-**C**=O), 164.2 (**C**=N), 155.6 (**C**-C=N), 143.3 (**C**-Cl), 142.3, 134.1, 131.2, 129.6, 127.4, 125.3, 124.3, 123.5, 121.7, 121.5, 66.4 (3C, N(**C**H₂CH₂)$_2$N-C=N (2C), $^+$N-**C**H₂ (1C)), 63.7 (O-CH₂-**C**H₂-N$^+$), 58.7 (O-**C**H₂-CH₂-N$^+$), 58.0 (2C, N(CH₂**C**H₂)$_2$N-C=N), 52.6, 52.1 (2C, $^+$N(**C**H₃)$_2$), 26.9, 26.6, 24.6, 23.3, 20.7 (**C**H₃-C=O).

MS (ESI), m/z: 263.85 [M-Br+H] [2+]

HPLC purity: 99%

5.8.2.2. *N*-(2-Acetoxyethyl)-8-(4-(8-chloro-5*H*-dibenzo[*b,e*][1,4]diazepin-11-yl)piperazin-1-yl)-*N,N*-dimethyloctan-1-aminium bromide 36
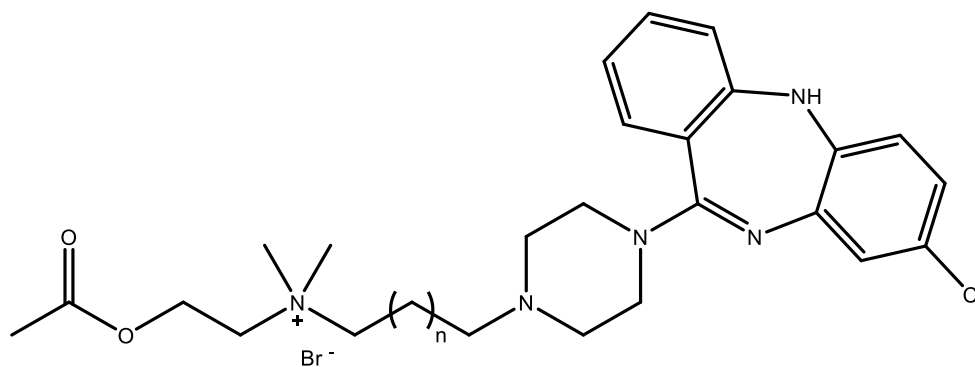
36, (n = 6)

(C$_{31}$H$_{45}$BrClN$_5$O$_2$, MW: 635.09 g/mol)

The intermediate **34** (165 mg, 0.41 mmol) and *N*-desmethyl clozapine **20** (85 mg, 0.27 mmol) were used as reactants, and the crystallized product was filtered under vacuum and washed with cold acetonitrile to give **36** (106 mg, 62% yield).

Compound **36**: straw yellow solid; mp = 190 °C; R$_f$ = 0.45 (silica gel, 0.2 M aqueous KNO$_3$/MeOH 2:3).

IR (ATR), ṽ [cm^{-1}]: 3300, 2974, 2929, 2858, 1737, 1615, 1462, 1380, 1238.

^{1}H NMR (400 MHz, MeOD, δ [ppm]): 7.45 − 7.32 (m, 2H, **H**-1$_{cloz-arom.}$, **H**-3$_{cloz-arom.}$), 7.12 − 7.02 (m, 2H, **H**-2$_{cloz-arom.}$, **H**-4$_{cloz-arom.}$), 6.99 (d, *J* = 2.3 Hz, 1H, **H**-9$_{cloz-arom.}$), 6.94 − 6.82 (m,

2H, **H**-6$_{cloz-arom.}$, **H**-7$_{cloz-arom.}$), 4.52 (br, 2H, O-C**H$_2$**-CH$_2$-N$^+$), 3.74 – 3.68 (m, 2H, O-CH$_2$-C**H$_2$**-N$^+$), 3.61 – 3.32 (m, 8H, N(C**H$_2$**C**H$_2$**)$_2$N), 3.47 – 3.40 (m, 2H, $^+$N-C**H$_2$**), 3.24 – 3.19 (m, 2H, $^+$N-CH$_2$-(CH$_2$)$_6$-C**H$_2$**), 3.18 (s, 6H, $^+$N(C**H$_3$**)$_2$), 2.11 (s, 3H, C**H$_3$**-C=O), 1.82 (br, 4H, $^+$N-CH$_2$-C**H$_2$**, $^+$N-CH$_2$-(CH$_2$)$_5$-C**H$_2$**), 1.45 (br, 8H, $^+$N-CH$_2$-CH$_2$-C**H$_2$**, $^+$N-CH$_2$-(CH$_2$)$_2$-C**H$_2$**, $^+$N-CH$_2$-(CH$_2$)$_3$-C**H$_2$**, $^+$N-CH$_2$-(CH$_2$)$_4$-C**H$_2$**).

^{13}C NMR (100 MHz, MeOD, δ [ppm]): 171.6 (CH$_3$-**C**=O), 164.2 (**C**=N), 155.6 (**C**-C=N), 143.3 (**C**-Cl), 142.7, 134.0, 131.2, 129.6, 127.4, 125.3, 124.3, 123.5, 121.7, 121.5, 66.6 (3C, N(**C**H$_2$CH$_2$)$_2$N-C=N (2C), $^+$N-**C**H$_2$ (1C)), 63.5 (O-CH$_2$-**C**H$_2$-N$^+$), 58.7 (O-**C**H$_2$-CH$_2$-N$^+$), 58.2 (2C, N(CH$_2$**C**H$_2$)$_2$N-C=N), 52.6, 52.0 (2C, $^+$N(**C**H$_3$)$_2$), 29.8, 29.7, 27.4, 27.1, 24.9, 23.5, 20.7 (**C**H$_3$-C=O).

MS (ESI), m/z: 277.90 [M-Br+H]$^{2+}$

HPLC purity: 99%

REFERENCES

6. References

[1]   Huang, Y.; Thathiah, A., Regulation of neuronal communication by G protein-coupled receptors. *FEBS Lett.* **2015,** *589* (14), 1607-1619.

[2]   Tiwari, P.; Dwivedi, S.; Singh, M. P.; Mishra, R.; Chandy, A., Basic and modern concepts on cholinergic receptor: A review. *Asian Pac. J. Trop. Dis.* **2013,** *3* (5), 413.

[3]   Waymire, J. C., Chapter 11: Acetylcholine Neurotransmission. *UTHealth* **2013**.

[4]   Amenta, F.; Tayebati, S., Pathways of acetylcholine synthesis, transport and release as targets for treatment of adult-onset cognitive dysfunction. *Curr. Med. Chem.* **2008,** *15* (5), 488-498.

[5]   Kawashima, K.; Fujii, T., Basic and clinical aspects of non-neuronal acetylcholine: overview of non-neuronal cholinergic systems and their biological significance. *J. Pharmacol. Sci.* **2008,** *106* (2), 167-173.

[6]   Ishii, M.; Kurachi, Y., Muscarinic acetylcholine receptors. *Curr. Pharm. Des.* **2006,** *12* (28), 3573-3581.

[7]   Picciotto, M. R.; Higley, M. J.; Mineur, Y. S., Acetylcholine as a neuromodulator: cholinergic signaling shapes nervous system function and behavior. *Neuron* **2012,** *76* (1), 116-129.

[8]   McCorry, L. K., Physiology of the autonomic nervous system. *Am. J. Pharm. Educ.* **2007,** *71* (4), 78.

[9]   Kirstein, S. L.; Insel, P. A., Autonomic nervous system pharmacogenomics: a progress report. *Pharmacol. Rev.* **2004,** *56* (1), 31-52.

[10]   Bjarnadóttir, T. K.; Gloriam, D. E.; Hellstrand, S. H.; Kristiansson, H.; Fredriksson, R.; Schiöth, H. B., Comprehensive repertoire and phylogenetic analysis of the G protein-coupled receptors in human and mouse. *Genomics* **2006,** *88* (3), 263-273.

[11]   Kochman, K., Superfamily of G-protein coupled receptors (GPCRs)-extraordinary and outstanding success of evolution. *Adv. Hyg. Exp. Med.* **2014,** *68*.

[12]   Ja, W. W.; Wiser, O.; Austin, R. J.; Jan, L. Y.; Roberts, R. W., Turning G proteins on and off using peptide ligands. *ACS Chem. Biol.* **2006,** *1* (9), 570-574.

[13]   Oldham, W. M.; Hamm, H. E., Heterotrimeric G protein activation by G-protein-coupled receptors. *Nat. Rev. Mol. Cell Biol.* **2008,** *9* (1), 60.

[14]   Wettschureck, N.; Offermanns, S., Mammalian G Proteins and Their Cell Type Specific Functions. *Physiol. Rev.* **2005,** *85* (4), 1159-1204.

[15]   Joost, P.; Methner, A., Phylogenetic analysis of 277 human G-protein-coupled receptors as a tool for the prediction of orphan receptor ligands. *Genome Biol.* **2002,** *3* (11), research0063. 1.

[16]   Kruse, A. C.; Kobilka, B. K.; Gautam, D.; Sexton, P. M.; Christopoulos, A.; Wess, J., Muscarinic acetylcholine receptors: novel opportunities for drug development. *Nat. Rev. Drug Discov.* **2014,** *13* (7), 549.

[17]   Scarr, E., Muscarinic receptors: their roles in disorders of the central nervous system and potential as therapeutic targets. *CNS Neurosci. Ther.* **2012,** *18* (5), 369-379.

[18]   Thiele, A., Muscarinic signaling in the brain. *Annu. Rev. Neurosci.* **2013,** *36*, 271-294.

[19]   Caulfield, M. P.; Birdsall, N. J., International Union of Pharmacology. XVII. Classification of muscarinic acetylcholine receptors. *Pharmacol. Rev.* **1998,** *50* (2), 279-290.

[20]   Michal, P.; El-Fakahany, E.; Doležal, V., Muscarinic M_2 receptors directly activate $G_{q/11}$ and G_s G-proteins. *J. Pharmacol. Exp. Ther.* **2007,** *320* (2), 607-614.

[21]   Aosaki, T.; Miura, M.; Suzuki, T.; Nishimura, K.; Masuda, M., Acetylcholine–dopamine balance hypothesis in the striatum: An update. *Geriatr. Gerontol. Int.* **2010,** *10*, S148-S157.

[22]   Shah, N.; Khurana, S.; Cheng, K.; Raufman, J.-P., Muscarinic receptors and ligands in cancer. *Am. J. Physiol. Cell Physiol.* **2009,** *296* (2), C221-C232.

[23]   Yeşilyurt, S.; Aras, İ.; Altınbaş, K.; Atagün, M. İ.; Kurt, E., Pathophysiology of clozapine induced sialorrhea and current treatment choices. *Dusunen Adam: J. Psychiatry Neurol. Sci.* **2010,** *23*, 275-281.

[24]   Bai, Y.-M.; Lin, C.-C.; Chen, J.-Y.; Liu, W.-C., Therapeutic effect of pirenzepine for clozapine-induced hypersalivation: a randomized, double-blind, placebo-controlled, cross-over study. *J. Clin. Psychopharmacol.* **2001,** *21* (6), 608-611.

[25]   Carmine, A.; Brogden, R., Pirenzepine.   A review of its pharmacodynamic and pharmacokinetic properties and therapeutic efficacy in peptic ulcer disease and other allied diseases. *Drugs* **1985,** *30* (2), 85-126.

[26]   Walline, J. J.; Lindsley, K.; Vedula, S. S.; Cotter, S. A.; Mutti, D. O.; Twelker, J. D., Interventions to slow progression of myopia in children. *Cochrane Database Syst. Rev.* **2011,** (12), CD004916.

[27]   Ostrin, L. A.; Frishman, L. J.; Glasser, A., Effects of pirenzepine on pupil size and accommodation in rhesus monkeys. *Invest. Ophthalmol. Vis. Sci.* **2004,** *45* (10), 3620-3628.

[28]   Kelly, D. L.; Wehring, H. J.; Vyas, G., Current status of clozapine in the United States. *Shanghai Arch. Psychiatry* **2012,** *24* (2), 110.

[29]   Meltzer, H. Y., An overview of the mechanism of action of clozapine. *J. Clin. Psychiatry* **1994**.

[30]   Barendrecht, M. M.; Oelke, M.; Laguna, M. P.; Michel, M. C., Is the use of parasympathomimetics for treating an underactive urinary bladder evidence-based? *BJU Int.* **2007,** *99* (4), 749-752.

[31]   Koumis, T.; Samuel, S., Tiotropium bromide: a new long-acting bronchodilator for the treatment of chronic obstructive pulmonary disease. *Clin. Ther.* **2005,** *27* (4), 377-392.

[32]   Sirohiwal, D.; Dahiya, K.; De, M., Efficacy of hyoscine-*N*- butyl bromide (Buscopan) suppositories as a cervical spasmolytic agent in labour. *Aust. N. Z. J. Obstet. Gynaecol.* **2005,** *45* (2), 128-129.

[33]   Mohr, K.; Schmitz, J.; Schrage, R.; Tränkle, C.; Holzgrabe, U., Molecular alliance—from orthosteric and allosteric ligands to dualsteric/bitopic agonists at G protein coupled receptors. *Angew. Chem. Int. Ed.* **2013,** *52* (2), 508-516.

[34]   Schmitz, J.; van der Mey, D.; Bermudez, M.; Klöckner, J.; Schrage, R.; Kostenis, E.; Tränkle, C.; Wolber, G.; Mohr, K.; Holzgrabe, U., Dualsteric muscarinic antagonists–orthosteric binding pose controls allosteric subtype selectivity. *J. Med. Chem.* **2014,** *57* (15), 6739-6750.

[35]   Bock, A.; Mohr, K., Dualsteric GPCR targeting and functional selectivity: the paradigmatic M_2 muscarinic acetylcholine receptor. *Drug Discov. Today: Technol.* **2013,** *10* (2), e245-e252.

[36] Kruse, A. C.; Ring, A. M.; Manglik, A.; Hu, J.; Hu, K.; Eitel, K.; Hübner, H.; Pardon, E.; Valant, C.; Sexton, P. M., Activation and allosteric modulation of a muscarinic acetylcholine receptor. *Nature* **2013,** *504* (7478), 101.

[37] Kruse, A. C.; Hu, J.; Pan, A. C.; Arlow, D. H.; Rosenbaum, D. M.; Rosemond, E.; Green, H. F.; Liu, T.; Chae, P. S.; Dror, R. O., Structure and dynamics of the M_3 muscarinic acetylcholine receptor. *Nature* **2012,** *482* (7386), 552.

[38] Wess, J.; Blin, N.; Mutschler, E.; Blüml, K., Muscarinic acetylcholine receptors: structural basis of ligand binding and G protein coupling. *Life Sci.* **1995,** *56* (11-12), 915-922.

[39] Haga, T., Molecular properties of muscarinic acetylcholine receptors. *Proc. Jpn. Acad. Ser. B Phys. Biol. Sci.* **2013,** *89* (6), 226-256.

[40] Bock, A.; Merten, N.; Schrage, R.; Dallanoce, C.; Bätz, J.; Klöckner, J.; Schmitz, J.; Matera, C.; Simon, K.; Kebig, A., The allosteric vestibule of a seven transmembrane helical receptor controls G-protein coupling. *Nat. Commun.* **2012,** *3*, 1044.

[41] Bock, A.; Bermudez, M.; Krebs, F.; Matera, C.; Chirinda, B.; Sydow, D.; Dallanoce, C.; Holzgrabe, U.; De Amici, M.; Lohse, M. J., Ligand binding ensembles determine graded agonist efficacies at a G protein-coupled receptor. *J. Biol. Chem.* **2016,** *291* (31), 16375-16389.

[42] Martinez-Archundia, M.; Cordomi, A.; Garriga, P.; Perez, J. J., Molecular modeling of the M_3 acetylcholine muscarinic receptor and its binding site. *BioMed Res. Int.* **2012,** *2012*.

[43] Mohr, K.; Tränkle, C.; Kostenis, E.; Barocelli, E.; De Amici, M.; Holzgrabe, U., Rational design of dualsteric GPCR ligands: quests and promise. *Br. J. Pharmacol.* **2010,** *159* (5), 997-1008.

[44] Ferré, S.; Casadó, V.; Devi, L. A.; Filizola, M.; Jockers, R.; Lohse, M. J.; Milligan, G.; Pin, J.-P.; Guitart, X., G protein–coupled receptor oligomerization revisited: functional and pharmacological perspectives. *Pharmacol. Rev.* **2014,** *66* (2), 413-434.

[45] Valant, C.; Robert Lane, J.; Sexton, P. M.; Christopoulos, A., The best of both worlds? Bitopic orthosteric/allosteric ligands of G protein–coupled receptors. *Annu. Rev. Pharmacol. Toxicol.* **2012,** *52*, 153-178.

[46] Schwyzer, R., ACTH: a short introductory review. *Ann. N.Y. Acad. Sci.* **1977,** *297* (1), 3-26.

[47]   Disingrini, T.; Muth, M.; Dallanoce, C.; Barocelli, E.; Bertoni, S.; Kellershohn, K.; Mohr, K.; De Amici, M.; Holzgrabe, U., Design, synthesis, and action of oxotremorine-related hybrid-type allosteric modulators of muscarinic acetylcholine receptors. *J. Med. Chem.* **2006,** *49* (1), 366-372.

[48]   Antony, J.; Kellershohn, K.; Mohr-Andrä, M.; Kebig, A.; Prilla, S.; Muth, M.; Heller, E.; Disingrini, T.; Dallanoce, C.; Bertoni, S., Dualsteric GPCR targeting: a novel route to binding and signaling pathway selectivity. *FASEB J.* **2009,** *23* (2), 442-450.

[49]   Dror, R. O.; Green, H. F.; Valant, C.; Borhani, D. W.; Valcourt, J. R.; Pan, A. C.; Arlow, D. H.; Canals, M.; Lane, J. R.; Rahmani, R., Structural basis for modulation of a G-protein-coupled receptor by allosteric drugs. *Nature* **2013,** *503* (7475), 295.

[50]   Chen, X.; Klöckner, J.; Holze, J.; Zimmermann, C.; Seemann, W. K.; Schrage, R.; Bock, A.; Mohr, K.; Tränkle, C.; Holzgrabe, U., Rational design of partial agonists for the muscarinic M_1 acetylcholine receptor. *J. Med. Chem.* **2014,** *58* (2), 560-576.

[51]   De Min, A.; Matera, C.; Bock, A.; Holze, J.; Kloeckner, J.; Muth, M.; Traenkle, C.; De Amici, M.; Kenakin, T.; Holzgrabe, U.; Dallanoce, C.; Kostenis, E.; Mohr, K.; Schrage, R., A new molecular mechanism to engineer protean agonism at a G protein-coupled receptor. *Mol. Pharmacol.* **2017,** *91* (4), 348-356.

[52]   Mohr, K.; Tränkle, C.; Holzgrabe, U., Structure/activity relationships of M_2 muscarinic allosteric modulators. *Recept. Channels* **2003,** *9* (4), 229-240.

[53]   Muth, M.; Bender, W.; Scharfenstein, O.; Holzgrabe, U.; Balatkova, E.; Tränkle, C.; Mohr, K., Systematic development of high affinity bis (ammonio) alkane-type allosteric enhancers of muscarinic ligand binding. *J. Med. Chem.* **2003,** *46* (6), 1031-1040.

[54]   Muth, M.; Sennwitz, M.; Mohr, K.; Holzgrabe, U., Muscarinic allosteric enhancers of ligand binding: pivotal pharmacophoric elements in hexamethonio-type agents. *J. Med. Chem.* **2005,** *48* (6), 2212-2217.

[55]   Holzgrabe, U.; Heller, E., A new synthetic route to compounds of the AFDX-type with affinity to muscarinic M_2-receptor. *Tetrahedron* **2003,** *59* (6), 781-787.

[56]   Tahtaoui, C.; Parrot, I.; Klotz, P.; Guillier, F.; Galzi, J.-L.; Hibert, M.; Ilien, B., Fluorescent pirenzepine derivatives as potential bitopic ligands of the human M_1 muscarinic receptor. *J. Med. Chem.* **2004,** *47* (17), 4300-4315.

[57]   Sur, C.; Mallorga, P. J.; Wittmann, M.; Jacobson, M. A.; Pascarella, D.; Williams, J. B.; Brandish, P. E.; Pettibone, D. J.; Scolnick, E. M.; Conn, P. J., *N*-desmethylclozapine, an allosteric agonist at muscarinic 1 receptor, potentiates *N*-methyl-D-aspartate receptor activity. *Proc. Natl. Acad. Sci. U. S. A.* **2003,** *100* (23), 13674-13679.

[58]   Riad, N. M.; Zlotos, D.; Holzgrabe, U., 2-Amino-*N*-(2-chloropyridin-3yl) benzamide. *IUCrData* **2017,** *2* (10), x171536.

[59]   Riad, N.; Zlotos, D.; Holzgrabe, U., 3-(2-Chloropyridin-3-yl) quinazoline-2, 4 (1*H*, 3*H*)-dione chloroform monosolvate. *IUCrData* **2017,** *2* (4), x170580.

[60]   Liegeois, J. F. F.; Bruhwyler, J.; Damas, J.; Nguyen, T. P.; Chleide, E. M.; Mercier, M. G.; Rogister, F. A.; Delarge, J. E., New pyridobenzodiazepine derivatives as potential antipsychotics: synthesis and neurochemical study. *J. Med. Chem.* **1993,** *36* (15), 2107-2114.

[61]   Riad, N. M.; Zlotos, D. P.; Holzgrabe, U., Crystal structure of 5, 11-dihydropyrido [2, 3-b][1, 4] benzodiazepin-6-one. *Acta Crystallogr. Sect. E Crystallogr. Commun.* **2015,** *71* (5), o304-o305.

[62]   Zare, H.; Ghanbari, M. M.; Jamali, M.; Aboodi, A., A novel and efficient strategy for the synthesis of various carbamates using carbamoyl chlorides under solvent-free and grinding conditions using microwave irradiation. *Chin. Chem. Lett.* **2012,** *23* (8), 883-886.

[63]   Karimipour, G.; Kowkabi, S.; Naghiha, A., New aminoporphyrins bearing urea derivative substituents: synthesis, characterization, antibacterial and antifungal activity. *Braz. Arch. Biol. Technol.* **2015,** *58* (3), 431-442.

[64]   Schmitz, J.; Heller, E.; Holzgrabe, U., A fast and efficient track to allosteric modulators of muscarinic receptors: microwave-assisted syntheses. *Monatsh. Chem.* **2007,** *138* (2), 171-174.

[65]   McRobb, F. M.; Crosby, I. T.; Yuriev, E.; Lane, J. R.; Capuano, B., Homobivalent ligands of the atypical antipsychotic clozapine: design, synthesis, and pharmacological evaluation. *J. Med. Chem.* **2012,** *55* (4), 1622-1634.

[66]   Kloeckner, J.; Schmitz, J.; Holzgrabe, U., Convergent, short synthesis of the muscarinic superagonist iperoxo. *Tetrahedron Lett.* **2010,** *51* (27), 3470-3472.

[67]   Geyer, F. Synthese potentieller dualsterischer Partialagonisten mit Selektivität zum M_1-Acetylcholinrezeptor. 2016.

[68]   Klöckner, J. V. Design Subtyp-selektiver Agonisten und Antagonisten muskarinischer Rezeptoren. **2013**.

[69]   Kellar, K. J.; Martino, A. M.; Hall, D. P.; Schwartz, R. D.; Taylor, R. L., High-affinity binding of [³H] acetylcholine to muscarinic cholinergic receptors. *J. Neurosci.* **1985,** *5* (6), 1577-1582.

[70]   Uppal, J. K.; Hazari, P. P.; Chuttani, K.; Allard, M.; Kaushik, N. K.; Mishra, A. K., Design, synthesis and biological evaluation of choline based SPECT imaging agent: Ga (III)-DO3A-EA-Choline. *Org. Biomol. Chem.* **2011,** *9* (5), 1591-1599.

[71]   Sekar, R. B.; Periasamy, A., Fluorescence resonance energy transfer (FRET) microscopy imaging of live cell protein localizations. *J. Cell Biol.* **2003,** *160* (5), 629-633.

[72]   Elangovan, M.; Day, R.; Periasamy, A., Nanosecond fluorescence resonance energy transfer-fluorescence lifetime imaging microscopy to localize the protein interactions in a single living cell. *J. Microsc.* **2002,** *205* (1), 3-14.

[73]   Vilardaga, J.-P.; Bünemann, M.; Feinstein, T. N.; Lambert, N.; Nikolaev, V. O.; Engelhardt, S.; Lohse, M. J.; Hoffmann, C., MINIREVIEW: GPCR and G proteins: drug efficacy and activation in live cells. *Mol. Endocrinol.* **2009,** *23* (5), 590-599.

[74]   Lohse, M. J.; Nuber, S.; Hoffmann, C., Fluorescence/bioluminescence resonance energy transfer techniques to study G-protein-coupled receptor activation and signaling. *Pharmacol. Rev.* **2012**, pr. 110.004309.

[75]   Messerer, R.; Kauk, M.; Volpato, D.; Alonso Canizal, M. C.; Klöckner, J.; Zabel, U.; Nuber, S.; Hoffmann, C.; Holzgrabe, U., FRET studies of quinolone-based bitopic ligands and their structural analogues at the muscarinic M_1 receptor. *ACS Chem. Biol.* **2017,** *12* (3), 833-843.

[76]   Hoffmann, C.; Gaietta, G.; Bünemann, M.; Adams, S. R.; Oberdorff-Maass, S.; Behr, B.; Vilardaga, J.-P.; Tsien, R. Y.; Ellisman, M. H.; Lohse, M. J., A FlAsH-based FRET approach to determine G protein–coupled receptor activation in living cells. *Nat. Methods* **2005,** *2* (3), 171.

[77]   Messerer, R.; Dallanoce, C.; Matera, C.; Wehle, S.; Flammini, L.; Chirinda, B.; Bock, A.; Irmen, M.; Tränkle, C.; Barocelli, E., Novel bipharmacophoric inhibitors of the cholinesterases with affinity to the muscarinic receptors M_1 and M_2. *MedChemComm* **2017,** *8* (6), 1346-1359.

[78]   Schmitz, J. Synthese von Liganden muscarinerger Rezeptoren-Allostere Modulatoren, bivalente Agonisten und Antagonisten. **2008**.

[79]   Muth, M. Synthese und Charakterisierung allosterer Modulatoren muscarinischer M_2-Rezeptoren: Strukturvariationen der Bis (ammonium) alkan-Verbindung W84. **2004**.

[80]   Matera, C.; Flammini, L.; Quadri, M.; Vivo, V.; Ballabeni, V.; Holzgrabe, U.; Mohr, K.; De Amici, M.; Barocelli, E.; Bertoni, S., Bis (ammonio) alkane-type agonists of muscarinic acetylcholine receptors: synthesis, in vitro functional characterization, and in vivo evaluation of their analgesic activity. *Eur. J. Med. Chem.* **2014,** *75*, 222-232.

[81]   Schrage, R.; Seemann, W.; Klöckner, J.; Dallanoce, C.; Racké, K.; Kostenis, E.; De Amici, M.; Holzgrabe, U.; Mohr, K., Agonists with supraphysiological efficacy at the muscarinic M_2 ACh receptor. *Br. J. Pharmacol.* **2013,** *169* (2), 357-370.
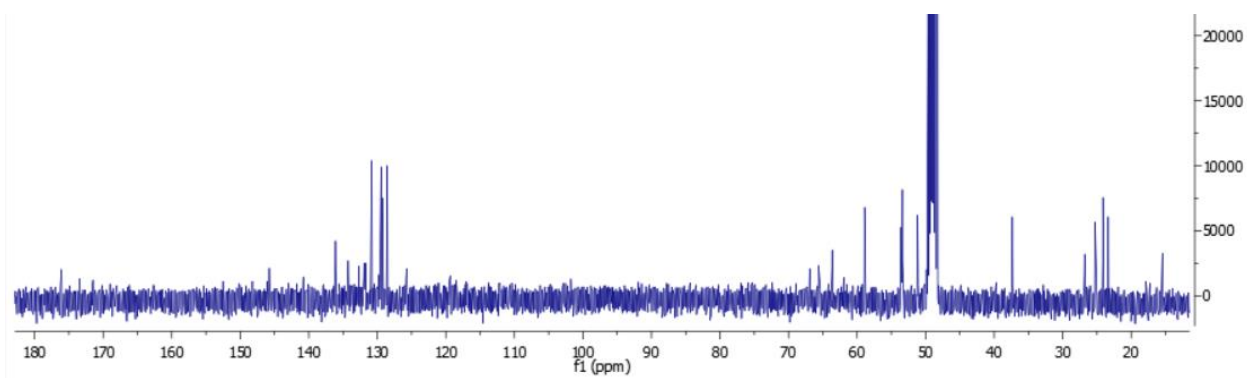
7. Appendix

7.1. Dualsteric ligand 13

7.1.1. NMR spectra
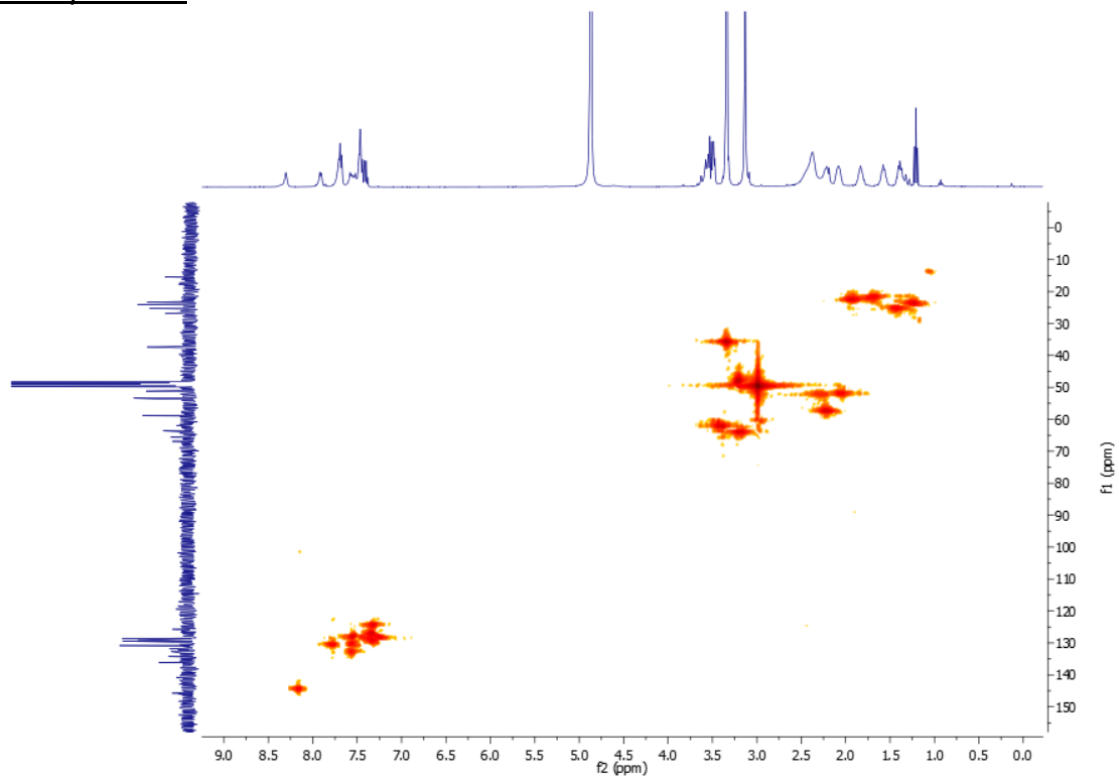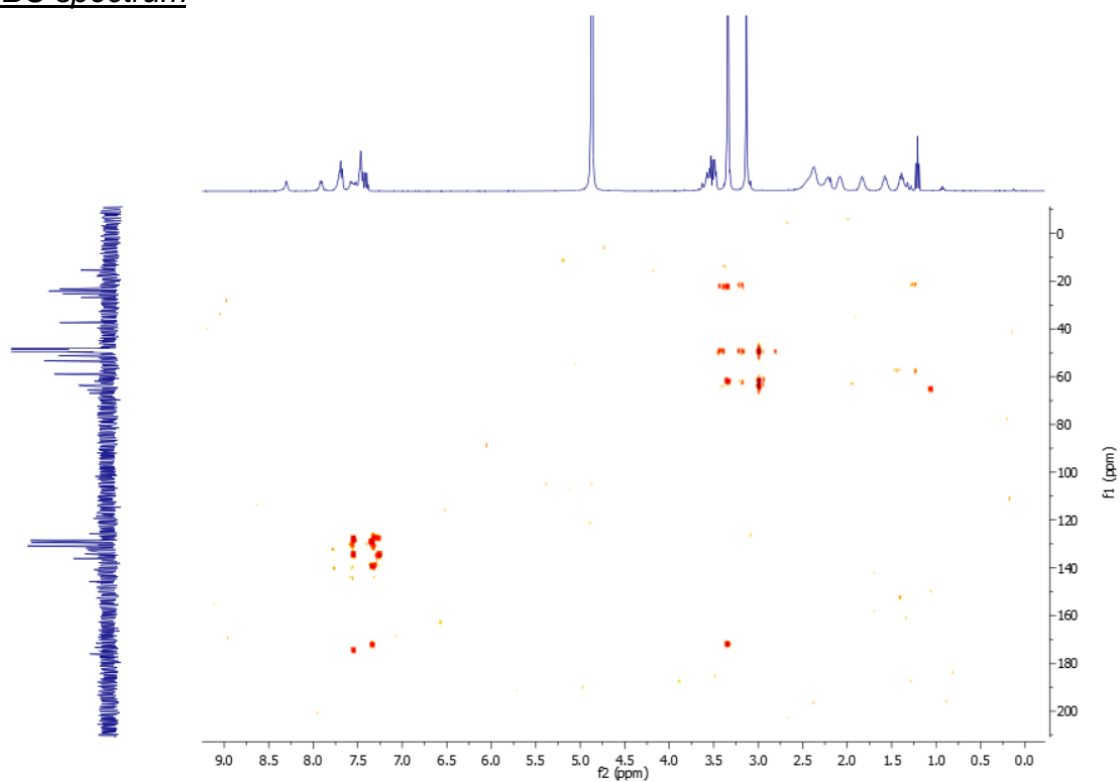
^{1}H-NMR spectrum
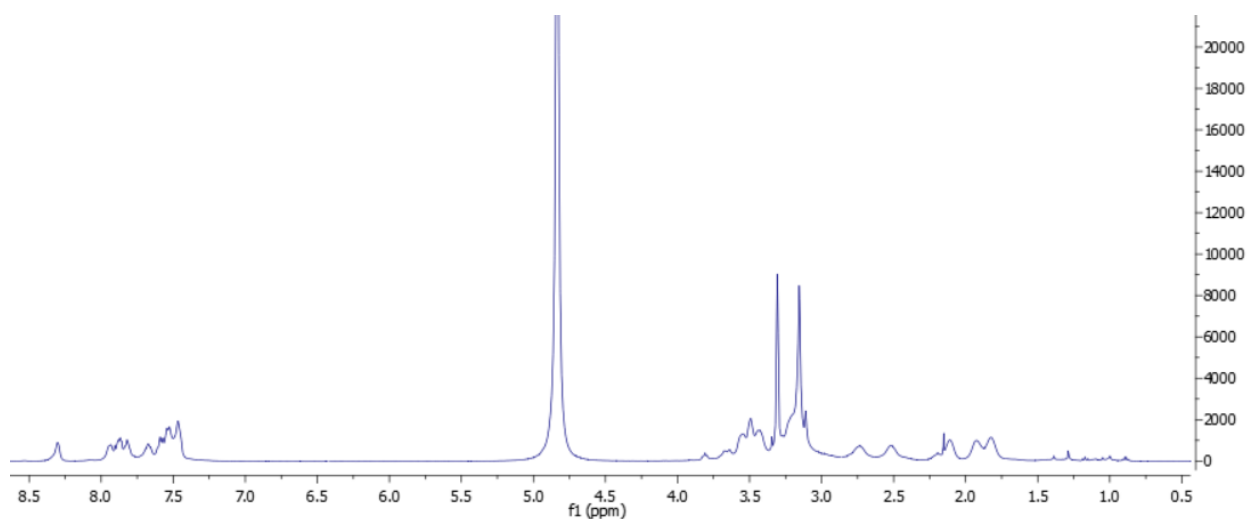
^{13}C-NMR spectrum
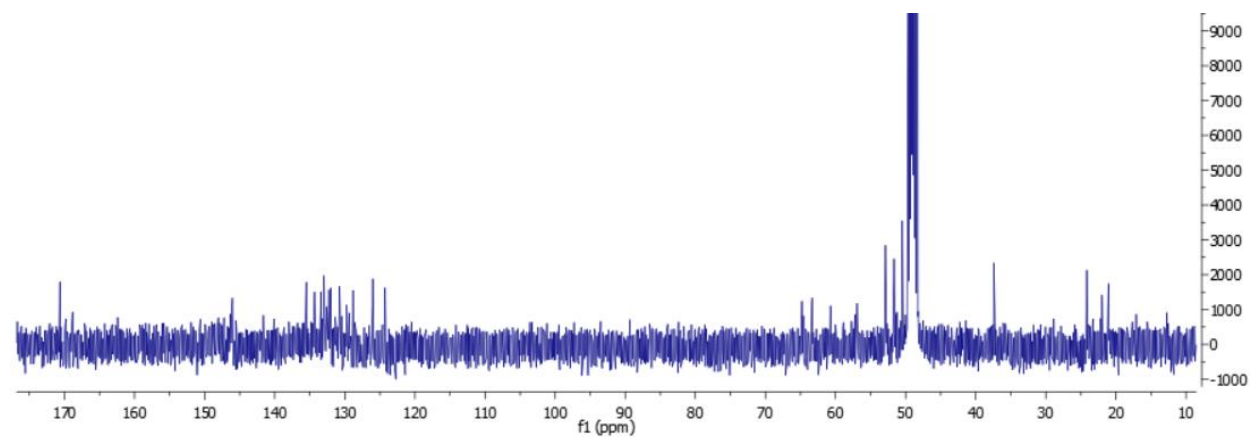
COSY spectrum
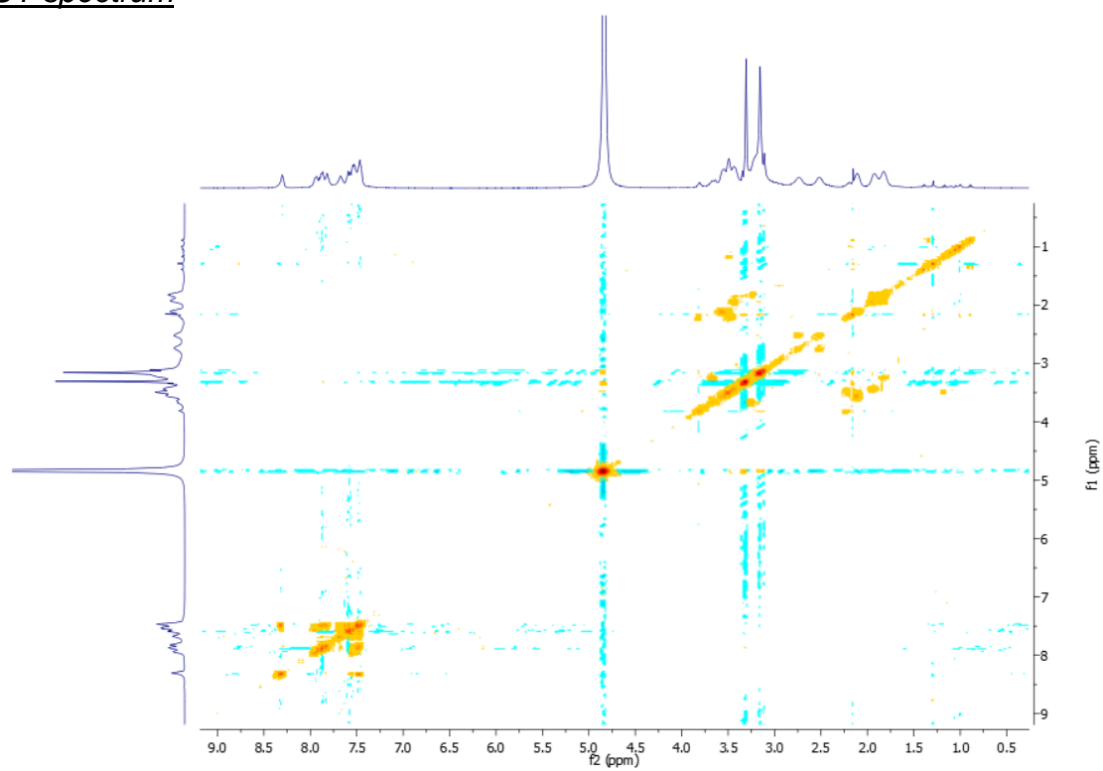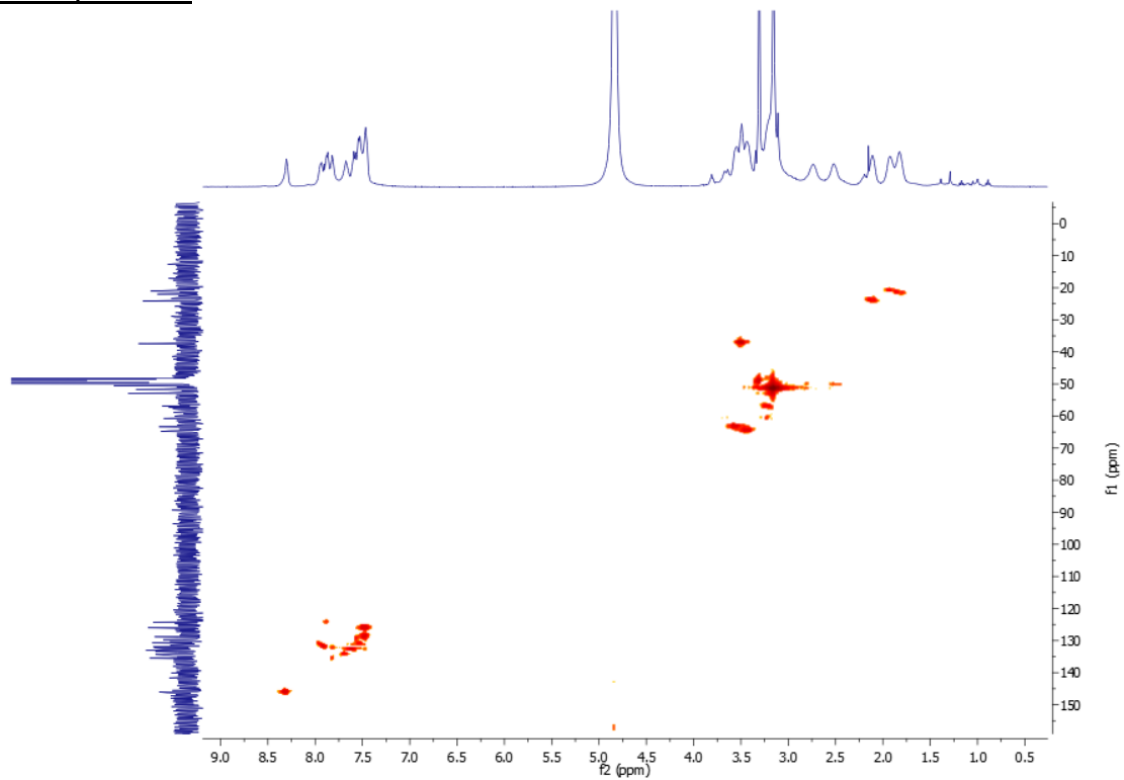
HMQC spectrum

HMBC spectrum
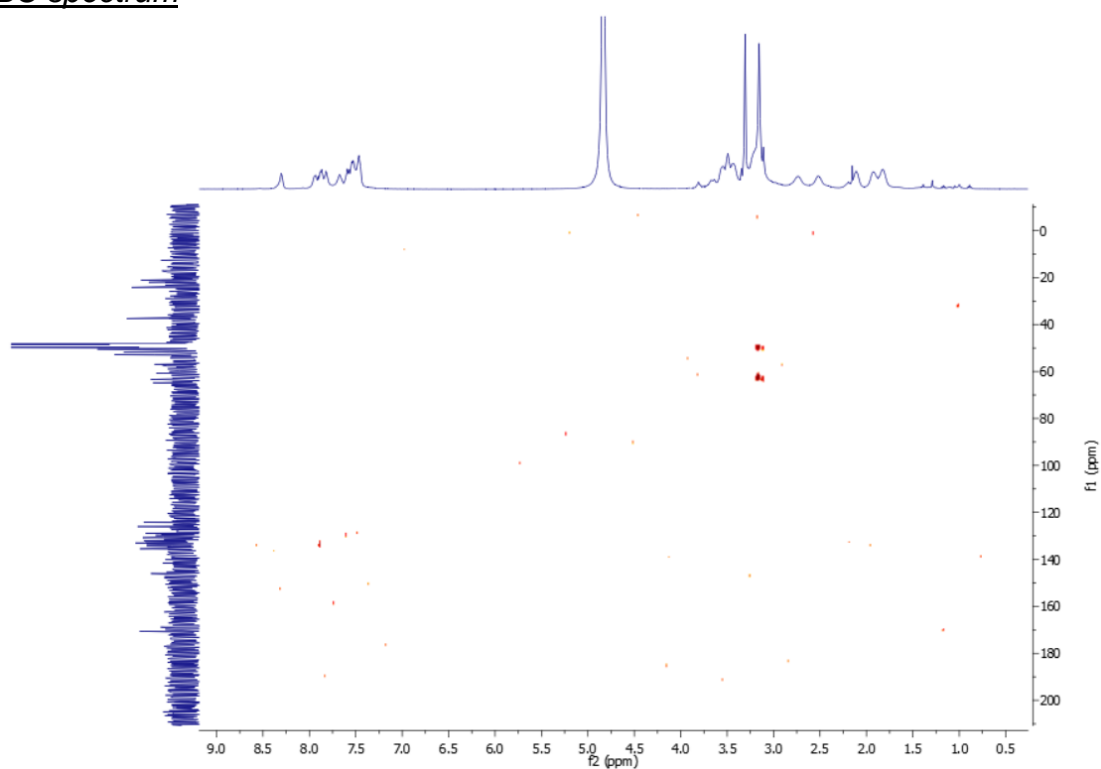
7.1.2. IR spectrum
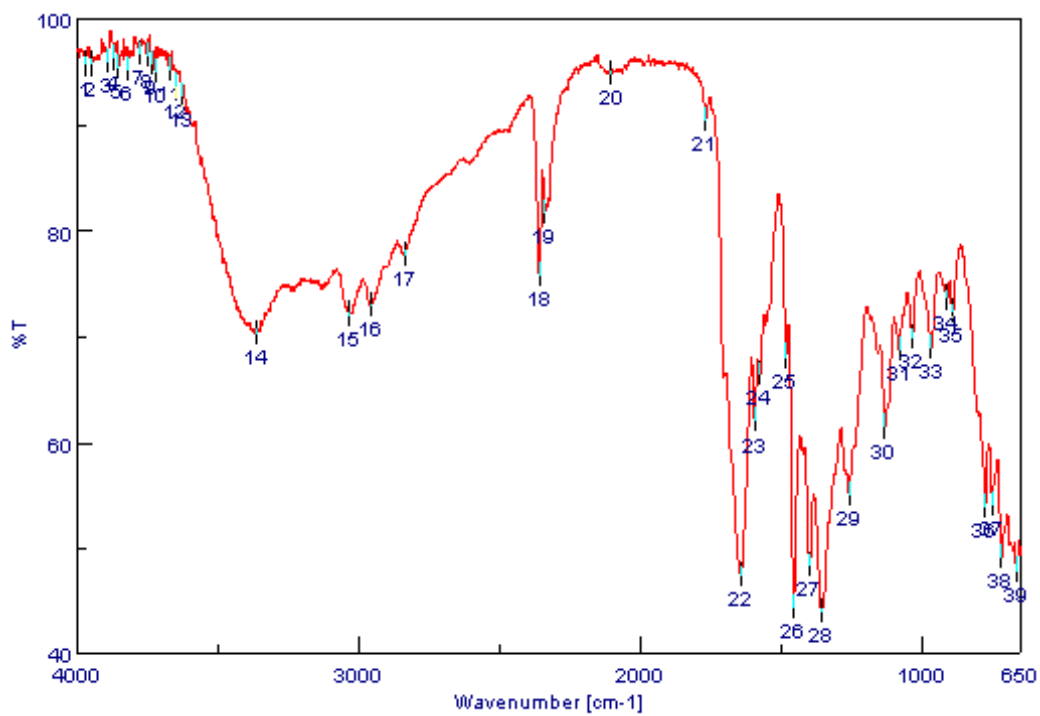
7.1.3. LC-MS spectrum (ESI)

\<Chromatogram\>

mV
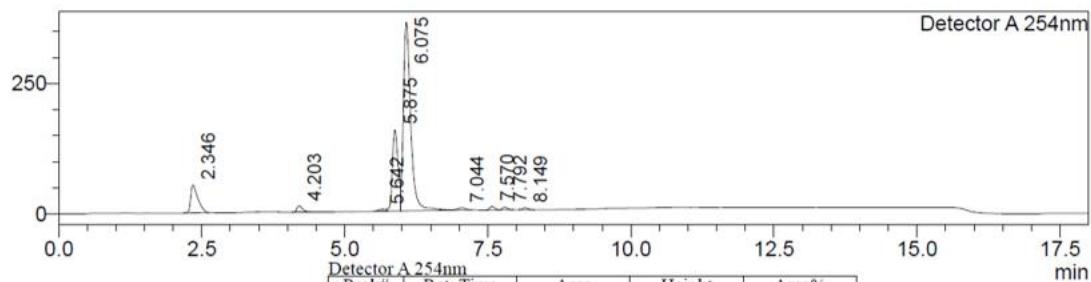
Peak#	Ret. Time	Area	Height	Area%
1	2.346	469591	53469	9.377
2	4.203	82508	12104	1.648
3	5.642	31004	3285	0.619
4	5.875	1068129	155278	21.329
5	6.075	3219233	361487	64.284
6	7.044	41864	4363	0.836
7	7.570	41918	6787	0.837
8	7.792	30437	5181	0.608
9	8.149	23168	3800	0.463
Total		5007852	605753	100.000

Line#:1   R.Time:6.453(Scan#:3873)
MassPeaks:441
Spectrum Mode:Averaged 6.450-6.457(3871-3875) Base Peak:321.60(1953115)
BG Mode:Calc Segment 1 - Event 1
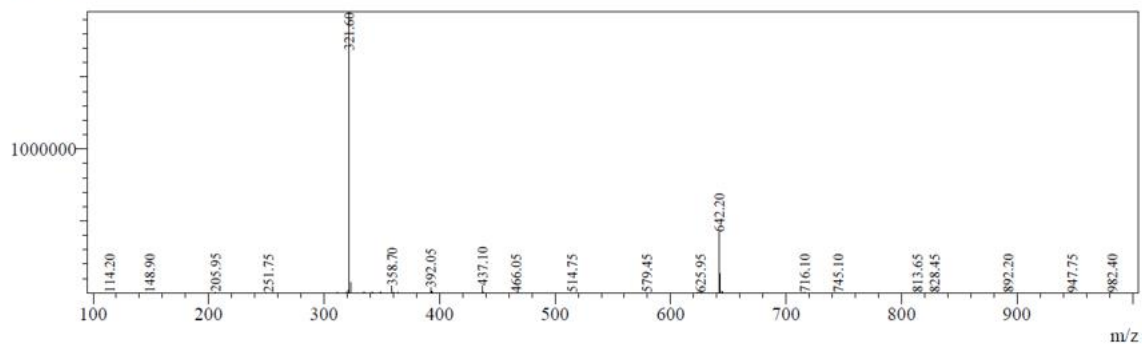
7.2. Dualsteric ligand 14

7.2.1. NMR spectra

¹H-NMR spectrum
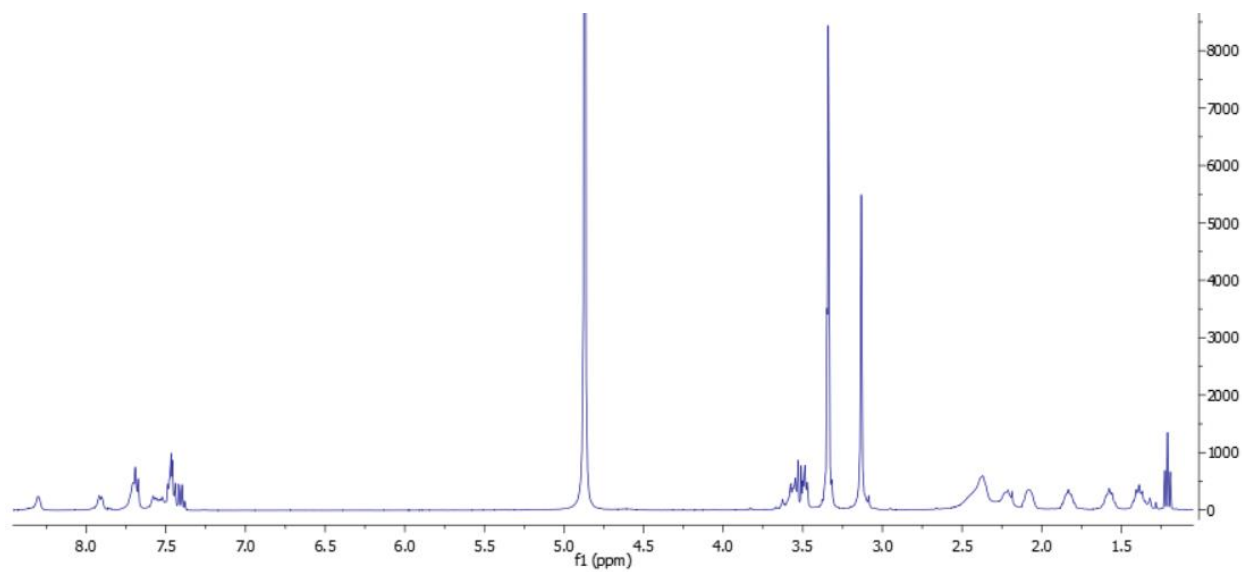
¹³C-NMR spectrum

COSY spectrum
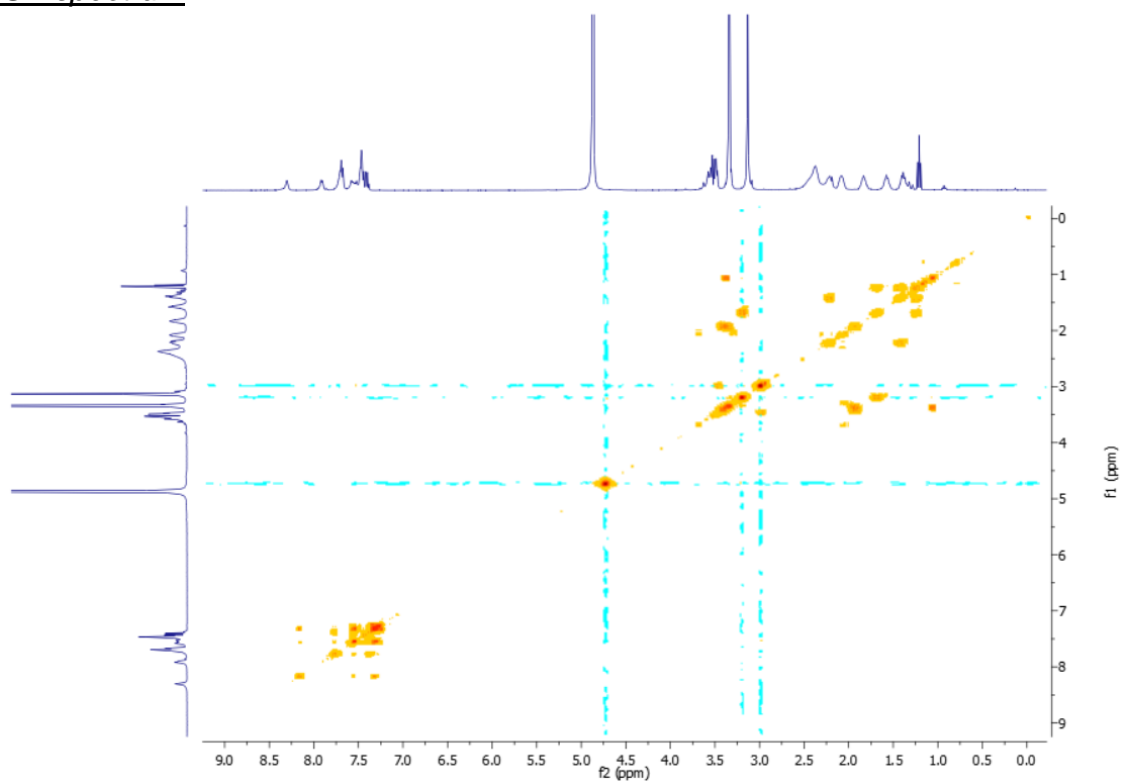
HMQC spectrum

HMBC spectrum

7.2.2. IR spectrum
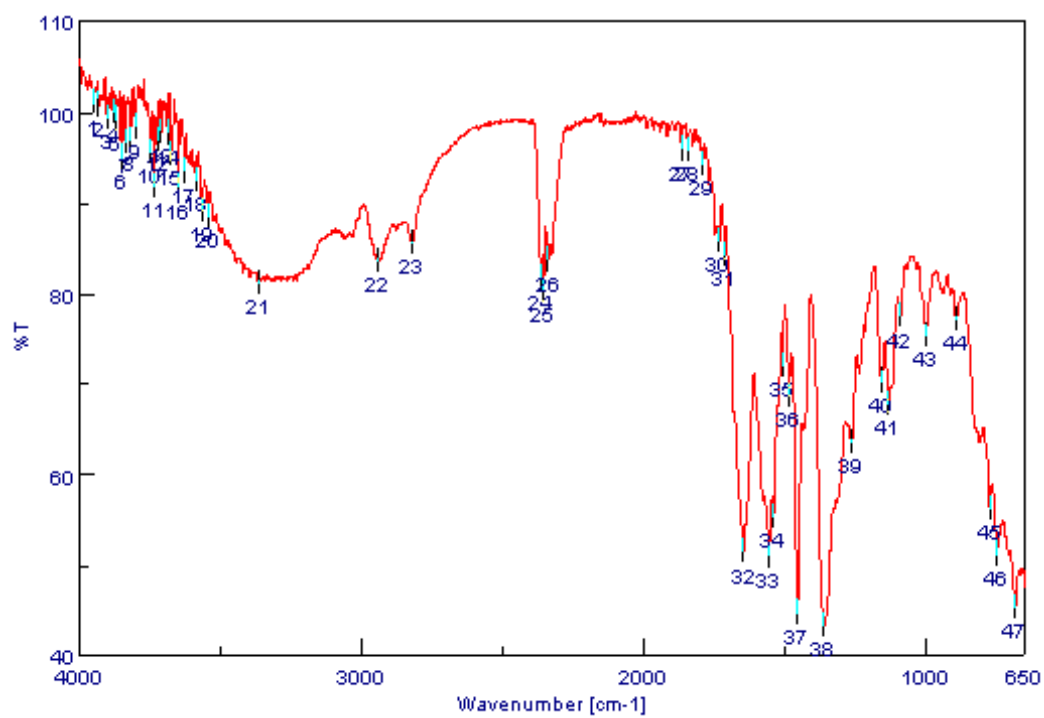
7.2.3. LC-MS spectrum (ESI)

\<Chromatogram\>

mV
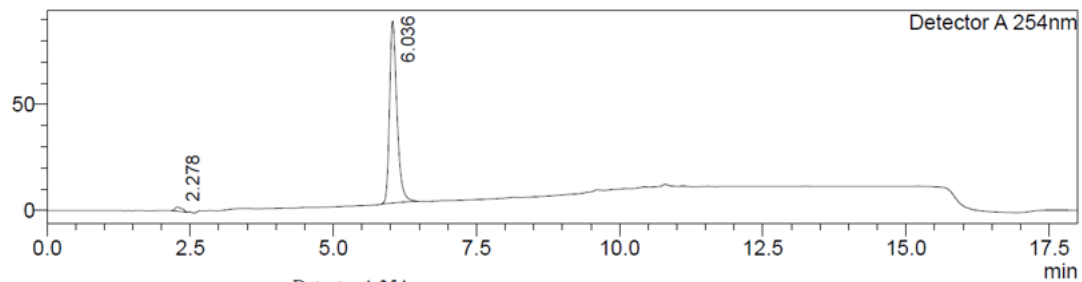
Detector A 254nm

Detector A 254nm

Peak#	Ret. Time	Area	Height	Area%
1	2.278	17542	2052	2.217
2	6.036	773867	85741	97.783
Total		791409	87792	100.000

Line#:1   R.Time:6.420(Scan#:3853)
MassPeaks:427
Spectrum Mode:Averaged 6.417-6.423(3851-3855) Base Peak:328.70(717471)
BG Mode:Calc Segment 1 - Event 1

m/z
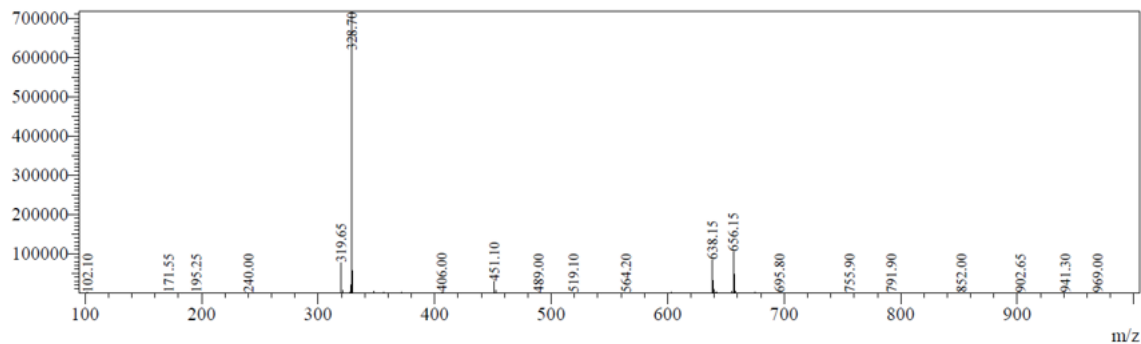
7.3. Dualsteric ligand 15

7.3.1. NMR spectra

¹H-NMR spectrum
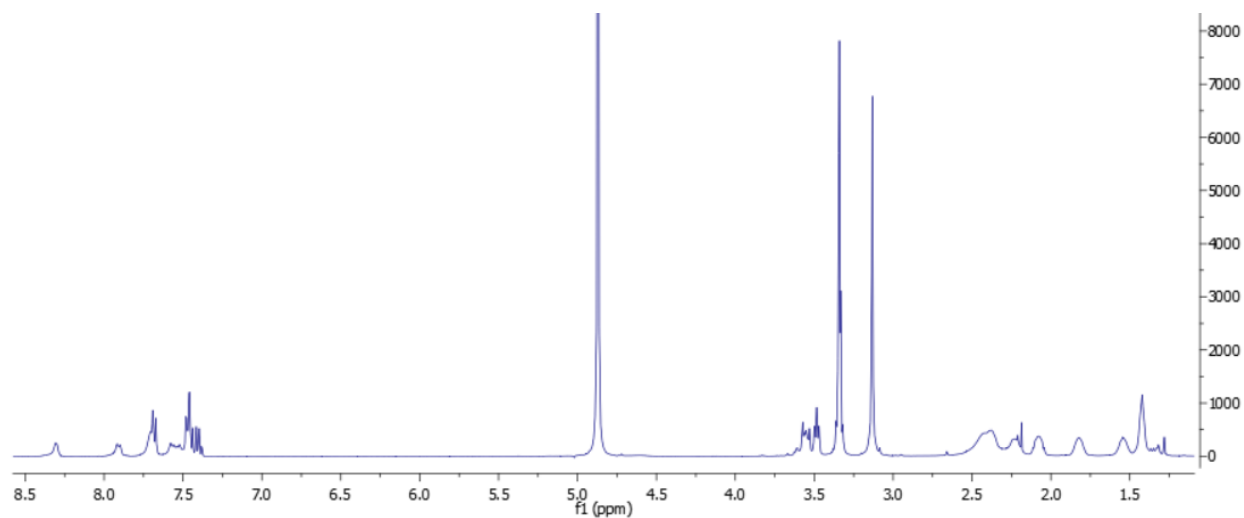
¹³C-NMR spectrum
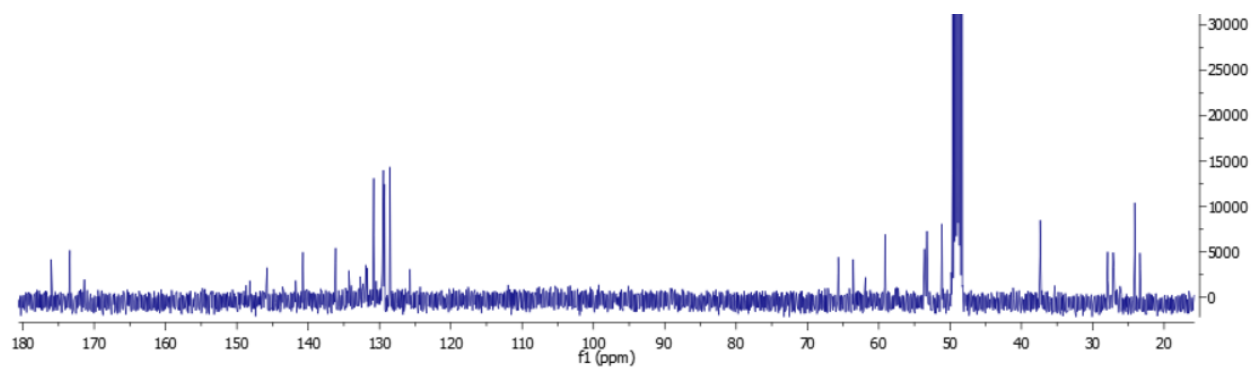
COSY spectrum
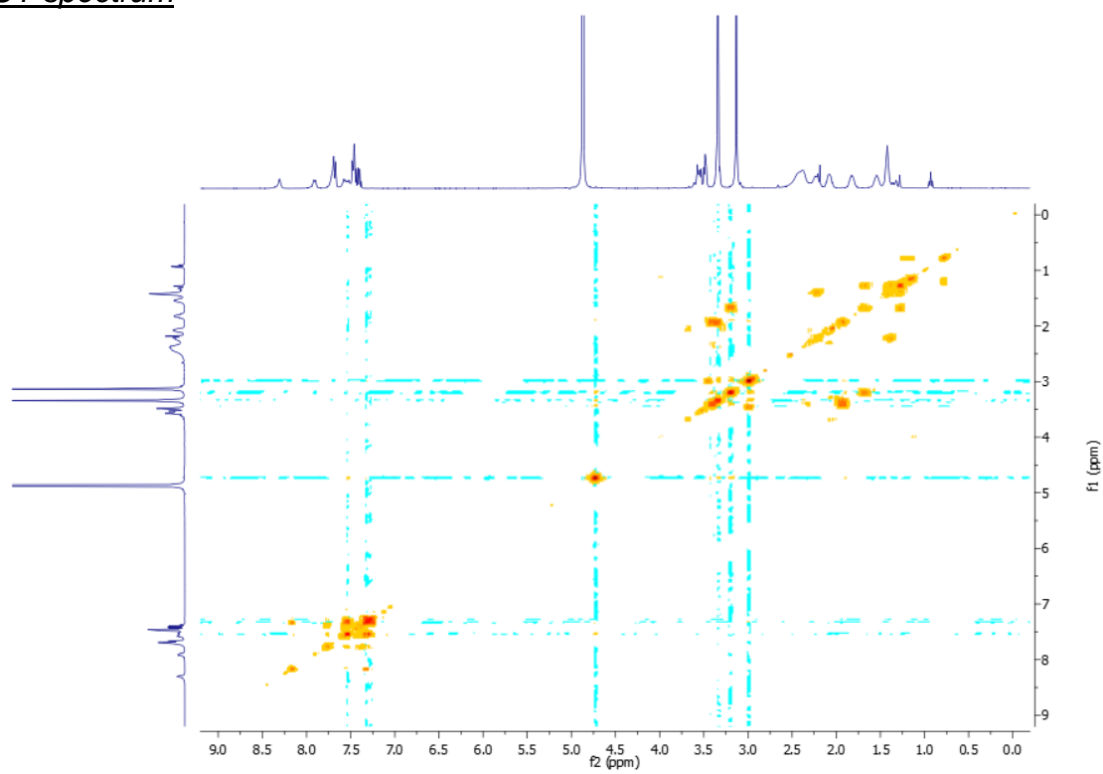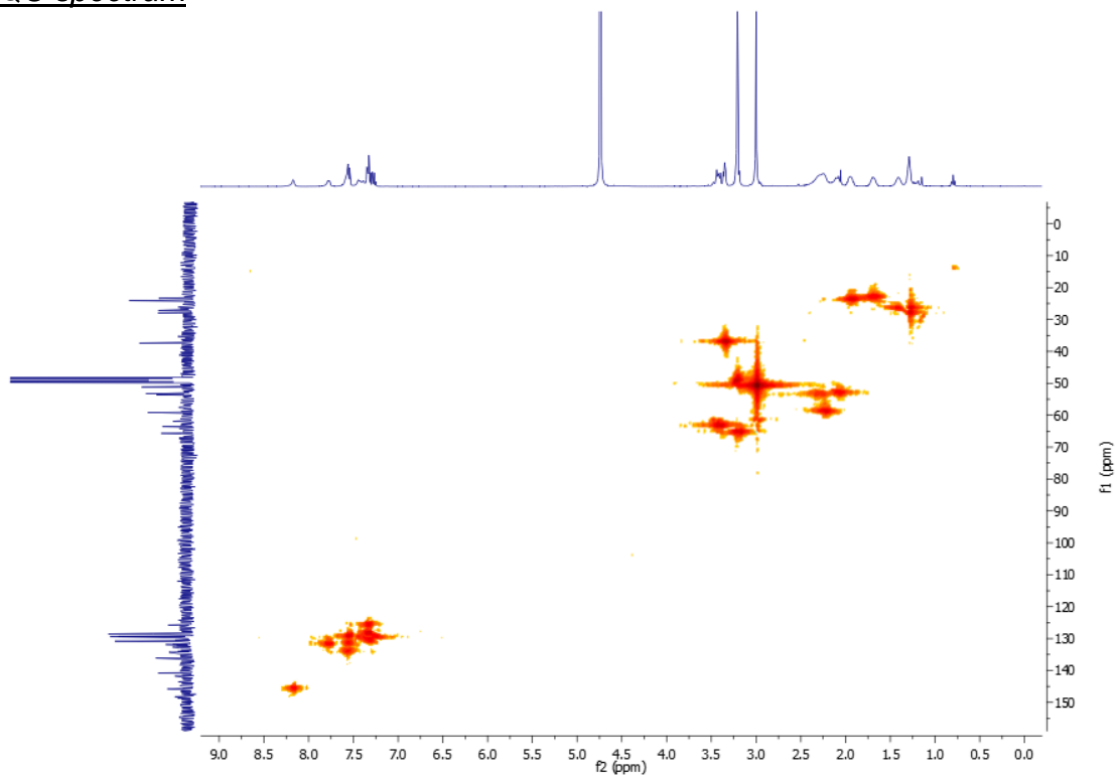
HMQC spectrum

HMBC spectrum
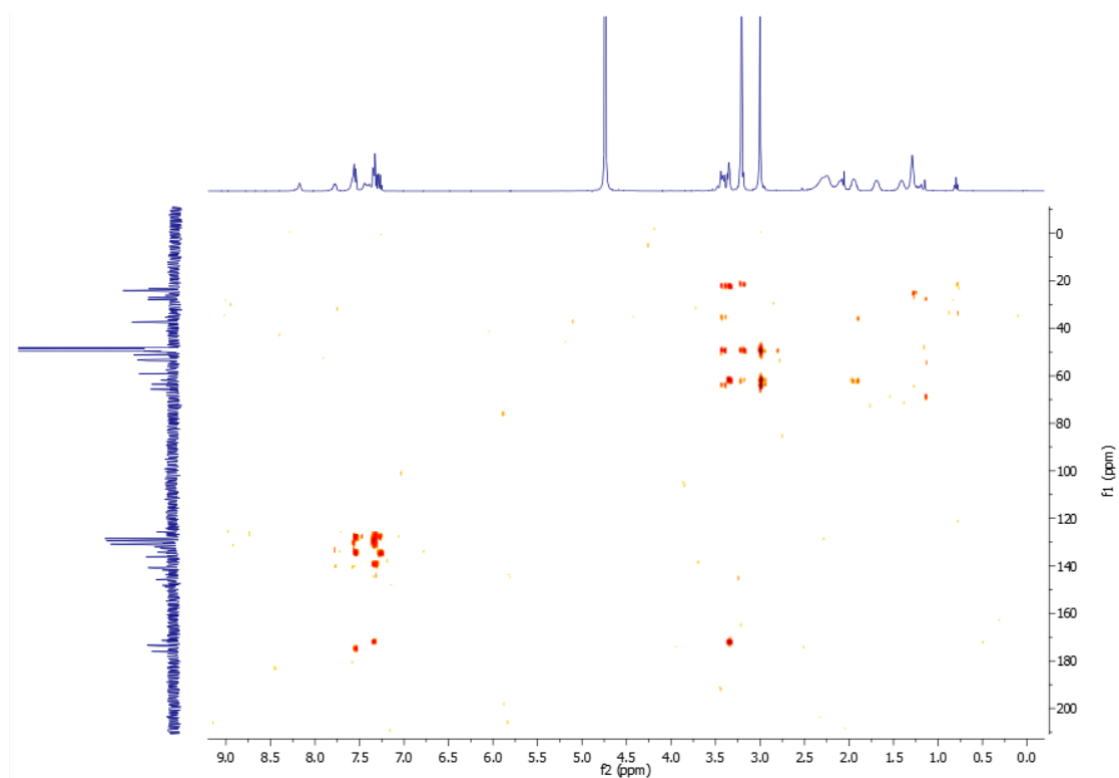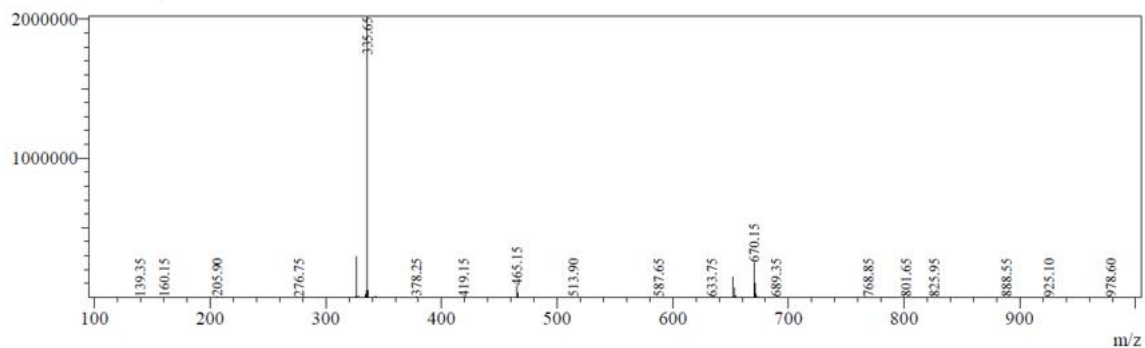

7.3.2. IR spectrum
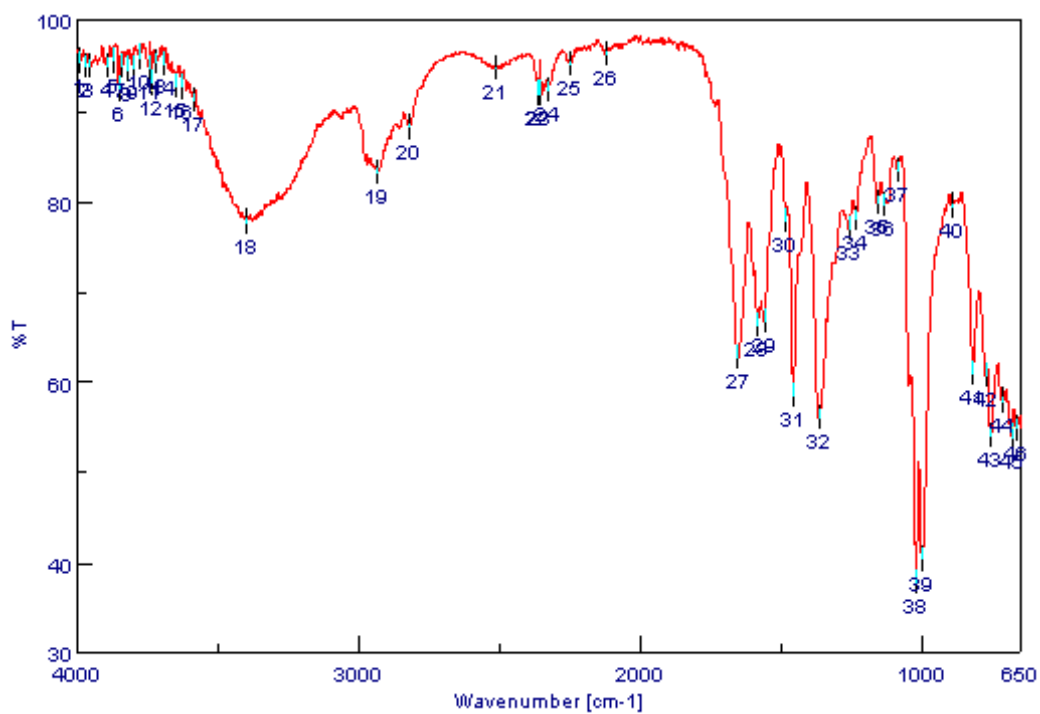
7.3.3. LC-MS spectrum (ESI)

\<Chromatogram\>

mV
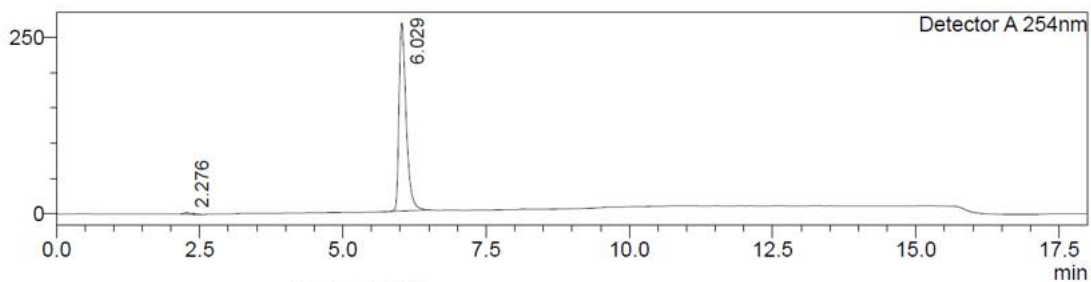
Detector A 254nm

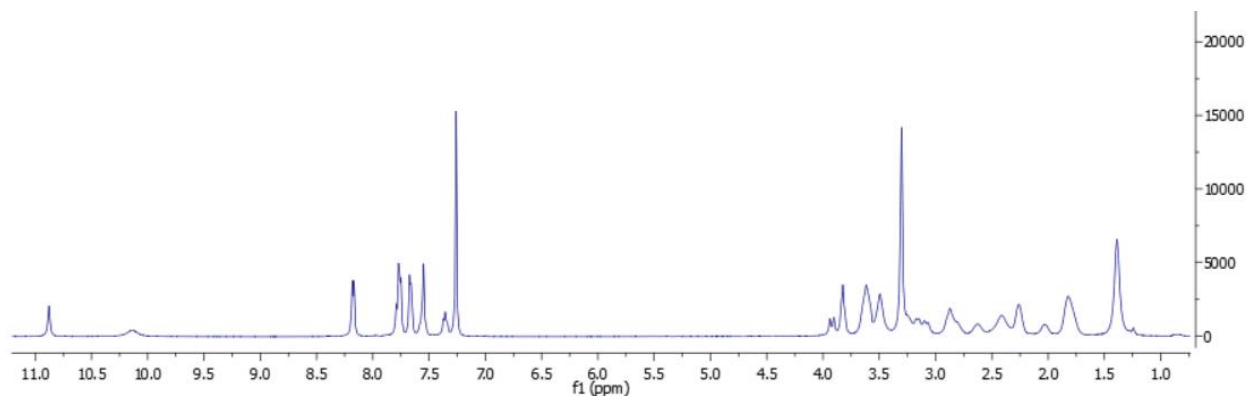| Detector A 254nm				
Peak#	Ret. Time	Area	Height	Area%
1	2.276	18584	2025	0.798
2	6.029	2308964	266188	99.202
Total		2327548	268213	100.000

Line#:1 R.Time:6.413(Scan#:3849)
MassPeaks:445
Spectrum Mode:Averaged 6.410-6.417(3847-3851) Base Peak:335.65(2021921)
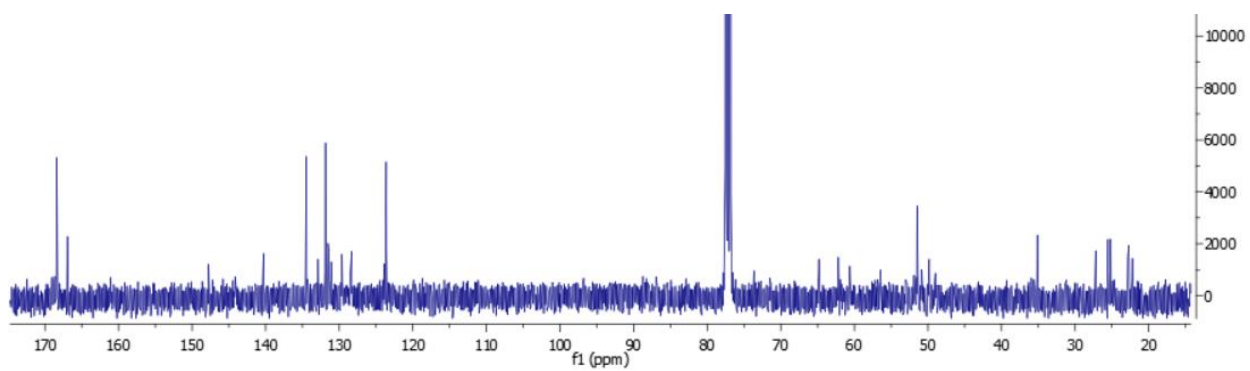BG Mode:Calc Segment 1 - Event 1

m/z

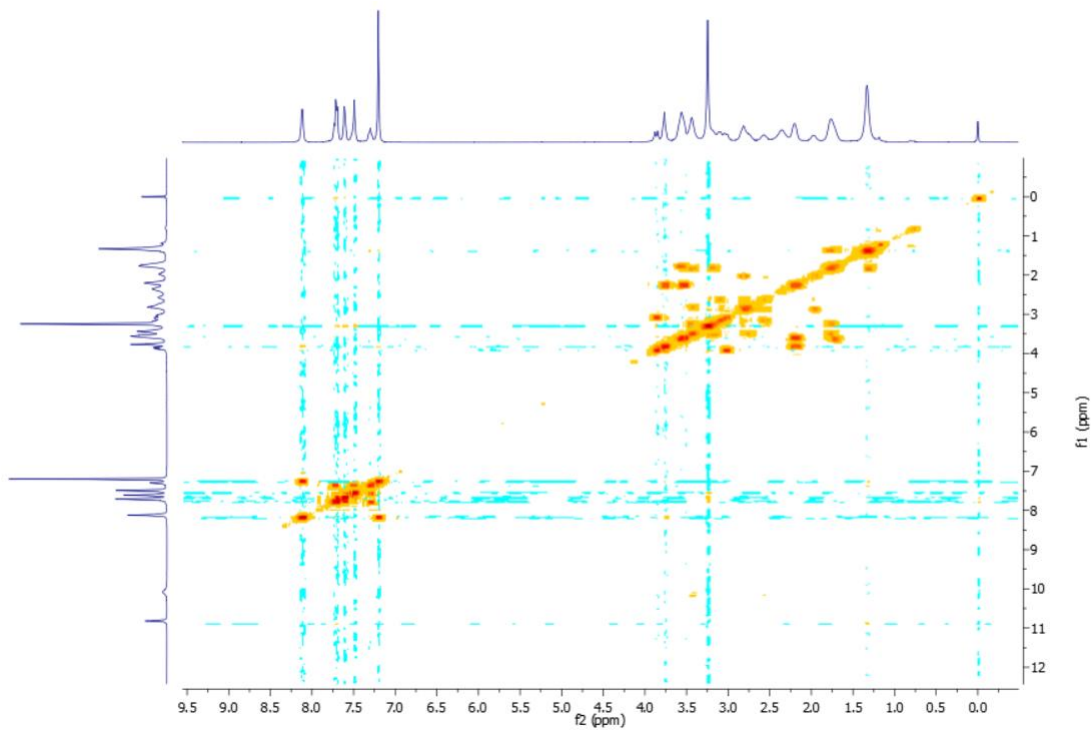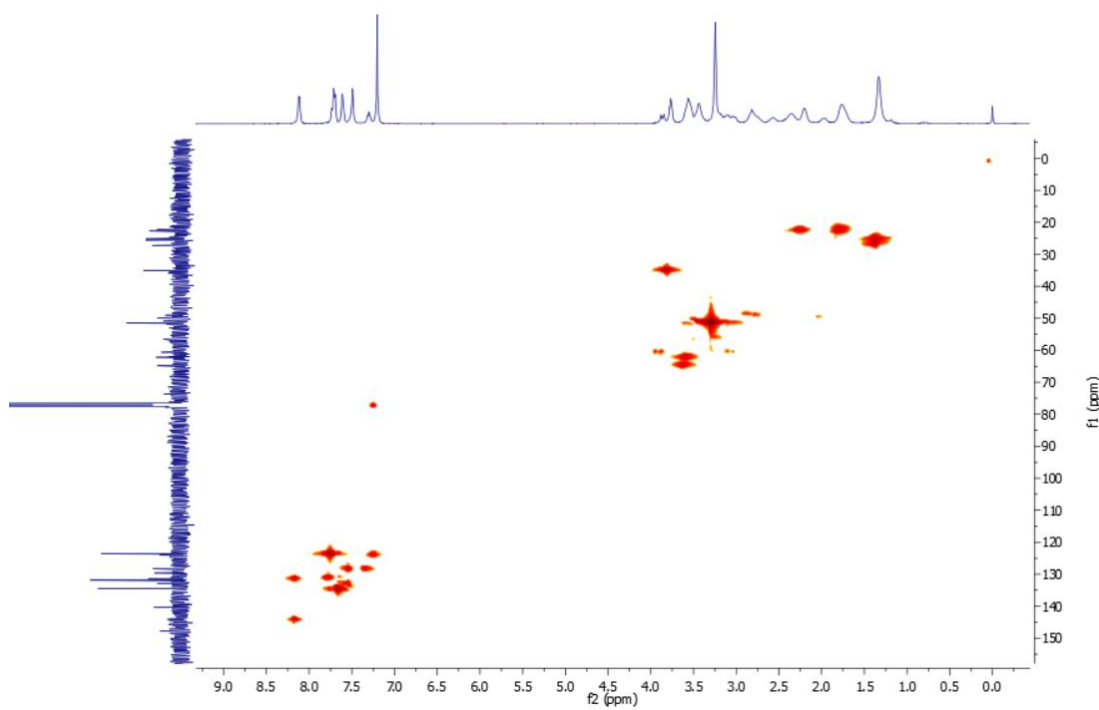## 7.4. Dualsteric ligand 16
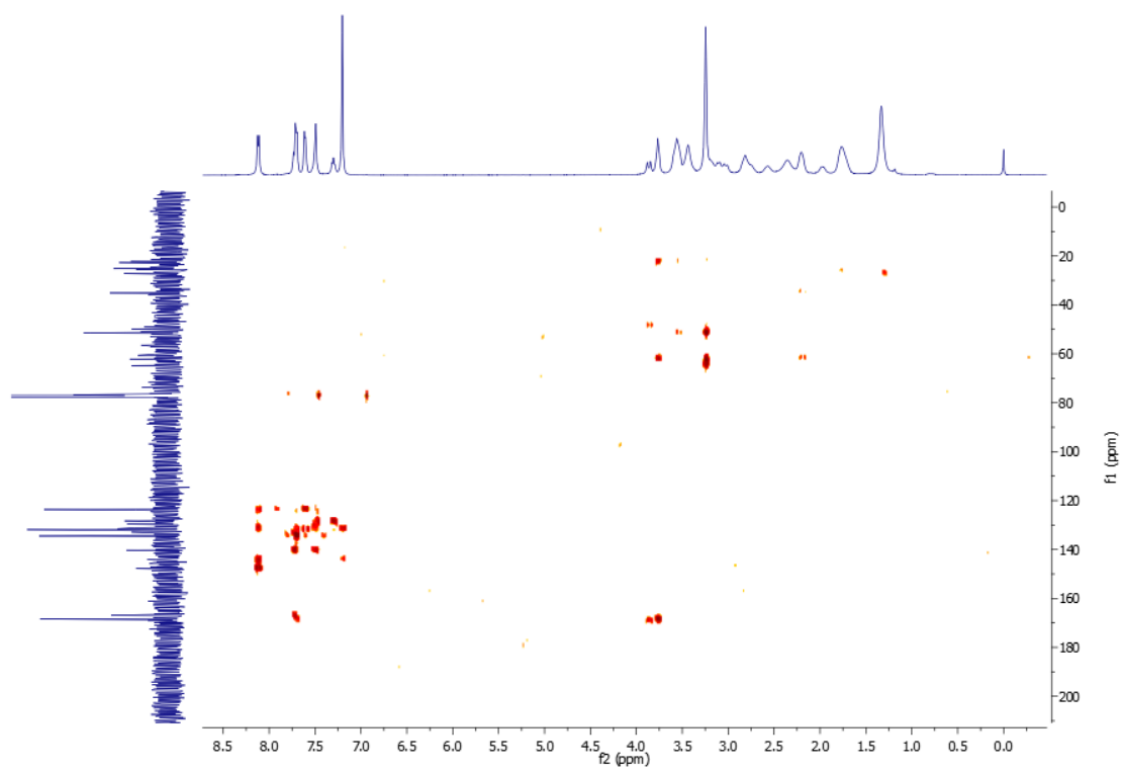
7.4.1. NMR spectra

¹H-NMR spectrum

¹³C-NMR spectrum

COSY spectrum

HMQC spectrum

HMBC spectrum

7.4.2. IR spectrum
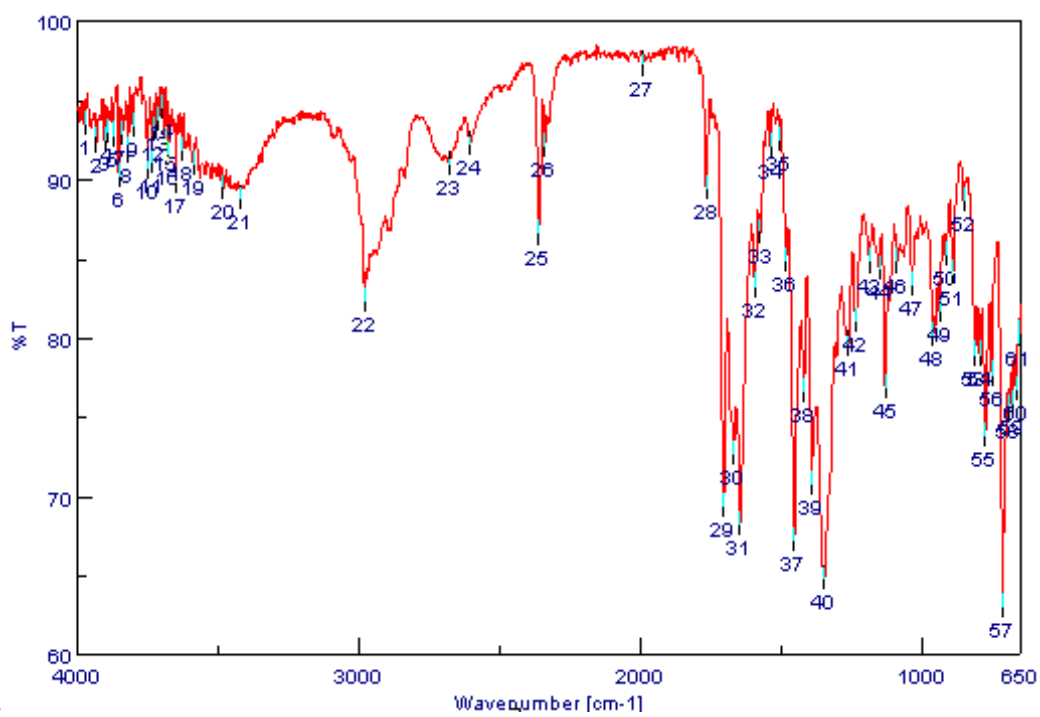
7.4.3. LC-MS spectrum (ESI)

\<Chromatogram\>

mV

Detector A 254nm
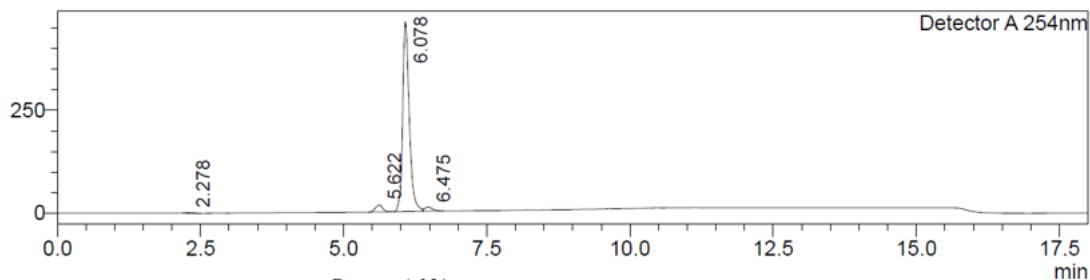
Peak#	Ret. Time	Area	Height	Area%
1	2.278	16760	1810	0.423
2	5.622	146097	16810	3.687
3	6.078	3703284	461120	93.470
4	6.475	95843	10004	2.419
Total		3961984	489744	100.000

Line#:1   R.Time:6.467(Scan#:3881)
MassPeaks:458
Spectrum Mode:Averaged 6.463-6.470(3879-3883) Base Peak:333.75(2935528)
BG Mode:Calc Segment 1 - Event 1
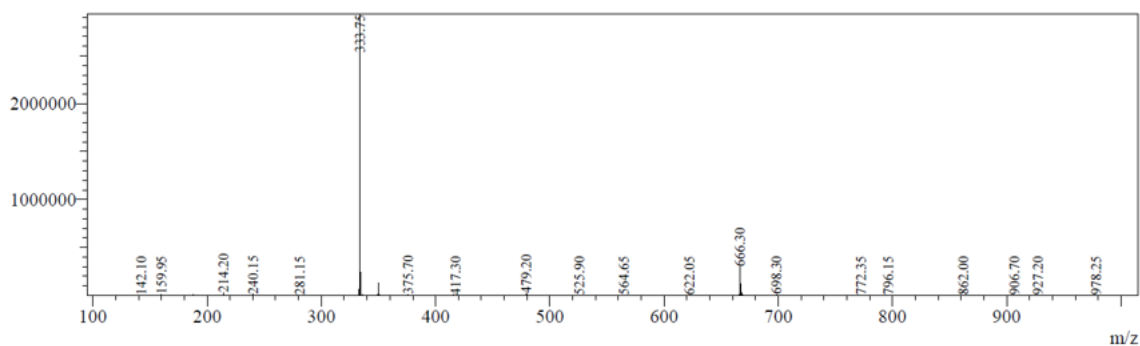
7.5. Dualsteric ligand 17

7.5.1. NMR spectra

1H-NMR spectrum

13C-NMR spectrum
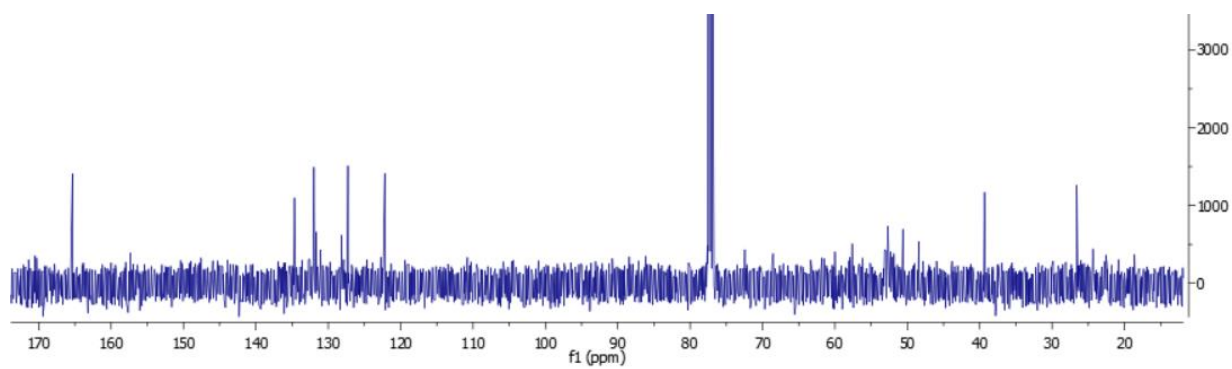
COSY spectrum
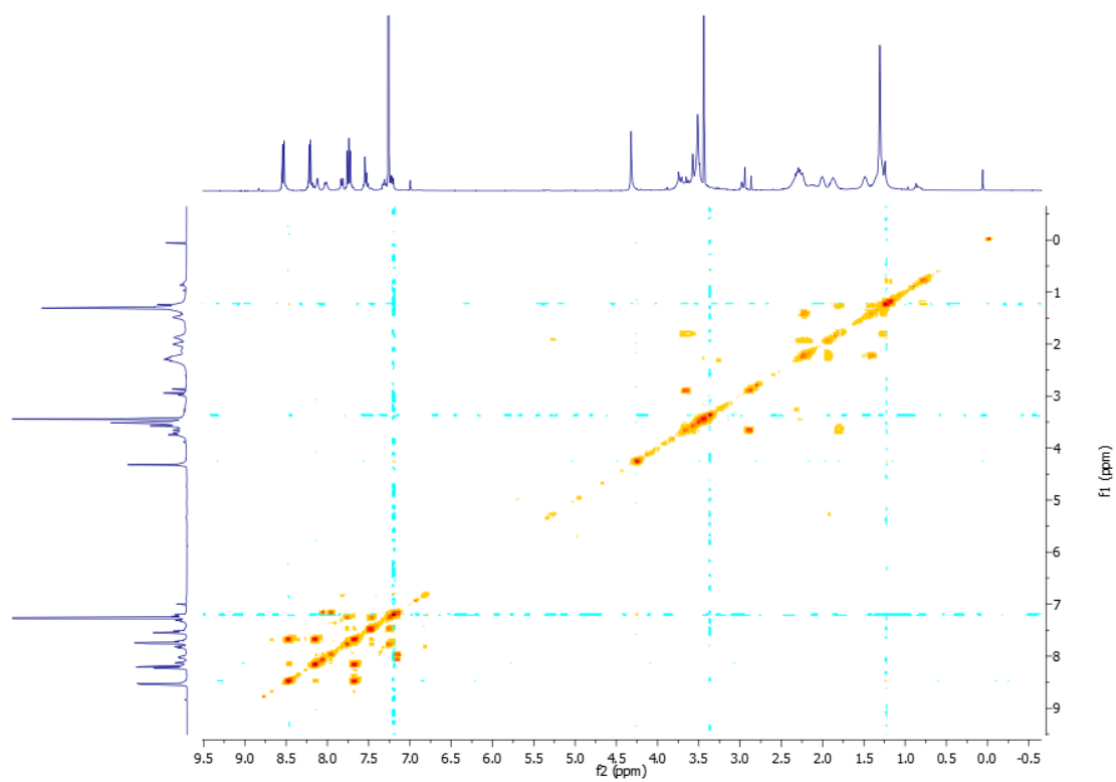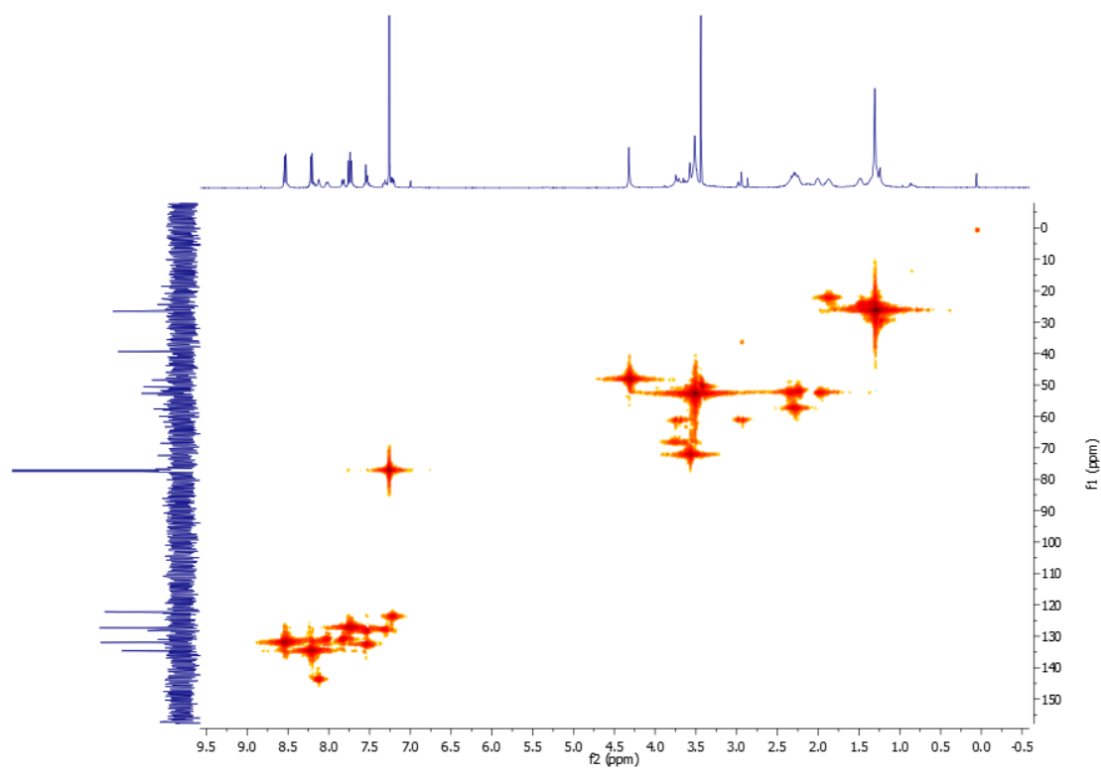
HMQC spectrum

HMBC spectrum
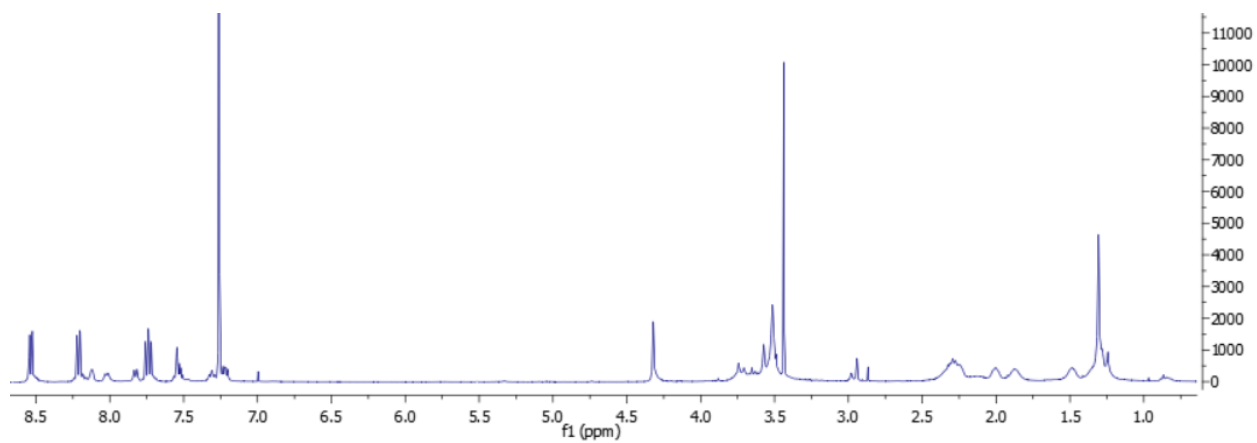

7.5.2. IR spectrum

7.5.3. LC-MS spectrum (ESI)

\<Chromatogram\>

mV
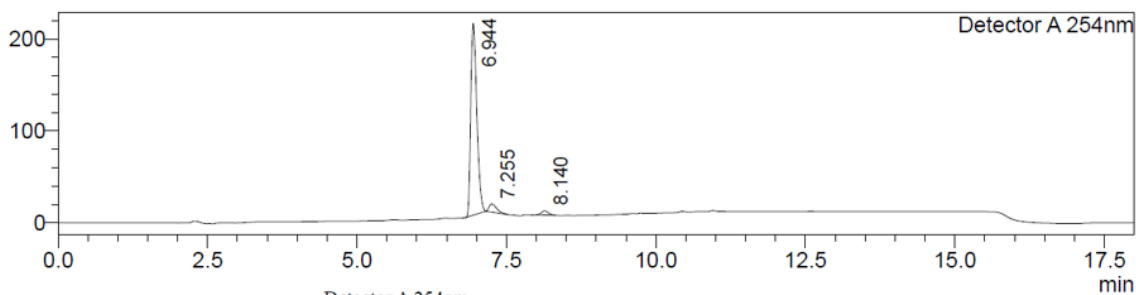
Detector A 254nm

Detector A 254nm

Peak#	Ret. Time	Area	Height	Area%
1	6.944	1472470	208173	92.498
2	7.255	80735	8905	5.072
3	8.140	38691	4704	2.431
Total		1591897	221783	100.000

Line#:1   R.Time:7.320(Scan#:4393)
MassPeaks:406
Spectrum Mode:Averaged 7.317-7.323(4391-4395) Base Peak:358.70(2184352)
BG Mode:Calc Segment 1 - Event 1

7.6. Dualsteric ligand 18

7.6.1. NMR spectra

^{1}H-NMR spectrum
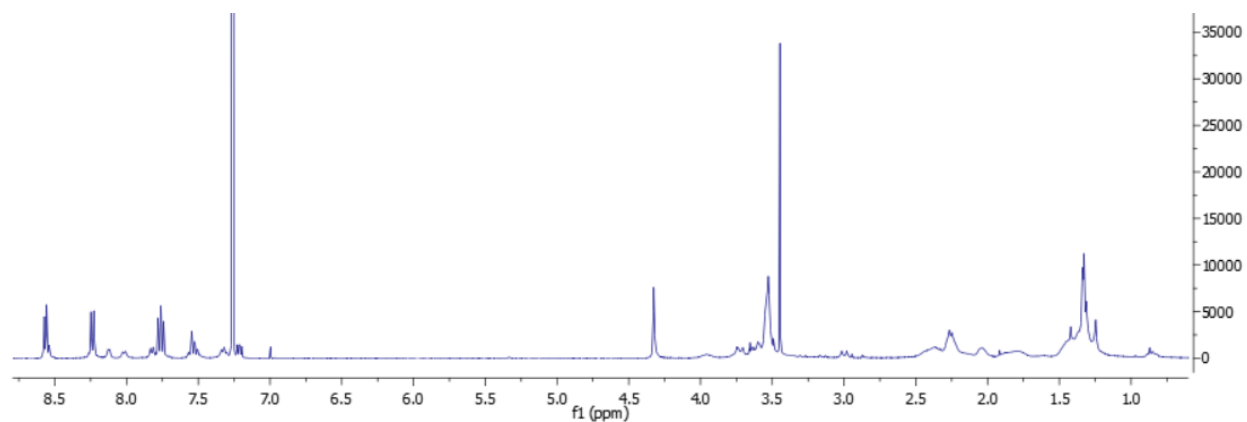
^{13}C-NMR spectrum
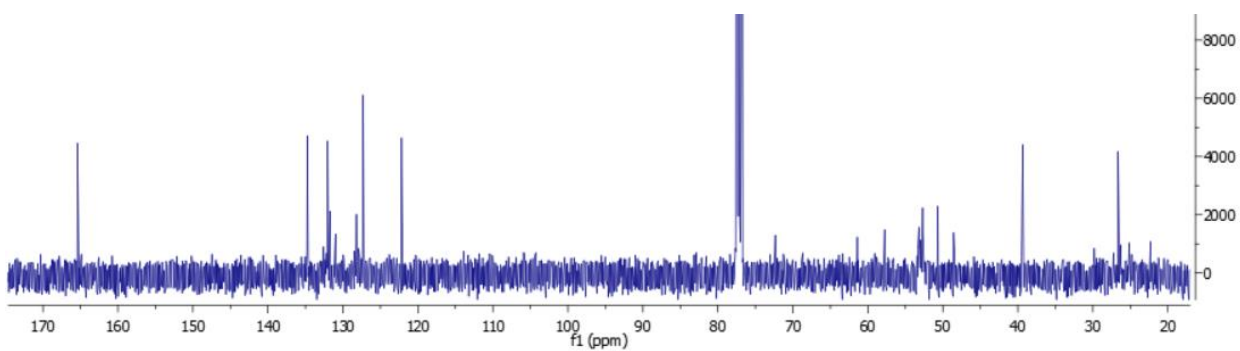
COSY spectrum
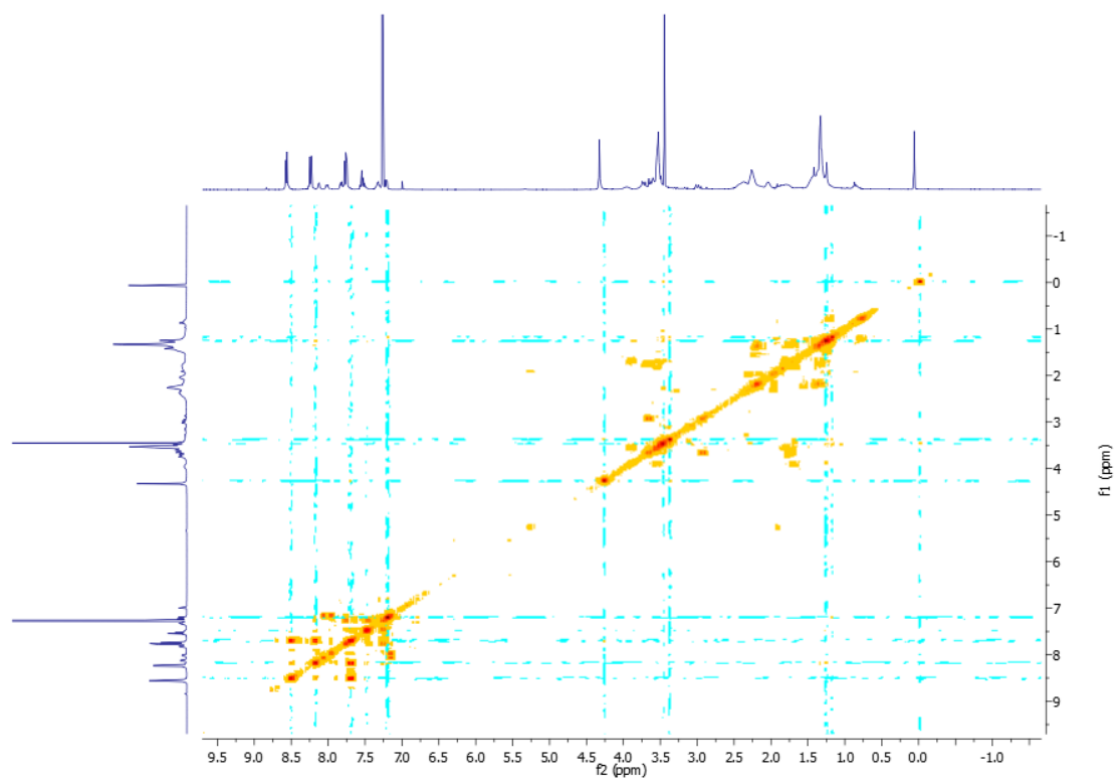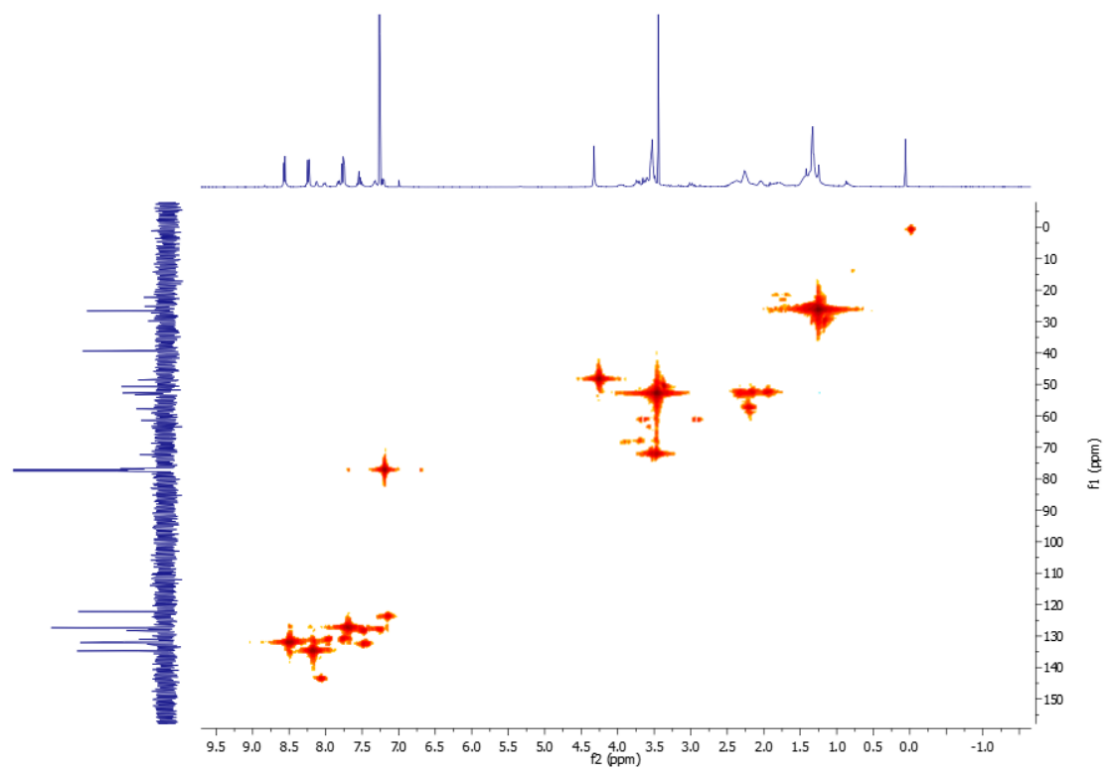
HMQC spectrum

HMBC spectrum
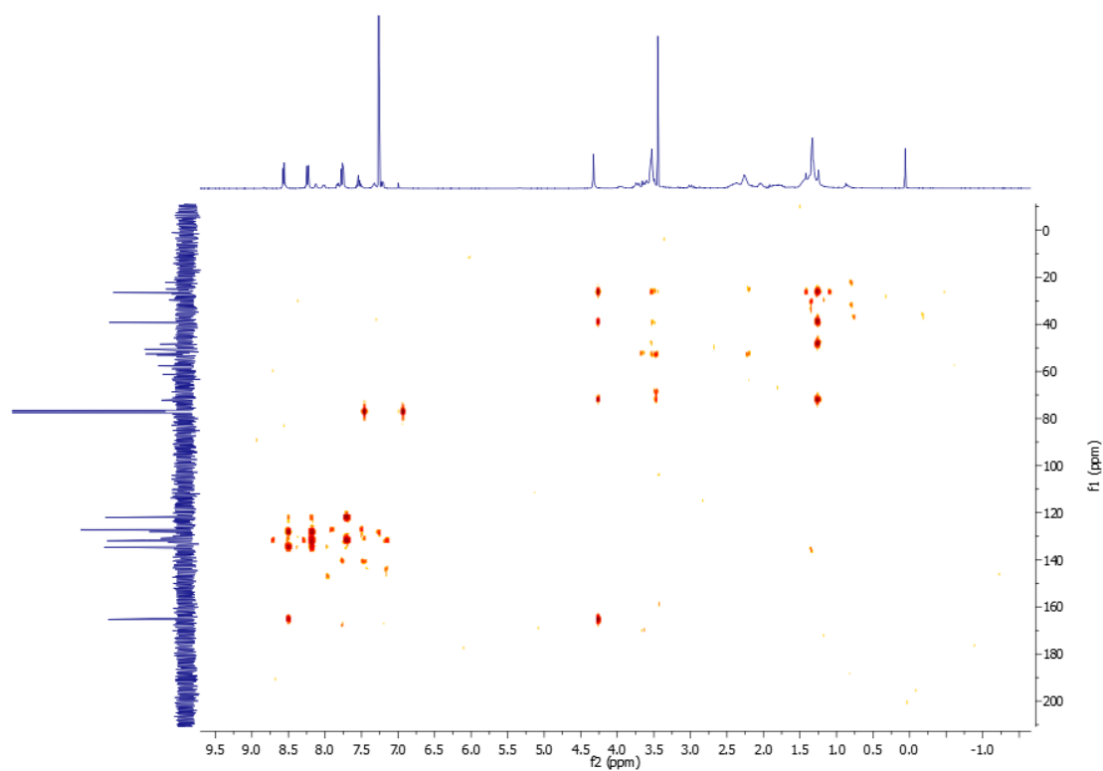
7.6.2. IR spectrum
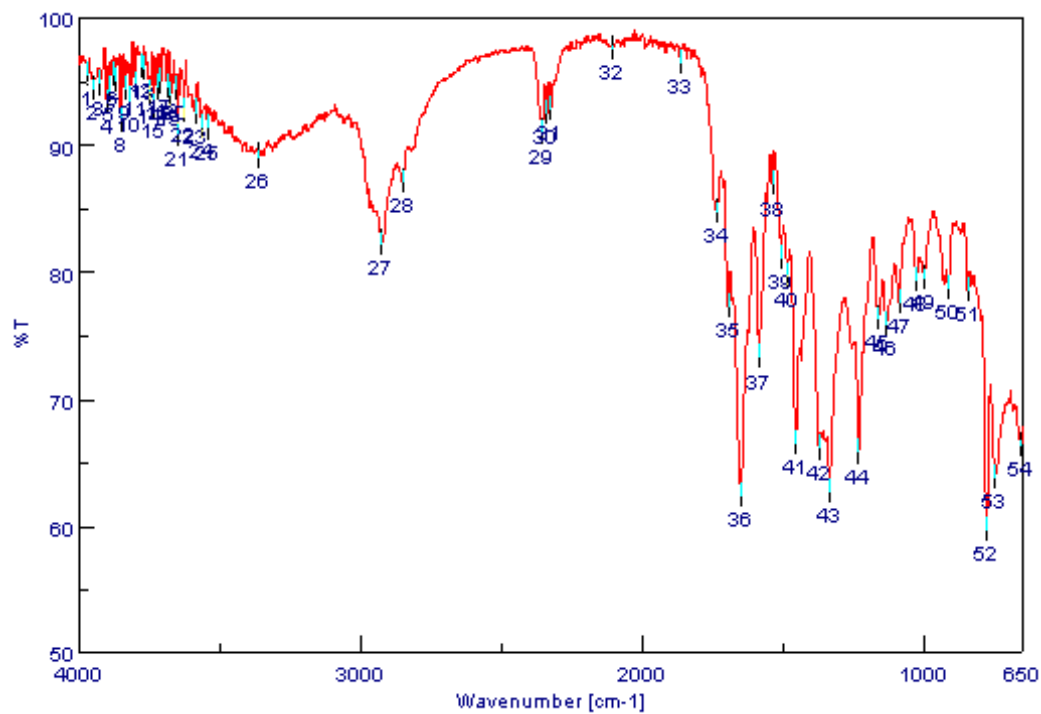
7.6.3. LC-MS spectrum (ESI)

\<Chromatogram\>

mV
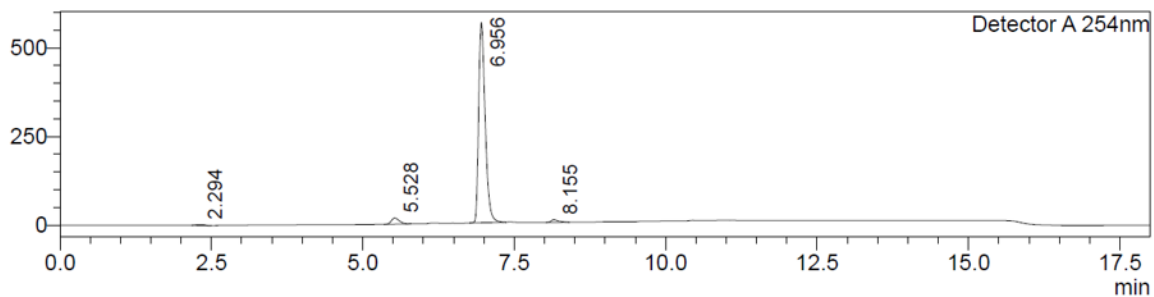
Detector A 254nm

Peak#	Ret. Time	Area	Height	Area%
1	2.294	22172	2271	0.496
2	5.528	156977	17081	3.514
3	6.956	4228178	563364	94.650
4	8.155	59850	7089	1.340
Total		4467177	589804	100.000

Line#:1 R.Time:7.353(Scan#:4413)
MassPeaks:424
Spectrum Mode:Averaged 7.350-7.357(4411-4415) Base Peak:365.75(4346722)
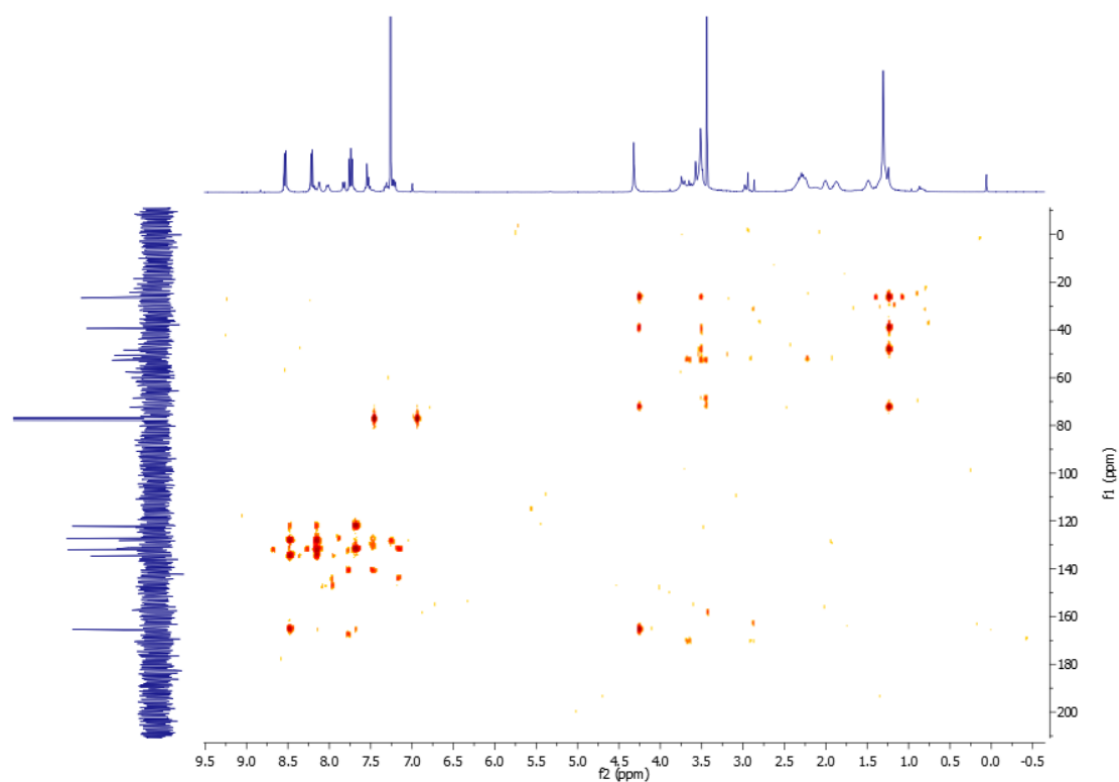BG Mode:Calc Segment 1 - Event 1
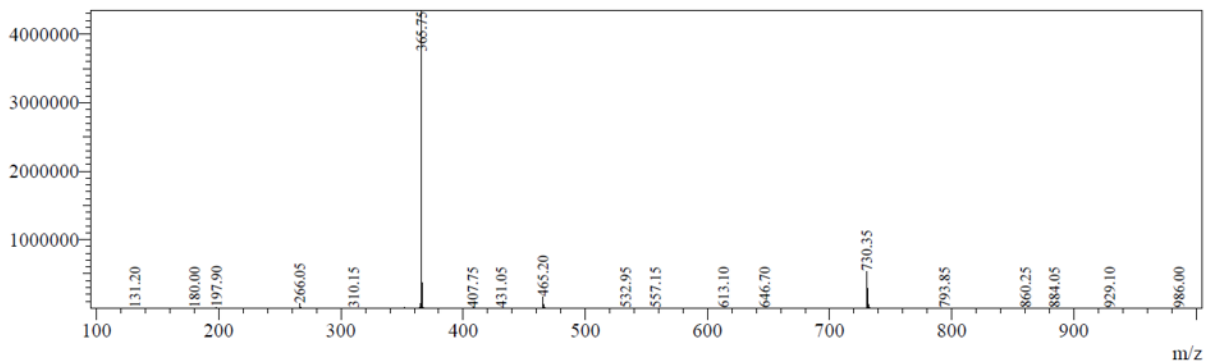
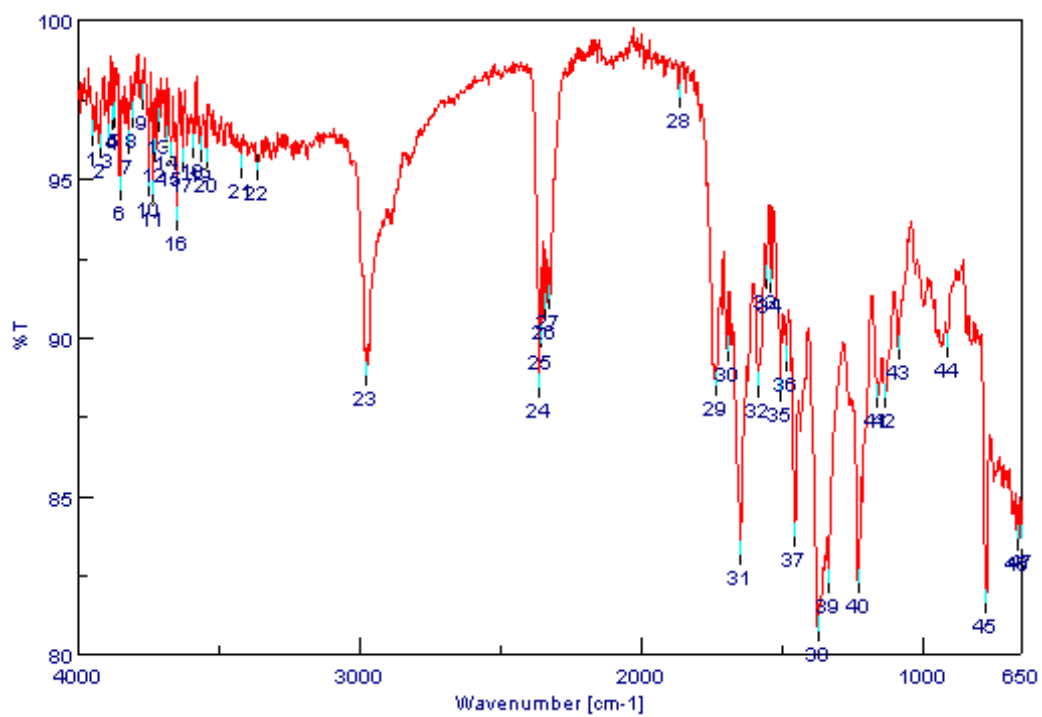## 7.7. Dualsteric ligand 19

7.7.1. NMR spectra

¹H-NMR spectrum
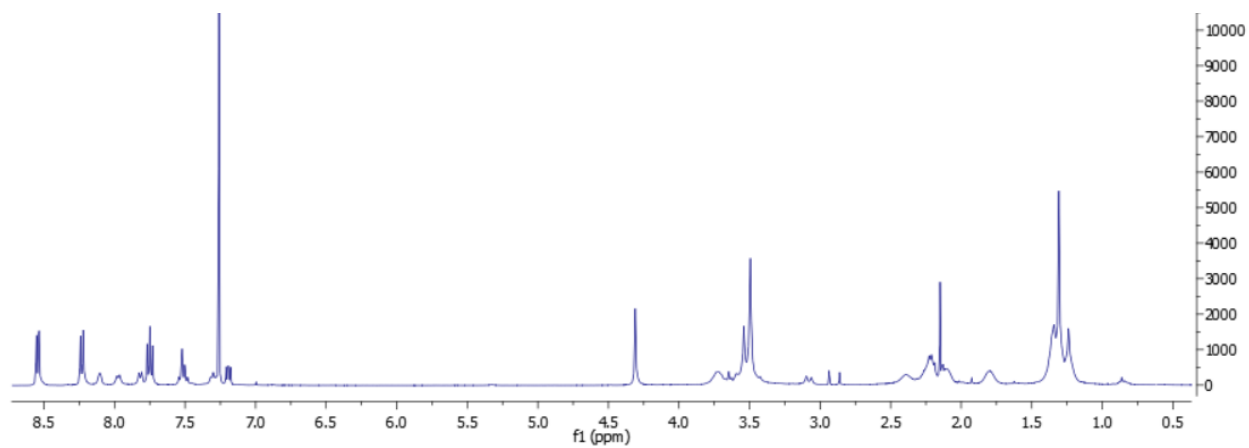
¹³C-NMR spectrum
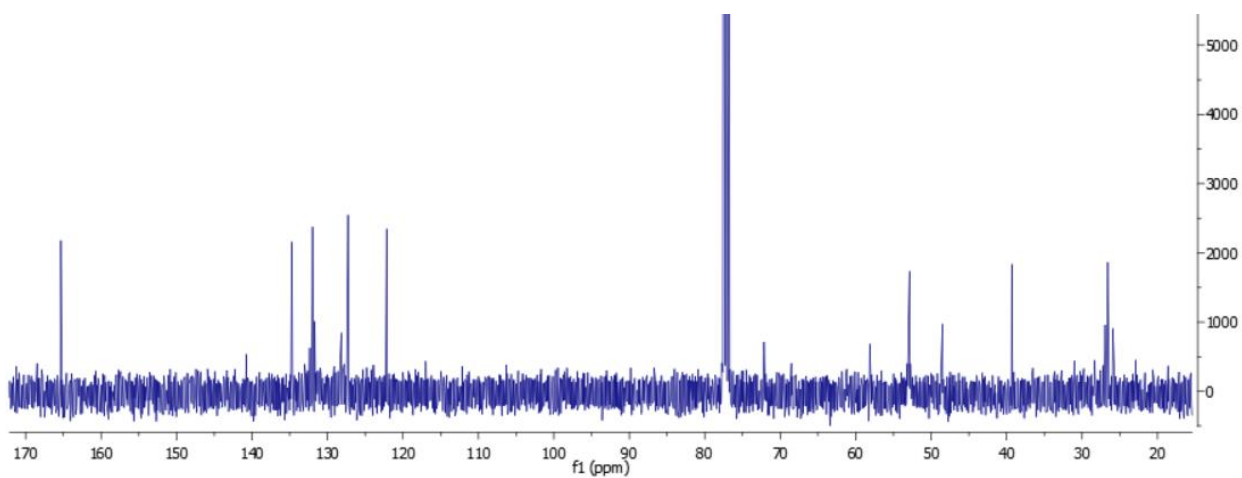
COSY spectrum
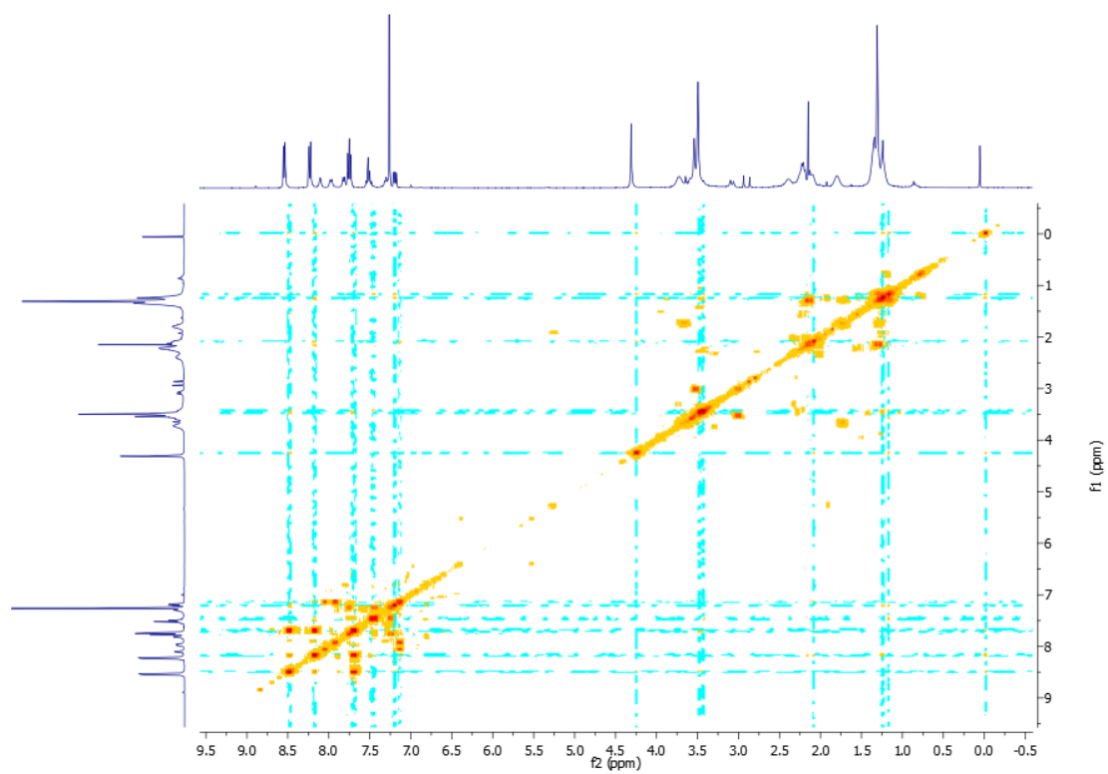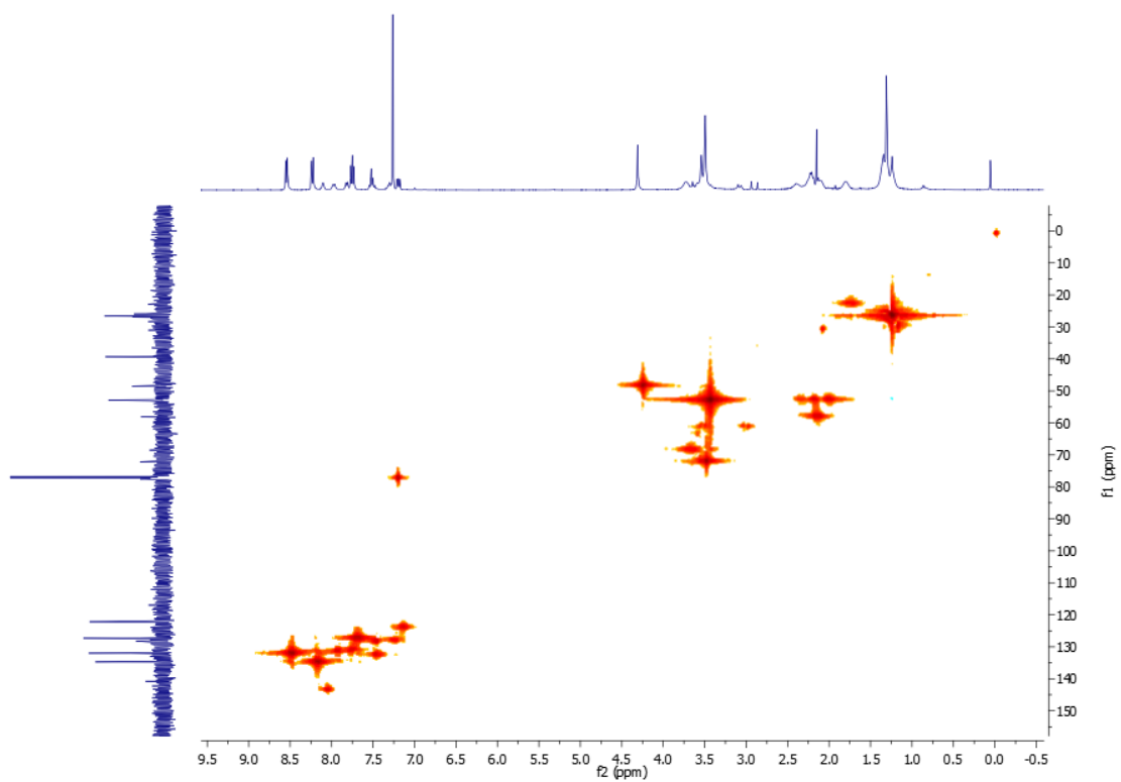
HMQC spectrum

HMBC spectrum
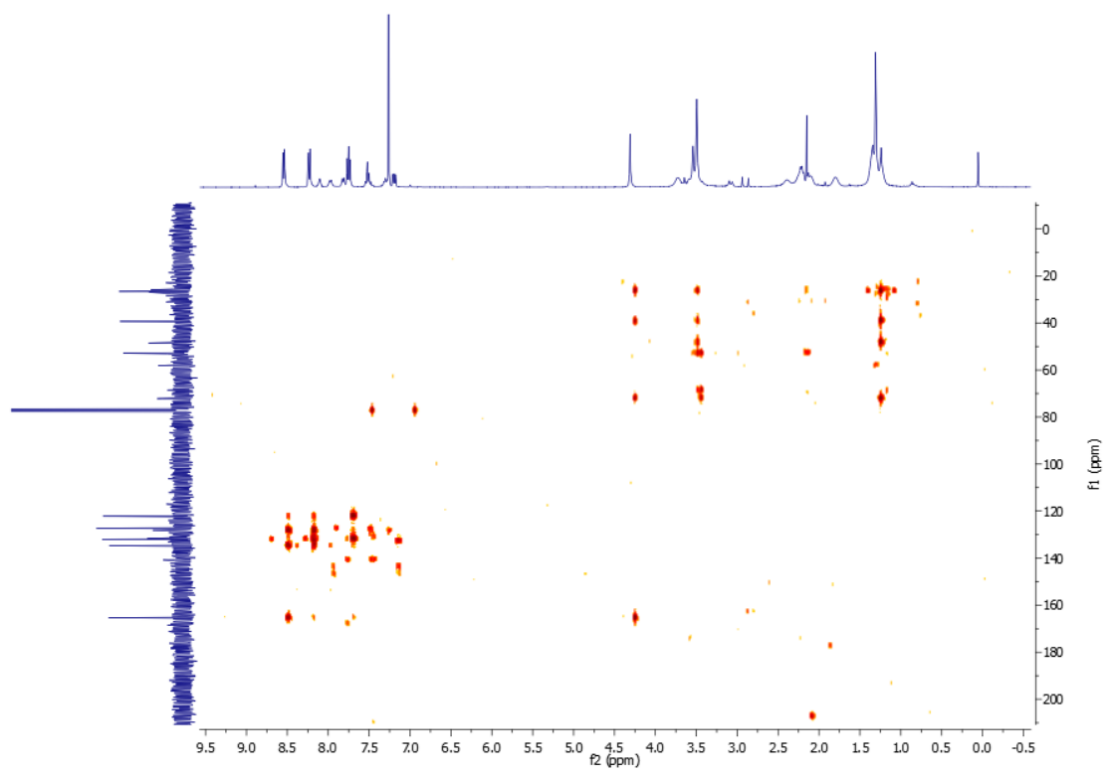
7.7.2. IR spectrum
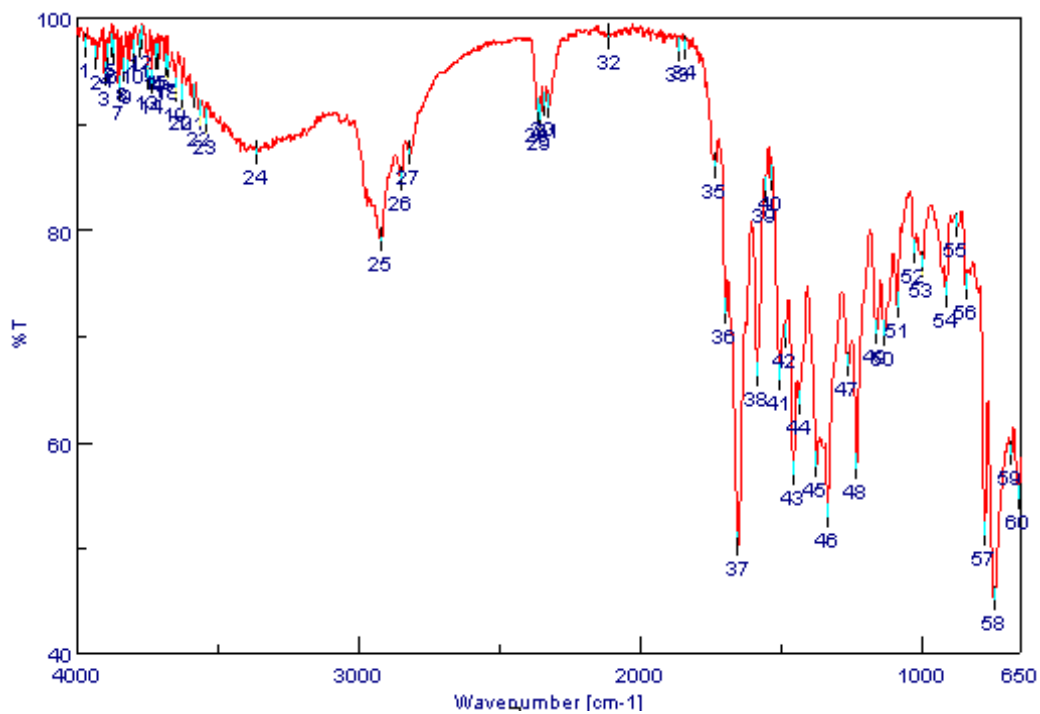
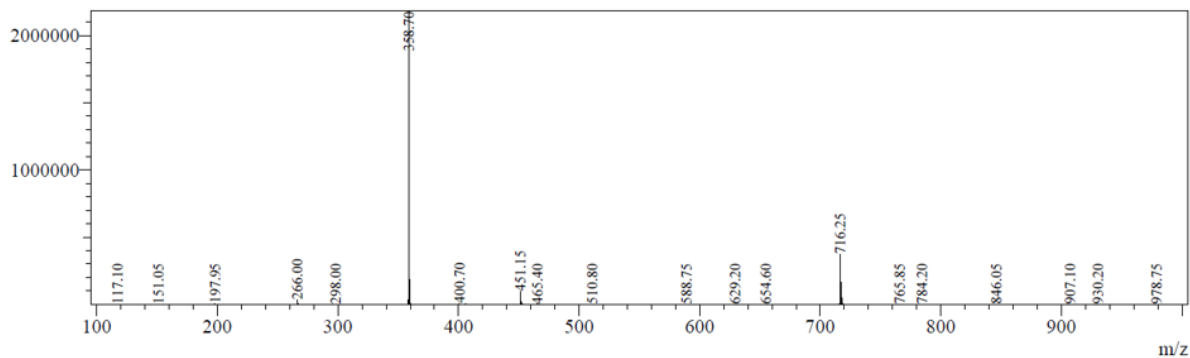## 7.7.3. LC-MS spectrum (ESI)

<Chromatogram>

mV

Detector A 254nm

Detector A 254nm
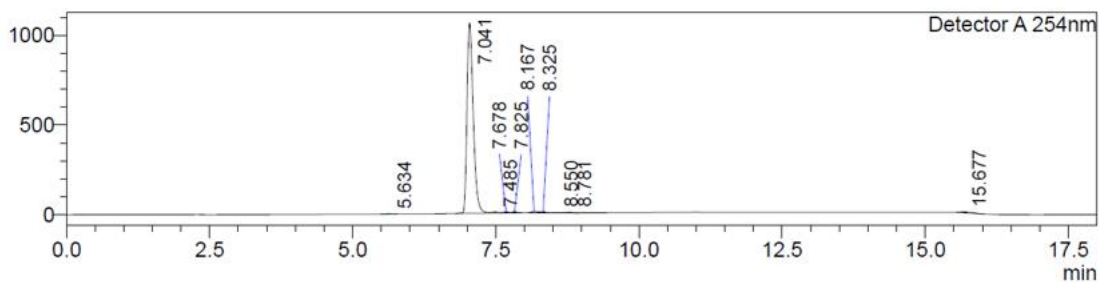
Peak#	Ret. Time	Area	Height	Area%
1	5.634	17014	2129	0.202
2	7.041	8041012	1059010	95.680
3	7.485	55788	5750	0.664
4	7.678	40225	5838	0.479
5	7.825	32945	5237	0.392
6	8.167	62558	8623	0.744
7	8.325	43482	5804	0.517
8	8.550	20672	1303	0.246
9	8.781	24262	4000	0.289
10	15.677	66122	4262	0.787
Total		8404081	1101955	100.000

Line#:1 R.Time:7.427(Scan#:4457)
MassPeaks:356
Spectrum Mode:Averaged 7.423-7.430(4455-4459) Base Peak:372.75(9353047)
BG Mode:Calc Segment 1 - Event 1
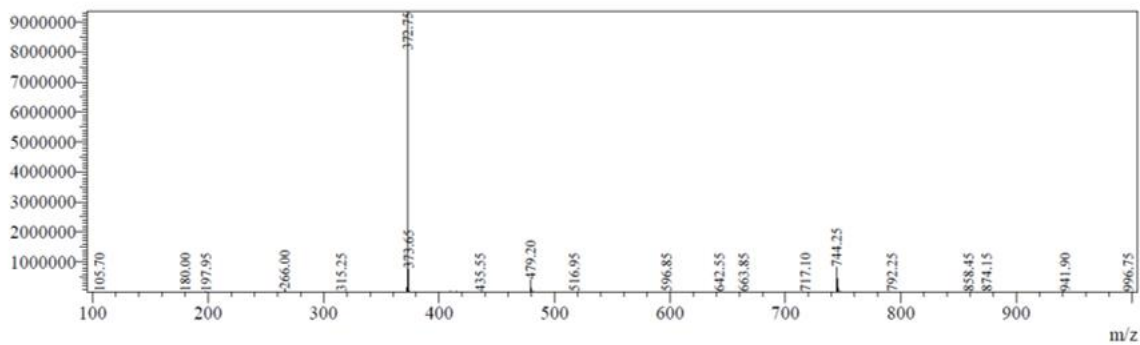
7.8. Dualsteric ligand 21

7.8.1. NMR spectra

¹H-NMR spectrum

¹³C-NMR spectrum
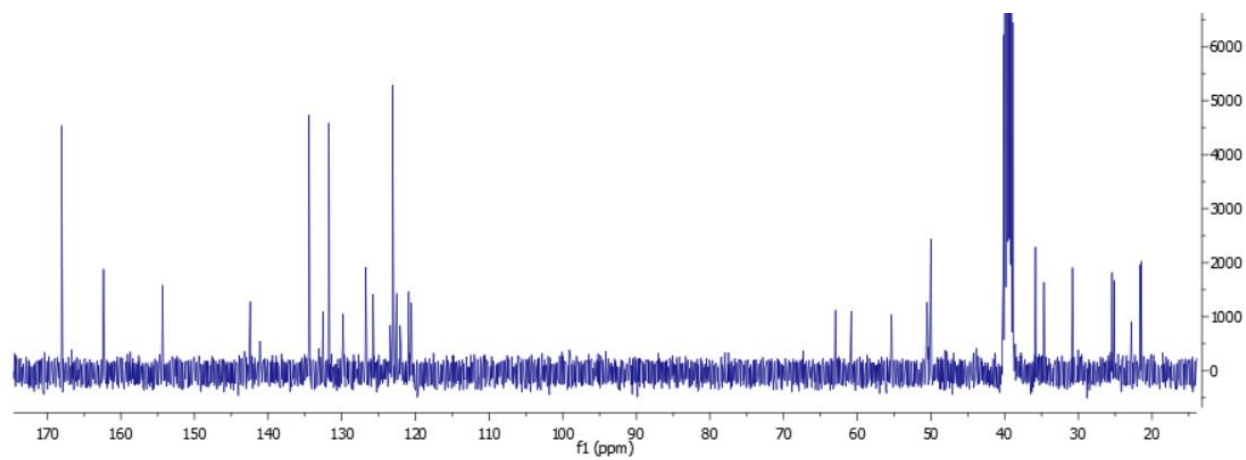
COSY spectrum
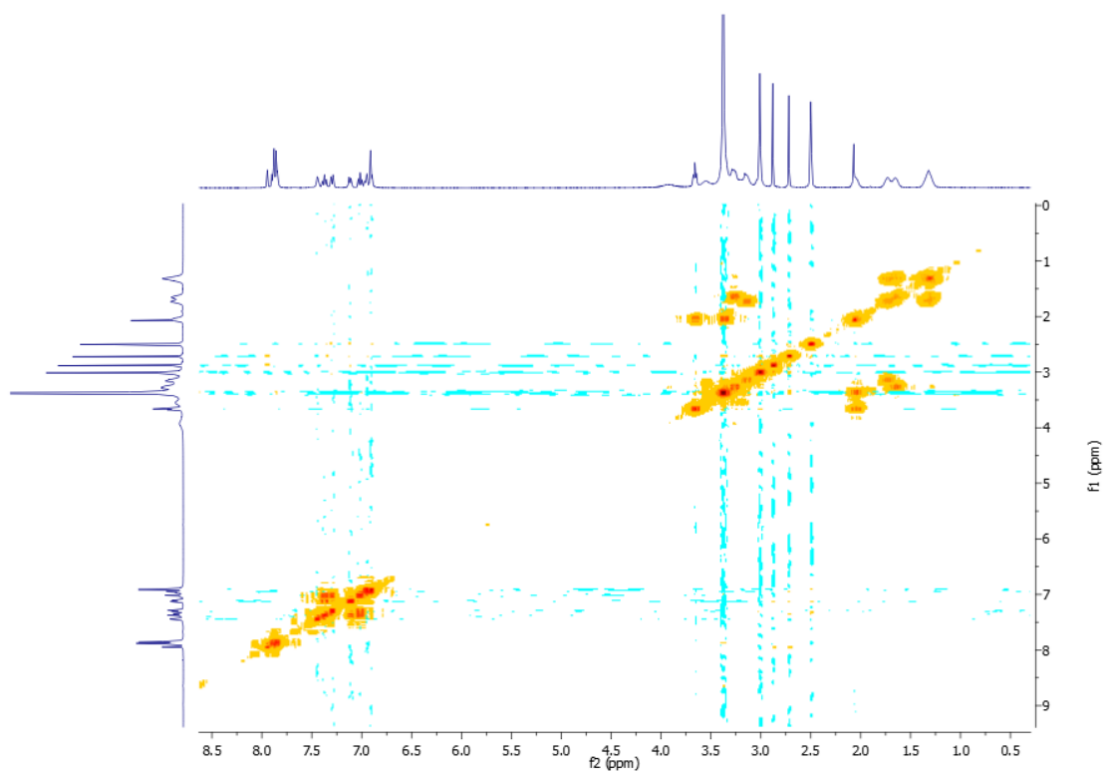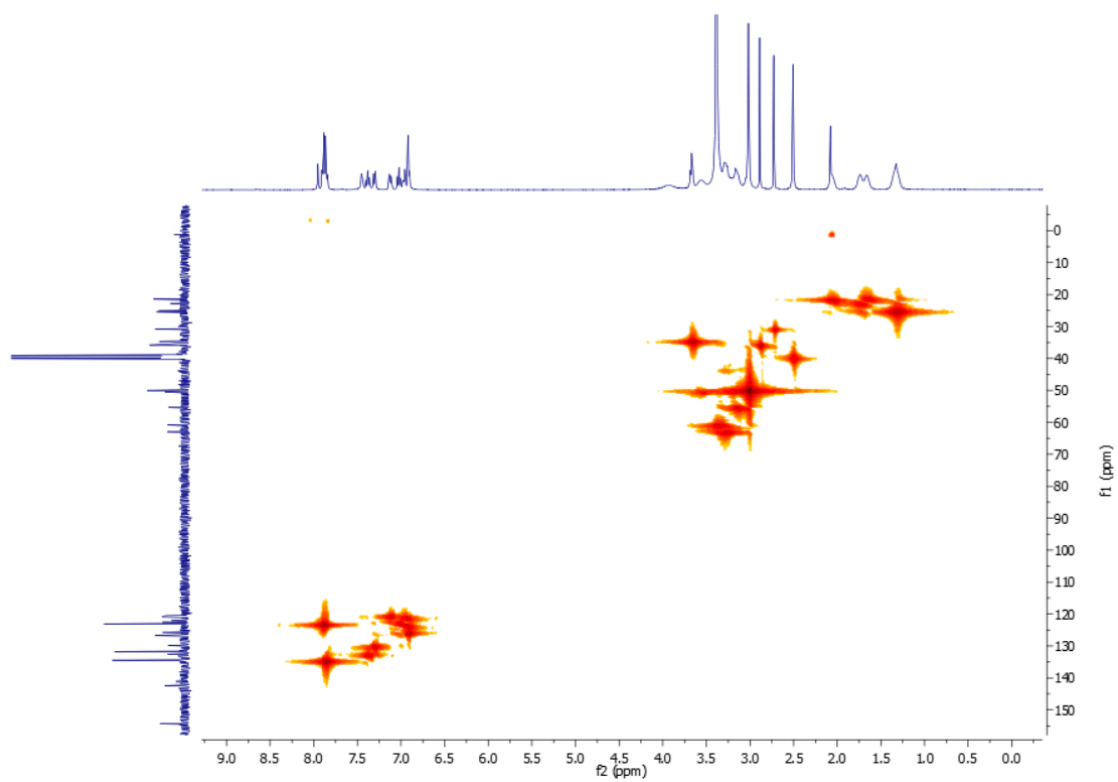
HMQC spectrum

HMBC spectrum

7.8.2. IR spectrum

sult of Peak Picking

.	Position	Intensity	No.	Position	Intensity
	3992.89	103	2	3932.14	100
	3922.5	101	4	3902.25	98
	3891.65	100	6	3881.04	100
	3870.43	99	8	3854.04	96
	3839.58	99	10	3821.26	98

7.8.3. LC-MS spectrum (ESI)

\<Chromatogram\>

mV
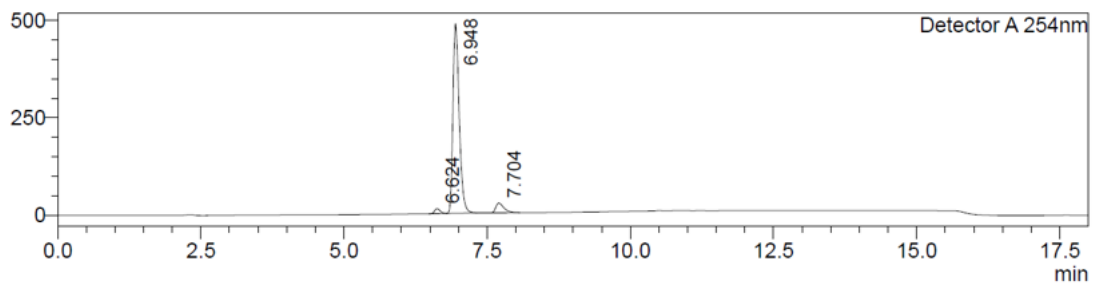
Detector A 254nm

Peak#	Ret. Time	Area	Height	Area%
1	6.624	88667	12936	2.191
2	6.948	3711292	486046	91.718
3	7.704	246436	24800	6.090
Total		4046394	523782	100.000

Line#:1 R.Time:7.320(Scan#:4393)
MassPeaks:469
Spectrum Mode:Averaged 7.317-7.323(4391-4395) Base Peak:314.40(2323972)
BG Mode:Calc Segment 1 - Event 1

m/z
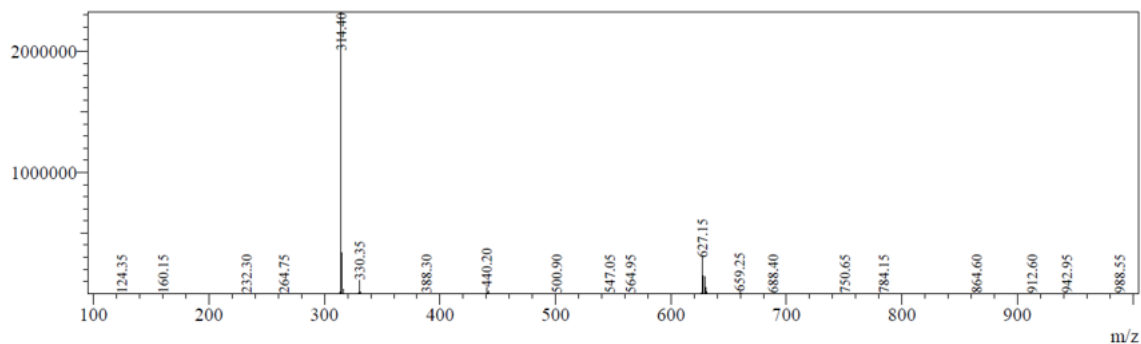
7.9. Dualsteric ligand 22

7.9.1. NMR spectra

<u>*1H-NMR spectrum*</u>
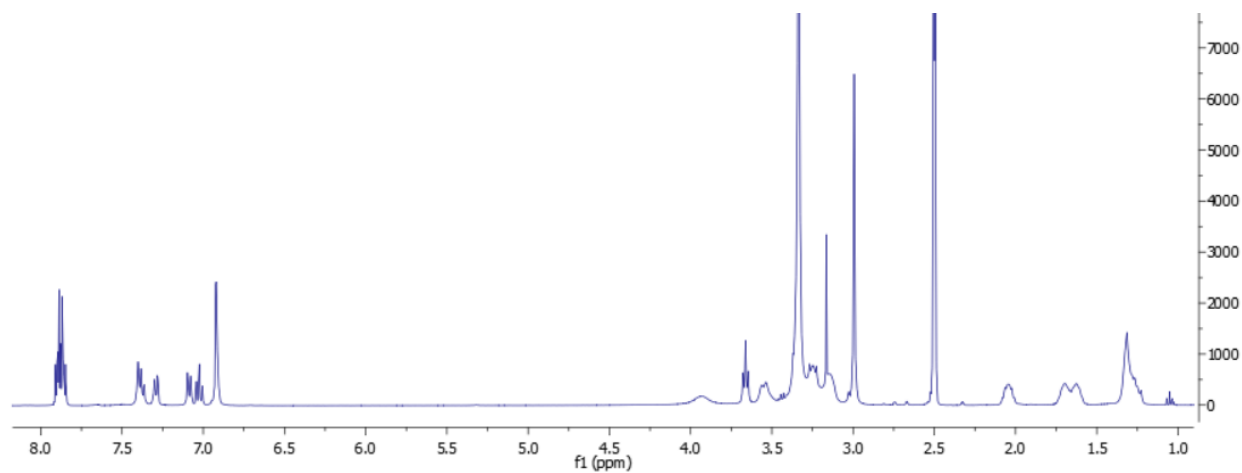
<u>*13C-NMR spectrum*</u>
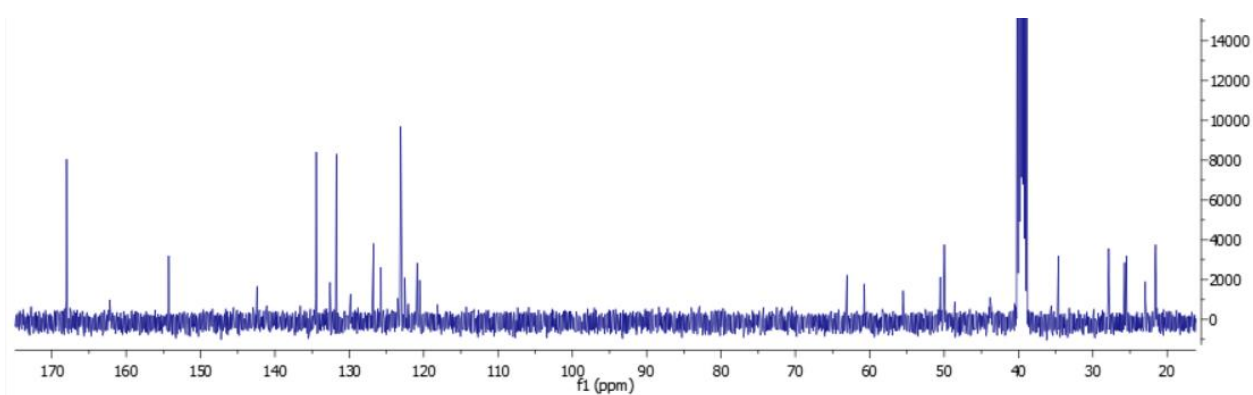
COSY spectrum
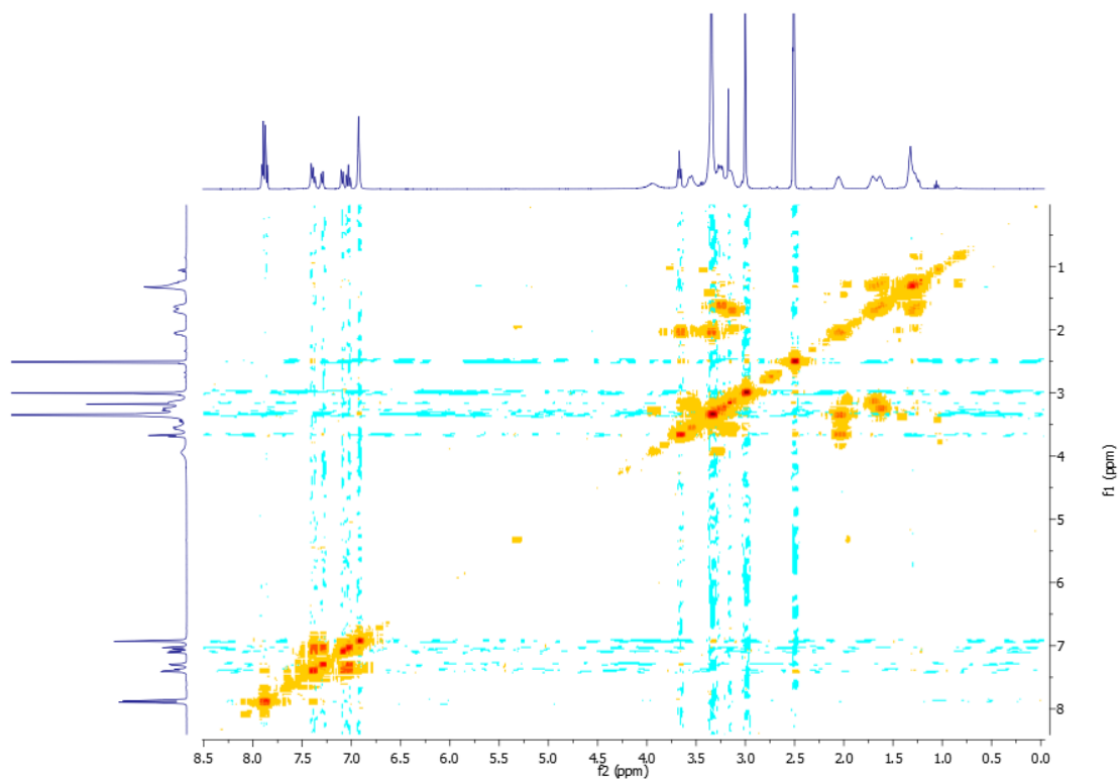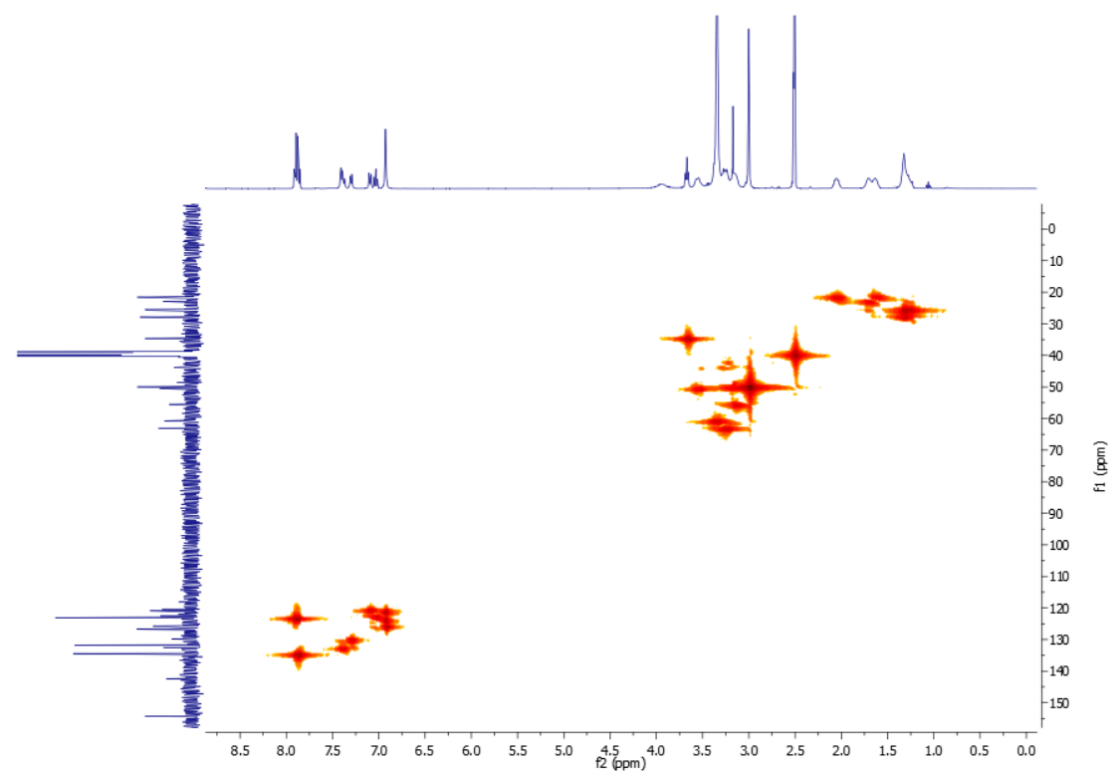
HMQC spectrum

HMBC spectrum
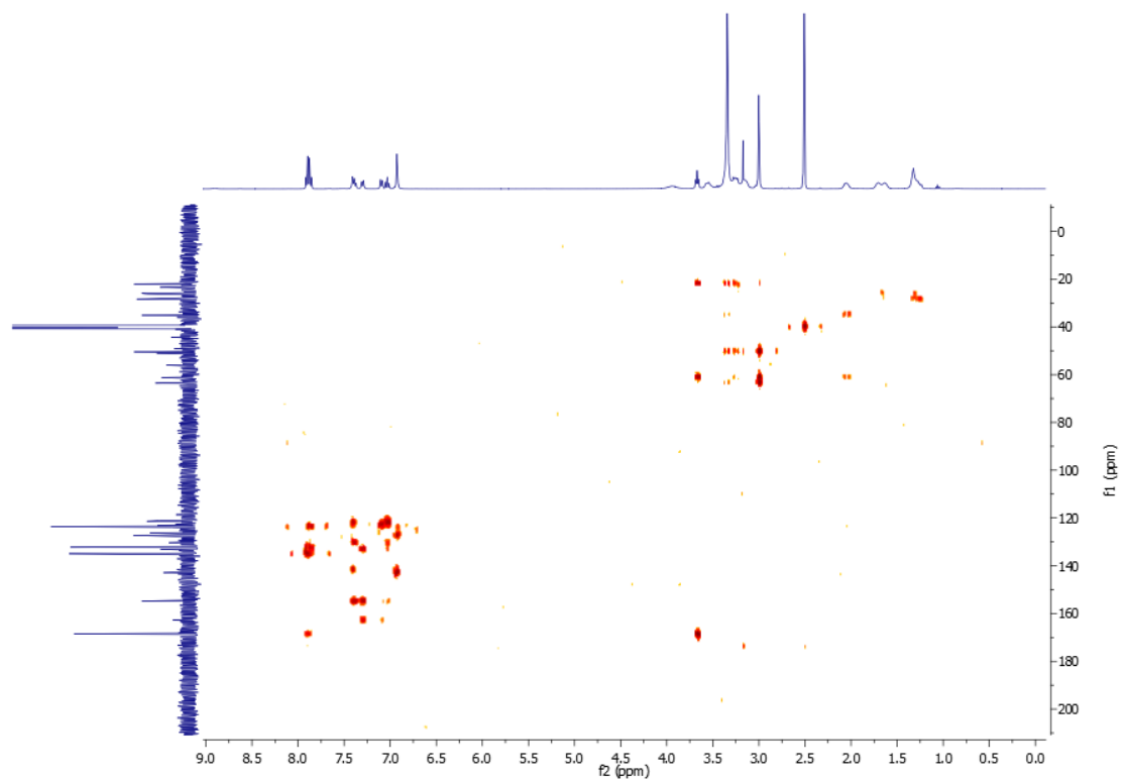
7.9.2. IR spectrum
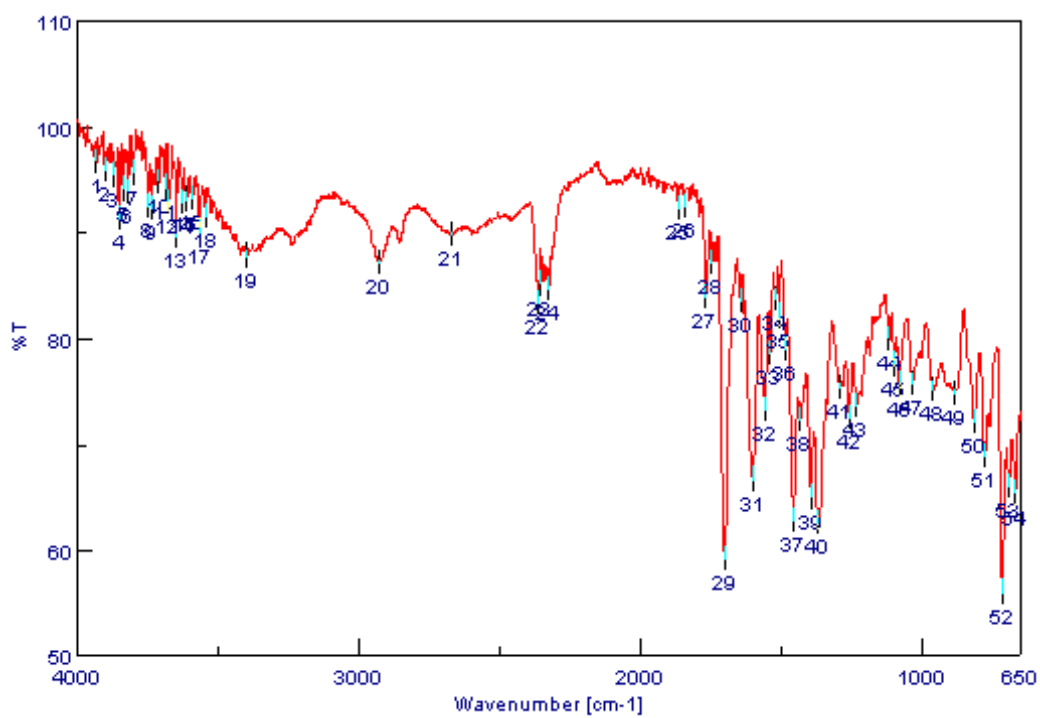
7.9.3. LC-MS spectrum (ESI)

\<Chromatogram\>

mV
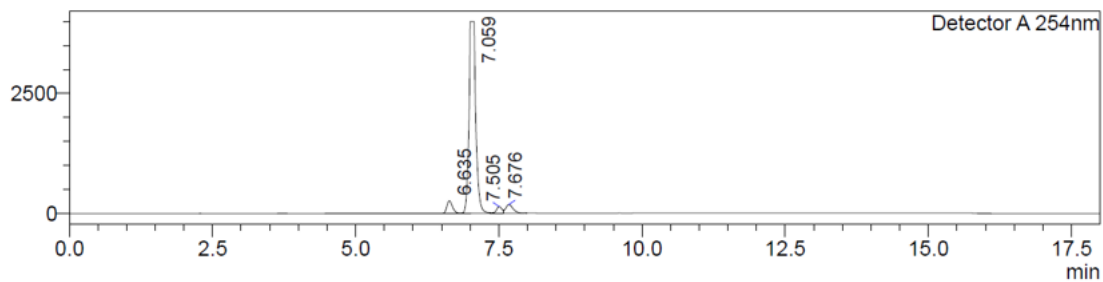
Detector A 254nm

Detector A 254nm

Peak#	Ret. Time	Area	Height	Area%
1	6.635	1823853	262884	4.891
2	7.059	32906386	3993160	88.247
3	7.505	945421	140587	2.535
4	7.676	1613333	181502	4.327
Total		37288993	4578133	100.000

Line#:1 R.Time:7.393(Scan#:4437)
MassPeaks:398
Spectrum Mode:Averaged 7.390-7.397(4435-4439) Base Peak:321.35(8284637)
BG Mode:Calc Segment 1 - Event 1
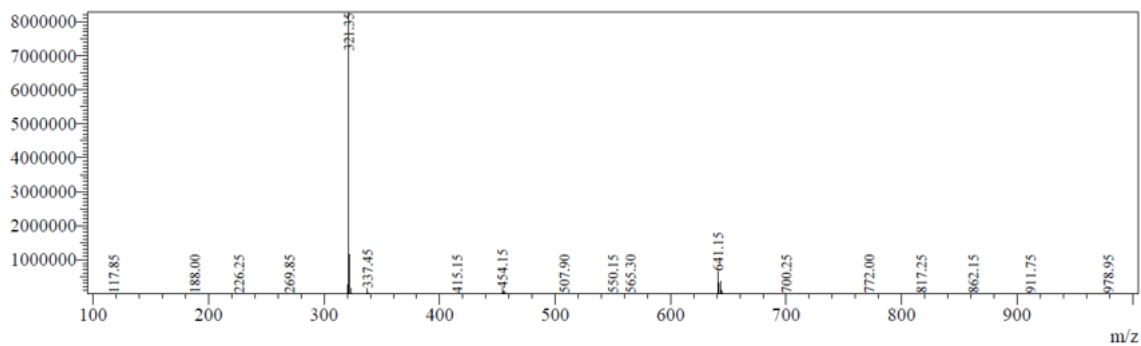
7.10. Dualsteric ligand 23

7.10.1. NMR spectra

¹H-NMR spectrum
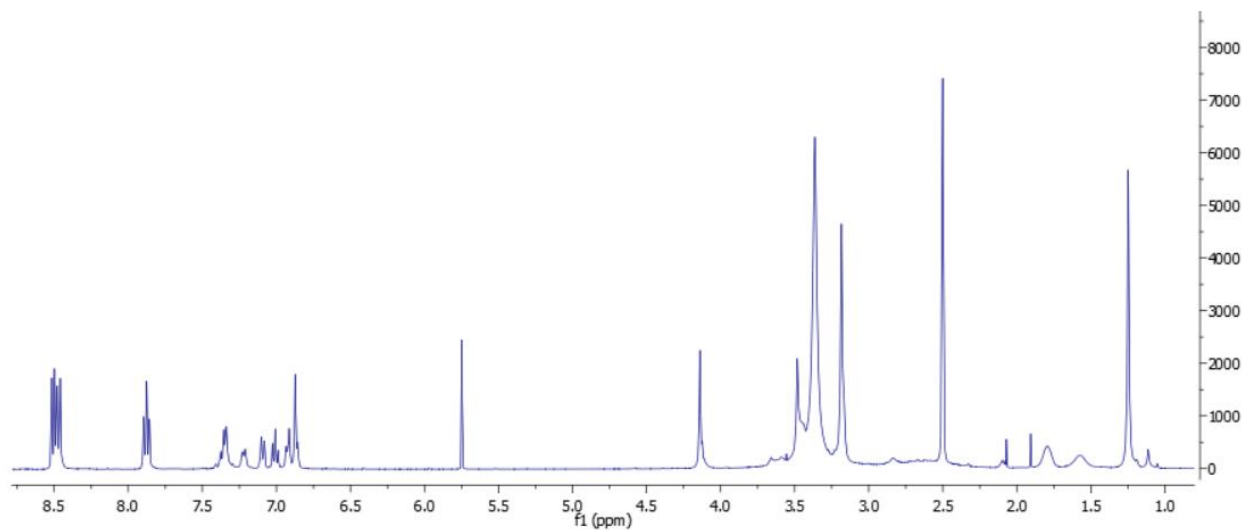
¹³C-NMR spectrum
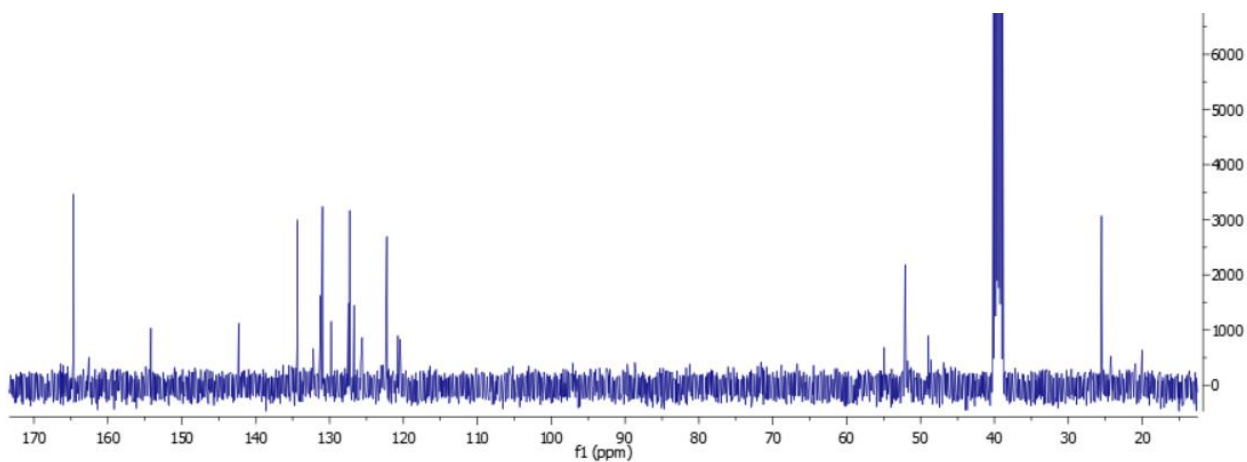
COSY spectrum
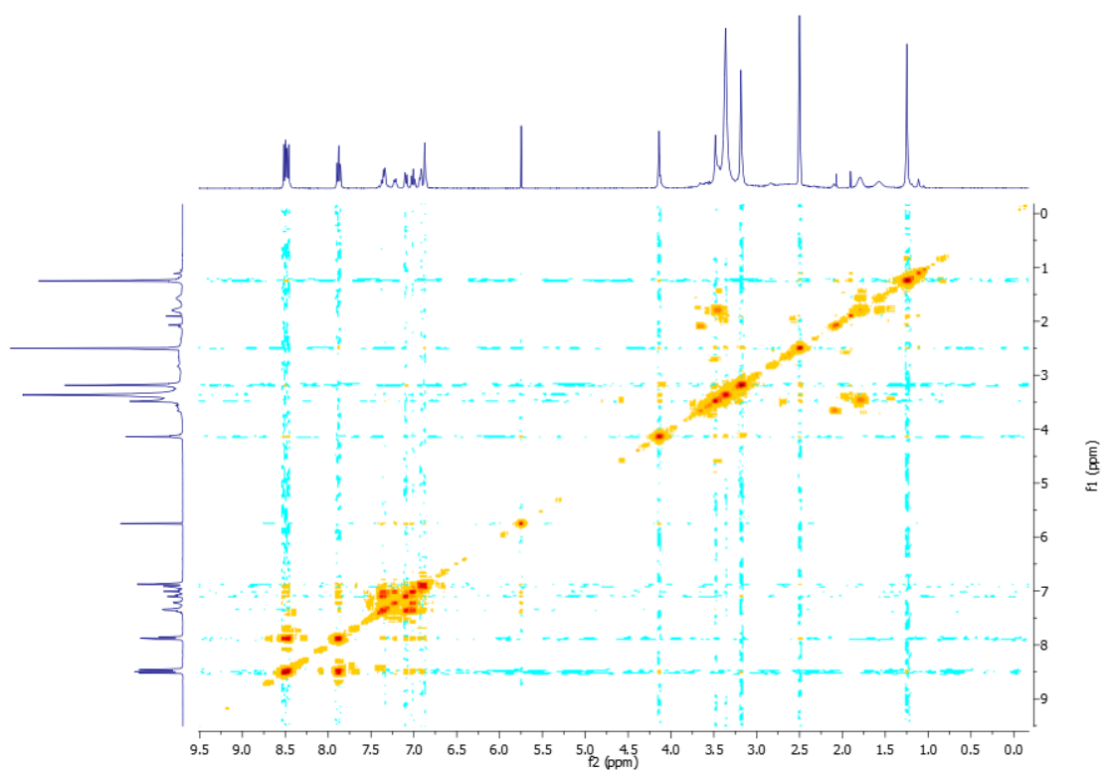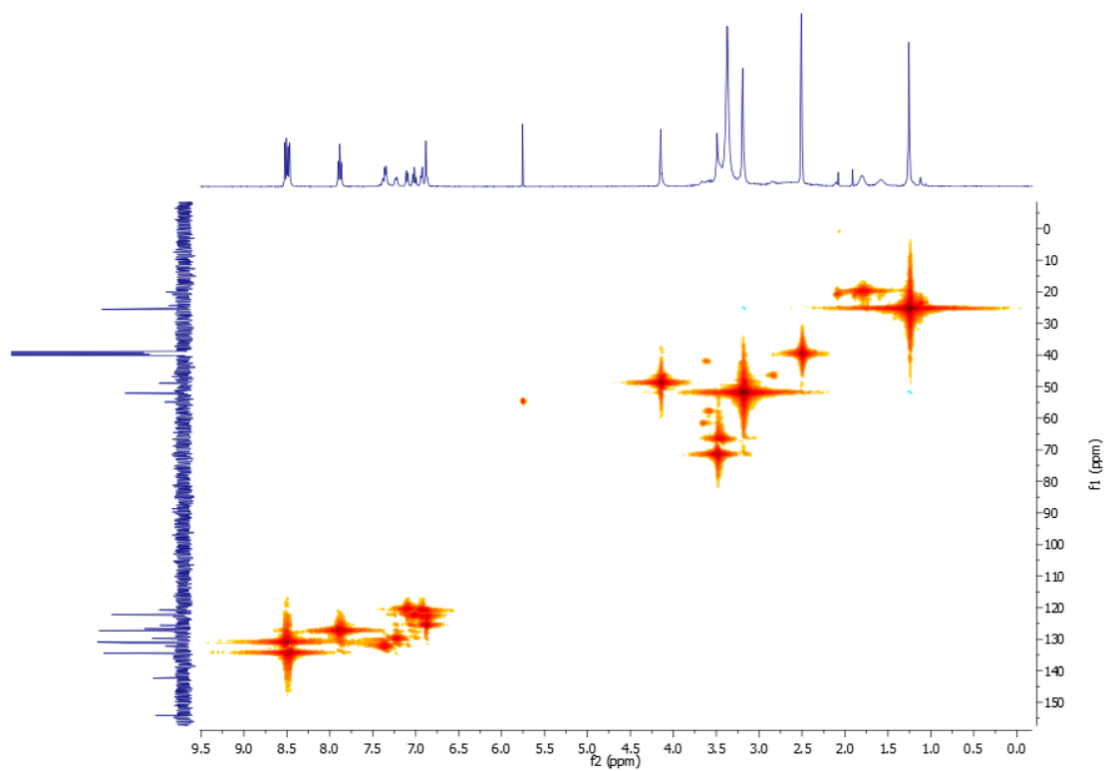
HMQC spectrum

HMBC spectrum
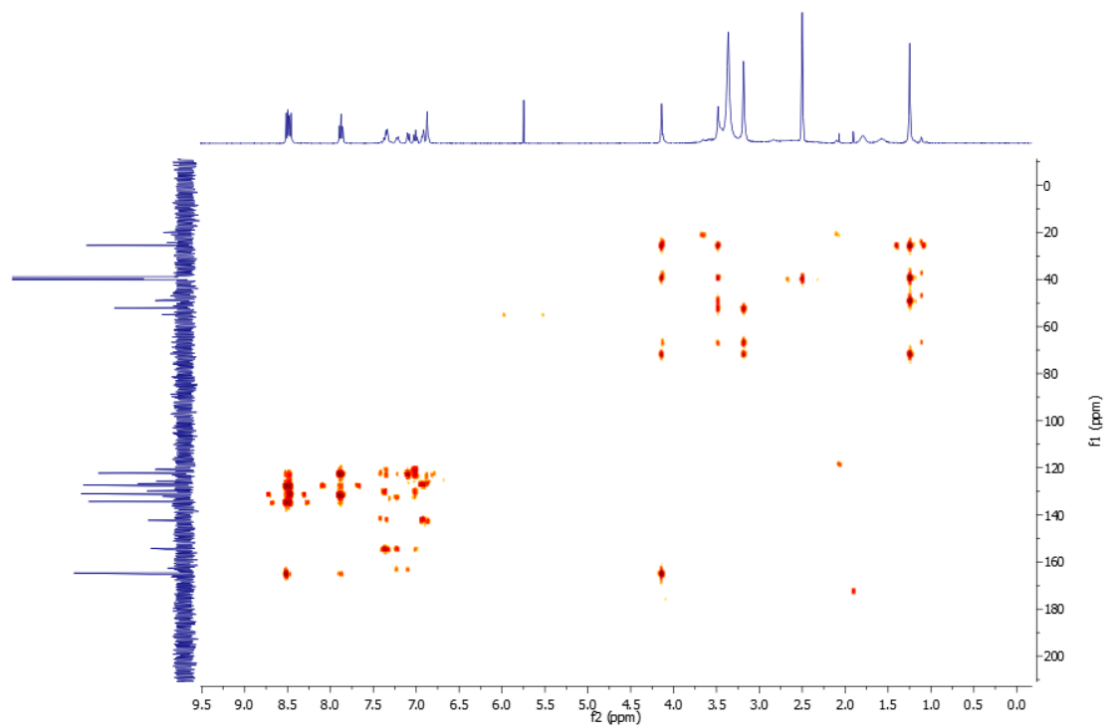
7.10.2. IR spectrum
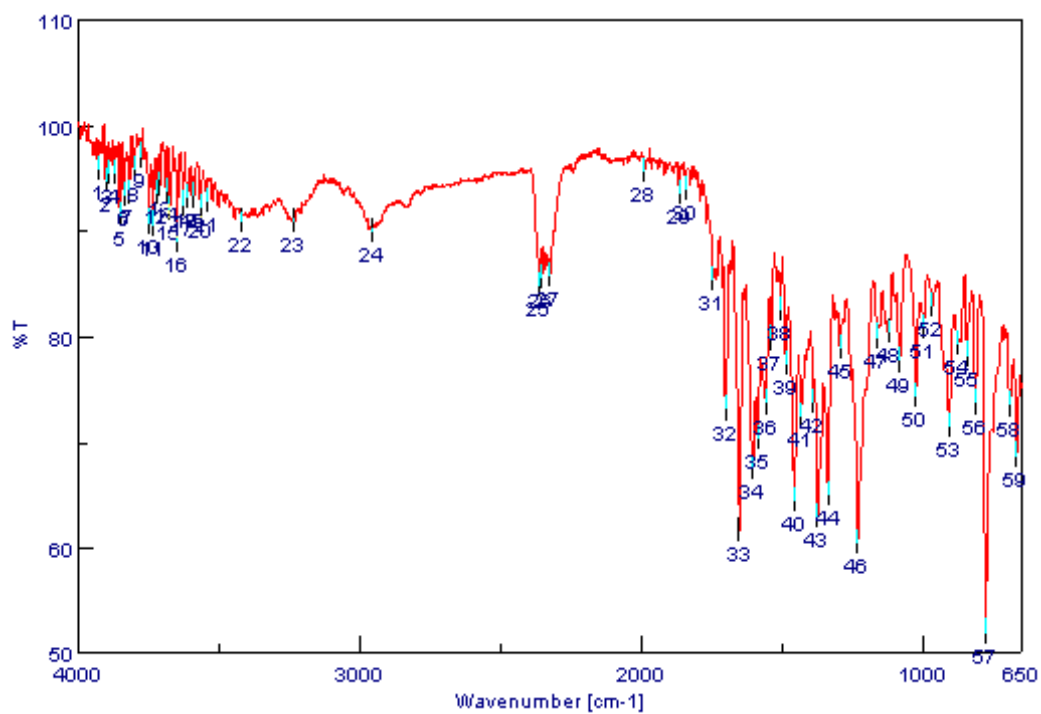
7.10.3. LC-MS spectrum (ESI)

\<Chromatogram\>

mV
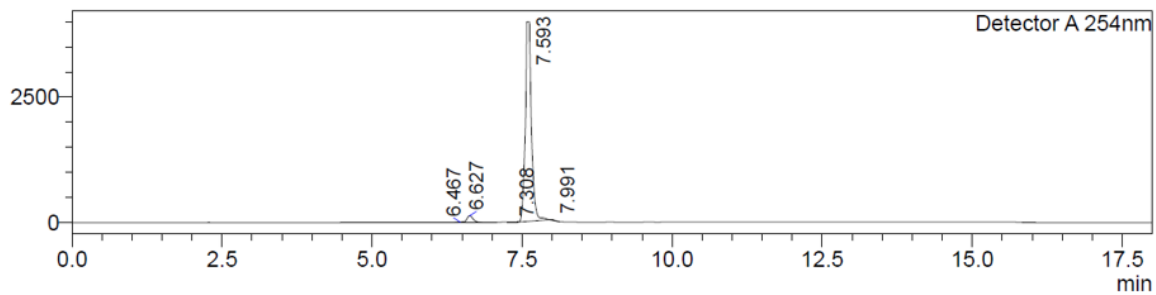
Detector A 254nm

Detector A 254nm

Peak#	Ret. Time	Area	Height	Area%
1	6.467	70136	9767	0.240
2	6.627	973464	134431	3.336
3	7.308	3992	836	0.014
4	7.593	28067476	3971673	96.194
5	7.991	62848	12158	0.215
Total		29177916	4128865	100.000

Line#:2   R.Time:7.953(Scan#:4773)
MassPeaks:339
Spectrum Mode:Averaged 7.950-7.957(4771-4775) Base Peak:339.35(6390378)
BG Mode:Calc Segment 1 - Event 1

m/z
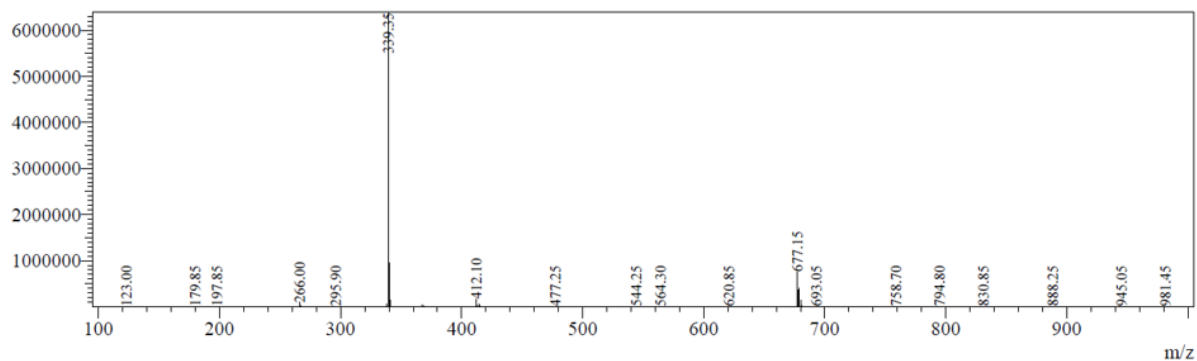
7.11. Dualsteric ligand 24

7.11.1. NMR spectra

¹H-NMR spectrum
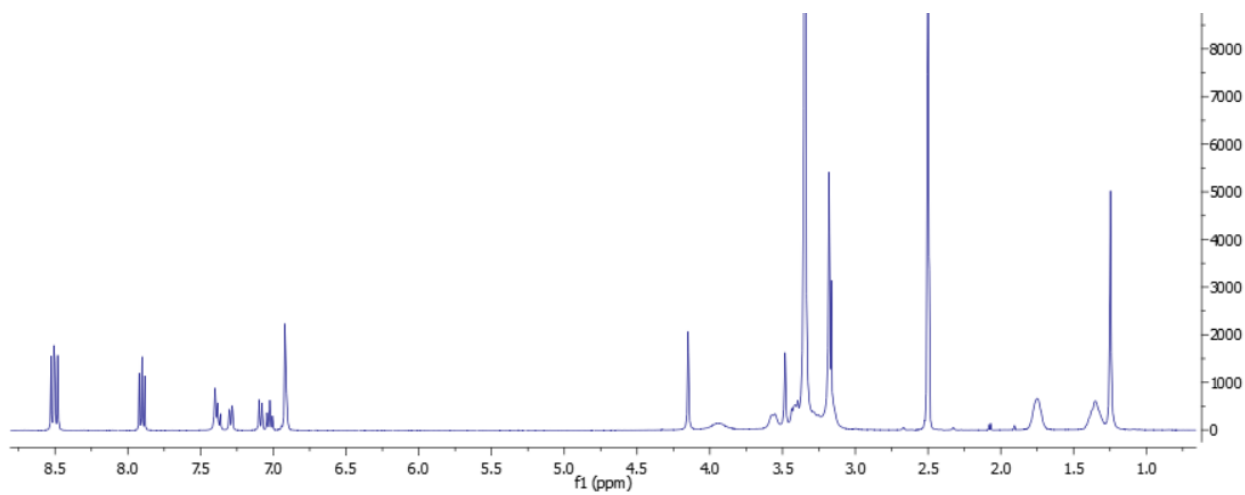
¹³C-NMR spectrum
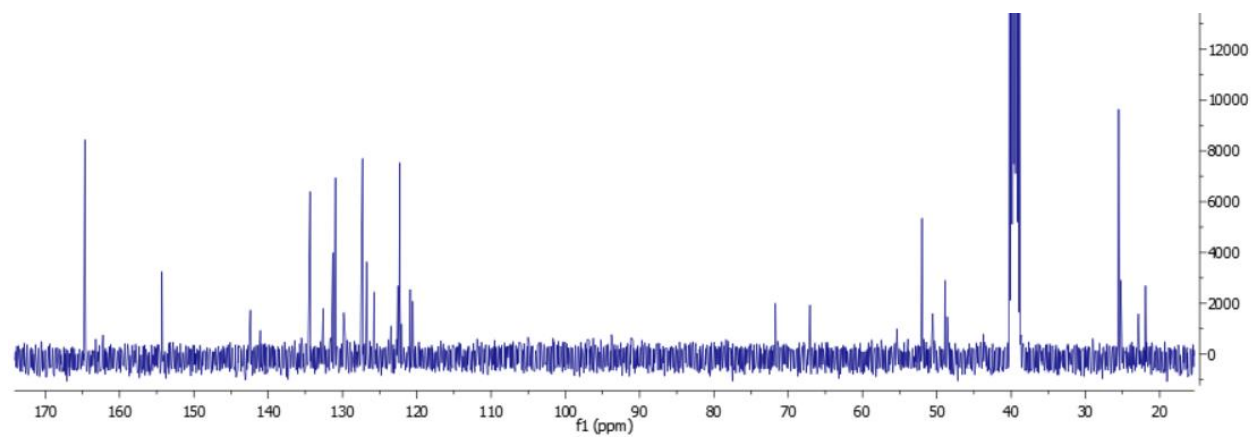
COSY spectrum
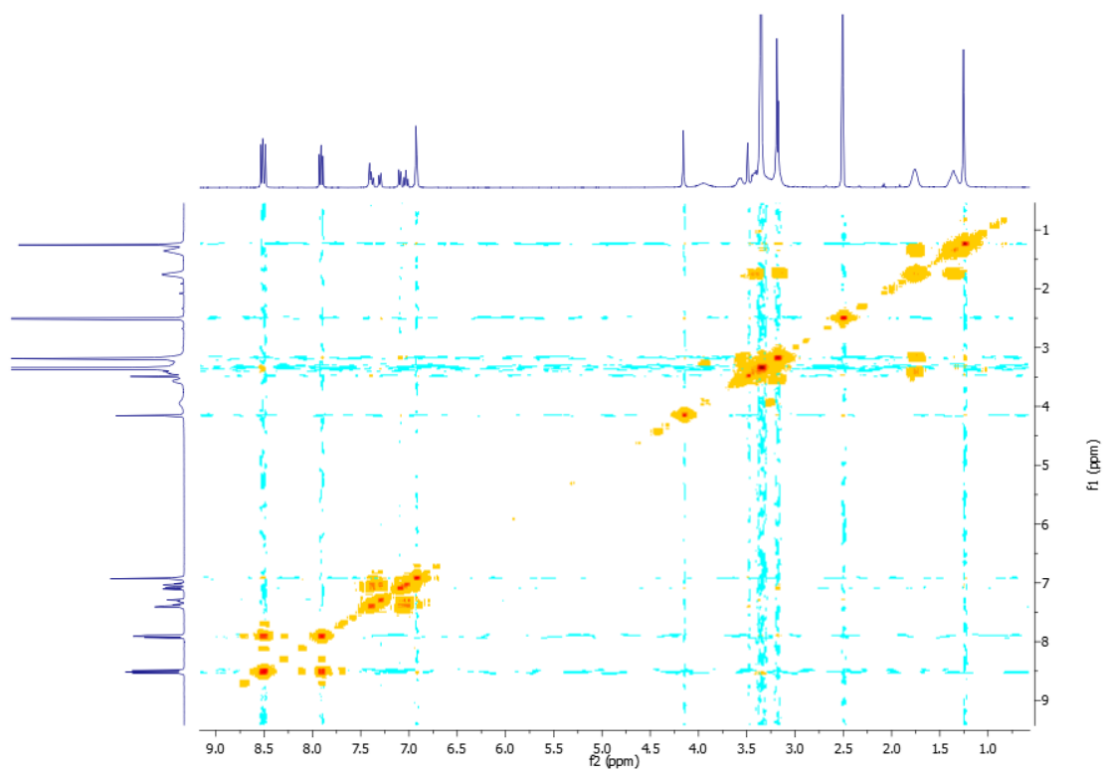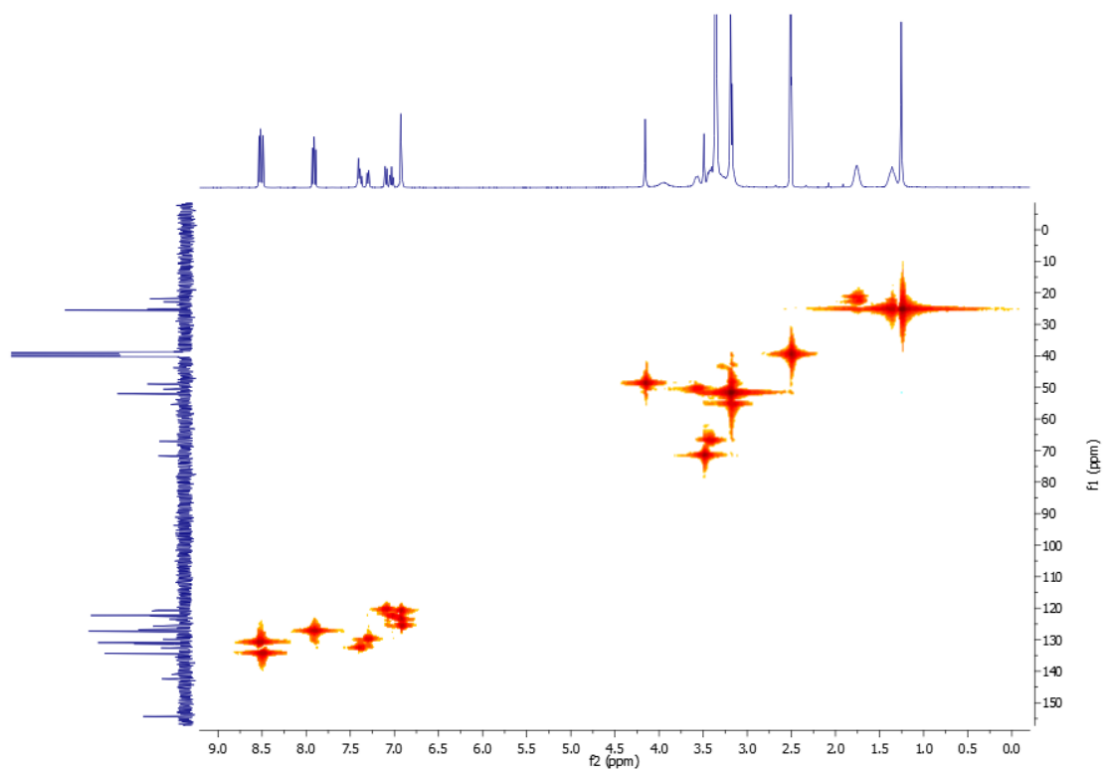
HMQC spectrum

HMBC spectrum
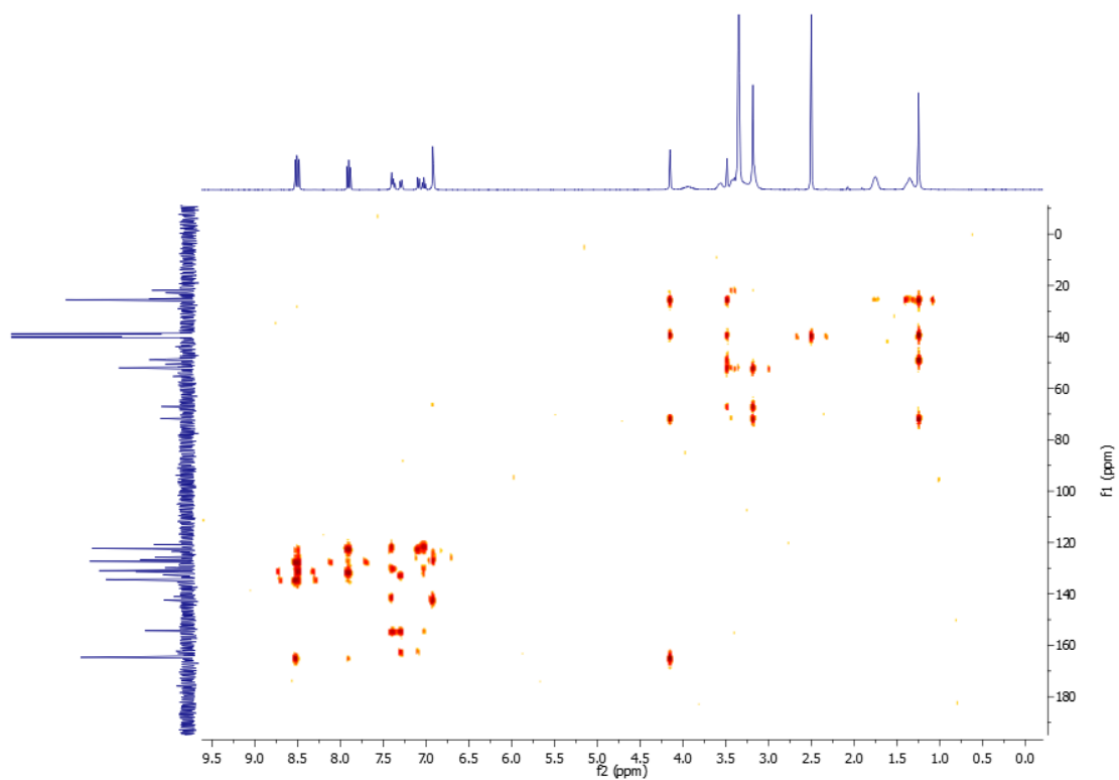
7.11.2. IR spectrum
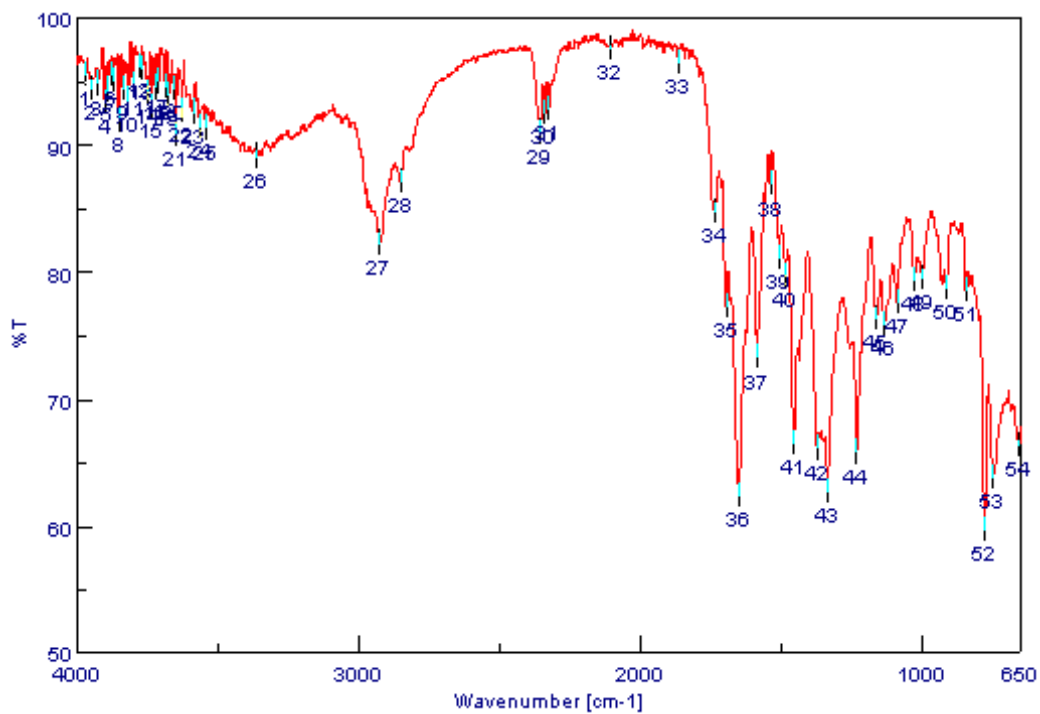
7.11.3. LC-MS spectrum (ESI)

\<Chromatogram\>

mV
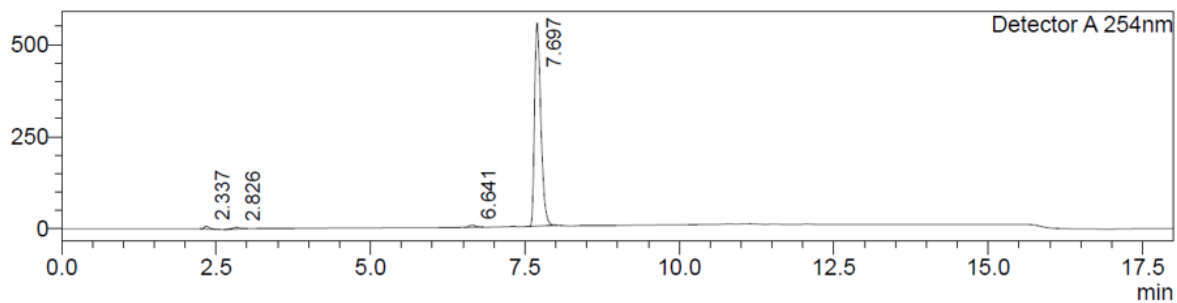
Detector A 254nm

Detector A 254nm

Peak#	Ret. Time	Area	Height	Area%
1	2.337	44826	7488	1.104
2	2.826	45683	4762	1.126
3	6.641	41128	6113	1.013
4	7.697	3926849	551833	96.757
Total		4058486	570195	100.000

Line#:1 R.Time:8.080(Scan#:4849)
MassPeaks:411
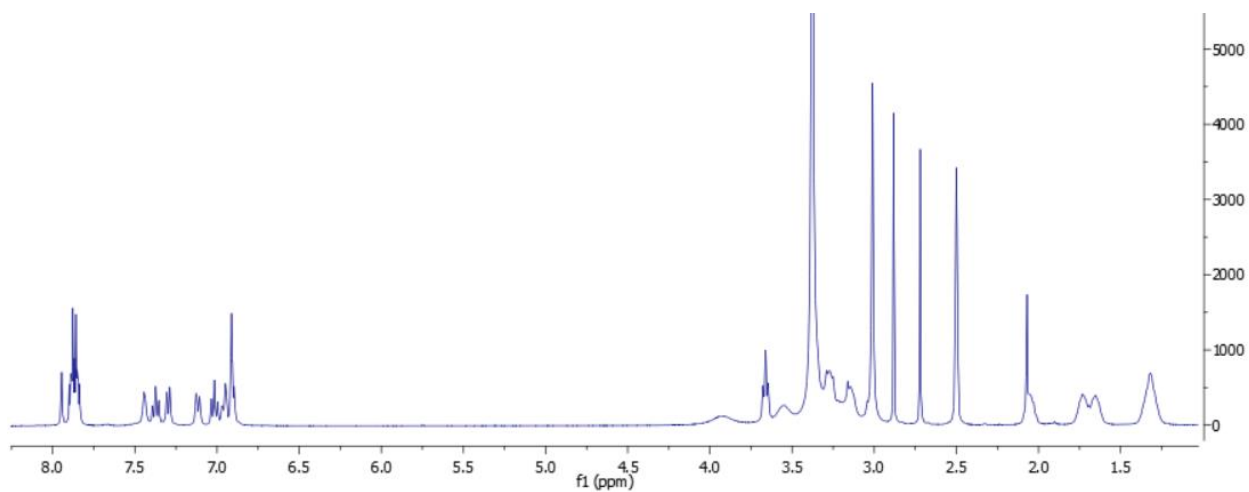Spectrum Mode:Averaged 8.077-8.083(4847-4851) Base Peak:353.40(3295313)
BG Mode:Calc Segment 1 - Event 1
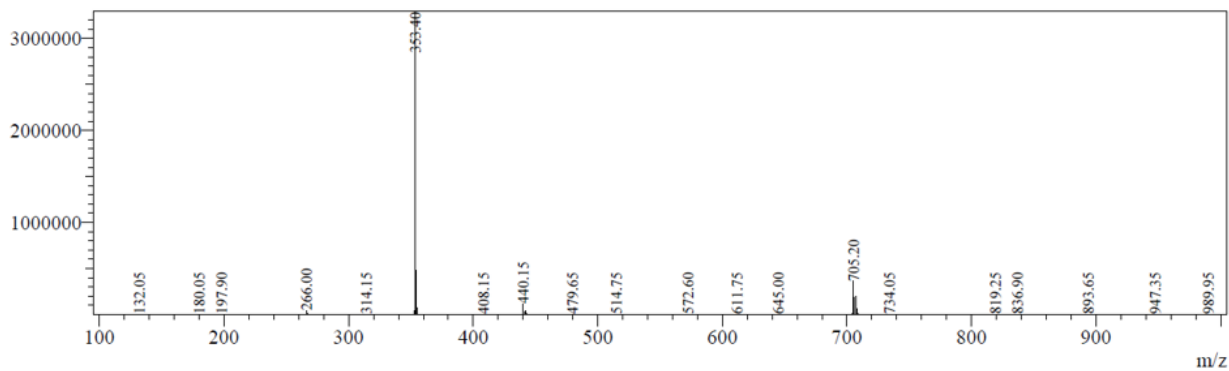
7.12. Dualsteric ligand 25
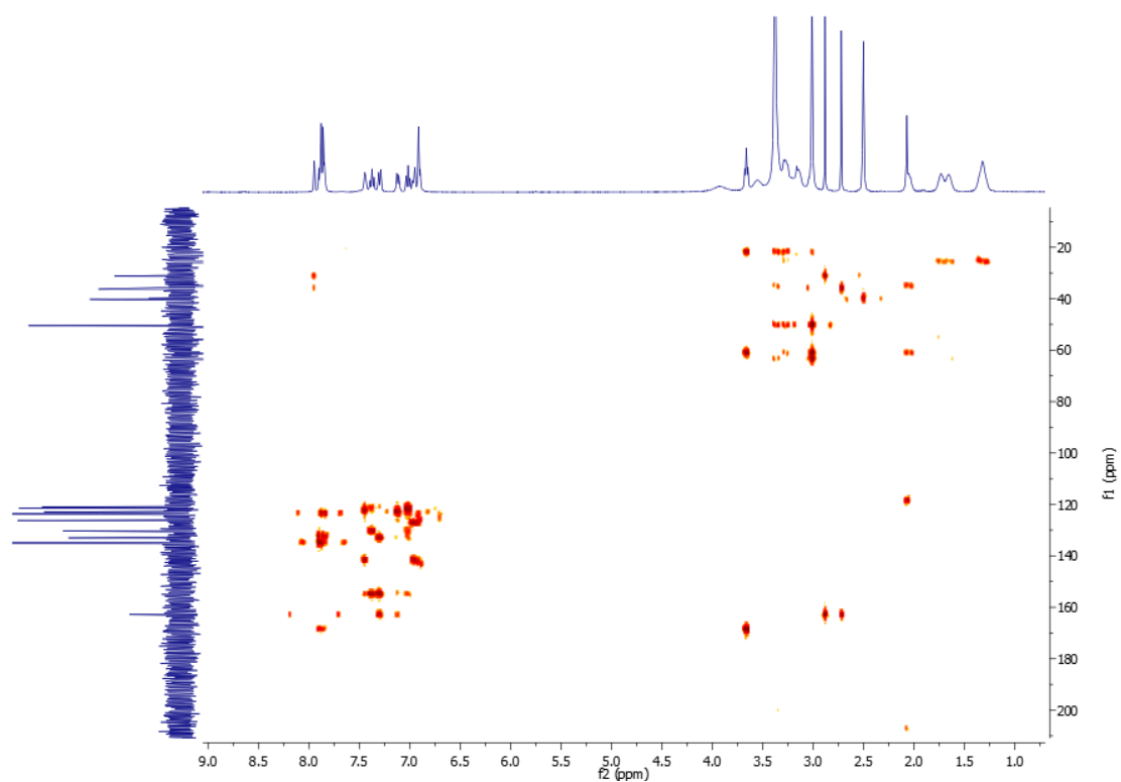
7.12.1. NMR spectra

1H-NMR spectrum
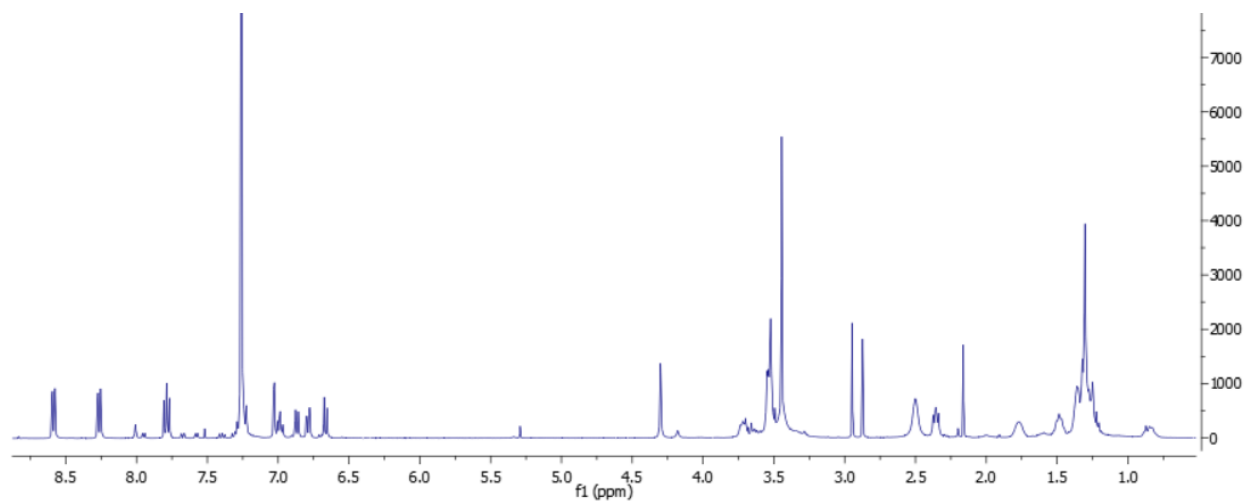
13C-NMR spectrum
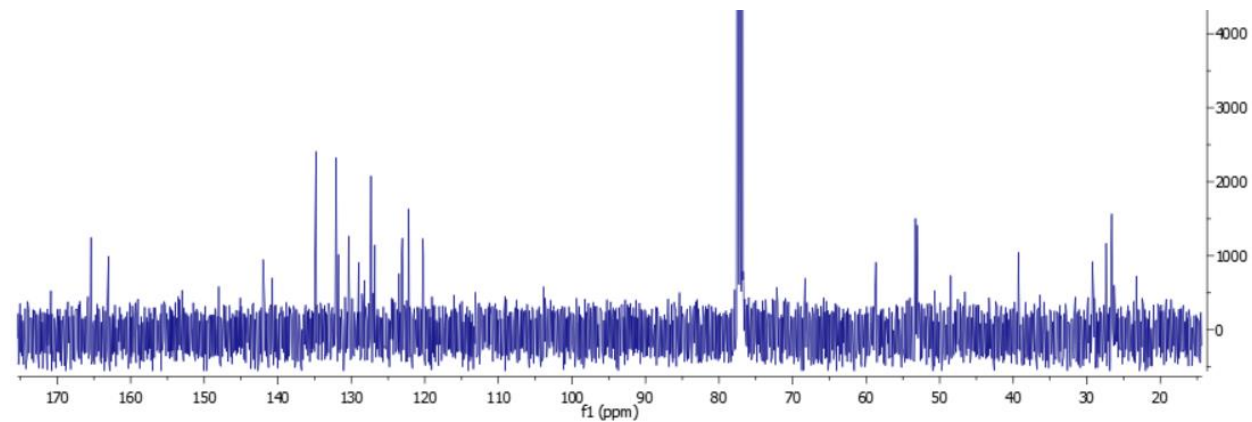
COSY spectrum
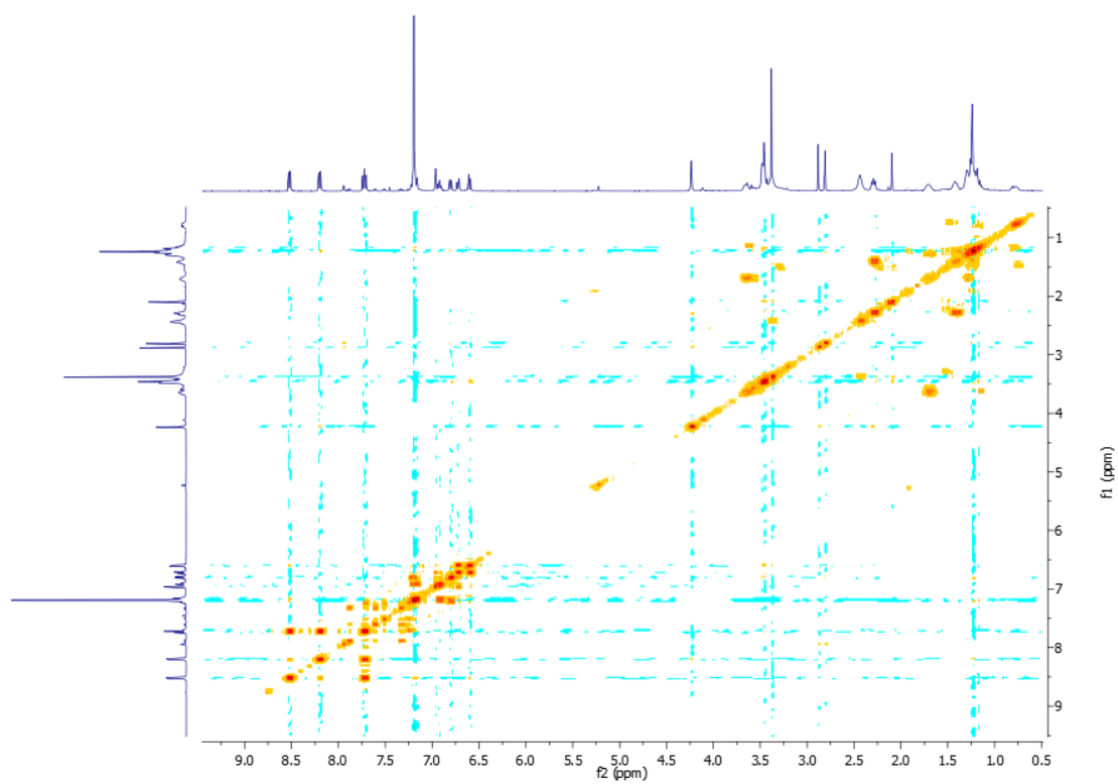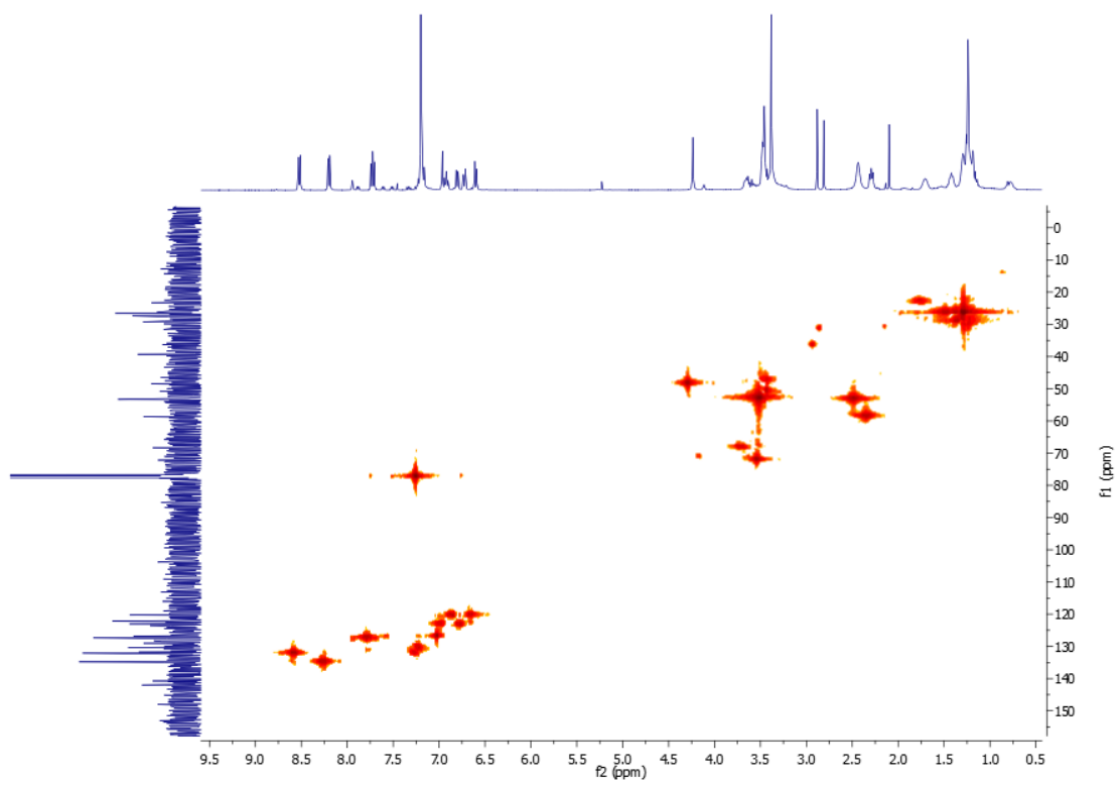
HMQC spectrum

HMBC spectrum
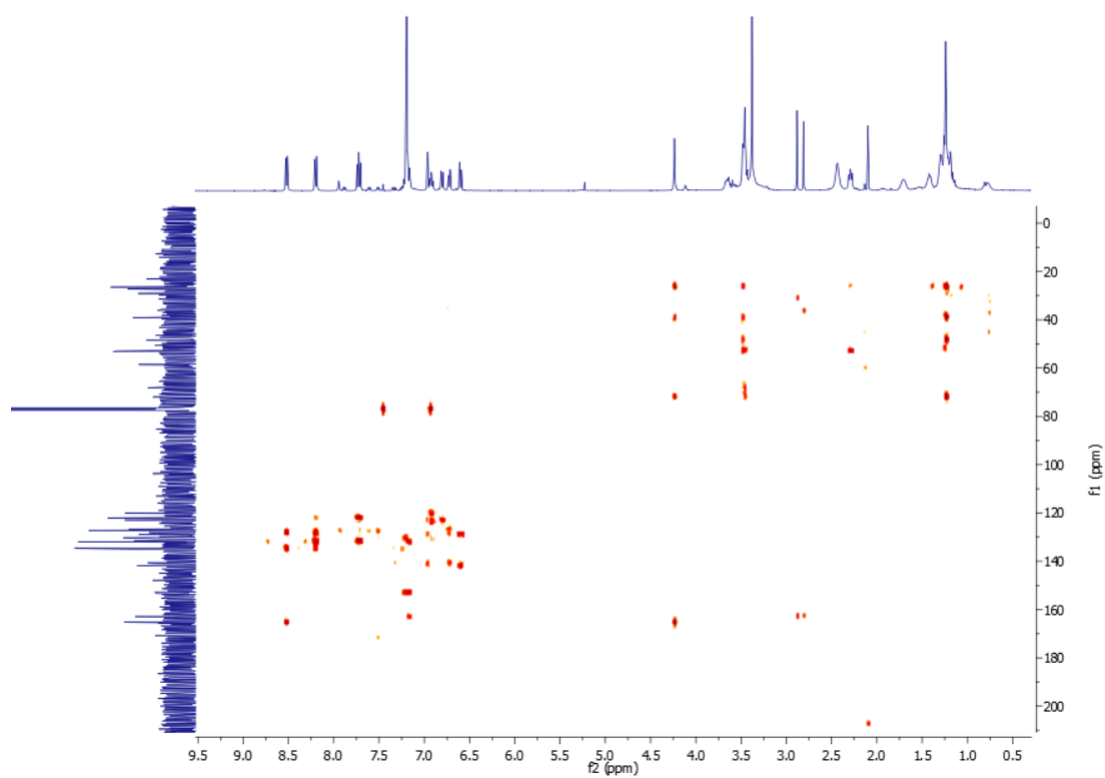
7.12.2. IR spectrum
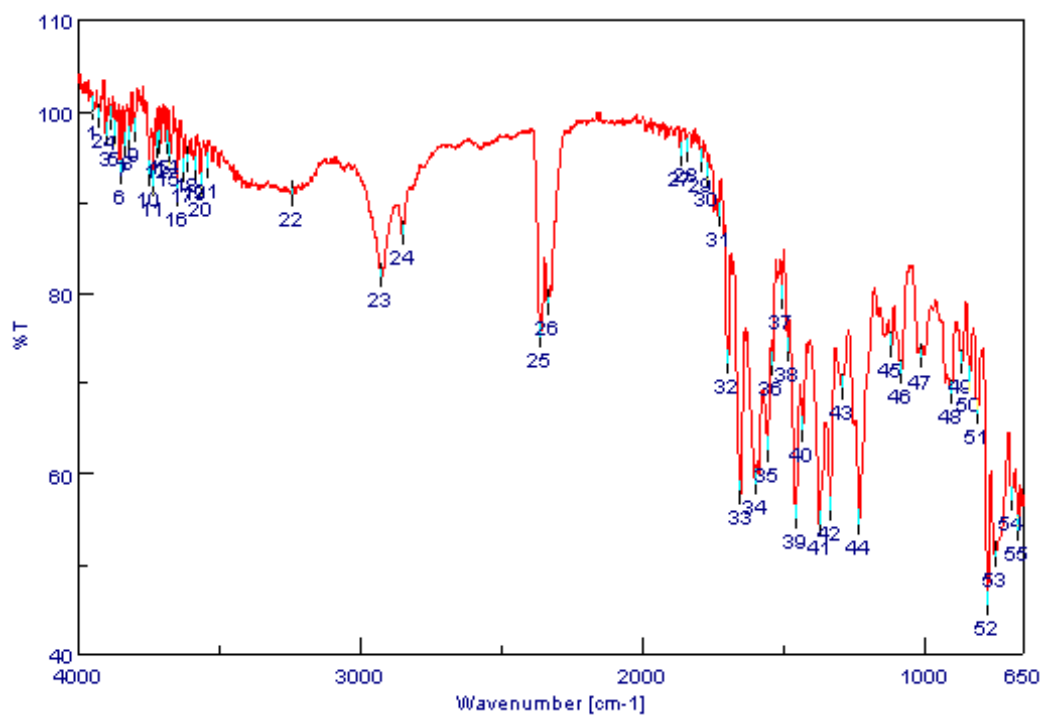
7.12.3. LC-MS spectrum (ESI)

<Chromatogram>

mV
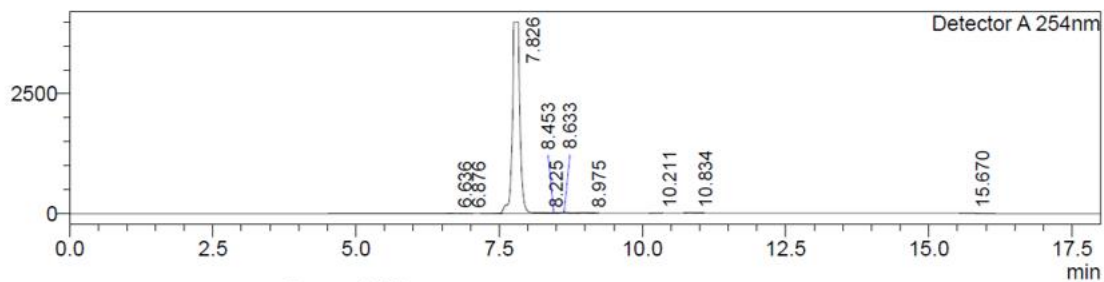
Detector A 254nm

Detector A 254nm

Peak#	Ret. Time	Area	Height	Area%
1	6.636	59148	9080	0.158
2	6.876	22968	2545	0.061
3	7.826	36987741	3991060	98.788
4	8.225	20761	3451	0.055
5	8.453	37900	5992	0.101
6	8.633	129175	15422	0.345
7	8.975	62599	9145	0.167
8	10.211	13528	2336	0.036
9	10.834	31529	4111	0.084
10	15.670	76337	4972	0.204
Total		37441687	4048115	100.000

Line#:1　R.Time:8.173(Scan#:4905)
MassPeaks:340
Spectrum Mode:Averaged 8.170-8.177(4903-4907)　Base Peak:360.50(10056614)
BG Mode:Calc　Segment 1 - Event 1
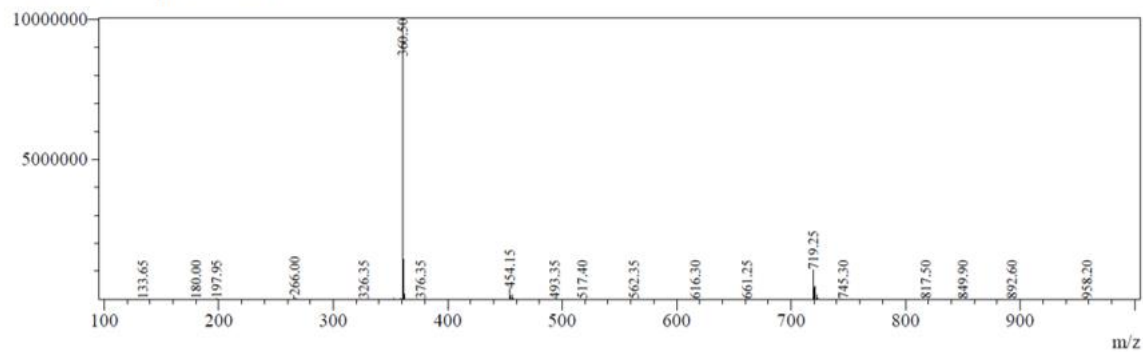
7.13. Dualsteric ligand 30

7.13.1. NMR spectra

^{1}H-NMR spectrum
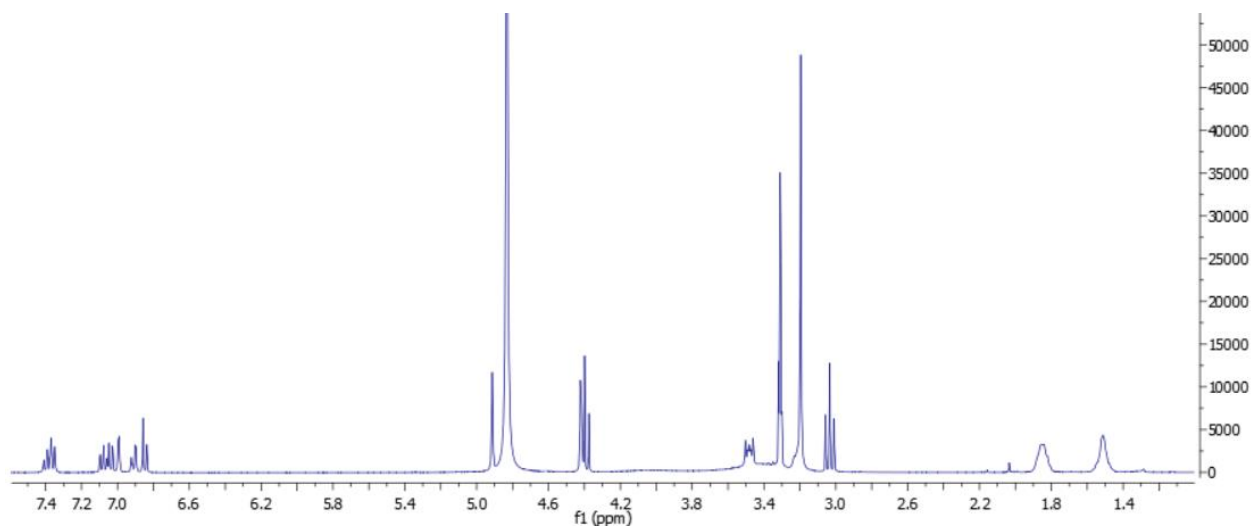
^{13}C-NMR spectrum
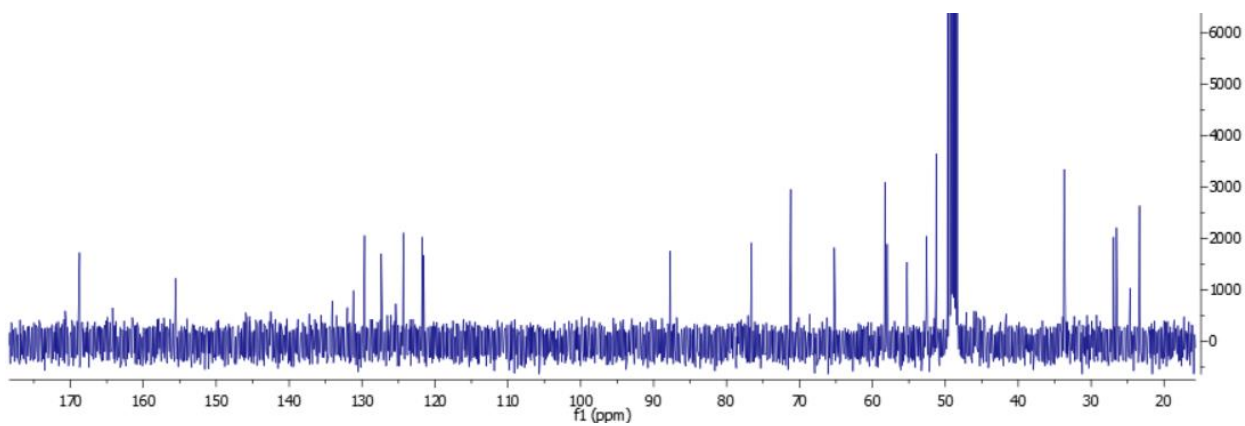
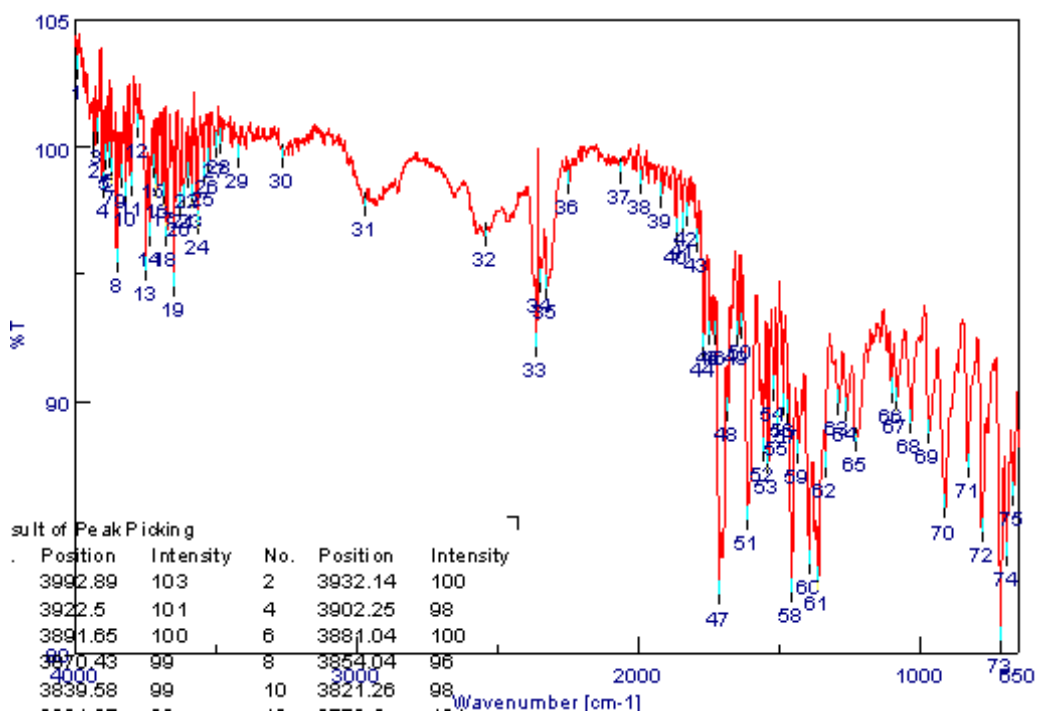## COSY spectrum
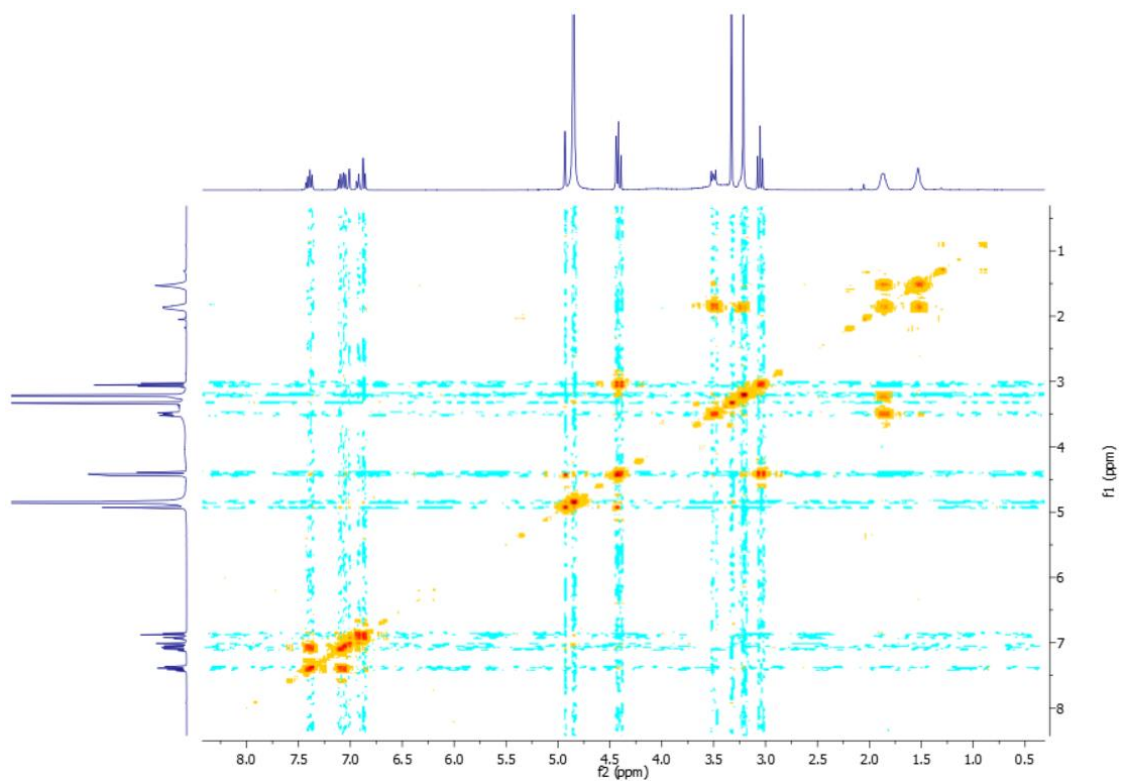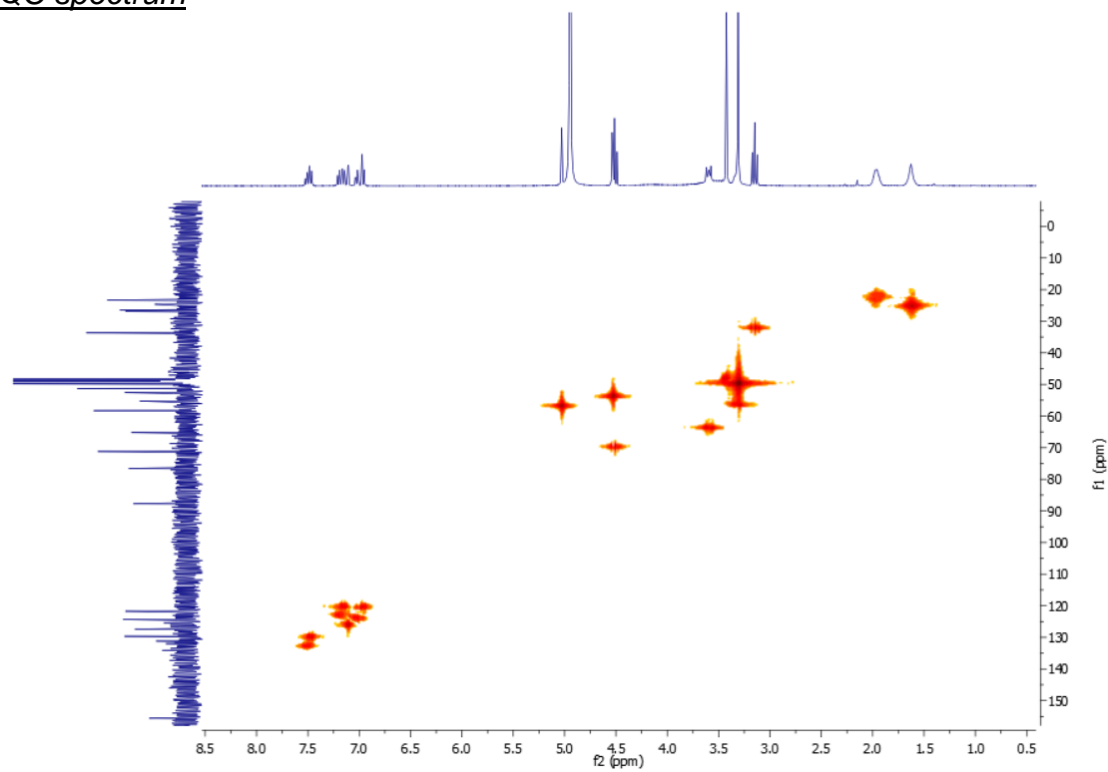
HMQC spectrum

HMBC spectrum
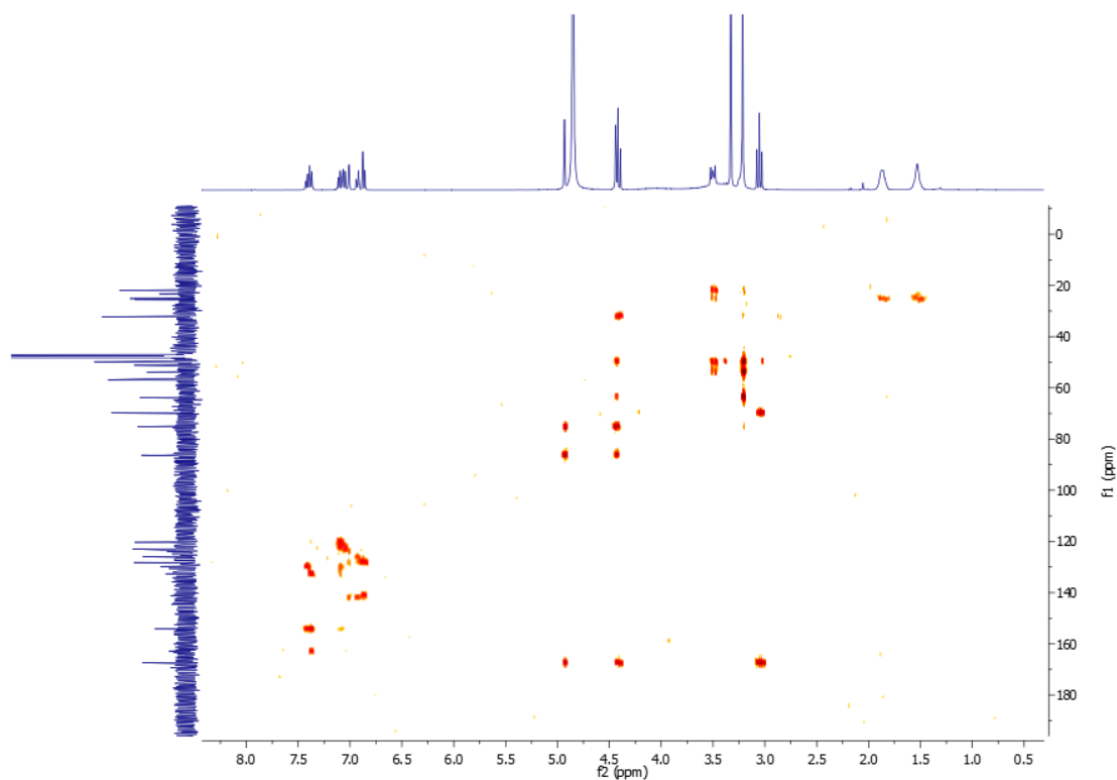
7.13.2. IR spectrum
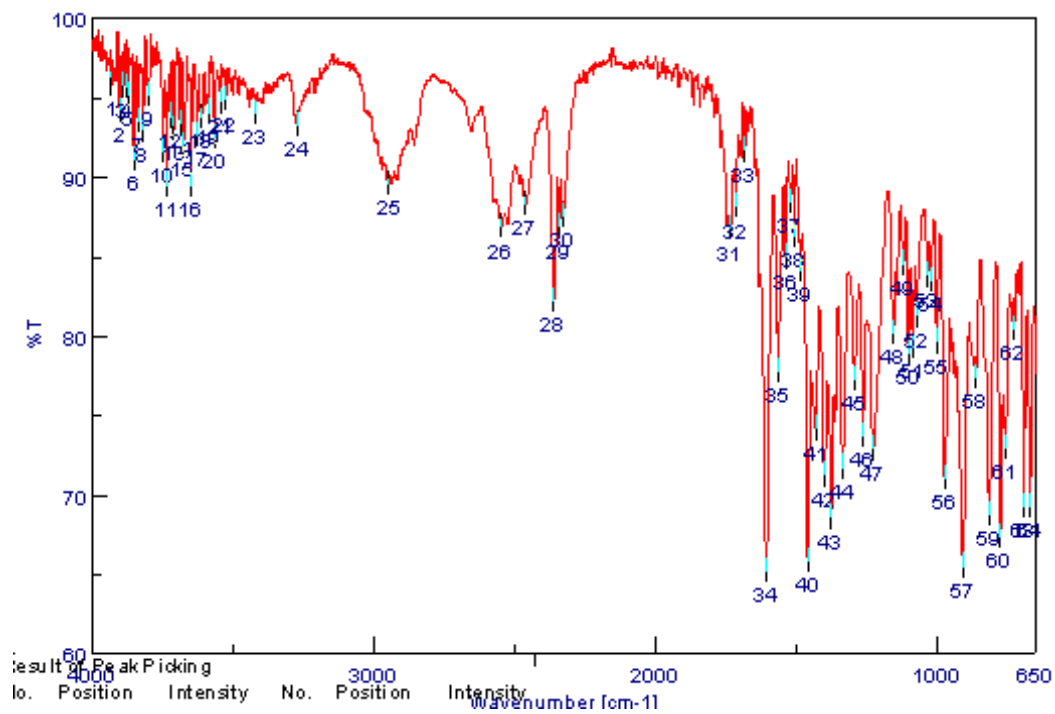
7.13.3. LC-MS spectrum (ESI)

<Chromatogram>

mV
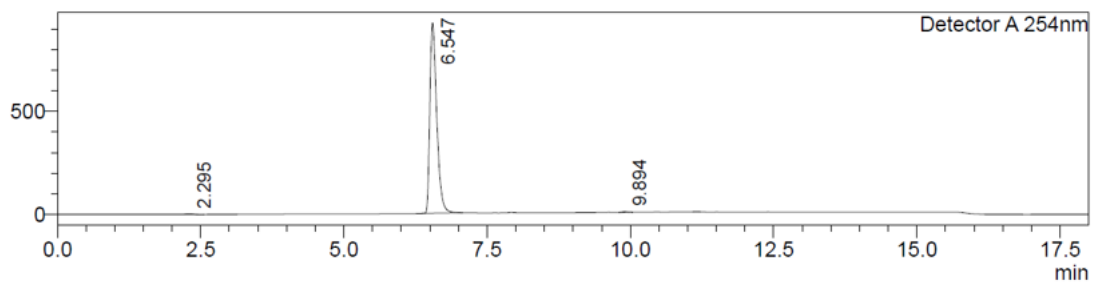
Detector A 254nm

Detector A 254nm				
Peak#	Ret. Time	Area	Height	Area%
1	2.295	24682	2676	0.317
2	6.547	7738017	923107	99.454
3	9.894	17801	2969	0.229
Total		7780500	928751	100.000

Line#:1   R.Time:6.927(Scan#:4157)
MassPeaks:384
Spectrum Mode:Averaged 6.923-6.930(4155-4159) Base Peak:289.35(2779691)
BG Mode:Calc Segment 1 - Event 1
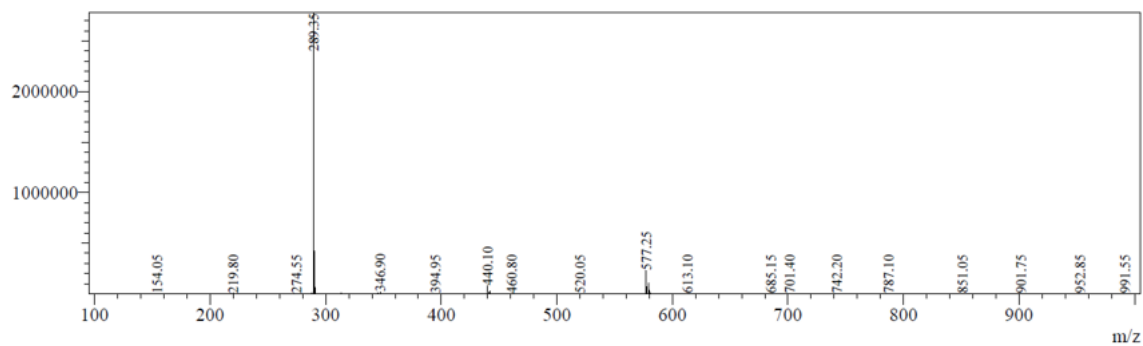
7.14. Dualsteric ligand 31

7.14.1. NMR spectra

¹H-NMR spectrum
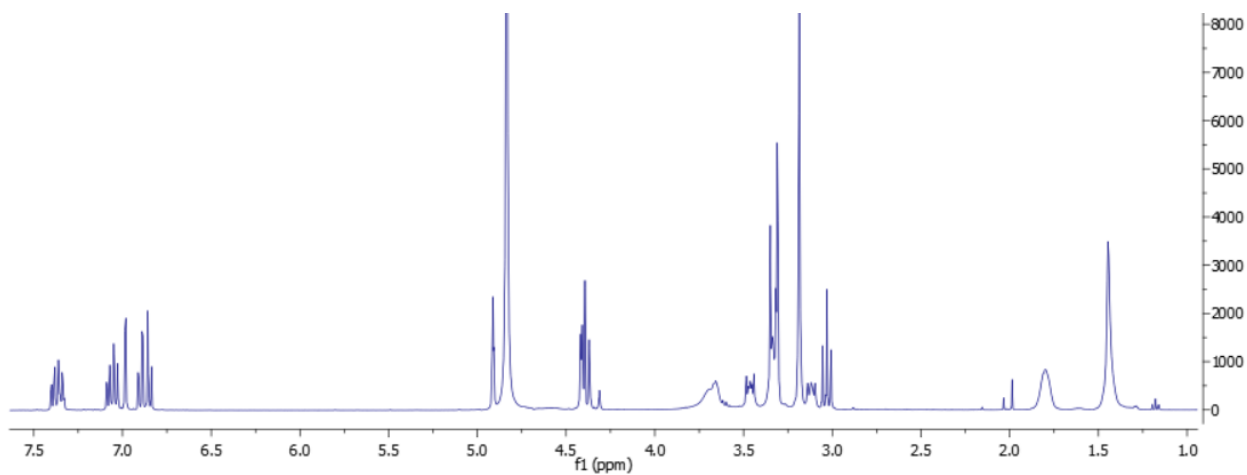
¹³C-NMR spectrum
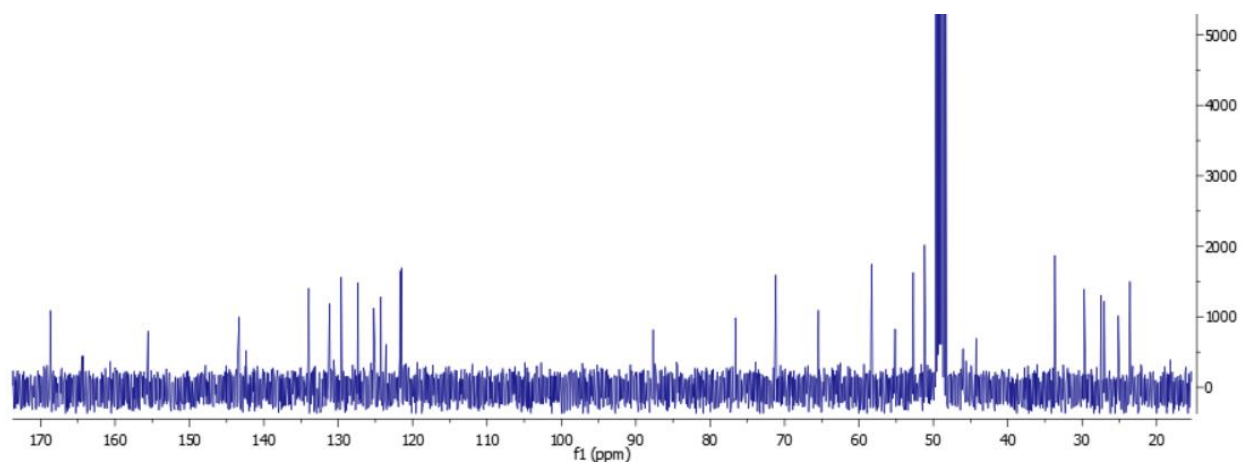
COSY spectrum
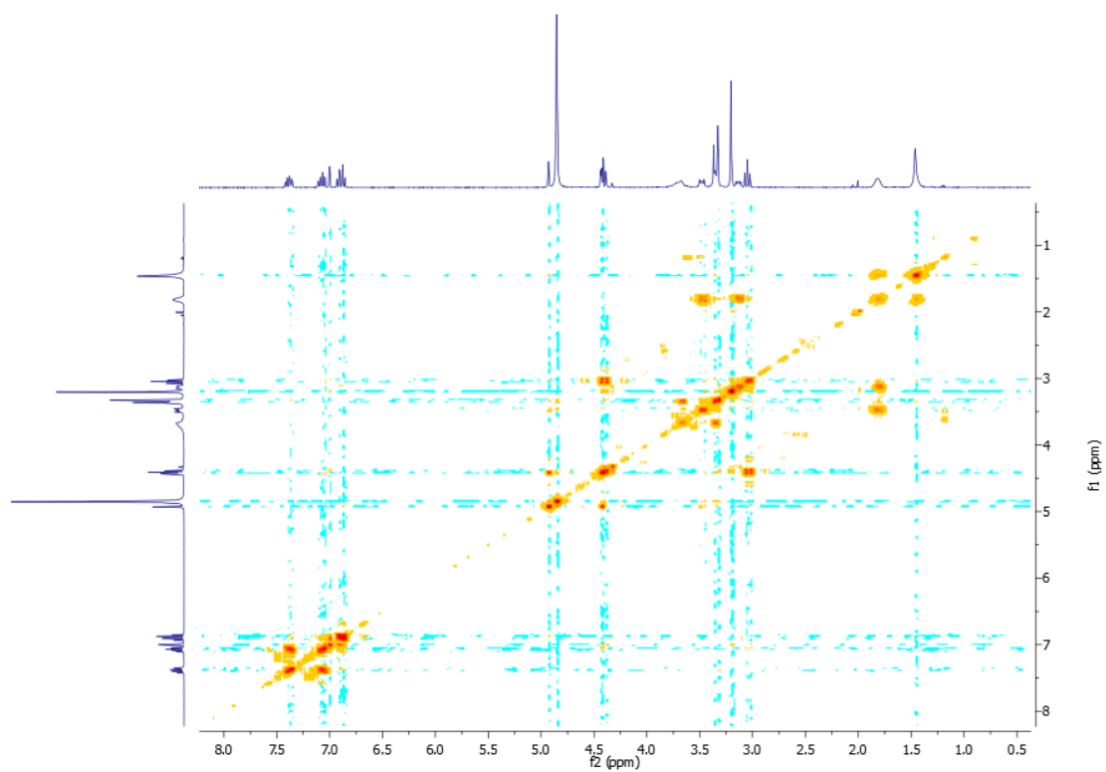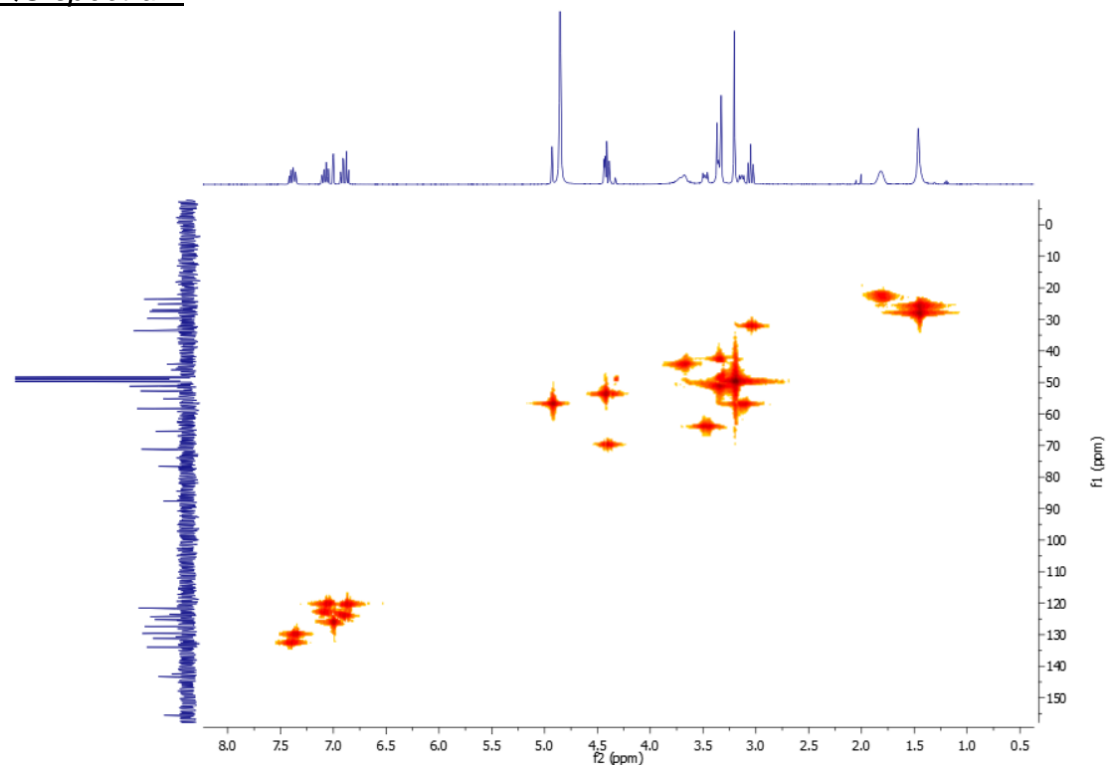
HMQC spectrum

HMBC spectrum
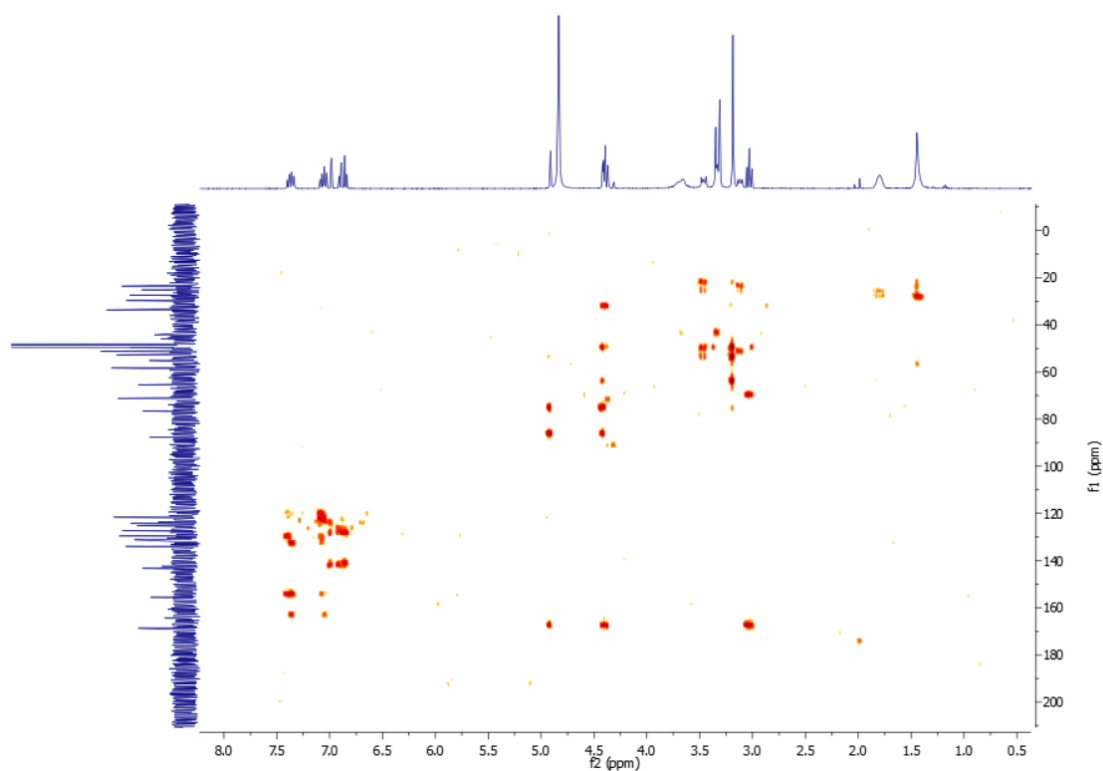
7.14.2. IR spectrum

7.14.3. LC-MS spectrum (ESI)

\<Chromatogram\>

mV

Detector A 254nm

2500 —

Peaks labeled: 2.273, 5.622, 6.385, 6.701, 6.925, 7.255, 7.808, 9.568, 10.834

0 —

0.0 2.5 5.0 7.5 10.0 12.5 15.0 17.5

min

Detector A 254nm
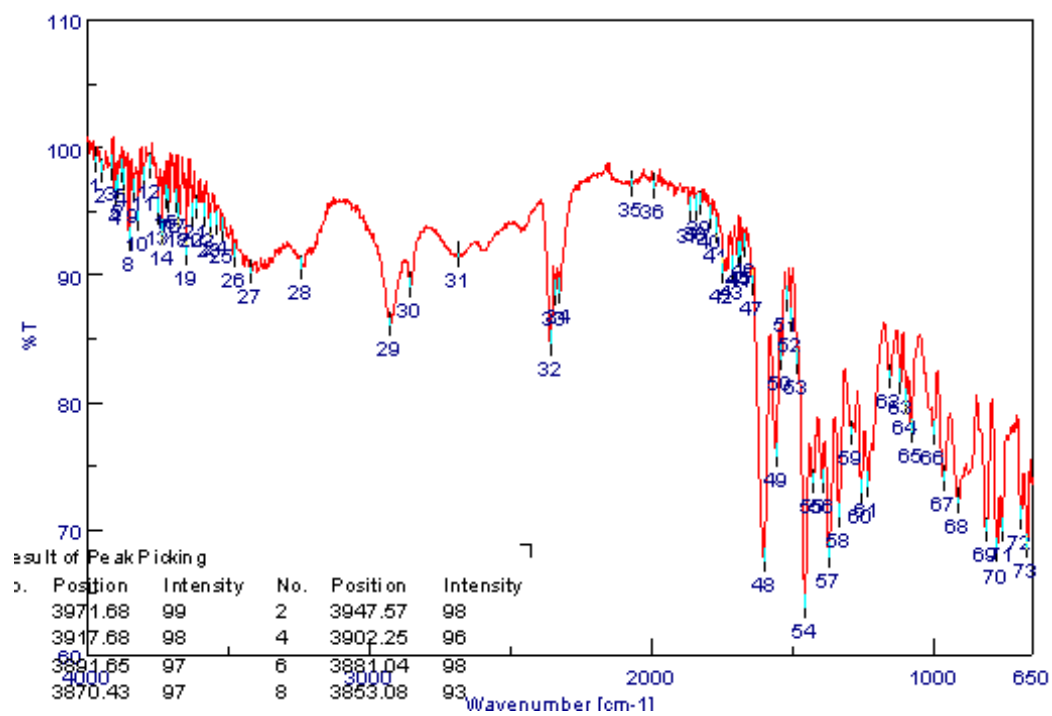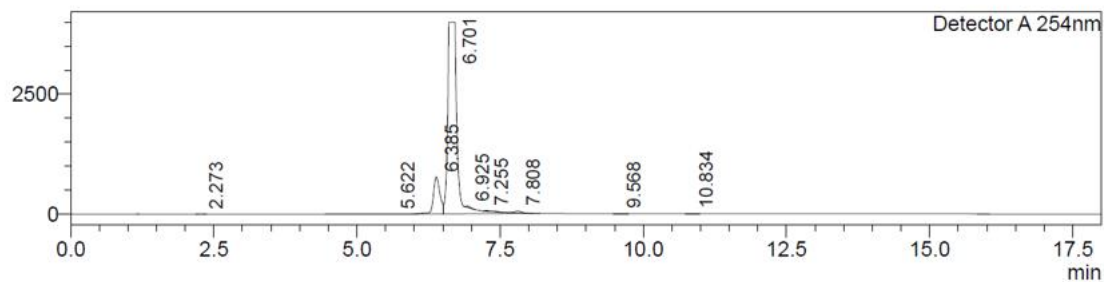
Peak#	Ret. Time	Area	Height	Area%
1	2.273	9152	1829	0.018
2	5.622	22345	2850	0.043
3	6.385	6213103	772227	11.918
4	6.701	45163666	3989902	86.634
5	6.925	152244	26287	0.292
6	7.255	214359	14810	0.411
7	7.808	321860	40701	0.617
8	9.568	21294	3390	0.041
9	10.834	13366	2170	0.026
Total		52131389	4854165	100.000

Line#:2 R.Time:7.077(Scan#:4247)
MassPeaks:367
Spectrum Mode:Averaged 7.073-7.080(4245-4249) Base Peak:303.35(7488256)
BG Mode:Calc Segment 1 - Event 1

7000000 —
6000000 —
5000000 —
4000000 —
3000000 —
2000000 —
1000000 —

m/z peaks labeled: 127.50, 184.25, 233.90, 277.00, 303.35, 346.25, 414.95, 468.15, 518.05, 558.80, 605.15, 649.15, 712.25, 736.75, 784.50, 841.35, 874.35, 931.15, 964.20

100 200 300 400 500 600 700 800 900

m/z
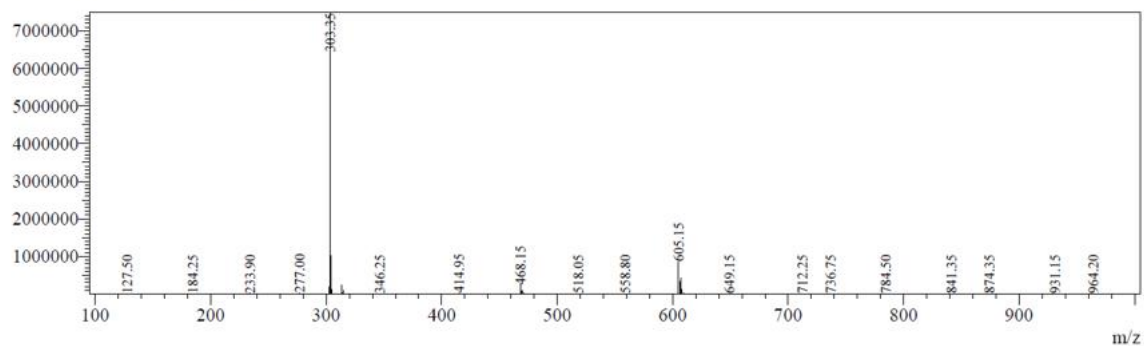
7.15. Dualsteric ligand 32

7.15.1. NMR spectra

¹H-NMR spectrum

¹³C-NMR spectrum
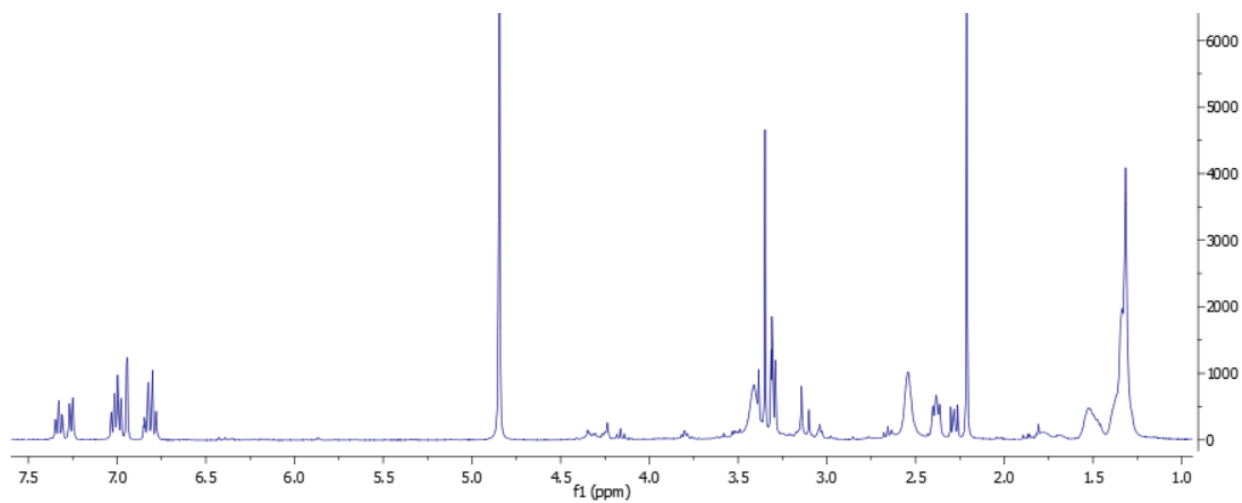
COSY spectrum
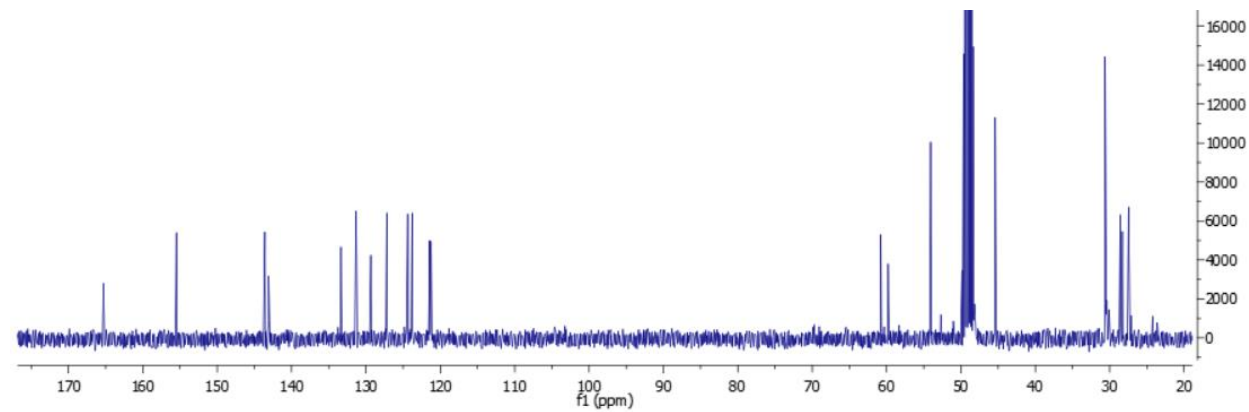
HMQC spectrum
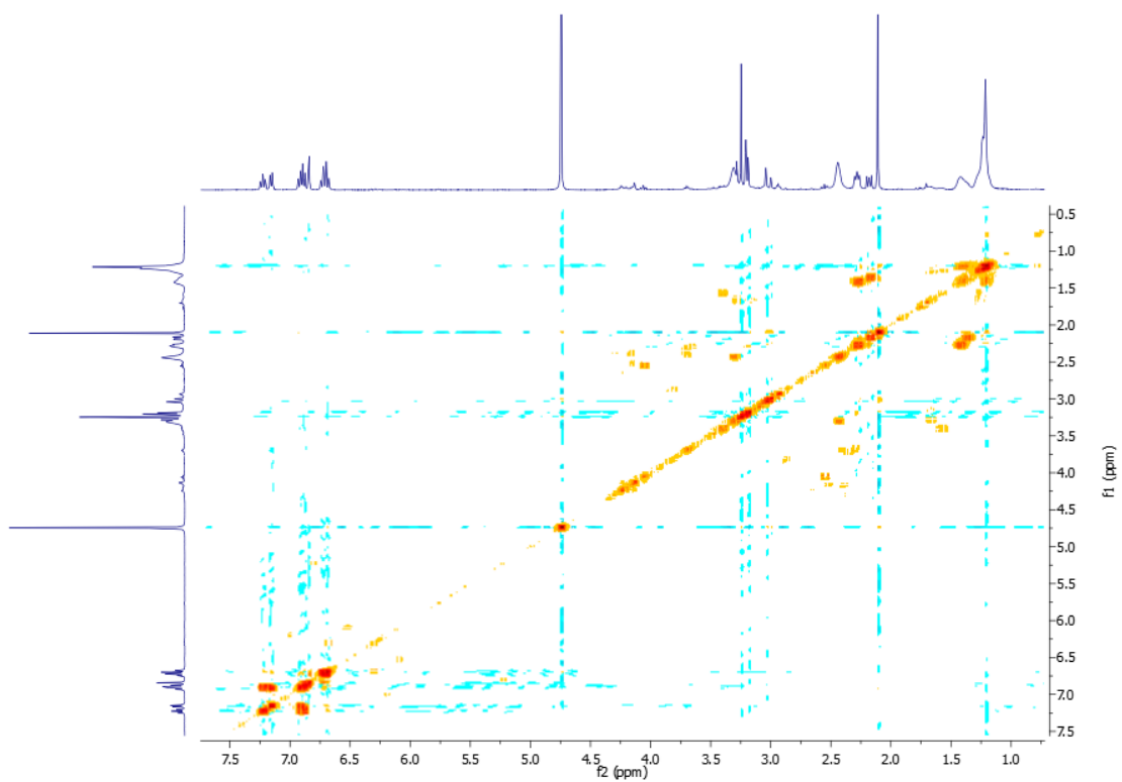
HMBC spectrum

7.15.2. IR spectrum
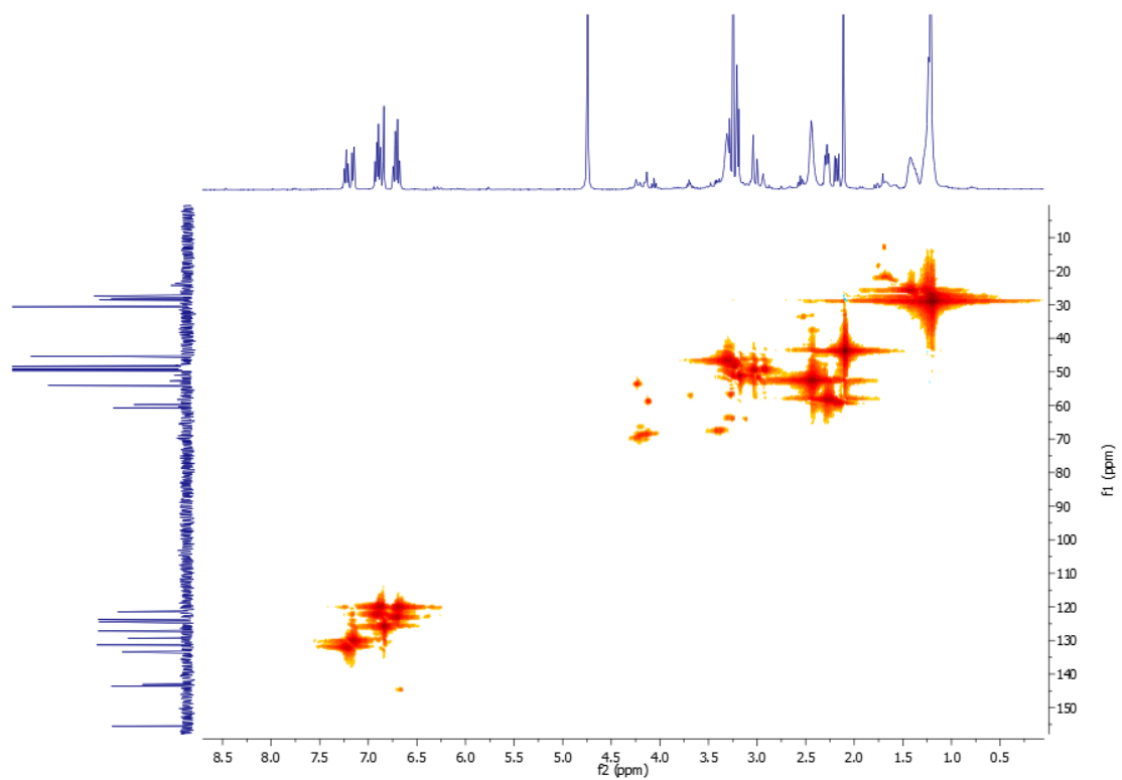
7.15.3. LC-MS spectrum (ESI)

\<Chromatogram\>

mV
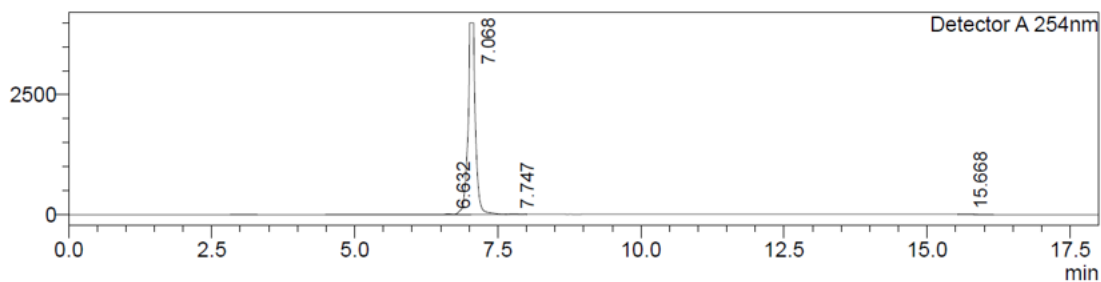
Detector A 254nm

Detector A 254nm				
Peak#	Ret. Time	Area	Height	Area%
1	6.632	99627	14976	0.274
2	7.068	36123392	3992670	99.269
3	7.747	93483	7891	0.257
4	15.668	72722	4713	0.200
Total		36389223	4020251	100.000

Line#:1 R.Time:7.447(Scan#:4469)
MassPeaks:360
Spectrum Mode:Averaged 7.443-7.450(4467-4471) Base Peak:317.40(8883100)
BG Mode:Calc Segment 1 - Event 1
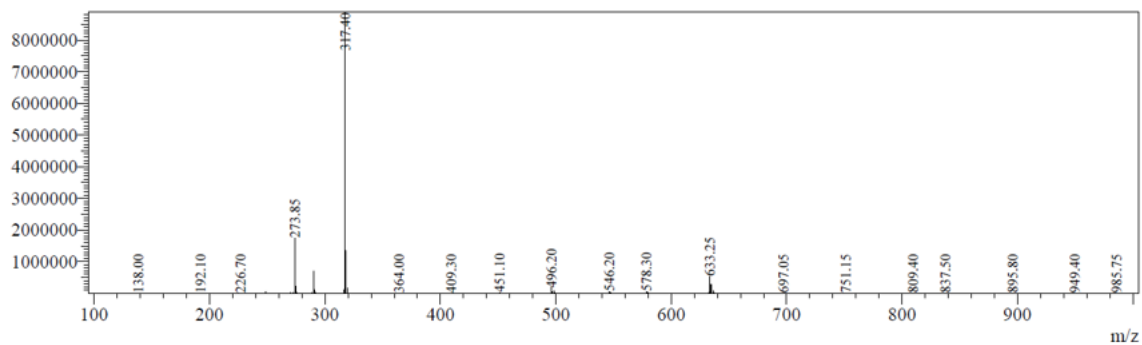
## 7.16. Dualsteric ligand 35

7.16.1. NMR spectra

*¹H-NMR spectrum*
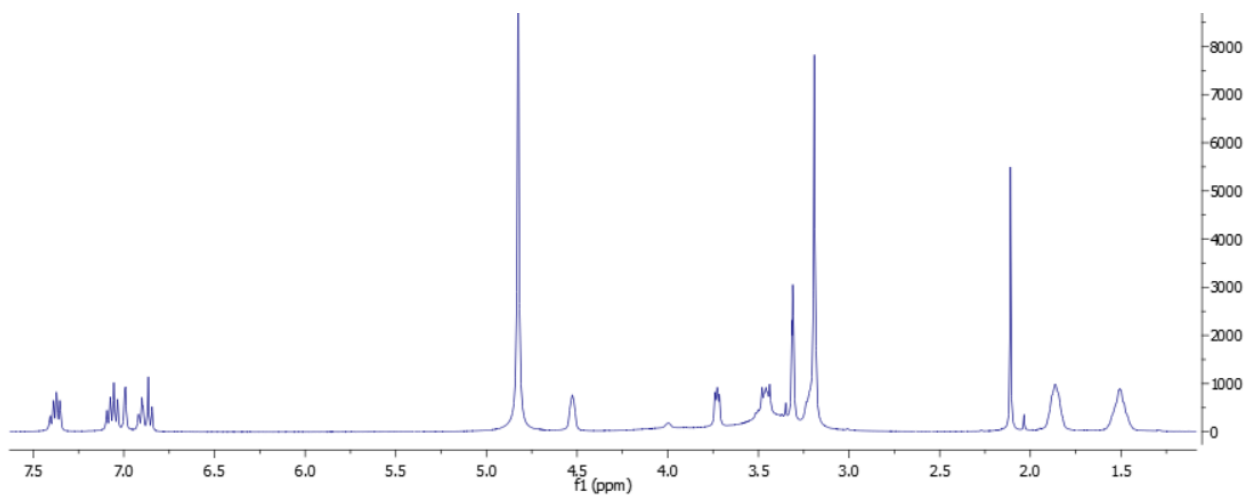
¹³C-NMR spectrum
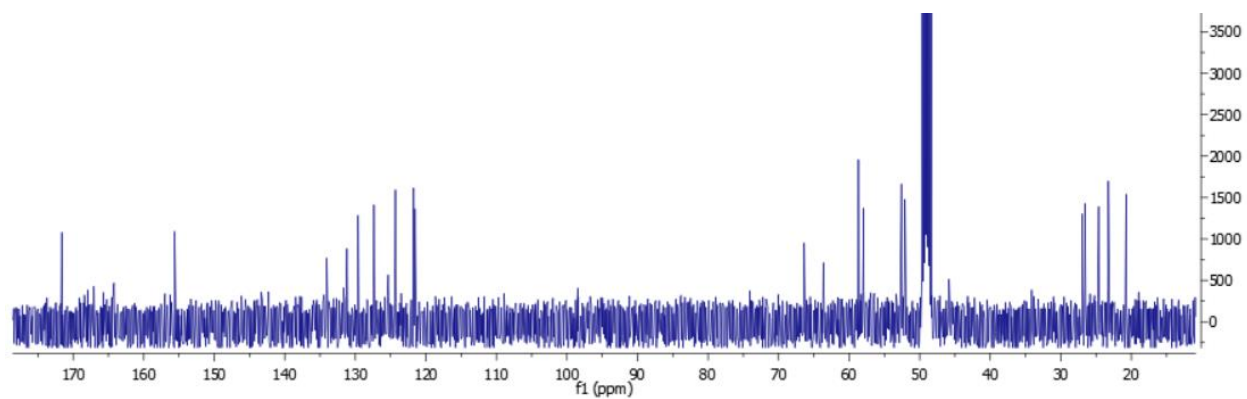
COSY spectrum
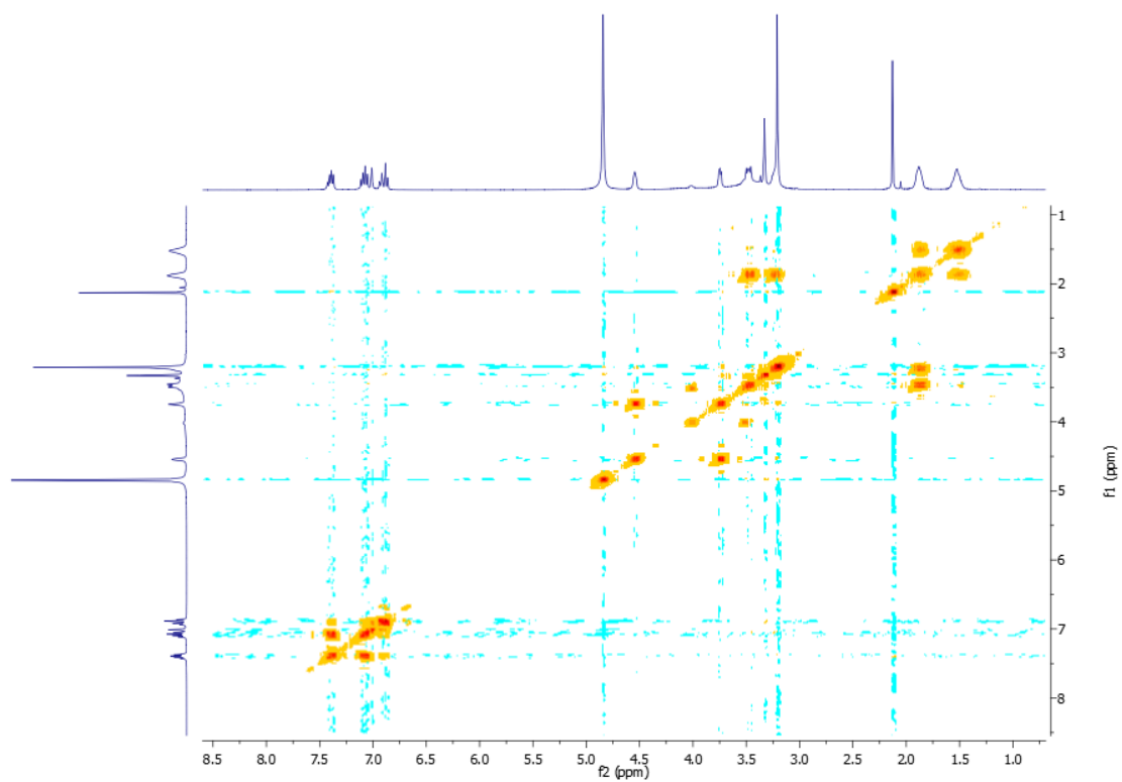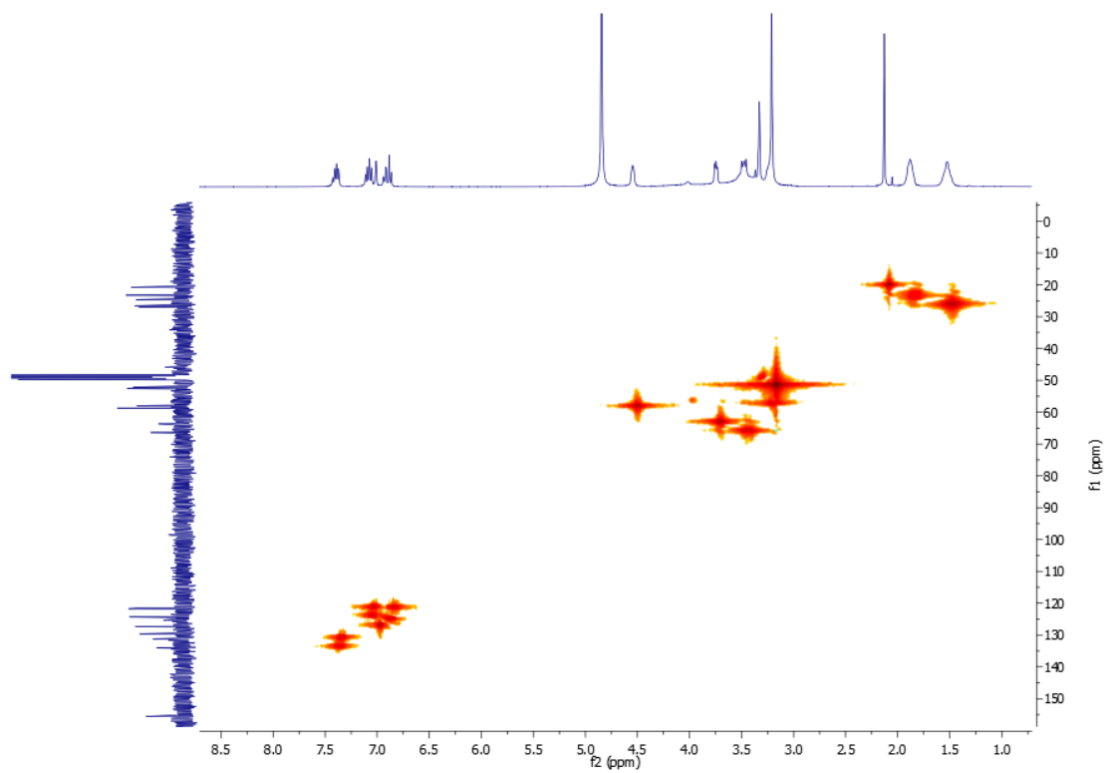
HMQC spectrum

HMBC spectrum
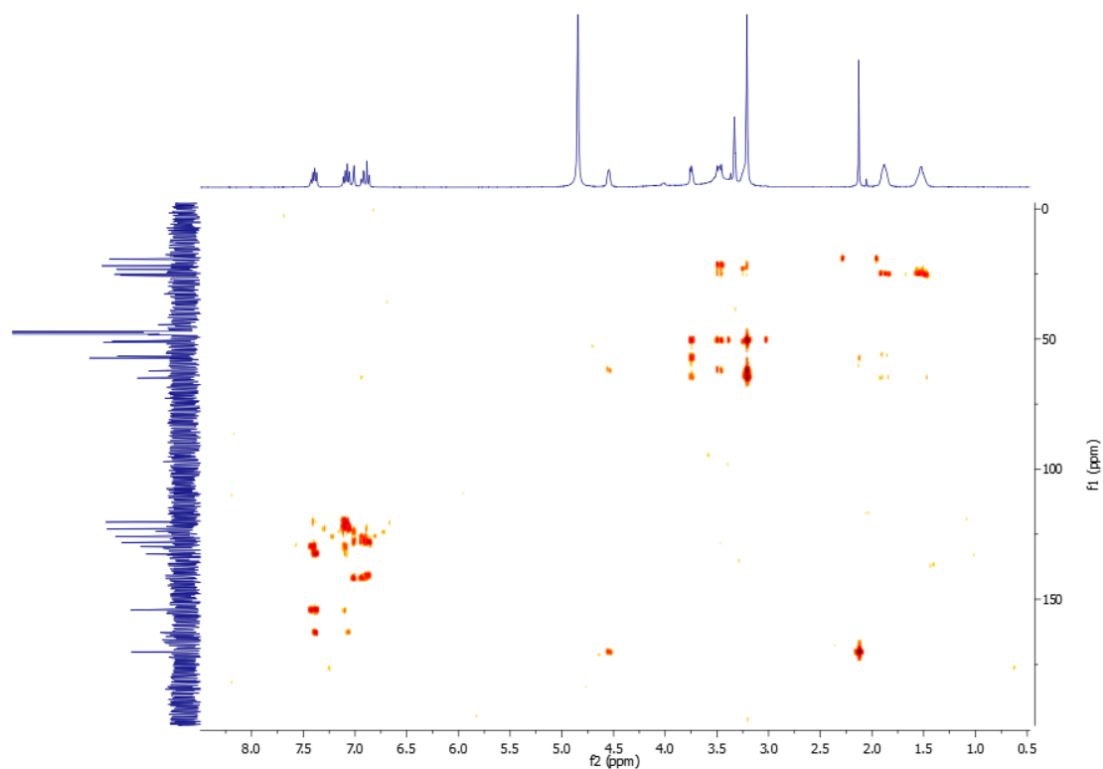
7.16.2. IR spectrum
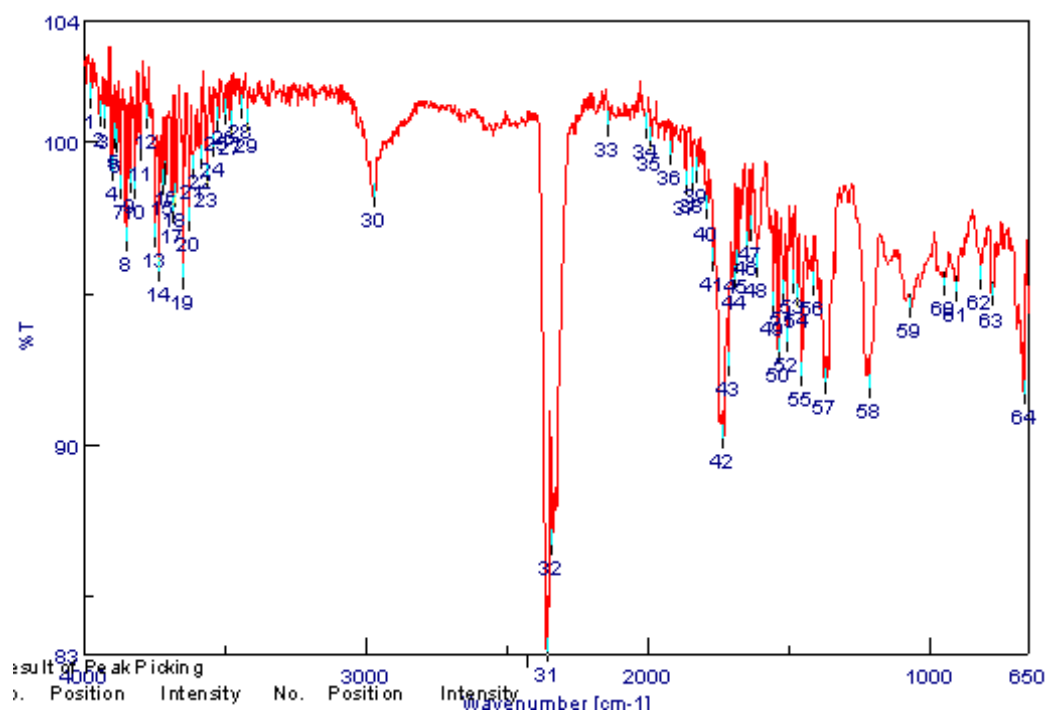
7.16.3. LC-MS spectrum (ESI)

<Chromatogram>

mV

Detector A 254nm

Detector A 254nm
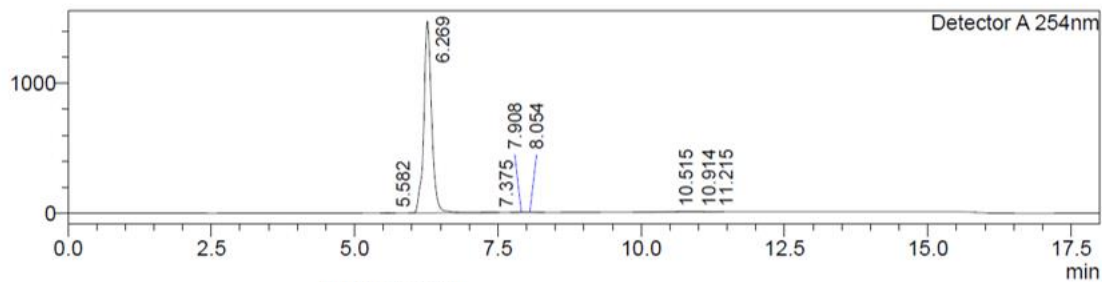
Peak#	Ret. Time	Area	Height	Area%
1	5.582	6055	795	0.043
2	6.269	14061006	1469314	99.350
3	7.375	4196	518	0.030
4	7.908	7609	929	0.054
5	8.054	13385	1409	0.095
6	10.515	23494	1601	0.166
7	10.914	26472	1046	0.187
8	11.215	10717	995	0.076
Total		14152934	1476608	100.000

Line#:1 R.Time:6.647(Scan#:3989)
MassPeaks:388
Spectrum Mode:Averaged 6.643-6.650(3987-3991) Base Peak:263.85(4021615)
BG Mode:Calc Segment 1 - Event 1
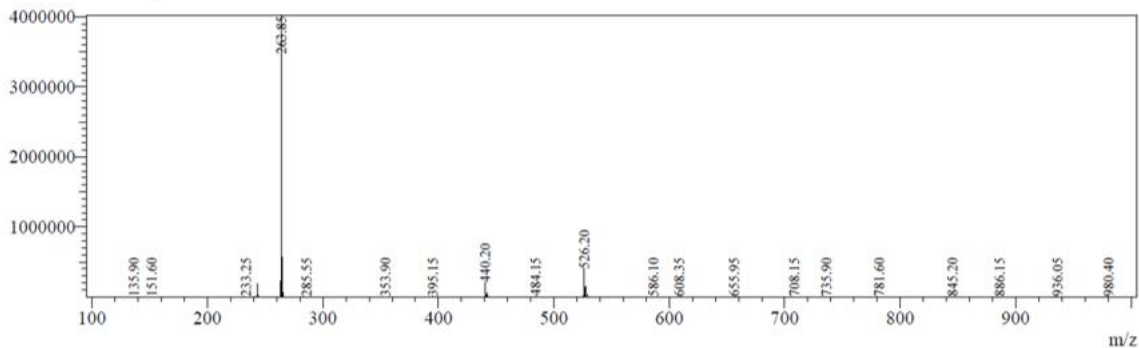
7.17. Dualsteric ligand 36

7.17.1. NMR spectra

¹H-NMR spectrum
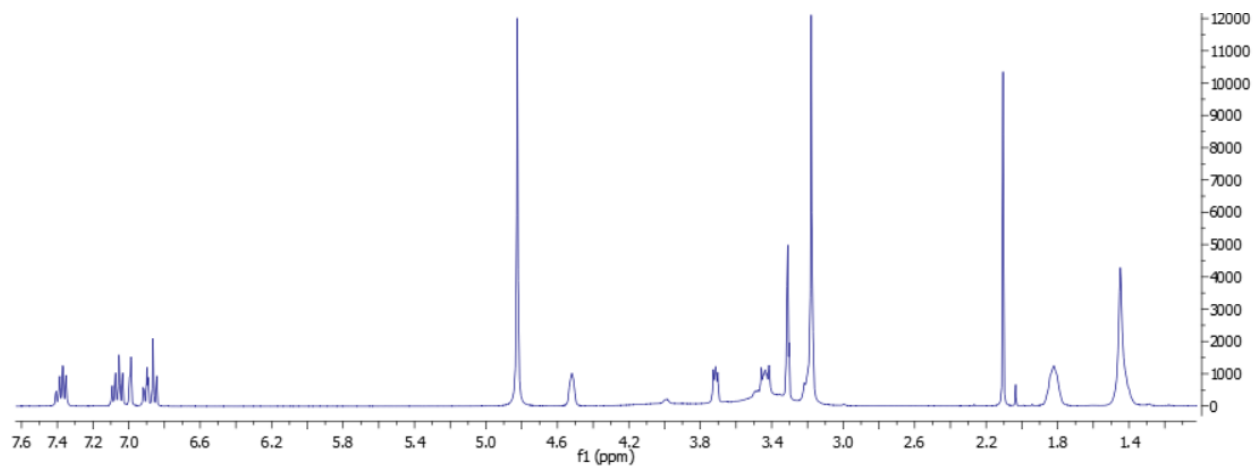
¹³C-NMR spectrum
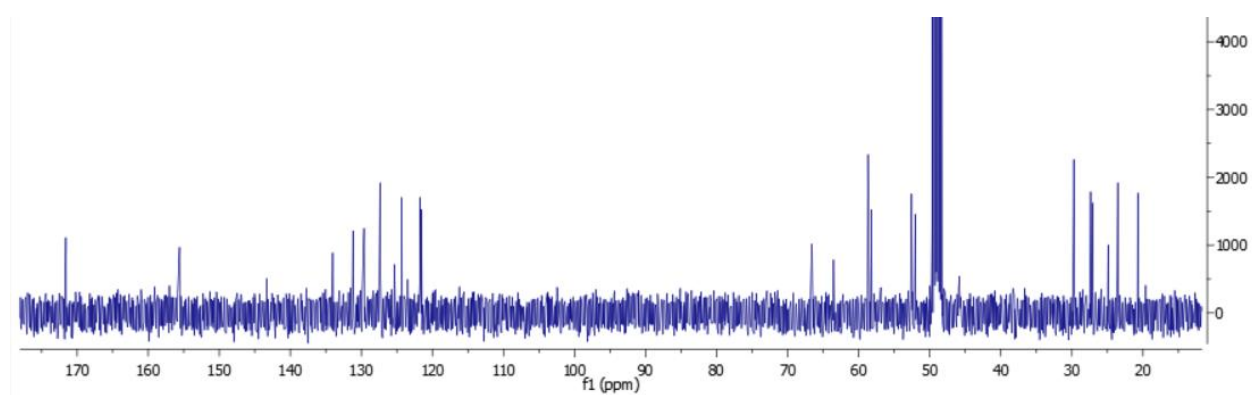
COSY spectrum
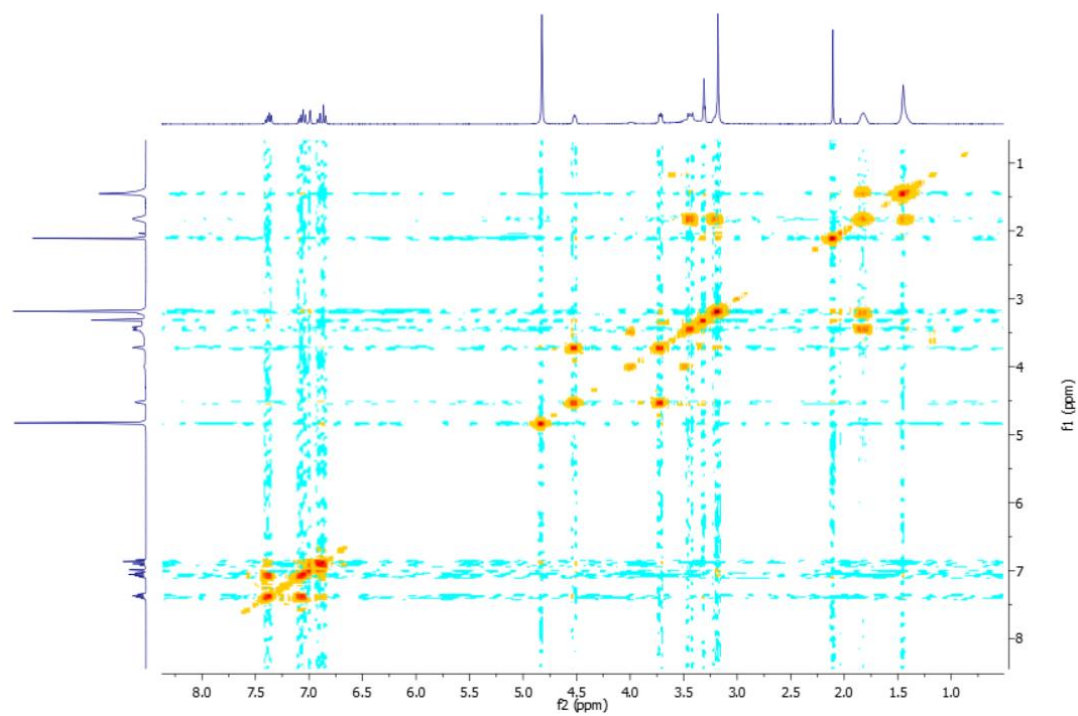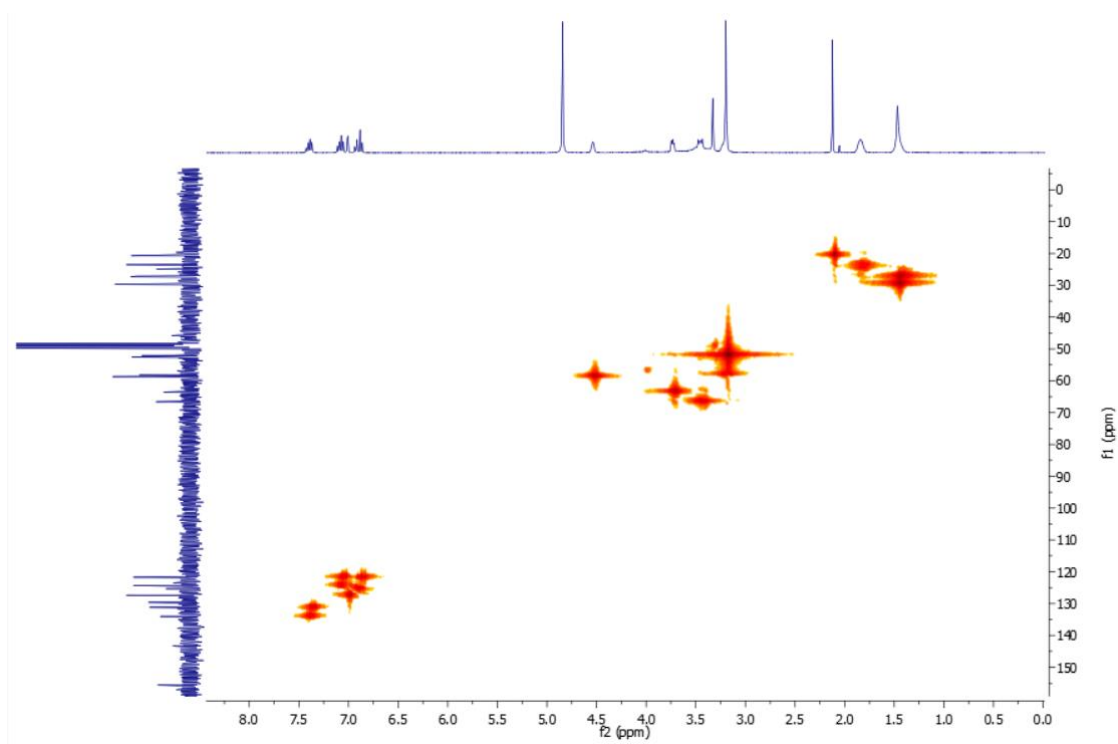
HMQC spectrum

HMBC spectrum

7.17.2. IR spectrum

esult	Peak Picking				
.	Position	Intensity	No.	Position	Intensity
	3950.46	99	2	3930.22	98
	3902.25	97	4	3891.65	98
	3882.97	99	6	3871.4	96
	3853.08	95	8	3838.61	97
	3820.29	96	10	3801.01	97
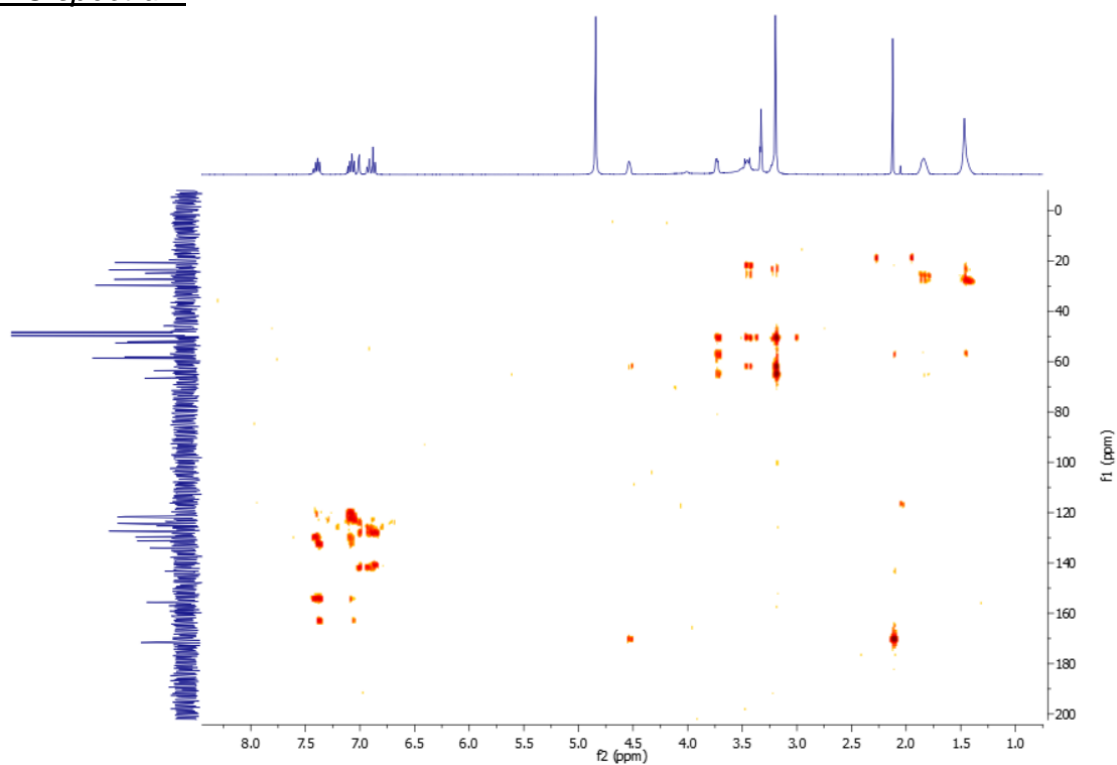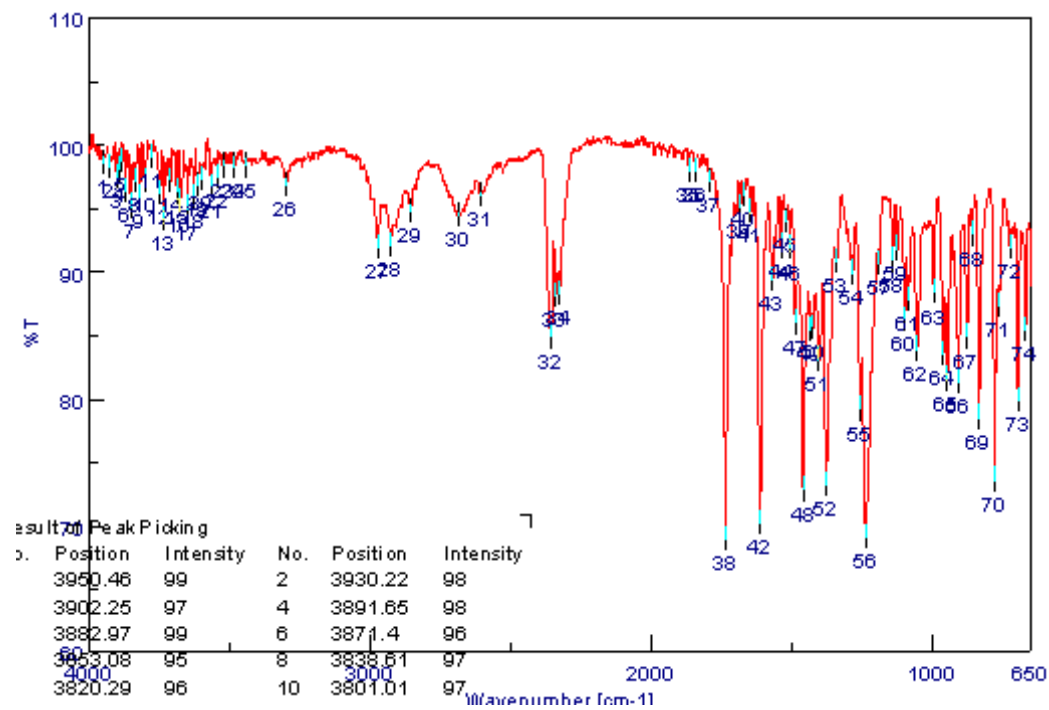
7.17.3. LC-MS spectrum (ESI)

\<Chromatogram\>

mV

Detector A 254nm

Detector A 254nm
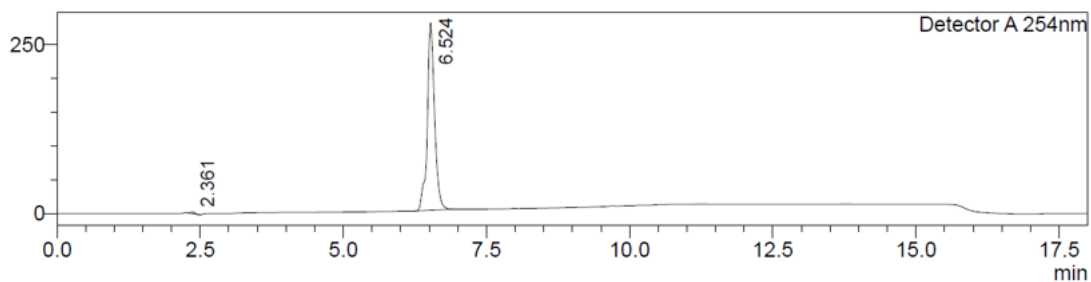
Peak#	Ret. Time	Area	Height	Area%
1	2.361	12048	2240	0.485
2	6.524	2472173	277266	99.515
Total		2484221	279506	100.000

Line#:1 R.Time:6.903(Scan#:4143)
MassPeaks:436
Spectrum Mode:Averaged 6.900-6.907(4141-4145) Base Peak:277.90(1748943)
BG Mode:Calc Segment 1 - Event 1
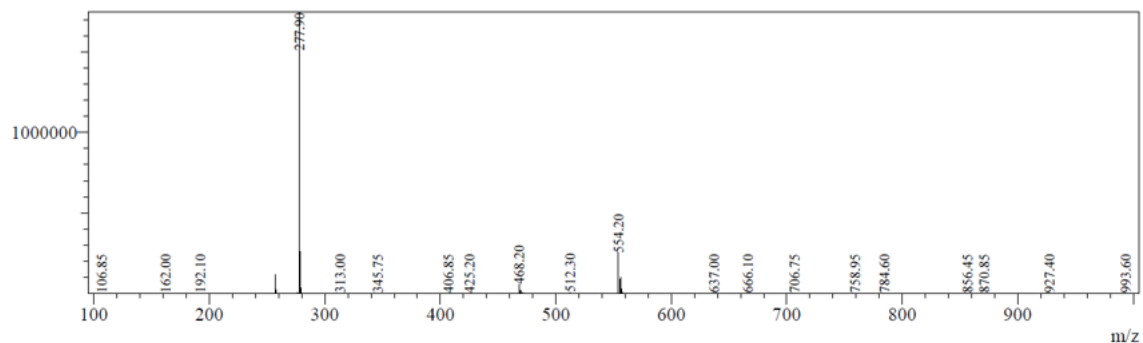
8. Supplementary information

8.1. Full crystallographic data of compound V

2-Amino-*N*-(2-chloropyridin-3yl)benzamide

Noura M. Riad, Darius P. Zlotos and Ulrike Holzgrabe

Crystal data:

$C_{12}H_{10}ClN_3O$	$F(000) = 512$
$M_r = 247.68$	$D_x = 1.518$ Mg m^{-3}
Monoclinic, $P2_1/c$	Mo *Kα* radiation, $\lambda = 0.71073$ Å
$a = 11.0965$ (9) A	Cell parameters from 2859 reflections
$b = 4.7669$ (4) Å	$\theta = 2.5–26.6°$
$c = 20.6624$ (17) Å	$\mu = 0.34$ mm^{-1}
$\beta = 97.556$ (3)°	$T = 100$ K
$V = 1083.47$ (15) Å^3	Block, colourless
$Z = 4$	0.57 × 0.39 × 0.21 mm

Data collection:

Bruker APEXII CCD diffractometer	2283 independent reflections
	1963 reflections with $I > 2\sigma(I)$
φ and *ω* scans	$R_{int} = 0.044$
Absorption correction: multi-scan	$\theta_{max} = 26.8°, \theta_{min} = 1.9°$
(SADABS; Bruker, 2013)	$h = -13 \rightarrow 14$
$T_{min} = 0.862, T_{max} = 0.957$	$k = -6 \rightarrow 5$
11807 measured reflections	$l = -25 \rightarrow 26$

Refinement:

Refinement on F^2	$wR(F^2) = 0.091$
Least-squares matrix: full	$S = 1.07$
$R[F^2 > 2\sigma(F^2)] = 0.037$	2283 reflections
155 parameters	$w = 1/[\sigma^2(F_o^2) + (0.0341P)^2 + 0.9297P]$
0 restraints	where $P = (F_o^2 + 2F_c^2)/3$
Primary atom site location: iterative	$(\Delta/\sigma)\text{max} < 0.001$
Hydrogen site location: mixed	$\Delta \rho_{max} = 0.35$ e Å^{-3}
H-atoms parameters constrained	$\Delta \rho_{min} = -0.44$ e Å^{-3}

Computer programs: *APEX2* and *SAINT*,[1] *olex2.solve*,[2] *SHELXL*,[3] and *OLEX2*.[4]

Geometry:

All e.s.d.'s (estimated standard deviation), except the e.s.d. in the dihedral angle between two l.s. planes, are estimated using the full covariance matrix. The cell e.s.d.'s are taken into account individually in the estimation of e.s.d.'s in distances, angles and torsion angles; correlations between e.s.d.'s in cell parameters are only used when they are defined by crystal symmetry. An approximate (isotropic) treatment of cell e.s.d.'s is used for estimating e.s.d.'s involving l.s. planes.

Fractional atomic coordinates and isotropic or equivalent isotropic displacement parameters (Å^2)

	x	y	z	$U_{iso}*/U_{eq}$
Cl1	0.81489 (4)	0.23796 (9)	0.39806 (2)	0.01471 (13)
O1	0.70743 (12)	0.9552 (3)	0.22843 (6)	0.0161 (3)
N3	0.70224 (13)	0.8909 (3)	0.09469 (7)	0.0137 (3)
H3A	0.7063	1.0033	0.1275	0.016*

H3B	0.7206	0.9803	0.0611	0.016*
N2	0.71512 (13)	0.5248 (3)	0.27552 (7)	0.0113 (3)
H2	0.7345	0.3474	0.2712	0.014*
N1	0.65077 (14)	0.5388 (3)	0.44509 (7)	0.0139 (3)
C8	0.78996 (15)	0.6915 (4)	0.11373 (9)	0.0112 (4)
C9	0.85353 (16)	0.5653 (4)	0.06707 (9)	0.0141 (4)
H9	0.8375	0.6234	0.0228	0.017*
C6	0.74137 (15)	0.7094 (4)	0.22874 (8)	0.0109 (4)
C2	0.65890 (15)	0.6017 (4)	0.33025 (8)	0.0099 (3)
C7	0.81176 (15)	0.5917 (4)	0.17868 (8)	0.0110 (4)
C5	0.56237 (17)	0.7324 (4)	0.44136 (9)	0.0159 (4)
H5	0.5291	0.7798	0.4800	0.019*
C11	0.96468 (16)	0.2701 (4)	0.14867 (9)	0.0146 (4)
H11	1.0256	0.1328	0.1606	0.018*
C12	0.90038 (15)	0.3850 (4)	0.19498 (9)	0.0126 (4)
H12	0.9166	0.3225	0.2389	0.015*
C3	0.56528 (15)	0.7972 (4)	0.32742 (9)	0.0131 (4)
H3	0.5346	0.8827	0.2871	0.016*
C4	0.51739 (16)	0.8661 (4)	0.38375 (9)	0.0147 (4)
H4	0.4548	1.0026	0.3830	0.018*
C1	0.69709 (15)	0.4811 (4)	0.39114 (9)	0.0113 (4)
C10	0.93868 (16)	0.3588 (4)	0.08413 (9)	0.0153 (4)
H10	0.9801	0.2760	0.0515	0.018*

Atomic displacement parameters ($\mathring{A}^2$)

	U^{11}	U^{22}	U^{33}	U^{12}	U^{13}	U^{23}
Cl1	0.0156 (2)	0.0151 (2)	0.0135 (2)	0.00489 (17)	0.00259 (16)	0.00396 (16)
O1	0.0258 (7)	0.0090 (6)	0.0148 (7)	0.0026 (5)	0.0075 (5)	0.0002 (5)
N3	0.0171 (8)	0.0138 (8)	0.0102 (8)	0.0010 (6)	0.0021 (6)	0.0025 (6)
N2	0.0156 (7)	0.0084 (7)	0.0105 (7)	0.0015 (6)	0.0042 (6)	−0.0009 (6)
N1	0.0171 (8)	0.0144 (8)	0.0111 (8)	−0.0010 (6)	0.0046 (6)	−0.0012 (6)

C8	0.0105 (8)	0.0097 (8)	0.0133 (9)	−0.0038 (7)	0.0017 (7)	−0.0004 (7)
C9	0.0159 (9)	0.0169 (9)	0.0101 (9)	−0.0045 (7)	0.0035 (7)	−0.0009 (7)
C6	0.0117 (8)	0.0101 (8)	0.0102 (8)	−0.0015 (7)	−0.0011 (7)	−0.0015 (6)
C2	0.0121 (8)	0.0082 (8)	0.0096 (8)	−0.0022 (7)	0.0025 (6)	−0.0017 (6)
C7	0.0124 (8)	0.0087 (8)	0.0121 (9)	−0.0029 (7)	0.0027 (7)	−0.0016 (7)
C5	0.0181 (9)	0.0170 (9)	0.0142 (9)	−0.0006 (8)	0.0078 (7)	−0.0040 (7)
C11	0.0123 (8)	0.0140 (9)	0.0179 (10)	−0.0005 (7)	0.0034 (7)	−0.0005 (7)
C12	0.0124 (8)	0.0124 (8)	0.0127 (9)	−0.0018 (7)	0.0012 (7)	−0.0001 (7)
C3	0.0121 (8)	0.0133 (9)	0.0135 (9)	−0.0017 (7)	0.0002 (7)	0.0005 (7)
C4	0.0116 (8)	0.0128 (9)	0.0203 (10)	0.0007 (7)	0.0041 (7)	−0.0022 (7)
C1	0.0115 (8)	0.0097 (8)	0.0125 (9)	−0.0006 (7)	0.0005 (7)	−0.0010 (7)
C10	0.0145 (9)	0.0170 (9)	0.0159 (10)	−0.0033 (7)	0.0070 (7)	−0.0042 (7)

Geometric parameters (Å, º)

Cl1—C1	1.7387 (17)	C6—C7	1.486 (2)
O1—C6	1.230 (2)	C2—C3	1.391 (2)
N3—H3A	0.8605	C2—C1	1.398 (2)
N3—H3B	0.8612	C7—C12	1.402 (2)
N3—C8	1.380 (2)	C5—H5	0.9500
N2—H2	0.8800	C5—C4	1.384 (3)
N2—C6	1.367 (2)	C11—H11	0.9500
N2—C2	1.410 (2)	C11—C12	1.380 (3)
N1—C5	1.342 (2)	C11—C10	1.393 (3)
N1—C1	1.316 (2)	C12—H12	0.9500
C8—C9	1.403 (2)	C3—H3	0.9500
C8—C7	1.414 (2)	C3—C4	1.381 (3)
C9—H9	0.9500	C4—H4	0.9500
C9—C10	1.378 (3)	C10—H10	0.9500
H3A—N3—H3B	109.4	N1—C5—H5	118.5
C8—N3—H3A	104.0	N1—C5—C4	122.98 (17)
C8—N3—H3B	109.8	C4—C5—H5	118.5

C6—N2—H2	118.0	C12—C11—H11	120.6
C6—N2—C2	123.91 (15)	C12—C11—C10	118.85 (17)
C2—N2—H2	118.0	C10—C11—H11	120.6
C1—N1—C5	117.33 (15)	C7—C12—H12	119.2
N3—C8—C9	119.93 (16)	C11—C12—C7	121.53 (17)
N3—C8—C7	121.89 (16)	C11—C12—H12	119.2
C9—C8—C7	117.98 (16)	C2—C3—H3	120.3
C8—C9—H9	119.3	C4—C3—C2	119.46 (16)
C10—C9—C8	121.36 (17)	C4—C3—H3	120.3
C10—C9—H9	119.3	C5—C4—H4	120.7
O1—C6—N2	121.56 (16)	C3—C4—C5	118.68 (17)
O1—C6—C7	122.99 (16)	C3—C4—H4	120.7
N2—C6—C7	115.44 (15)	N1—C1—Cl1	116.28 (13)
C3—C2—N2	123.17 (15)	N1—C1—C2	124.78 (16)
C3—C2—C1	116.73 (16)	C2—C1—Cl1	118.94 (13)
C1—C2—N2	120.10 (15)	C9—C10—C11	120.71 (17)
C8—C7—C6	119.58 (15)	C9—C10—H10	119.6
C12—C7—C8	119.44 (16)	C11—C10—H10	119.6
C12—C7—C6	120.98 (15)		

O1—C6—C7—C8	−33.5 (2)	C6—N2—C2—C3	39.1 (2)
O1—C6—C7—C12	145.85 (17)	C6—N2—C2—C1	−140.53 (17)
N3—C8—C9—C10	−177.76 (16)	C6—C7—C12—C11	178.71 (16)
N3—C8—C7—C6	−1.9 (2)	C2—N2—C6—O1	−6.5 (3)
N3—C8—C7—C12	178.73 (15)	C2—N2—C6—C7	174.11 (14)
N2—C6—C7—C8	145.84 (16)	C2—C3—C4—C5	−1.6 (3)
N2—C6—C7—C12	−34.8 (2)	C7—C8—C9—C10	−2.8 (3)
N2—C2—C3—C4	−178.27 (16)	C5—N1—C1—Cl1	177.95 (13)
N2—C2—C1—Cl1	0.4 (2)	C5—N1—C1—C2	−1.6 (3)
N2—C2—C1—N1	179.89 (16)	C12—C11—C10—C9	2.4 (3)
N1—C5—C4—C3	0.2 (3)	C3—C2—C1—Cl1	−179.30 (13)
C8—C9—C10—C11	−0.4 (3)	C3—C2—C1—N1	0.2 (3)
C8—C7—C12—C11	−1.9 (3)	C1—N1—C5—C4	1.4 (3)
C9—C8—C7—C6	−176.72 (15)	C1—C2—C3—C4	1.4 (2)
C9—C8—C7—C12	3.9 (2)	C10—C11—C12—C7	−1.3 (3)

Hydrogen-bond geometry (Å, º)

D—H⋯A	D—H	H⋯A	D⋯A	D—H⋯A
N3—H3A⋯O1	0.86	2.10	2.7734 (19)	135
N2—H2⋯O1^{i}	0.88	2.07	2.882 (2)	152
N3—H3B⋯N1^{ii}	0.86	2.42	3.087 (2)	134

Symmetry codes: (i) *x*, *y*−1, *z*; (ii) *x*, −*y*+3/2, *z*−1/2.

References:

[1]   Bruker *APEX2, SAINT and SADABS*, Bruker AXS Inc.: Madison, Wisconsin, USA, **2013**.

[2]   Bourhis, L. J.; Dolomanov, O. V.; Gildea, R. J.; Howard, J. A. K.; Puschmann, H., *Acta Cryst. A* **2015,** *71*, 59–75.

[3]   Sheldrick, G. M., *Acta Cryst. A* **2008,** *64*, 112–122.

[4]   Dolomanov, O. V.; Bourhis, L. J.; Gildea, R. J.; Howard, J. A. K.; Puschmann, H., *J. Appl. Cryst.* **2009,** *42*, 339-341.

8.2. Full crystallographic data of compound VI

3-(2-Chloropyridin-3-yl)quinazoline-2,4(1*H*,3*H*)-dione chloroform monosolvate

Noura M. Riad, Darius P. Zlotos and Ulrike Holzgrabe

Reprinted from: Riad, N.; Zlotos, D.; Holzgrabe, U., 3-(2-Chloropyridin-3-yl) quinazoline-2, 4 (1*H*, 3*H*)-dione chloroform monosolvate. *IUCrData* **2017,** *2* (4), x170580.

Crystal data:

$C_{13}H_8ClN_3O_2 \cdot CHCl_3$

$M_r = 393.04$

Monoclinic, $P2_1/c$

$a = 5.6382\,(11)$ A

$b = 13.622\,(3)$ Å

$c = 20.662\,(4)$ Å

$\beta = 92.289\,(6)°$

$V = 1585.7\,(5)$ Å^3

$Z = 4$

$F(000) = 792$

$D_x = 1.646$ Mg m^{-3}

Mo *Kα* radiation, $\lambda = 0.71073$ Å

Cell parameters from 3659 reflections

$\theta = 2.5–26.4°$

$\mu = 0.76$ mm^{-1}

$T = 100$ K

Block, colourless

$0.59 \times 0.32 \times 0.26$ mm

Data collection:

Bruker APEXII CCD
  diffractometer

φ and ω scans

Absorption correction: multi-scan

(SADABS; Bruker, 2013)

$T_{min} = 0.656$, $T_{max} = 0.980$

15463 measured reflections

3370 independent reflections

2796 reflections with $I > 2\sigma(I)$

$R_{int} = 0.054$

$\theta_{max} = 26.8°$, $\theta_{min} = 1.8°$

$h = -7 \rightarrow 7$

$k = -17 \rightarrow 16$

$l = -26 \rightarrow 26$

Refinement:

Refinement on F^2	$wR(F^2)$ = 0.109
Least-squares matrix: full	S = 1.08
$R[F^2 > 2\sigma(F^2)]$ = 0.040	3370 reflections
208 parameters	$w = 1/[\sigma^2(F_o^2) + (0.0529P)^2 + 0.6894P]$
0 restraints	where $P = (F_o^2 + 2F_c^2)/3$
Primary atom site location: structure-invariant	(Δ/σ)max = 0.001
direct methods	$\Delta\rho_{max}$ = 0.45 e Å^{-3}
Secondary atom site location: difference	$\Delta\rho_{min}$ = −0.49 e Å^{-3}
Fourier map	Hydrogen site location: inferred from
H-atoms parameters constrained	neighbouring sites

Computer programs: *APEX2* and *SAINT*,[1] *olex2.solve*,[2] *SHELXL*2014,[3] *Mercury*,[4] *OLEX2*,[5] *enCIFer*,[6] and *publCIF*.[7]

Geometry:

All e.s.d.'s (estimated standard deviation), except the e.s.d. in the dihedral angle between two l.s. planes, are estimated using the full covariance matrix. The cell e.s.d.'s are taken into account individually in the estimation of e.s.d.'s in distances, angles and torsion angles; correlations between e.s.d.'s in cell parameters are only used when they are defined by crystal symmetry. An approximate (isotropic) treatment of cell e.s.d.'s is used for estimating e.s.d.'s involving l.s. planes.

Fractional atomic coordinates and isotropic or equivalent isotropic displacement parameters (Å^2)

	x	y	z	U_{iso}*/U_{eq}
Cl1	0.12965 (11)	0.78921 (4)	0.58061 (3)	0.02149 (16)

Cl2	0.36470 (11)	0.13451 (5)	0.50999 (3)	0.02813 (17)
Cl3	0.40964 (14)	0.12297 (5)	0.64924 (3)	0.03261 (19)
Cl4	−0.03576 (12)	0.07201 (5)	0.58295 (4)	0.03620 (19)
O2	0.1523 (3)	0.60895 (12)	0.73418 (7)	0.0176 (4)
O1	0.5724 (3)	0.60283 (12)	0.55085 (8)	0.0213 (4)
N2	0.3498 (3)	0.60913 (13)	0.64027 (9)	0.0136 (4)
N1	0.4692 (4)	0.87525 (14)	0.64811 (9)	0.0186 (4)
N3	0.2842 (4)	0.48850 (14)	0.56200 (9)	0.0172 (4)
H3	0.3204	0.4603	0.5254	0.021*
C10	−0.2711 (4)	0.36988 (17)	0.66329 (12)	0.0217 (5)
H10	−0.3989	0.3427	0.6859	0.026*
C11	−0.1409 (4)	0.44692 (16)	0.69008 (11)	0.0172 (5)
H11	−0.1781	0.4724	0.7313	0.021*
C5	0.6601 (4)	0.87655 (17)	0.68915 (11)	0.0191 (5)
H5	0.7306	0.9381	0.6997	0.023*
C6	0.4117 (4)	0.56808 (16)	0.58157 (10)	0.0158 (5)
C4	0.7592 (4)	0.79289 (17)	0.71677 (11)	0.0186 (5)
H4	0.8932	0.7968	0.7460	0.022*
C12	0.0464 (4)	0.48717 (16)	0.65602 (10)	0.0139 (4)
C9	−0.2150 (4)	0.33221 (17)	0.60333 (12)	0.0226 (5)
H9	−0.3059	0.2795	0.5853	0.027*
C3	0.6576 (4)	0.70314 (16)	0.70056 (11)	0.0168 (5)
H3A	0.7219	0.6441	0.7184	0.020*
C8	−0.0304 (5)	0.36989 (17)	0.56961 (12)	0.0209 (5)
H8	0.0080	0.3428	0.5290	0.025*
C7	0.1001 (4)	0.44849 (16)	0.59596 (11)	0.0156 (5)
C13	0.1806 (4)	0.57113 (16)	0.68188 (10)	0.0137 (4)
C2	0.4630 (4)	0.70030 (16)	0.65844 (10)	0.0135 (4)
C1	0.3755 (4)	0.78838 (16)	0.63368 (10)	0.0154 (5)
C14	0.2739 (4)	0.07115 (17)	0.57913 (11)	0.0181 (5)
H14	0.3274	0.0014	0.5759	0.022*

Atomic displacement parameters ($\mathring{A}^2$)

	U^{11}	U^{22}	U^{33}	U^{12}	U^{13}	U^{23}
Cl1	0.0248 (3)	0.0162 (3)	0.0229 (3)	0.0005 (2)	−0.0065 (2)	0.0010 (2)
Cl2	0.0266 (3)	0.0344 (4)	0.0234 (3)	−0.0062 (3)	0.0005 (2)	0.0095 (2)
Cl3	0.0510 (5)	0.0250 (3)	0.0219 (3)	−0.0152 (3)	0.0019 (3)	−0.0036 (2)
Cl4	0.0211 (3)	0.0288 (4)	0.0594 (5)	−0.0018 (3)	0.0103 (3)	0.0094 (3)
O2	0.0216 (9)	0.0148 (8)	0.0166 (8)	−0.0002 (7)	0.0025 (6)	−0.0021 (6)
O1	0.0281 (10)	0.0146 (8)	0.0218 (9)	−0.0078 (7)	0.0100 (7)	−0.0063 (6)
N2	0.0179 (10)	0.0071 (9)	0.0159 (9)	−0.0027 (7)	0.0020 (7)	−0.0021 (7)
N1	0.0277 (11)	0.0089 (9)	0.0191 (10)	−0.0023 (8)	0.0004 (8)	0.0001 (7)
N3	0.0237 (11)	0.0113 (9)	0.0168 (9)	−0.0052 (8)	0.0040 (8)	−0.0045 (7)
C10	0.0199 (13)	0.0121 (12)	0.0331 (14)	−0.0036 (10)	0.0026 (10)	0.0036 (9)
C11	0.0175 (12)	0.0120 (11)	0.0222 (12)	0.0021 (9)	0.0019 (9)	0.0026 (9)
C5	0.0266 (13)	0.0110 (11)	0.0197 (12)	−0.0048 (10)	0.0023 (9)	−0.0029 (8)
C6	0.0203 (12)	0.0096 (11)	0.0175 (11)	−0.0009 (9)	0.0018 (9)	−0.0006 (8)
C4	0.0192 (12)	0.0172 (12)	0.0194 (12)	−0.0025 (10)	−0.0010 (9)	−0.0026 (9)
C12	0.0153 (11)	0.0074 (10)	0.0189 (11)	0.0017 (9)	−0.0008 (8)	0.0022 (8)
C9	0.0228 (13)	0.0104 (11)	0.0344 (14)	−0.0053 (10)	−0.0006 (10)	−0.0018 (10)
C3	0.0206 (12)	0.0111 (11)	0.0190 (11)	0.0020 (9)	0.0035 (9)	−0.0009 (8)
C8	0.0274 (13)	0.0115 (11)	0.0239 (12)	−0.0021 (10)	0.0010 (10)	−0.0032 (9)
C7	0.0183 (12)	0.0081 (10)	0.0203 (11)	0.0006 (9)	0.0003 (9)	0.0014 (8)
C13	0.0150 (11)	0.0098 (10)	0.0165 (11)	0.0043 (9)	0.0009 (8)	0.0021 (8)
C2	0.0172 (11)	0.0089 (10)	0.0148 (10)	−0.0018 (9)	0.0053 (8)	−0.0020 (8)
C1	0.0197 (12)	0.0113 (11)	0.0152 (11)	−0.0011 (9)	0.0009 (8)	−0.0004 (8)
C14	0.0210 (12)	0.0113 (11)	0.0221 (12)	−0.0012 (10)	0.0024 (9)	−0.0004 (9)

Geometric parameters (Å, º)

Cl1—C1	1.733 (2)	C11—H11	0.9500
Cl2—C14	1.763 (2)	C11—C12	1.404 (3)
Cl3—C14	1.759 (2)	C5—H5	0.9500
Cl4—C14	1.751 (2)	C5—C4	1.383 (3)
O2—C13	1.214 (3)	C4—H4	0.9500
O1—C6	1.222 (3)	C4—C3	1.385 (3)
N2—C6	1.393 (3)	C12—C7	1.392 (3)
N2—C13	1.408 (3)	C12—C13	1.461 (3)
N2—C2	1.439 (3)	C9—H9	0.9500
N1—C5	1.343 (3)	C9—C8	1.375 (4)
N1—C1	1.325 (3)	C3—H3A	0.9500
N3—H3	0.8800	C3—C2	1.373 (3)
N3—C6	1.354 (3)	C8—H8	0.9500
N3—C7	1.387 (3)	C8—C7	1.397 (3)
C10—H10	0.9500	C2—C1	1.387 (3)
C10—C11	1.383 (3)	C14—H14	1.0000
C10—C9	1.389 (3)		
C6—N2—C13	125.71 (19)	C8—C9—C10	121.2 (2)
C6—N2—C2	116.71 (18)	C8—C9—H9	119.4
C13—N2—C2	117.53 (18)	C4—C3—H3A	120.3
C1—N1—C5	117.1 (2)	C2—C3—C4	119.3 (2)
C6—N3—H3	117.9	C2—C3—H3A	120.3
C6—N3—C7	124.24 (19)	C9—C8—H8	120.5
C7—N3—H3	117.9	C9—C8—C7	119.1 (2)
C11—C10—H10	120.0	C7—C8—H8	120.5
C11—C10—C9	120.1 (2)	N3—C7—C12	119.7 (2)
C9—C10—H10	120.0	N3—C7—C8	119.8 (2)
C10—C11—H11	120.2	C12—C7—C8	120.5 (2)
C10—C11—C12	119.6 (2)	O2—C13—N2	120.3 (2)
C12—C11—H11	120.2	O2—C13—C12	125.0 (2)
N1—C5—H5	118.3	N2—C13—C12	114.72 (18)
N1—C5—C4	123.4 (2)	C3—C2—N2	121.6 (2)

C4—C5—H5	118.3	C3—C2—C1	118.2 (2)
O1—C6—N2	120.9 (2)	C1—C2—N2	120.2 (2)
O1—C6—N3	123.4 (2)	N1—C1—Cl1	115.99 (17)
N3—C6—N2	115.66 (19)	N1—C1—C2	123.8 (2)
C5—C4—H4	120.9	C2—C1—Cl1	120.18 (17)
C5—C4—C3	118.1 (2)	Cl2—C14—H14	108.3
C3—C4—H4	120.9	Cl3—C14—Cl2	109.87 (12)
C11—C12—C13	120.8 (2)	Cl3—C14—H14	108.3
C7—C12—C11	119.6 (2)	Cl4—C14—Cl2	110.84 (13)
C7—C12—C13	119.6 (2)	Cl4—C14—Cl3	111.24 (13)
C10—C9—H9	119.4	Cl4—C14—H14	108.3
N2—C2—C1—Cl1	−0.1 (3)	C4—C3—C2—C1	0.0 (3)
N2—C2—C1—N1	179.9 (2)	C9—C10—C11—C12	0.6 (4)
N1—C5—C4—C3	0.8 (4)	C9—C8—C7—N3	−178.8 (2)
C10—C11—C12—C7	−0.5 (3)	C9—C8—C7—C12	1.0 (4)
C10—C11—C12—C13	177.5 (2)	C3—C2—C1—Cl1	−179.73 (17)
C10—C9—C8—C7	−1.0 (4)	C3—C2—C1—N1	0.2 (3)
C11—C10—C9—C8	0.2 (4)	C7—N3—C6—O1	−179.5 (2)
C11—C12—C7—N3	179.6 (2)	C7—N3—C6—N2	0.9 (3)
C11—C12—C7—C8	−0.3 (3)	C7—C12—C13—O2	−178.2 (2)
C11—C12—C13—O2	3.9 (3)	C7—C12—C13—N2	3.1 (3)
C11—C12—C13—N2	−174.84 (19)	C13—N2—C6—O1	−175.0 (2)
C5—N1—C1—Cl1	−179.98 (17)	C13—N2—C6—N3	4.6 (3)
C5—N1—C1—C2	0.1 (3)	C13—N2—C2—C3	84.3 (3)
C5—C4—C3—C2	−0.5 (3)	C13—N2—C2—C1	−95.3 (2)
C6—N2—C13—O2	174.7 (2)	C13—C12—C7—N3	1.6 (3)
C6—N2—C13—C12	−6.5 (3)	C13—C12—C7—C8	−178.3 (2)
C6—N2—C2—C3	−98.0 (3)	C2—N2—C6—O1	7.4 (3)
C6—N2—C2—C1	82.4 (3)	C2—N2—C6—N3	−172.91 (19)
C6—N3—C7—C12	−3.9 (3)	C2—N2—C13—O2	−7.8 (3)
C6—N3—C7—C8	176.0 (2)	C2—N2—C13—C12	171.01 (19)
C4—C3—C2—N2	−179.6 (2)	C1—N1—C5—C4	−0.6 (4)

Hydrogen-bond geometry (Å, º)

D—H···*A*	*D*—H	H···*A*	*D*···*A*	*D*—H···*A*
N3—H3···O1[i]	0.88	1.91	2.791 (3)	175
C14—H14···N1[ii]	1.00	2.39	3.200 (3)	137
C3—H3*A*···O2[iii]	0.95	2.48	3.123 (3)	125

Symmetry codes: (i) −*x*+1, −*y*+1, −*z*+1; (ii) *x*, *y*−1, *z*; (iii) *x*+1, *y*, *z*.

References:

[1]   Bruker, *APEX2, SAINT and SADABS*, Bruker AXS Inc.: Madison, Wisconsin, USA, **2013**.

[2]   Bourhis, L. J.; Dolomanov, O. V.; Gildea, R. J.; Howard, J. A. K.; Puschmann, H., *Acta Cryst. A* **2015,** *71*, 59–75.

[3]   Sheldrick, G. M., *Acta Cryst. C* **2015,** *71*, 3–8.

[4]   Macrae, C. F.; Bruno, I. J.; Chisholm, J. A.; Edgington, P. R.; McCabe, P.; Pidcock, E.; Rodriguez-Monge, L.; Taylor, R.; van de Streek, J.; Wood, P. A., *J. Appl. Cryst.* **2008,** *41*, 466–470.

[5]   Dolomanov, O. V.; Bourhis, L. J.; Gildea, R. J.; Howard, J. A. K.; Puschmann, H., *J. Appl. Cryst.* **2009,** *42*, 339-341.

[6]   Allen, F. H.; Johnson, O.; Shields, G. P.; Smith, B. R.; Towler, M., *J. Appl. Cryst.* **2004,** *37*, 335–338.

[7]   Westrip, S. P., *J. Appl. Cryst.* **2010,** *43*, 920–925.

8.3. Full crystallographic data of compound VII

Crystal structure of 5,11-dihydropyrido [2,3-*b*][1,4]benzodiazepin-6-one

Noura M. Riad, Darius P. Zlotos and Ulrike Holzgrabe

Reprinted from: Riad, N. M.; Zlotos, D. P.; Holzgrabe, U., Crystal structure of 5, 11-dihydropyrido [2, 3-*b*][1, 4] benzodiazepin-6-one. *Acta Crystallographica Section E: Crystallographic Communications* **2015,** *71* (5), 304-305.

Crystal data:

$C_{12}H_9N_3O$	$Z = 2$
$M_r = 211.22$	F(000) = 220
Triclinic, $P1^-$	Dx = 1.494 Mg m^{-3}
$a = 3.7598\ (5)$ Å	Mo $K\alpha$ radiation, λ = 0.71073 Å
$b = 10.2467\ (14)$ Å	Cell parameters from 1512 reflections
$c = 12.8768\ (17)$ Å	θ = 2.3–26.2°
$\alpha = 104.628\ (6)$°	$\mu = 0.10$ mm^{-1}
$\beta = 96.616\ (5)$°	$T = 100$ K
$\gamma = 98.009\ (4)$°	Plate, colourless
$V = 469.43\ (11)$ Å^3	0.35 × 0.26 × 0.06 mm

Data collection:

Bruker APEXII CCD diffractometer	2000 independent reflections
	1467 reflections with $I > 2\sigma(I)$
φ and ω scans	$R_{int} = 0.035$
Absorption correction: multi-scan	$\theta_{max} = 26.8$°, $\theta_{min} = 1.7$°
(SADABS; Bruker, 2013)	$h = -4{\rightarrow}4$
$T_{min} = 0.898$, $T_{max} = 0.959$	$k = -12{\rightarrow}12$
6425 measured reflections	$l = -16{\rightarrow}16$

Refinement:

Refinement on F^2	$wR(F^2) = 0.110$
Least-squares matrix: full	$S = 1.06$
$R[F^2 > 2\sigma(F^2)] = 0.041$	2000 reflections
153 parameters	$w = 1/[\sigma^2(F_o^2) + (0.0437P)^2 + 0.2092P]$
0 restraints	where $P = (F_o^2 + 2F_c^2)/3$
Primary atom site location: iterative	$(\Delta/\sigma)max < 0.001$
Hydrogen site location: mixed	$\Delta\rho_{max} = 0.23$ e Å^{-3}
H atoms treated by a mixture of independent and constrained refinement	$\Delta\rho_{min} = -0.22$ e Å^{-3}

The N- and C-bound H atoms were included in calculated positions and refined as riding: N2—H = 0.86 Å, C—H and N3 —H = 0.93 Å with $U_{iso}(H) = 1.2U_{eq}(C)$.

Data collection: *APEX2;*[1] cell refinement: *SAINT;*[1] data reduction: *SAINT;*[1] program(s) used to solve structure: *OLEX2.solve;*[2] program(s) used to refine structure: *SHELXL97;*[3] molecular graphics: *OLEX2;*[4] software used to prepare material for publication: *OLEX2,* Mercury,[5] and *enCIFer.*[6]

Absorption correction: SADABS-2012/1 (Bruker,2012) was used for absorption correction. wR2(int) was 0.0475 before and 0.0419 after correction. The ratio of minimum to maximum transmission is 0.9367. The $\lambda/2$ correction factor is 0.0015.

Geometry:

All e.s.d.'s (estimated standard deviation), except the e.s.d. in the dihedral angle between two l.s. planes, are estimated using the full covariance matrix. The cell e.s.d.'s are taken into account individually in the estimation of e.s.d.'s in distances, angles and torsion angles; correlations between e.s.d.'s in cell parameters are only used when they are defined by crystal symmetry. An approximate (isotropic) treatment of cell e.s.d.'s is used for estimating e.s.d.'s involving l.s. planes.

Fractional atomic coordinates and isotropic or equivalent isotropic displacement parameters ($Å^2$)

	x	y	z	$U_{iso}*/U_{eq}$
O1	0.3371 (4)	0.33046 (14)	0.49729 (10)	0.0196 (3)
N3	0.4460 (4)	0.42582 (15)	0.83790 (13)	0.0152 (4)
N1	0.3852 (4)	0.64248 (15)	0.93418 (12)	0.0157 (4)
N2	0.3945 (4)	0.51349 (17)	0.63963 (13)	0.0163 (4)
C4	0.3379 (5)	0.59565 (19)	0.74023 (14)	0.0143 (4)
C12	0.3836 (5)	0.55643 (19)	0.83732 (14)	0.0133 (4)
C1	0.3340 (5)	0.7706 (2)	0.93750 (16)	0.0174 (4)
H1	0.3431	0.8320	1.0051	0.021*
C10	0.0818 (5)	0.20571 (19)	0.81375 (15)	0.0148 (4)
H10	0.1291	0.2203	0.8887	0.018*
C3	0.2728 (5)	0.72576 (19)	0.74596 (15)	0.0168 (4)
H3A	0.2314	0.7535	0.6829	0.020*
C6	0.1477 (5)	0.28402 (18)	0.65494 (14)	0.0137 (4)
C7	−0.0602 (5)	0.15952 (19)	0.59213 (15)	0.0162 (4)
H7	−0.1071	0.1434	0.5171	0.019*
C11	0.2231 (5)	0.30746 (18)	0.76774 (14)	0.0130 (4)
C5	0.2998 (5)	0.37759 (19)	0.59331 (14)	0.0150 (4)
C2	0.2691 (5)	0.81567 (19)	0.84655 (15)	0.0170 (4)
H2A	0.2239	0.9039	0.8521	0.020*
C8	−0.1979 (5)	0.0597 (2)	0.63858 (16)	0.0177 (4)
H8	−0.3366	−0.0226	0.5956	0.021*
C9	−0.1254 (5)	0.08462 (19)	0.75055 (15)	0.0168 (4)
H9	−0.2180	0.0187	0.7831	0.020*
H3	0.497 (6)	0.419 (2)	0.9087 (19)	0.027 (6)*
H2	0.467 (6)	0.557 (2)	0.5943 (19)	0.031 (7)*

Atomic displacement parameters (Å²)

	U^{11}	U^{22}	U^{33}	U^{12}	U^{13}	U^{23}
O1	0.0270 (8)	0.0201 (7)	0.0118 (7)	0.0026 (6)	0.0058 (6)	0.0042 (6)
N3	0.0192 (9)	0.0143 (8)	0.0113 (8)	0.0023 (7)	−0.0008 (7)	0.0036 (7)
N1	0.0174 (8)	0.0157 (8)	0.0137 (8)	0.0016 (7)	0.0032 (6)	0.0039 (7)
N2	0.0212 (9)	0.0165 (9)	0.0122 (8)	0.0010 (7)	0.0043 (7)	0.0062 (7)
C4	0.0119 (9)	0.0174 (10)	0.0125 (9)	−0.0007 (8)	0.0012 (7)	0.0041 (8)
C12	0.0101 (9)	0.0155 (10)	0.0143 (9)	−0.0002 (7)	0.0015 (7)	0.0053 (8)
C1	0.0159 (10)	0.0178 (10)	0.0173 (10)	0.0024 (8)	0.0046 (8)	0.0018 (8)
C10	0.0158 (9)	0.0184 (10)	0.0128 (9)	0.0052 (8)	0.0031 (7)	0.0072 (8)
C3	0.0153 (10)	0.0203 (10)	0.0166 (10)	0.0021 (8)	0.0011 (8)	0.0097 (8)
C6	0.0117 (9)	0.0151 (10)	0.0154 (9)	0.0038 (8)	0.0046 (7)	0.0043 (8)
C7	0.0150 (10)	0.0192 (10)	0.0145 (9)	0.0047 (8)	0.0005 (7)	0.0044 (8)
C11	0.0105 (9)	0.0148 (9)	0.0139 (9)	0.0040 (7)	0.0027 (7)	0.0032 (8)
C5	0.0135 (9)	0.0193 (10)	0.0127 (9)	0.0029 (8)	0.0013 (7)	0.0056 (8)
C2	0.0160 (10)	0.0163 (10)	0.0209 (10)	0.0047 (8)	0.0045 (8)	0.0071 (9)
C8	0.0139 (10)	0.0151 (10)	0.0215 (10)	0.0012 (8)	0.0004 (8)	0.0024 (8)
C9	0.0135 (9)	0.0175 (10)	0.0229 (11)	0.0039 (8)	0.0054 (8)	0.0102 (9)

Geometric parameters (Å, º)

O1—C5	1.240 (2)	C10—C11	1.396 (3)
N3—C12	1.392 (2)	C10—C9	1.372 (3)
N3—C11	1.406 (2)	C3—H3A	0.9300
N3—H3	0.93 (2)	C3—C2	1.390 (3)
N1—C12	1.332 (2)	C6—C7	1.396 (3)
N1—C1	1.344 (2)	C6—C11	1.399 (2)
N2—C4	1.412 (2)	C6—C5	1.487 (3)
N2—C5	1.347 (2)	C7—H7	0.9300
N2—H2	0.87 (3)	C7—C8	1.380 (3)
C4—C12	1.406 (3)	C2—H2A	0.9300
C4—C3	1.374 (3)	C8—H8	0.9300
C1—H1	0.9300	C8—C9	1.387 (3)
C1—C2	1.372 (3)	C9—H9	0.9300
C10—H10	0.9300		
C12—N3—C11	121.58 (15)	C7—C6—C11	119.17 (17)
C12—N3—H3	110.9 (13)	C7—C6—C5	115.70 (16)
C11—N3—H3	112.7 (13)	C11—C6—C5	124.91 (17)
C12—N1—C1	117.87 (16)	C6—C7—H7	119.2
C4—N2—H2	115.9 (15)	C8—C7—C6	121.68 (18)
C5—N2—C4	130.98 (17)	C8—C7—H7	119.2
C5—N2—H2	112.2 (15)	C10—C11—N3	117.55 (16)
C12—C4—N2	123.05 (17)	C10—C11—C6	118.58 (17)
C3—C4—N2	118.46 (17)	C6—C11—N3	123.83 (17)
C3—C4—C12	118.12 (17)	O1—C5—N2	119.17 (17)
N3—C12—C4	121.47 (16)	O1—C5—C6	119.73 (17)
N1—C12—N3	115.93 (16)	N2—C5—C6	121.09 (16)
N1—C12—C4	122.55 (17)	C1—C2—C3	118.16 (18)
N1—C1—H1	118.2	C1—C2—H2A	120.9
N1—C1—C2	123.52 (18)	C3—C2—H2A	120.9
C2—C1—H1	118.2	C7—C8—H8	120.7
	119.4		118.69 (18)

C11—C10—H10		C7—C8—C9	
C9—C10—H10	119.4	C9—C8—H8	120.7
C9—C10—C11	121.27 (17)	C10—C9—C8	120.60 (18)
C4—C3—H3A	120.2	C10—C9—H9	119.7
C4—C3—C2	119.64 (17)	C8—C9—H9	119.7
C2—C3—H3A	120.2		
N1—C1—C2—C3	−3.0 (3)	C7—C6—C11—C10	−1.0 (3)
N2—C4—C12—N3	−7.9 (3)	C7—C6—C5—O1	−22.0 (3)
N2—C4—C12—N1	169.29 (18)	C7—C6—C5—N2	157.23 (17)
N2—C4—C3—C2	−170.60 (17)	C7—C8—C9—C10	−0.5 (3)
C4—N2—C5—O1	170.53 (18)	C11—N3—C12—N1	132.19 (18)
C4—N2—C5—C6	−8.7 (3)	C11—N3—C12—C4	−50.5 (2)
C4—C3—C2—C1	0.4 (3)	C11—C10—C9—C8	0.5 (3)
C12—N3—C11—C10	−129.09 (19)	C11—C6—C7—C8	1.0 (3)
C12—N3—C11—C6	53.5 (2)	C11—C6—C5—O1	152.47 (18)
C12—N1—C1—C2	2.1 (3)	C11—C6—C5—N2	−28.3 (3)
C12—C4—C3—C2	2.7 (3)	C5—N2—C4—C12	42.4 (3)
C1—N1—C12—N3	178.56 (16)	C5—N2—C4—C3	−144.7 (2)
C1—N1—C12—C4	1.3 (3)	C5—C6—C7—C8	175.82 (17)
C3—C4—C12—N3	179.21 (17)	C5—C6—C11—N3	2.0 (3)
C3—C4—C12—N1	−3.6 (3)	C5—C6—C11—C10	−175.34 (17)
C6—C7—C8—C9	−0.2 (3)	C9—C10—C11—N3	−177.23 (16)
C7—C6—C11—N3	176.35 (17)	C9—C10—C11—C6	0.3 (3)

Hydrogen-bond geometry (Å, º)

D—H···A	D—H	H···A	D···A	D—H···A
N2—H2···O1^i	0.87 (2)	1.98 (2)	2.840 (2)	175 (2)
N3—H3···N1^ii	0.93 (2)	2.28 (2)	3.200 (2)	168.7 (19)

Symmetry codes: (i) −x+1, −y+1, −z+1; (ii) −x+1, −y+1, −z+2.

References:

[1]   Bruker, *APEX2, SAINT and SADABS*, Bruker AXS Inc.: Madison, Wisconsin, USA, **2013**.

[2]   Bourhis, L. J.; Dolomanov, O. V.; Gildea, R. J.; Howard, J. A. K.; Puschmann, H., *Acta Cryst. A* **2015,** *71*, 59–75.

[3]   Sheldrick, G. M., *Acta Cryst. A* **2008,** *64*, 112–122.

[4]   Dolomanov, O. V.; Bourhis, L. J.; Gildea, R. J.; Howard, J. A. K.; Puschmann, H., *J. Appl. Cryst.* **2009,** *42*, 339-341.

[5]   Macrae, C. F.; Edgington, P. R.; McCabe, P.; Pidcock, E.; Shields, G. P.; Taylor, R.; Towler, M.; van de Streek, J., *J. Appl. Cryst.* **2006,** *39*, 453–457.

[6]   Allen, F. H.; Johnson, O.; Shields, G. P.; Smith, B. R.; Towler, M., *J. Appl. Cryst.* **2004,** *37*, 335–338.